



National Library
of Canada

Bibliothèque nationale
du Canada

Acquisitions and
Bibliographic Services Branch

Direction des acquisitions et
des services bibliographiques

395 Wellington Street
Ottawa, Ontario
K1A 0N4

395, rue Wellington
Ottawa (Ontario)
K1A 0N4

Your file - Votre référence

Our file - Notre référence

NOTICE

The quality of this microform is heavily dependent upon the quality of the original thesis submitted for microfilming. Every effort has been made to ensure the highest quality of reproduction possible.

If pages are missing, contact the university which granted the degree.

Some pages may have indistinct print especially if the original pages were typed with a poor typewriter ribbon or if the university sent us an inferior photocopy.

Reproduction in full or in part of this microform is governed by the Canadian Copyright Act, R.S.C. 1970, c. C-30, and subsequent amendments.

AVIS

La qualité de cette microforme dépend grandement de la qualité de la thèse soumise au microfilmage. Nous avons tout fait pour assurer une qualité supérieure de reproduction.

S'il manque des pages, veuillez communiquer avec l'université qui a conféré le grade.

La qualité d'impression de certaines pages peut laisser à désirer, surtout si les pages originales ont été dactylographiées à l'aide d'un ruban usé ou si l'université nous a fait parvenir une photocopie de qualité inférieure.

La reproduction, même partielle, de cette microforme est soumise à la Loi canadienne sur le droit d'auteur, SRC 1970, c. C-30, et ses amendements subséquents.

Canada

**A Fundamental Study of the Fracture and Fatigue
Characteristics of Single Wood Pulp Fibres:
Application to Mechanical Refiners**

by

Wadood Y. Hamad B.Sc., M.Eng.

Fracture and Fatigue Control Laboratory,
Department of Mechanical Engineering,
McGill University,
Montréal, Canada.

January, 1994

A Thesis submitted to the Faculty of Graduate Studies and Research
in partial fulfilment of the requirements of the degree of
Doctor of Philosophy

© Wadood Y. Hamad 1994.



National Library
of Canada

Acquisitions and
Bibliographic Services Branch

395 Wellington Street
Ottawa, Ontario
K1A 0N4

Bibliothèque nationale
du Canada

Direction des acquisitions et
des services bibliographiques

395, rue Wellington
Ottawa (Ontario)
K1A 0N4

Your file *Votre référence*

Our file *Notre référence*

The author has granted an irrevocable non-exclusive licence allowing the National Library of Canada to reproduce, loan, distribute or sell copies of his/her thesis by any means and in any form or format, making this thesis available to interested persons.

L'auteur a accordé une licence irrévocable et non exclusive permettant à la Bibliothèque nationale du Canada de reproduire, prêter, distribuer ou vendre des copies de sa thèse de quelque manière et sous quelque forme que ce soit pour mettre des exemplaires de cette thèse à la disposition des personnes intéressées.

The author retains ownership of the copyright in his/her thesis. Neither the thesis nor substantial extracts from it may be printed or otherwise reproduced without his/her permission.

L'auteur conserve la propriété du droit d'auteur qui protège sa thèse. Ni la thèse ni des extraits substantiels de celle-ci ne doivent être imprimés ou autrement reproduits sans son autorisation.

ISBN 0-315-94629-6

Canada

Fracture and Fatigue Characterisation of Single Wood Pulp Fibres

For my dearest and most cherished,

Nadia, Sara and Zaid.

Lest times prove cruel and become a catalyst to oblivion.

The analysis of scientific research merely begins with a description of how it is misapplied and misdistributed. The next step must be an unequivocal statement that scientific activity in a technological society is not, and cannot be, politically neutral or value free.

Bill Zimmerman *et al.*
'People's Science' in *The Racial Economy of
Science — Toward a Democratic Future.*

Abstract

An in-depth investigation is carried out to characterise the damage accumulation mechanisms and fatigue growth in single wood pulp fibres, which may be thought of as concentrically-layered, filamentary composite tubes that are approximately: 1–3 mm long, 20–40 μm in cross-section. The novel experimental methodology principally consists of the *in situ* apparatuses, on the one hand, which comprise the in-house designed and built *single-fibre tensiometer*, in conjunction with the confocal laser scanning microscope (CLSM) and, on the other, the computer hardware and periphery. The tensiometer's prime components, the loading jaws, are specifically designed to best emulate the force actions to which wood pulp fibres are subjected while between the discs of mechanical refiners (viz.: cyclic shear, radial compression and tension); and incorporate a mechanical fixation mechanism to ensure proper mounting of the single fibres. Moreover, the CLSM, which functions by scanning a diffraction-limited spot of light relative to the specimen in a raster-type scan, is a powerful tool for obtaining qualitative information on the morphology of fractured surfaces and structural behaviour of the fibres being fatigued, as well as providing accurate visual records of the history of crack propagation. The entire fully-automated set-up is controlled, in real time, via a computer algorithm specifically written for displacement-control fatigue-testing, while making efficient utilisation in terms of execution time, memory allocation, signal conversion and data acquisition.

The engendered conclusions may be summed up as follows. From a litany of tenuously-oriented microcracks, dominant macrocracks propagate along the axis of the fibre which may sharply deflect in the presence of natural bias (e.g. pits in the fibre wall). The material property degradation characteristics further include: volumetric expansion due to internal fibrillation in the cell wall, extensive external fibrillation, gradual delamination of the layers and partial peeling-off of the cell wall material. Cumulative damage due to cyclic shear is shown to be the most significant, further supported by the high structural collapsibility of the fibre wall layers. The mechanisms of fracture are either due to the development of transverse cracks at regions of high stress concentration (such as bordered pits), or owing to the gradual slippage of the fibre wall layers.

Résumé

Une étude approfondie a été afin de caractériser les mécanismes d'accumulation de la détérioration et la propagation de la fatigue d'une seule fibre de pâte de bois; on peut représenter ces fibres sous la forme de tubes composites filamenteux à couches concentriques d'environ 1 à 3 mm de long et de 20 à 40 μm de diamètre. Ce nouveau dispositif expérimental comprend principalement: des appareils *in situ* (un *tensiomètre* contenant une fibre conçu et fabriqué dans notre laboratoire, un microscope confocal à balayage laser [MCBL]); et, du matériel informatique et des périphériques. Les principaux éléments du tensiomètre, c'est-à-dire les mâchoires de chargement, sont spécifiquement conçus pour imiter le mieux possible les forces auxquelles les fibres de pâte de bois sont soumises entre les disques du raffineur mécanique (c'est-à-dire : cisaillement cyclique, compression radiale et tension); ces éléments comprennent un mécanisme de fixation mécanique qui assure le montage adéquat des fibres. De plus, le MCBL, qui fonctionne par balayage de type récurrent d'un point lumineux à diffraction limitée, constitue un outil puissant pour la cueillette d'informations qualitatives sur la morphologie de surfaces fracturées et sur les comportements structurels des fibres soumises à des essais de fatigue; l'instrument permet également de réaliser des enregistrements visuels précis de la propagation des fissures. L'ensemble de l'appareil, entièrement automatisé, est contrôlé en temps réel par un algorithme spécialement conçu pour les essais de fatigue à déplacement contrôlé; l'appareil est également d'une utilisation efficace pour ce qui est du temps d'exécution, de l'affectation de la mémoire, de la conversion des signaux et de la saisie des données.

Les conclusions dégagées peuvent se résumer de la façon suivante. À partir d'une série de microfissures d'orientation aléatoire, des macrofissures dominantes se propagent le long de l'axe de la fibre et peuvent être brusquement défléchies en présence de déformations naturelles (par ex., petites cavités dans la paroi de la fibre). Les caractéristiques de dégradation des propriétés du matériau comprennent en outre : l'expansion volumétrique due à la fibrillation interne dans la paroi cellulaire, la fibrillation externe étendue, la délamination graduelle des couches et le décollage partiel du matériau de la paroi cellulaire. La détérioration cumulée due au cisaillement cyclique se révèle être la plus importante de ces caractéristiques, ce qu'atteste en outre

la forte propension à l'affaissement structurel des couches de la paroi des fibres. Les mécanismes de fracture sont dus soit à l'apparition de fissures transversales dans les régions de forte concentration de contraintes (par ex., dans les cavités bordées), soit au glissement graduel des couches de la paroi des fibres.

Prologue

It is often the case that a researcher is gainsaid the very opportunity to transcend the mere surroundings of one's area of research to encompass palpable material conditions which would play a significant role in shaping one's thoughts and, hence, the manner in which one conducts research and, more importantly, the purpose and goal of so doing. While it may be beyond the scope of this treatise to delve, at least at this juncture, in propounding some of the ideas enunciated hereinbefore; I should, nonetheless, not be parsimonious in so far as acknowledging some of those who did, directly or indirectly, influence the very prospects I espouse. First and foremost, my most sincere gratitude and boundless admiration go to my parents and aunt, whose company I have been deprived of for well over a decade, for their unparalleled support, affection and guidance over the past twenty-seven years. Moreover, my advancement had particularly been due, in many a respect, to the unwavering dedication and support, in every sense of the word, of my uncle, Tariq — an inspiration *par excellence* — and his wife, Avis. My current state could not at all be realised without the altruism of all of them, which at times bordered on the edge of *naïveté*: Whatever I say shall stand bare relative to their deeds during some harsh times.

I extend my sincere thanks to my supervisor, Professor James W. Provan, for introducing a most interesting topic, and for his insatiable appetite for pursuing scientific research. His continued guidance, encouragement and tireless interest at each and every step of the way made the experience not only intellectually satisfying, but, indeed, a delectable one. His humility and unique sense of respect for fellow human beings, traits lacking nowadays, give, at least, myself a hopeful look into the future.

Moreover, I should like to acknowledge the support and help proffered by Dr. A. Karnis, of Paprican, Pointe Claire, during the course of the research: for providing various pulp samples, engaging in discussions and clarifying practical aspects of mechanical refining. I further extend my thanks to Professor D. R. Axelrad for his objective criticism and for bringing to my attention motley aspects of the field of micromechanics. Thanks are further due, for giving me the opportunity to explore and canvass various considerations of fibre physics and chemistry, to the following

persons: Dr. D. Page, Dr. R. Amiri, both of Paprican, Pointe Claire, and Professor D. Gray, Department of Chemistry.

I should like to acknowledge the generous support of the *Mechanical and Chemimechanical Wood-Pulps Centre of Excellence Network* through a research studentship to undertake the subject research.

My sincere thanks further go to Mr. Antonio Miccozi of the Machine Tool Laboratory, Department of Mechanical Engineering, for his impeccable workmanship in assisting with the manufacture of the single-fibre tensiometer and the very delicate and tiny loading jaws: his patience and perseverance to perform difficult tasks are indeed commendable. None of the research ideas one hopes to tackle could possibly materialise without the dedication of such persons as Tony; he and his colleagues deserve every recognition. I further wish to express my sincere gratitude to Ms. Jane Trecarten and the Montreal General Hospital Research Institute (Centre for Research in Neuroscience) for allowing the utilisation of their CLSM. Ms. Trecarten's invaluable assistance and her creating a pleasant atmosphere to ensure the smooth running of the research, are deeply appreciated. Thanks are in order to the Physical Sciences and Engineering Library, McGill University, the Pulp and Paper Research Institute Library, both at Pointe Claire and at McGill University, for their assistance in acquiring many references from rather dispersed and remote areas of the world.

It would not be possible not to mention the support I have received from my close friends, most notably, Mr. Rafid Yousif, Dr. Hassan al-Kaisi, Mrs. Kathy al-Kaisi and Dr. Ali Shikara. For in spite of the vast distances that separate them from the author they never failed to express their support and affection, in far too many ways to enumerate. Moreover, I am indebted to all the teachers during the course of my education; in particular, profound thanks go to my physics teacher while at Manchester, England, Mr. Alan G. Dobbins, who instilled in me the love of physics and maths — whose trance will be everlasting.

Last but not least, I should like to express my warm thanks to my colleagues and friends at the department: Ms. Nadia Kosseim, Mr. Christian Semler and my office mates, for the numerous reflections, discussions and exchange of ideas on not only scientific research, but on the state of affairs worldwide.

Contents

Abstract	iv
Résumé	v
Prologue	vii
Table of Contents	ix
List of Figures	xiii
List of Tables	xxvi
Nomenclature	xxvii
1 Preliminary Discourse	1
2 Wood Fibres: Structure and Composition	6
2.1 Morphological Aspects of Wood	6
2.1.1 Wood Structure	7
2.1.2 Fibre Morphology	9
2.1.3 The Physical Nature of Cell Wall Structure	14
2.2 Chemical Constituents of Wood Fibres	20
2.2.1 Cellulose	20
2.2.2 Hemicellulose	22
2.2.3 Lignin	23
2.2.4 Extractives	23
2.2.5 Distribution of Chemical Components in Wood Fibres	23

3	Pulping Processes	26
3.1	What is Pulping?	26
3.2	Chemical Pulping	30
3.3	Mechanical Pulping	31
3.3.1	Characteristics of Refiner Mechanical Pulping	32
3.4	Chemimechanical Pulping	36
4	Fibre Physics	37
4.1	Solid Mechanics of Cell Wall Components	37
4.1.1	Composite Characteristics of Wood fibres	38
4.1.2	Anisotropy of the Fibre Wall	39
4.2	Mechanical Properties of Single Wood Fibres	46
4.2.1	Fibre Strength	47
4.2.2	Fibre Strain Behaviour	49
4.3	Mechanics of Fibrous Structures	51
4.3.1	Molecular Properties of Hydrogen Bonds	52
5	Fatigue of Wood	56
5.1	Fatigue Characterisation in Refining	56
5.2	Fundamentals of Energy Consumption and Mechanical Deformation of Wood	58
5.2.1	Temperature Dependence	60
5.2.2	Frequency Dependence	61
5.2.3	Effects of Loading Mode	62
5.2.4	Effects of Sulphonation	62
5.2.5	Fibre Flexibility	63
6	Scope and Aims of Thesis	65
7	Experimental Methodology	69
7.1	Prelude	69
7.2	Philosophy of Experimental Approach	70
7.3	The Single-Fibre Tensiometer	74

CONTENTS

xi

7.3.1	Loading Jaws	77
7.3.1.1	Shear-Loading Jaws	78
7.3.1.2	Radially-Compressive-Loading Jaws	79
7.3.1.3	Tensile-Loading Jaws	83
7.3.2	Load Cell	87
7.3.3	Stepping Motor	88
7.4	Confocal Laser Scanning Microscopy	89
7.4.1	Fundamentals of Optical Image Formation	89
7.4.2	The CLSM: System Description	91
7.5	Electronic Hardware and Software	94
8	Experimental Results: Discussion and Analysis	99
8.1	General Remarks on Functional and Procedural Considerations	99
8.2	Image Analysis	109
8.3	Morphological Features of Fibres: A Cumulative Fatigue Damage Analysis	115
8.3.1	Crack Formation and Propagation	116
8.3.2	Characteristic Material Degradation Properties	127
8.3.3	Structural Integrity of the Fibre Wall	134
8.4	Micro-mechanisms of Fibre Fatigue-Failure: A Theory	143
9	Rheological Aspects of Papermaking Fibres	150
9.1	Towards a Microscopic Theory of Fibre Development	150
9.2	Practical Implications of Current Findings: A Synopsis	157
10	Conclusions	159
10.1	Concluding Remarks	159
10.2	Proposals for Future Research	162
	Statement of Originality and Contributions to Knowledge	164
	Bibliography	166

CONTENTS

xii

A	Finite-Element Modelling and Analysis	191
A.1	A Brief Overview	191
A.2	Modelling and Analysis	192
B	Calibrations	196
B.1	Photonic Sensor Calibration	196
B.2	Single-Fibre Tensiometer and Stepping Motor Calibration	202
B.2.1	Automatic-Cycling Mode	202
B.2.2	Step-by-step Cycling Mode	207
B.3	Load-Cell Calibration	212
B.4	Vertical Displacement Calibration of the Tensiometer and Support/Stage Set-up	214
C	Illustrations and Schemas	218
D	Fatigue-Testing Algorithm	224
D.1	Program	224
E	Supplementary Results	237

List of Figures

2.1	Schematic representation of a four-year old pine trunk [241].	8
2.2	Different concepts of cell wall layers of a typical fibre or tracheid, showing fibrillar and/or microfibrillar directions: (a) from Wardrop and Bland [284]; (b) from Harada <i>et al.</i> [108]; (c) from Forgacs [79].	11
2.3	A confocal laser scanning micrograph of a wood pulp fibre depicting the helical fibrillar orientation (a), along with a schema of the latter (b), of the S_2 layer of the cell wall.	13
2.4	Cell wall organisation of a typical fibre or tracheid, showing fibrillar and/or microfibrillar textures [283].	15
2.5	A confocal laser scanning micrograph of a <i>pinus banksiana</i> (jack pine) pulp fibre showing pinoid pitting.	16
2.6	Orientation of microfibrils around pits in different layers [108].	17
2.7	Schematic representation of several theories of component structures in fibres (adapted from [233]).	19
2.8	Constituents of wood (adapted from reference [37]).	21
2.9	Cellobiose, the monomer of cellulose.	25
3.1	A schematic representation of the three most common refiner configurations [47].	34
3.2	Typical refiner plate designs illustrating beater bar sections and refining sections (<i>courtesy of Dr. A. Karnis, Paprican, Pointe Claire, Canada</i>).	35

4.1	A model of a sub-microscopic element in a layer of a fibre wall (adapted from reference [273]).	40
4.2	A model of a basic unit cell wall. The unit contains a single rectangular anisotropic filament surrounded by a matrix of thickness, t (adapted from reference [175]).	45
4.3	A wood fibre in its flattened form, defining the principal axes 1, 2, 3 of the S_2 layer and the fibre axes X, Y, Z (single-layer model concept after [70]).	48
4.4	A schematic representation of the tension buckling phenomenon. Left, spirally-wound tube which, according to theory, buckles under axial strain to the form indicated on the right (adapted from reference [214]).	50
4.5	The direction of coupled shear stress in a fibre of high fibril angle, due to tensile strain (adapted from reference [212]).	51
4.6	Three distinct length scales in which materials may be considered. . .	53
4.7	A structural model of repeating unit cells of natural cellulose (adapted from reference [123]).	55
5.1	A schema illustrating an impression of fibres trapped between the passing stator and rotor bars of a disc refiner. The stresses that the fibres experience under these conditions are responsible for the cumulative fatigue damage phenomenon.	57
5.2	A diagrammatic depiction of the energy supplied to a sample of wood in cyclic compression, and the energy absorbed in one cyclic compression (adapted from reference [247]).	59
7.1	Testing system block diagram.	72
7.2	Strain distribution of a two-layered wood fibre subjected to uniform tangential displacement (5% of the fibre length), and has a fibril angle of 20° . The picture shows one-quarter of the fibre owing to geometrical symmetry of the structure (for further details, refer to Appendix A). .	73
7.3	A schematic diagram of the single-fibre tensiometer used for fatigue-testing wood pulp fibres.	75

- 7.4 A photograph showing the single fibre tensiometer residing in the support/stage mechanism, specifically designed to allow movement in the horizontal plane, and vertically, accurate to 1 μm using a sensitive micrometer screw-head. 76
- 7.5 A schema of the loading jaws used for fatigue-testing fibres under uniform, cyclic shear: (a) a three-dimensional representation of the jaws; (b) a two-dimensional profile. 80
- 7.6 A photographic depiction of the shear-loading jaws residing in the jackets. 81
- 7.7 A schema of the loading jaws used for testing fibres under cyclic radial compression. 82
- 7.8 A photographic illustration of the radially-compressive-loading jaws set-up. 84
- 7.9 A schematic diagram of the tensile-loading jaws. 85
- 7.10 A photographic representation of the tensile-loading jaws, *in situ*. . . 86
- 7.11 Schematic arrangement of a reflection mode scanning optical microscope (adapted, however with slight modifications, from reference [286]). 92
- 7.12 The origin of depth discrimination or optical sectioning property of confocal optical systems (adapted from reference [286]). 92
- 7.13 The optical arrangement of various forms of scanning optical microscopes. (a) A form of conventional scanning microscope. (b) Conventional microscope. (After reference [286].) 93
- 7.14 The Leitz FLUOVERT-FS CLSM assembly. 95
- 7.15 Complete experimental set-up for fatigue-testing of single wood pulp fibres. 97
- 8.1 Schematic representation of the fibre posturing as the applicator prods, to and fro, along the fibre specimen during shear-mode testing. 101
- 8.2 Fluorescence confocal micrographs of the clamped end of fibres mounted in the fixation mechanism (after the completion of testing): (a) shear-mode testing; (b) radial compression; and (c) tension. 102
- 8.3 Schematic illustration of fibre deflection under radial compression testing. 105

- 8.4 Graphical depiction of the applicator movement and fibre deflection, as incorporated in the fatigue-testing algorithm. 105
- 8.5 Diagrammatic representation of the relationship between fibre extension and the amplitude of cycling in tensile-mode fatigue-testing. . . . 106
- 8.6 Schematic illustration of surface and cross-sectional image scanning in a Leitz CLSM system. 111
- 8.7 Light refraction in media of identical and different refractive indices to expound effects of mounting media on the spherical aberration of confocal images, when using oil-based objective lenses: (a) When passing through a mounting medium of low refractive index, rays from the periphery of the objective lens converge to a focal point different from the one formed by rays closer to the optical axis, thus inducing spherical aberration. (b) However, if the refractive indices of both, the immersion oil and mounting medium, are the same, rays from all parts of the lens are focussed on the same focal plane. (N.B. In both cases, the thickness of the covering glass is assumed to be very small, hence causing no change in the path of the rays.) 114
- 8.8 Fluorescence confocal micrographs of a jack pine (*Pinus banksiana*) subjected to 1050 cycles in shear (sample #2 in Table 8.1) depicting: (a) dominant longitudinal macrocrack; (b) occurrence of transversely-oriented macrocracks; and (c) geometrical orientations of the macrocracks peculiar to this species type. 117
- 8.9 Propagation of a dominant longitudinal macrocrack in a loblolly pine subjected to 1200 cycles in shear at 0.0262 Hz (refining energy = 6.4 GJ/t; CTMP). 119
- 8.10 A fluorescent confocal micrograph depicting the crack propagation at an early stage of the sample fatigue life. The sample is: jack pine RMP (washed); refined at 4.4 GJ/t and experienced 350 cycles in shear at 0.0262 Hz. 119

8.11 (a) Mature macrocracks as well as evidence of cracks taking the shape of bordered pits (regions of high stress concentration) in a jack pine RMP (6.5 GJ/t) which experienced 1750 cycles in shear at 0.0262 Hz. Clearly illustrated in the micrograph as well, is the phenomenon of peeling-off of parts of the external layer of the cell wall material. (b) Slow crack growth leading to the opening of the macrocracks as the number of cycles is increased by about 20% (i.e., to 2100 cycles) for a pulp fibre of identical properties as that in (a). 121

8.12 Fluorescence confocal micrographs of a jack pine pulp fibre (RMP, refining energy = 6.5 GJ/t) subjected to radial compression, 3400 cycles at 0.187 Hz: (a) Depicts the apparent volumetric expansion resulting from internal fibrillation in the fibre cell wall. Also shown is the propagation of a dominant longitudinal crack. (b) The crack from (a) continues until it is sharply deflected owing to natural bias. Another macrocrack (the upper of the two shown) is formed in this region of high stress concentration which also propagates longitudinally. 123

8.13 Fluorescence confocal micrographs depicting developed longitudinal macrocracks in pulp fibres subjected to cyclic radial compression, for two cases: (a) jack pine RMP (8.5 GJ/t) subjected to 5000 cycles at 0.187 Hz; and (b) black spruce RMP (8.5 GJ/t) subjected to 5400 cycles at 0.187 Hz. Also shown here is the volumetric expansion of the filamentary composite fibre. 124

8.14 Inchoative crack formation in a loblolly pine fibre (CTMP, 6.4 GJ/t) cycled 6500 times in tension at 0.187 Hz. 126

8.15 The prominent partial delamination of the external wall layers, while leaving parts still attached to the fibre body, is a consequence of the cycle-dependent damage accumulation in the fibre cell wall which translates into destabilising the framework-matrix interaction of each layer of the laminated composite tube—externally first, then, successively inwards. A concomitant consequence of material degradation and immanent structural changes is the occurrence of fibrillation in the external (as well as internal) cell wall layers. These morphologies are illustrated in the fluorescence, confocal micrographs of: (a) jack pine pulp fibre (RMP, 6.5 GJ/t) subjected to 1050 cycles in shear at 0.0262 Hz; and (b) a fibre similar to (a), however subjected to 2100 cycles. . 129

8.16 A significant consequence of the internal fibrillation of, and the maturation of macrocracks in, the fibre cell wall material is the occurrence of volumetric expansion: (a) Developed macrocracks in the external layer of the cell wall—which are, in this case, oriented along the helical micrographs of the S_2 layer—allow a faster rate of cell wall breakdown owing to the resulting structural instability of the framework-matrix interaction. (Fibre sample: jack pine RMP, refined at 6.5 GJ/t, subjected to 2100 cycles in shear at 0.0262 Hz.) (b) The loosening of the structure of the laminated composite fibre resulting from random degradation of the inter-fibrillar matrix, induce the complete separation of whole chunks of cell wall material. (Fibre sample: jack pine RMP, refined at 6.5 GJ/t, subjected to 1050 cycles in shear at 0.0262 Hz.) 130

8.17 Fluorescence, confocal micrographs of a wood pulp fibre (jack pine, RMP, refined 6.5 GJ/t) subjected to 3400 cycles in radial compression (at 0.187 Hz) illustrating the characteristic material degradation phenomena due to the cumulative damage after a large-enough number of cycles: (a) developed, longitudinal macrocracks contributing to the general weakening of the framework-matrix interaction symbolised by the partial delamination and extensive internal fibrillation of the cell wall material, which also results in the local volumetric expansion of the fibre; and (b) the unravelling (peeling-off) of parts of the external layer material while leaving the remainder of the layer still attached to the fibre body. 132

8.18 Pulp fibres tested under cyclic tensile stroke only show insignificant degree of damage accumulation represented by partial delamination, and weak external fibrillation, of the external layer of the cell wall. This fluorescence confocal micrograph is of a loblolly pine (CTMP, refined at 6.4 GJ/t) cycled 6500 times at 0.187 Hz. 133

8.19 Fluorescence confocal micrographs of fibre cross-sections, 30 μm apart, indicating global structural integrity of the cell wall at incipient levels of fatigue damage accumulation — 350 cycles in shear. (Cf. the surface morphology of the same fibre shown in Figure 8.10.) 135

8.20 Cross-sectional fluorescence confocal images, 30 μm apart, of a loblolly pine CTMP (refined at 6.4 GJ/t) subjected to 1200 cycles in shear at 0.0262 Hz. Moderate structural collapse of the fibre cell wall is noticed, characteristic material degradation of the surface morphology notwithstanding. 136

- 8.21 In contrast to the above figure, a higher-refining-energy pulp fibre (8.7 GJ/t, jack pine RMP) cycled to the same number of cycles in shear exhibits more degradation of the fibre cell wall material characterised by more pronounced inter-laminar separation and cell wall collapse. Clearly evident, too, is the presence of slip planes and micro-compressions in the cell wall, and partial delamination of the external layer of the laminated composite tube. 136
- 8.22 Material damage accumulation in pulp fibres, after a certain fatigue life limit (around 1200 cycles), seems to be solely dictated by the number of cycles to which the fibre is subjected; moreover, damage rapidly cumulates as cycling exceeds this level. The above cross-sectional confocal micrographs are of two different fibres: (a)–(c) belong to a jack pine RMP, refined at 6.5 GJ/t and cycled to 1750 in shear at 0.0262 Hz; whereas (d)–(e) refer to a fibre only different from the above in that it is cycled to 2100 times in shear. The micrographs attest to the developed stage of the material chemical degradation, and subsequent loss of structural integrity, of the cell wall. (All optical cross-sections are obtained 30 μm apart.) 138
- 8.23 The cell wall structural integrity of fibres subjected to cyclic radial compression testing is hardly affected since the material damage accumulation occurs at an insignificant rate to cause the collapse of the inter-fibrillar matrix. The above confocal micrographs illustrate the cross-sections, 30 μm apart, of a motley combination of pulp fibres: (a)–(b) refer to loblolly pine CTMP, refined at 6.4 GJ/t, cycled 350 times at 0.187 Hz; (c)–(d) to jack pine RMP, refined at 6.5 GJ/t, cycled 600 times at 0.187 Hz; (e)–(f) to jack pine RMP, refined at 6.5 GJ/t, cycled 2700 times at 0.187 Hz; and (g)–(h) to black spruce RMP, refined at 6.5 GJ/t, cycled 5400 times at 0.187 Hz. 139

- 8.24 The localised material degradation in the external layers of pulp fibres subjected to cyclic tensile stroke becomes effaced as we traverse the cell wall cross-section: A trend strikingly similar to cyclic radial compression. The above confocal micrographs depict cross-sections, 30 μm apart, of fibres whose characteristics are as follows: (a)–(b) refer to black spruce RMP, refined at 4.3 GJ/t, subjected to 6000 cycles in tension at 0.187 Hz; and (c)–(d) to jack pine RMP, refined at 8.7 GJ/t, subjected to 6000 cycles in tension at 0.187 Hz (extractives, in this case, are removed from the cell wall). 141
- 8.25 Intact fibres of whatever species exhibit natural non-uniformity in cross-section owing to differing rates of cell wall development. Confocal micrographs show cross-sections, 30 μm apart, of: (a)–(b) intact black spruce RMP, refined at 8.5 GJ/t; and (c)–(d) intact jack pine RMP, refined at 8.7 GJ/t (whose extractives have been removed). . . 142
- 8.26 Fluorescence confocal micrographs illustrating the cumulative build up of plastic deformation as microcracks propagate along the cell wall layer. The gradual formation of developed macrocracks in any one layer ultimately leads to the slippage of layers, or what may be termed as *tearing action*—clearly depicted in (d). (Fibre sample: Jack pine RMP, refined at 6.5 GJ/t, subjected to 1200 cycles of shear displacement at 0.0262 Hz.) 145
- 8.27 Schematic representation of the model describing inchoate fatigue crack growth in pulp fibres (subjected to cyclic shear, radial compression or tension) under the influence of shear stress. 147
- 8.28 A schema of the stress distribution with developed longitudinal crack growth. 148
- 8.29 Supportive evidence of the proposed stress-distribution hypothesis shown in Figure 8.28. Depicted above are fluorescence confocal images of: (a) jack pine RMP, refined at 8.7 GJ/t, subjected to 1200 cycles in shear at 0.0262 Hz; (b) black spruce RMP, refined at 8.5 GJ/t, also cycled 1200 times in shear. 149

9.1	A schematic representation of the chip reduction process and stages to produce a papermaking pulp (adapted from reference [131]).	152
9.2	Scanning electron micrographs of a pulp refined at 7.0 GJ/t depicting: (a) the partial removal of P and S_1 layers (mag. 2500x); and (b) exposure and disruption of the S_2 layer (mag. 1000x). (<i>Courtesy of Dr. A. Karnis, PAPRICAN, Pointe Claire, Canada.</i>)	153
9.3	A schema illustrating the mechanism of fibre development, that is characterised by: (i) the fibre separation stage, in which the chips are reduced to shives and long intact fibres; and (ii) the peeling-off stage, where parts of the fibre cell wall material are eventually removed to form short fibres and fines. (Adapted with modification from reference [131].)	155
A.1	Schematics of the three-dimensional, finite-element model of a single pulp fibre, along with the boundary conditions for the application of a uniform tangential displacement.	194
A.2	Geometric model and finite-element mesh used for analysing the two-layered pulp fibre model.	195
A.3	Strain distribution for a pulp fibre with 30° fibril angle.	195
B.1	Schematic of a photonic sensor.	197
B.2	Output characteristics of the photonic sensor.	198
B.3	Deflection of a cantilever beam.	199
B.4	Photonic sensor calibration curve.	200
B.5	Automatic-mode calibration program.	203
B.6	Displacement versus wait-time plot for step rate=3 (automatic mode).	206
B.7	Step-by-step mode calibration program.	208
B.8	Displacement versus number of steps plots, step rate=3 (step-by-step mode).	211
B.9	Load cell calibration under static load.	213
B.10	Pictorial representation of the vertical displacement calibration of the tensiometer-support set-up.	214

B.11	Plots of vertical displacement calibration of the tensiometer-support set-up.	216
C.1	Photographic depiction of the interior of the μ mac-5000 microcomputer.	219
C.2	Block diagram of the μ mac-5000 microcomputer.	220
C.3	Schematic representation of the motor driver.	221
C.4	A schema of the 2x amplifier.	223
E.1	The underlying themes typifying fatigue cumulative damage are chemical degradation and structural breakdown of the cell wall material. The latter are evinced by particular phenomena, e.g., the propagation of cracks, inter-laminar separation, and partial peeling-off, of the cell wall material — travelling successively inwards. (a) Shows a pulp fibre sample: Jack pine RMP, refined at 4.4 GJ/t whose extractives are removed, subjected to 350 cycles in shear at 0.0262 Hz. (b) Similar to (a) except that the extractives are <i>not</i> removed, and the fibre is cycled 1200 times.	238
E.2	The above micrographs depict the typical material property degradation phenomena characterising damage accumulation due to cyclic-shear loading: A myriad of microcracks combine to form a dominant macrocrack spanning the length of the fibre. Regions of high stress concentration, such as bordered pits, force the cracks to re-orient themselves around these regions of natural bias. Moreover, intensive material degradation cumulates with cycling causing the eventual peeling-off of parts of the external cell wall layers (a). Concomitantly, the cell wall also undergoes extensive external fibrillation (b), as well as internal fibrillation; the latter being evinced by the apparent volumetric expansion of the cell wall layers (c). It should be noted that the transverse cracks are responsible for one mode of failure, as explained <i>in extenso</i> in Chapter 8. (Tested sample is: Jack pine RMP, refined at 6.5 GJ/t, subjected to 1050 cycles in shear at 0.0262 Hz.)	239

- E.3 Owing to the continued chemical degradation and structural breakdown — which traverses across the fibre width, the structural integrity of the laminated composite fibre is successively compromised as evinced by the clear cell wall collapse, and inter-laminar delamination as well. Cross-sectional micrographs (a)–(d), which are 30 μm apart, are of black spruce RMP, refined at 8.5 GJ/t, and subjected to 1200 cycles in shear at 0.0262 Hz. Whilst these shown in (e)–(g) are of jack pine RMP, refined at 6.5 GJ/t, and cycled 1750 times in shear. 240
- E.4 The propagation of developed cracks in the manner illustrated in the above micrograph, provides further support to theory proposed for the micro-mechanisms of fibre fatigue-failure (see section 8.4, Chapter 8): Essentially, the crack initiates at the surface and propagates longitudinally until deflected by the presence of natural bias. The shown photomicrograph is of jack pine RMP, refined at 6.5 GJ/t, subjected to 1050 cycles in shear. 241
- E.5 Although, under radial compression testing, a much larger number of cycles is required to effectively cause the material degradation and structural breakdown, in the fibre cell wall material, the overall mechanisms of failure and material property degradation phenomena are principally the same as for shear-testing. Shown above are such characteristics of: (a) jack pine RMP, refined at 6.5 GJ/t, subjected to 3400 cycles at 0.187 Hz; (b) black spruce RMP, refined at 8.5 GJ/t, subjected to 5400 cycles. 242
- E.6 The cell wall collapse, due to radial compression testing, is by far less than that due to shear-testing since the extent of damage accumulation is less pronounced here. Cross-sectional images (a)–(b), 30 μm apart, are of jack pine RMP, refined at 6.5 GJ/t, and subjected to 3400 cycles at 0.187 Hz. 243

- E.7 In the micrograph shown here, a pulp fibre was forced to rupture by driving the steel-alloy wire, housed in the applicator, through it. As clearly evidenced, the rupture is oriented along the dominant cracks which indicates the pre-eminence of the latter. This particular fibre is jack pine RMP, refined at 6.5 GJ/t, and radially compressed 2700 times at a frequency of 0.187 Hz. 244
- E.8 Cyclic tension stroke is the least effective mode at which material degradation could occur, even as the number of cycles exceeds 6000 — i.e. three-fold the maximum experienced under shear testing. Hence, very insignificant degradation phenomena and structural collapse would be expected: Micrograph (a) shows external fibrillation in the external layer of the fibre cell wall; whilst (b)–(c) depict two cross-sectional micrographs, 30 μm apart, of the above region. The tested fibre is: jack pine RMP, refined at 8.5 GJ/t, cycled 6100 times at 0.187 Hz. . . . 245

List of Tables

2.1	Calculated distribution of the components in the cell wall layers of spruce tracheids (adapted from reference [77]).	25
3.1	Survey of pulping processes (adapted from reference [77]).	27
4.1	Calculated elastic constants for a collapsed pulp fibre assumed to only have an S_2 layer versus a typical three-layered fibre (adapted from reference [179]).	43
8.1	Specifications concerning wood-pulp fibre samples used in shear-loading mode fatigue-testing. (The author acknowledges Dr. A. Karnis, Mechanical Pulping Division, PAPRICAN, Pointe Claire, for supplying all the pulp samples.)	104
8.2	Specifications concerning wood-pulp fibre samples used in radial-compression fatigue-testing.	107
8.3	Specifications concerning wood-pulp fibre samples used in tensile-mode fatigue-testing.	108
B.1	Calibration data of photonic sensor.	201
B.2	Stepping motor calibration — automatic mode.	204
B.3	Stepping motor calibration — automatic mode (Cont'd.).	205
B.4	Stepping Motor Calibration — step-by-step mode (step rate=3) [1 st run].	209
B.5	Stepping Motor Calibration — step-by-step mode (step rate=3) [2 nd run].	210
B.6	Calibration of the ± 1 -lb load cell.	213
B.7	Data for the vertical displacement of the tensiometer-support set-up.	217

Nomenclature

S_1	Outer layer of the secondary wall of a softwood fibre.
S_2	Middle layer of the secondary wall of a softwood fibre.
S_3	Inner layer of the secondary wall of a softwood fibre.
P	Primary wall of a softwood fibre.
ML or I	Inter-cellular substance, referred to as the Middle lamella, which bonds adjacent fibres together.
θ	Fibril angle, i.e., the angle the helix of the S_2 layer makes with the fibre axis.
S_{12}	Intermediate laminae between those of the S_1 and S_2 layers.
S_{23}	Intermediate laminae between those of the S_2 and S_3 layers.
T	Tertiary wall of a softwood fibre (refer to Figure 2.2).
RMP	Refiner mechanical pulp.
PRMP	Pressurised refiner mechanical pulp.
TMP	Thermo-mechanical pulp.
CTMP	Chemi-thermomechanical pulp.
α	Angle difference between filament alignment and the axial direction of the fibre (in the model of sub-microscopic element in a layer of a fibre wall).
E_L, E_T	Moduli of elasticity of a cell wall lamina parallel and perpendicular to the mean fibrillar direction of the lamina, respectively.
G_{LT}	Shear modulus of rigidity of a cell wall lamina in the plane of the lamina.
ν_{LT}	Poisson's ratio for cell wall lamina, giving ratios for contraction in the direction indicated by the 2 nd subscript to extension under stress in the direction indicated by the 1 st subscript.
ϵ_{LT}	In-plane shear strain of a cell wall lamina.
E	Young's modulus of elasticity.
I	Area moment of inertia.
CLSM	Confocal laser scanning microscope.
SEM	Scanning electron microscope.
Ω	Optimal rate of operation of stepping motor.
δ	Total to-and-fro movement of applicator.

- f Frequency of fatigue-testing = $f(\Omega, \delta)$.
- x_{min} Minimum, precise, permissible displacement the stepping motor delivers.
- y Deflection at the fibre centre (which equals the amplitude of cycling in the case of radial compression testing).
- l_{av} Average fibre length.
- A Amplitude (in the case of tension testing).
- x Fibre extension (under tension testing).

Chapter 1

Preliminary Discourse

Paper, traditionally defined as a felted sheet of fibres formed on a fine screen from a water suspension [75], was first invented by T'sai Lun in China as early as 100 A.D. using a suspension of bamboo, rags, bark of tree or mulberry fibres. The Chinese subsequently developed papermaking into a highly skilled art, and many beautiful examples of ancient illustrations on paper are still in existence.¹ Several centuries thereafter, the art of papermaking reached the Middle East, at which period the cultural advances of the Arab-Islamic civilisation provided the material basis for its development. Owing to Europe's proximity to the then centre of the world, it also became cognisant of this art.

The art of making paper also arose independently in Mesoamerica sometime before 660 A.D. As with their counterparts in the Orient, Maya, Toltec, Aztec and Zapotec papermakers utilised the bark fibres of trees of the Moraceae family. They devised their own techniques of fibre separation, washing, beating, felting, couching, sizing, drying, hot pressing, coating and converting.² By the beginning of the 15th century, a number of paper mills existed in Spain, Italy, Germany and France; whilst the first paper mill in North America was established in 1690 [256]. Today manual labour has given way to colossal paper machines, and wood has replaced rags as the chief raw material.

¹For example, the British Museum Library, London, England.

²This portion is excerpted from reference [176], Introduction.

Within the context of a humanistic, universal view of *paper* and *civilisation*, the role of the “humanity” of paper is most aptly enunciated by Mark [176] in “its influence on civilisation as its geographical and cultural distribution has widened; the increasing diversity in its use; and its central role in providing a convenient vehicle for acquisition, storage, and dissemination of both tangible goods (as in packaging), and these same functions applied to intangible areas, such as communication and their infinitely diverse applications of human knowledge.”

Let us now turn our attention to examining technical aspects pertinent to modern papermaking. Wood, the most abundant source of papermaking fibres, is virtually the only source utilised in North America, hence the emphasis on wood as the raw material for pulping. Softwood³ tracheids generally comprise over 90% of the volumetric composition of coniferous woods, while tracheid wall substance accounts for over 95% of the weight of such woods [172]. Tracheids which are hollow tubes, the inner cavity being called the lumen, are members of that large category of materials called “natural fibres”. The cell wall structure is essentially comprised of an outer primary wall and a three-layered secondary wall, with each layer having a characteristic orientation of cellulosic fibrils; adjacent tracheids are separated by a layer called the middle lamella. The manufacture of paper essentially takes place in two stages: The production of pulp from wood and the making of paper from pulp — the latter fibrous raw material is usually of vegetable origin, but animal, mineral or synthetic fibres may be used for special applications. The wood may be pulped chemically, mechanically, thermally or by a combination thereof. However, owing to the relatively high strength of the pulp and the usage of secondary wood products, refiner mechanical pulping has been gaining burgeoning popularity in recent decades: thus, the prime motivation for our study.

The study of wood fibres, in general, shares a common meeting ground amongst broad disciplines: physical, chemical and biological, pure and applied, sciences. A broad background of the botanical and chemical nature, as well as a thorough comprehension of the structure and physical properties of fibres, are required before we

³Softwoods are the tree species predominantly used for the production of pulp in Canada — refer to Chapter 2.

can delve into achieving our real objective: The determination and characterisation of fatigue-failure mechanisms and morphological behaviour of wood pulp fibres subjected to cyclic mechanical action. Why be concerned with fatigue of pulp fibres in the first place?

In refining, the heart of mechanical pulping, wood chips are mechanically defibred to a pulp appropriate for papermaking, whereby a suitable amount of mechanical flexing of the fibres takes place. This process is a highly specialised attrition process whose object is to separate fibres while retaining their integrity, through subjecting the wood chips to cyclic deformation, and to induce flexibility and fibrillation into these fibres. By elucidating the mechanisms of damage accumulation — that is, crack formation and characteristic material property degradation phenomena —, their extent and the morphology of fatigued fibres, one will be in a position to fathom and explicate the structural changes occurring in pulp fibres during the process of mechanical treatment: It is vitally important to gain a deeper understanding of the way single fibres respond to synthesised cyclic mechanical action, under conditions emulating the force-actions imparted on pulp fibres between the discs of mechanical refiners, so as to ultimately assess the conditions responsible for producing “good” papermaking fibres and, in retrospect, be able to modify current refiner furnishes in order to conform with the sought-after results.

It should further be noted that our concern chiefly centres on the hitherto uninaugurated fatigue-testing of *single* pulp fibres, rather than assemblies thereof: At this stage, it is deemed of import to painstakingly identify the phenomena as well as the fundamental material property degradation characteristics of single pulp fibres in order to pave the road for future considerations — such as, the quantification of these characteristics and the inclusion of fibre-fibre interfacial effects on the structural behaviour of the fibrous network. To attain the goal enunciated hereinbefore, we are required to elucidate the mechanisms of fibre failure under conditions emulating mechanical refiners. The approach undertaken essentially involves an in-depth (microscopical) experimental investigation; and three-dimensional, finite-element modelling and analysis of a single pulp fibre is summarily carried out to qualitatively validate specific trends engendered from the experimental results. The body of the thesis is

structured along themes pithily described below.

- A comprehensive review, along with an in-depth analysis, of the literature are proffered in accord with the following formation:

Chapter 2 discusses the physical structure and chemical composition of wood fibres.

Chapter 3 presents an overview of the principles behind the various pulping processes with particular emphasis on mechanical pulping.

Chapter 4 canvasses, *in extenso*, the mechanical behaviour of wood pulp fibres with a coverage of the basis for modelling wood tracheids for the purposes of performing quantitative studies, such as the determination of elastic constants of the cell wall components.

Chapter 5 provides an insight into the few macroscopic studies performed to characterise the fatigue behaviour and energy consumption in the mechanical deformation of wood.

- Thenceforward, the realm of the current research is profusely dealt with as follows:

Chapter 6 clearly pronounces the scope and purpose of the thesis.

Chapter 7 definitively details, with an artist's care, the mechanisms, apparatuses and overall methodology of the novel experimental technique developed for the purposes of performing fatigue-testing of single pulp fibres.

Chapter 8 begins by expressing the underlying functional and procedural considerations in performing the experiment as well as image analysis. Thenceforth, canvassed at length are the findings of this research; along with the proposed theory for the micro-mechanisms of fatigue-failure in pulp fibres.

Chapter 9 describes how the outcome of the current research is used to further advance the theory of fibre development — specific to the arena of

mechanical pulping, which refers to changes occurring in the fibre properties during refining. A synoptic treatment of the practical implications of the material property degradation phenomena is subsequently given.

Chapter 10 concludes the thesis with particular emphasis on the last three chapters in relation to the scope and aims of this research; and further sheds some light on proposals for future research.

- The claim to contributing and advancing the cause of science and technology is enunciated in the **Statement of Originality and Contributions to Knowledge**.
- Finally, the thesis includes five appendices which are, in turn, organised in the following manner:

Appendix A contains a summary of the three-dimensional, finite-element modelling and analysis, whose results confirm the general trend of highly localised strain regions recognised throughout the experimental results.

Appendix B explains, in detail, the modality in which the apparatuses were calibrated, and presents the outcome of a series of performed calibrations.

Appendix C contains illustrations and schemas of the interior of the $\mu\text{mac-5000}$ and the motor driver.

Appendix D lists the fatigue-testing algorithm used in the control and operation of the entire experimental set-up.

Appendix E provides supplementary micrographical evidence of the results dealt with in Chapter 8.

Chapter 2

Wood Fibres: Structure and Composition

2.1 Morphological Aspects of Wood

Wood is the most abundant source of papermaking and is virtually the only source utilised in North America, though straw, seed and bamboo are the dominant raw materials in some other regions of the world. Botanically, woods are classified into two main groups: softwoods, or *gymnosperms*, and hardwoods, or *angiosperms* [125]. The former group constitutes the most predominant tree species used for the production of pulp in Canada. However, in localised areas where the supply of coniferous trees has been depleted, hardwoods have been receiving burgeoning use, particularly poplar as the primary source of wood.

Significant variations in wood structure, fibre structure and chemical composition exist within the two groups of trees. Concomitantly, the selection of the source of wood is important with respect to pulping and papermaking. Softwoods are composed almost entirely of large, tapering cells called *tracheids*; hardwoods of relatively long fibres of narrow diameter, as well as much shorter, wider cells called *vessels*. Because of these unique characteristics, softwoods are more suitable for pulping especially in the case of mechanical pulping, in which almost all the fine material of wood remains. Hence, in subsequent parts of this thesis, the discussion will solely focus

on the structure and chemistry of softwoods. Nonetheless, the general concepts and developments set forth in the course of our research are fundamentally applicable to hardwoods.

2.1.1 Wood Structure

Wood is the principal source of cellulosic fibres for pulp and paper manufacture. It provides about 93% of the world's virgin fibre requirement, while the other sources contribute the remainder [256]. Trees have three basic structural components: the crown, roots and trunk; each one having a specific purpose. The crown is composed of the leaves and small branches at the uppermost part of the tree. This is where the photosynthesis occurs, enabling the tree to grow. The roots, as well as anchoring the tree firmly to the ground, serve as the transport system for the mineral nutrients and water from the soil. The trunk provides structural support for the crown, storage for food, and conduit for photosynthesised food downwards and water and nutrients upwards. The trunk is the main source of wood and fibre in the pulp and paper industry. However, whole tree pulping in which the crown and the roots are used in addition to the trunk, is occasionally found in the Pulp and Paper Industry [72, 73, 222].

A typical cross-section of a softwood trunk is illustrated in Figure 2.1. The three basic components are: the cambium, xylem and phloem. The cambium is a thin layer located between the phloem, or the inner bark, and the xylem, or wood. The growth of wood cells occurs within this layer. The rate of growth is dependent upon the season. In springtime, the growth is rapid and the wood cells produced have thin walls and large inner cavities, or lumens. However, when growth occurs more slowly, as during summertime, the cells formed have thick walls and small lumens. Wood fibres so formed are called earlywood (or springwood) and latewood (or summerwood), respectively.

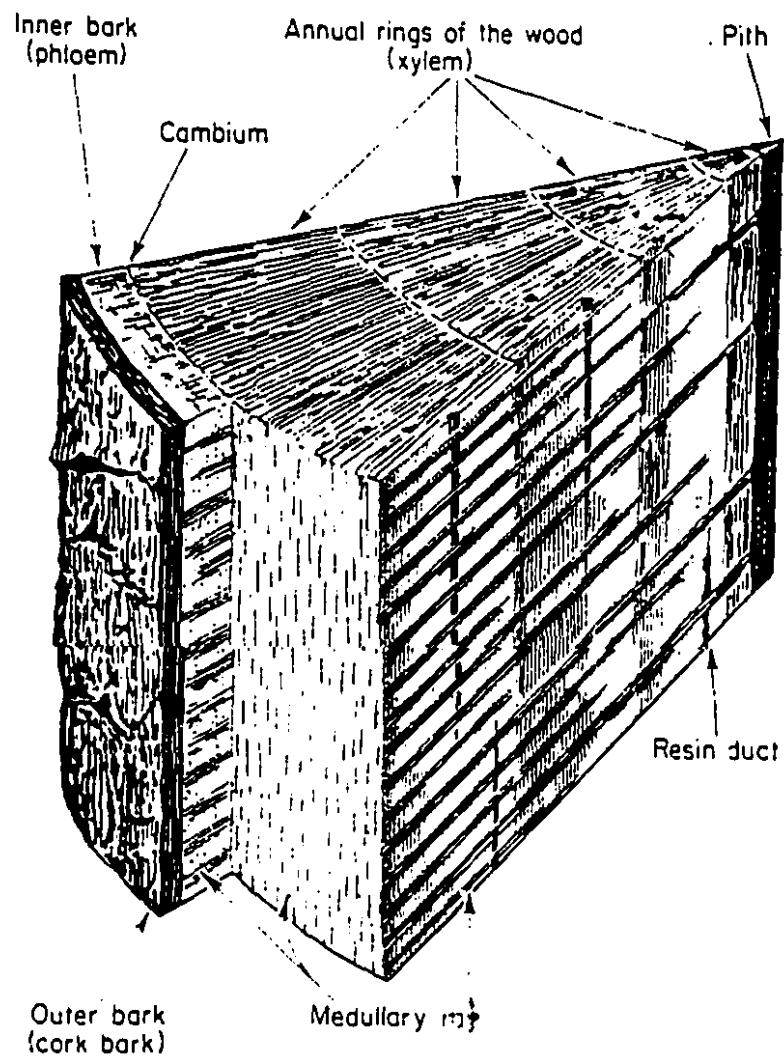


Figure 2.1: Schematic representation of a four-year old pine trunk [241].

2.1.2 Fibre Morphology

In softwoods, the two main types of cells are the *tracheids* and the *parenchyma cells*. Tracheids form the major bulk of softwoods, about 95% by volume [241, 77] and, hence, are the most important source of papermaking fibres. They are 3–5 mm in length and 25–50 μm in diameter [77], and are oriented longitudinally in the tree. The only living tracheid cells are those located alongside the cambium. The bulk of the xylem is therefore composed of dead tracheids which act as structural units and allow for the transport of fluids by means of the lumen and the inter-connecting pits. Parenchyma cells, on the other hand, are generally shorter and thinner than tracheids and are located throughout the xylem. They serve for food storage and for transport of fluids. One type of parenchyma cells in particular, the ray cell, is a ribbon-like aggregate which transports fluids to and from the cambium and inner bark.

In a native cellulosic fibre, the number of long-chain cellulose molecules which pass through a given cross-section is approximately one or two thousand million [86, 89]. The fibrils observed with light microscopes have actually been revealed to be aggregations of finer filamentous units called *microfibrils*. Some authors considered these microfibrils the basic supermolecular structural units in plant cell walls [59, 225, 226], whereas others presented evidence that the microfibrils were, in turn, composed of finer (ca. 35Å x 35Å or smaller) 'elementary microfibrils' [89, 194, 199]. The principal, if not exclusive, constituent of microfibrils and/or elementary fibrils is *cellulose*. The orientation of cellulosic chains has been shown to be the same as that of the fibrils [172]. The definition and functional description of microfibrils, which form the skeleton of the cell wall are quite complex. A compendious review is presented hereunder.

Fibrillar and subfibrillar organisation varies considerably between organisms, but most structural plant cell walls contain a thin primary wall and a thick concentrically-layered secondary wall. The living cells lay down the primary wall first. This wall is usually composed of a matrix of pectic materials plus polyuronides and other hemicelluloses strengthened by a loose network of cellulosic microfibrils. Mühlethaler [193] aptly described the dispersed microfibrillar texture of the primary wall as deposited

“in fabric-like manner”. The secondary wall layers formed subsequently as the cell matures have a much more parallel arrangement of microfibrils.

The cell wall structure of a typical unbeaten softwood tracheid is shown schematically in Figure 2.2. The lignified cell wall of a tracheid, which is a hollow tube whose inner cavity is called the lumen, possesses — as alluded to hereinbefore — a very thin primary, cambial wall, P, whose thickness averages $0.1 \mu\text{m}$ [9]. Wardrop [282] has shown that the fibrils on the inner side of P tend to have a much more transverse orientation with respect to the cell than those on the outside. In any case, the cellulosic fibrils seem to be rather tenuously arranged. Further inside the primary wall are found: the thin outer layer, S_1 ($0.08\text{--}0.2 \mu\text{m}$ thick), broad central layer, S_2 ($1\text{--}10 \mu\text{m}$ thick) and thin layer, S_3 ($0.1 \mu\text{m}$ thick) of the secondary wall [71, 141]. The orientation of the fibrils is different in each layer: the S_1 is made up of a cross-fibrillar network, the S_3 has a transverse orientation; and both layers having the fibrils oriented at large angles to the long axis of the cell (i.e. the fibre axis). Whereas the S_2 layer, where the main bulk of the fibre (90% of the fibre mass) is located, is characterised by helically-oriented fibrils which are more longitudinally directed than in the S_1 or S_3 [172]. The angle the helix makes with the fibre axis is termed the ‘fibril angle’, which is approximately constant throughout the length of a single fibre [70, 142, 204, 210, 212, 214, 215, 216].

It is worthwhile noting that within a given layer, most of the microfibrils wind helically in a predominant S or Z sense and are continuous, passing over the end of the tracheid and back into the helical pattern. There is always a minority of microfibrils interweaving with those following the principal helical orientation [39]. (The reader’s attention is directed to Figure 2.3.) Moreover, the S_2 layer, being the densest, contains a large number of laminae, and although the helical inclination is not precisely the same in each lamina — only approximately so —, neither is there any evidence for the reversal of the sense of the predominant helix [82]. The usual sense of the S_2 helix in conifers seems to be right-handed, or Z [30]; however, exceptions do exist [82]. Adjacent tracheids are bonded together by inter-cellular substance consisting principally of pectopolyuronides and lignin in the middle lamella, ML, between cells [68, 77, 237]. Lignin and other non-cellulosic substances are also interspersed

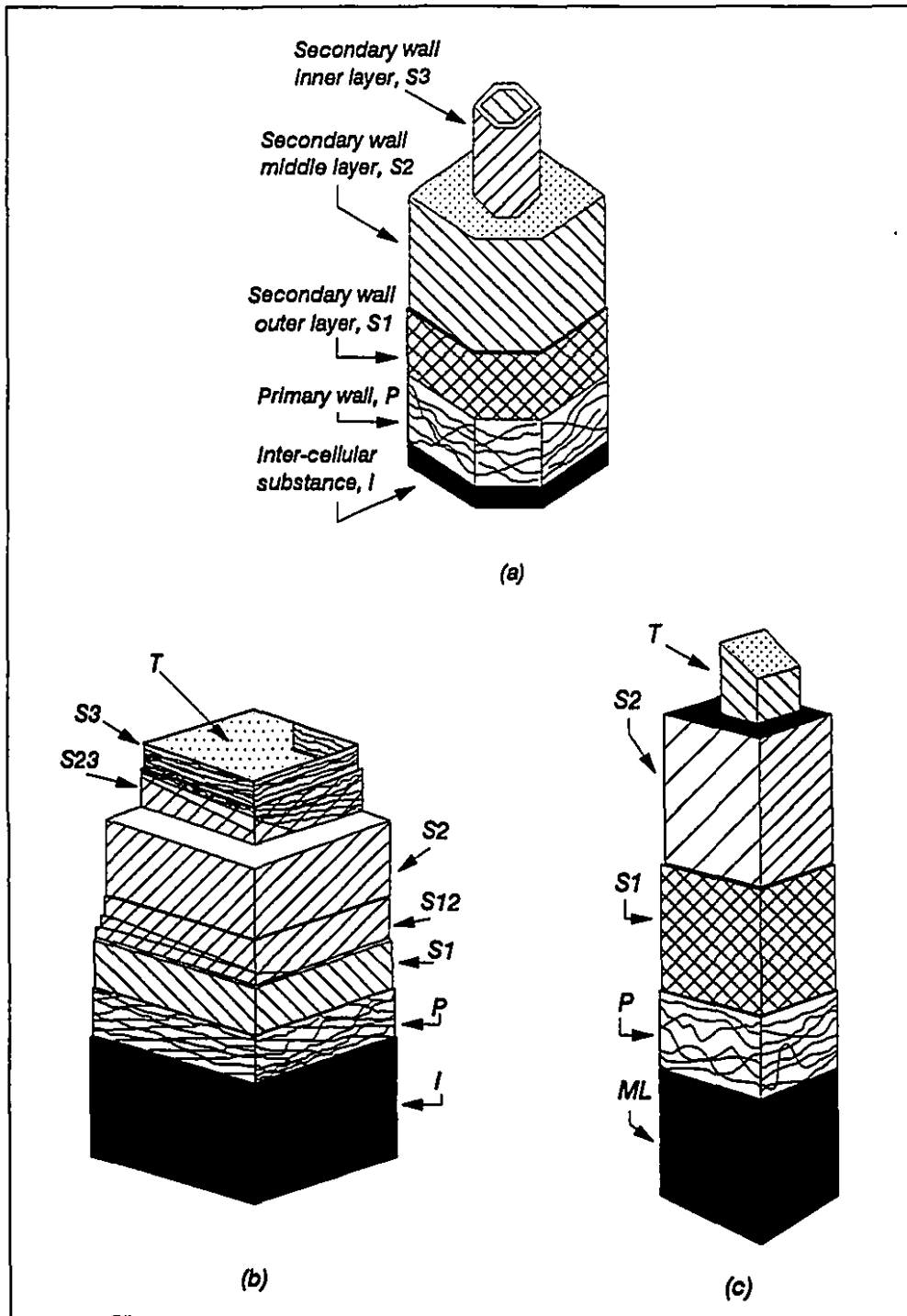
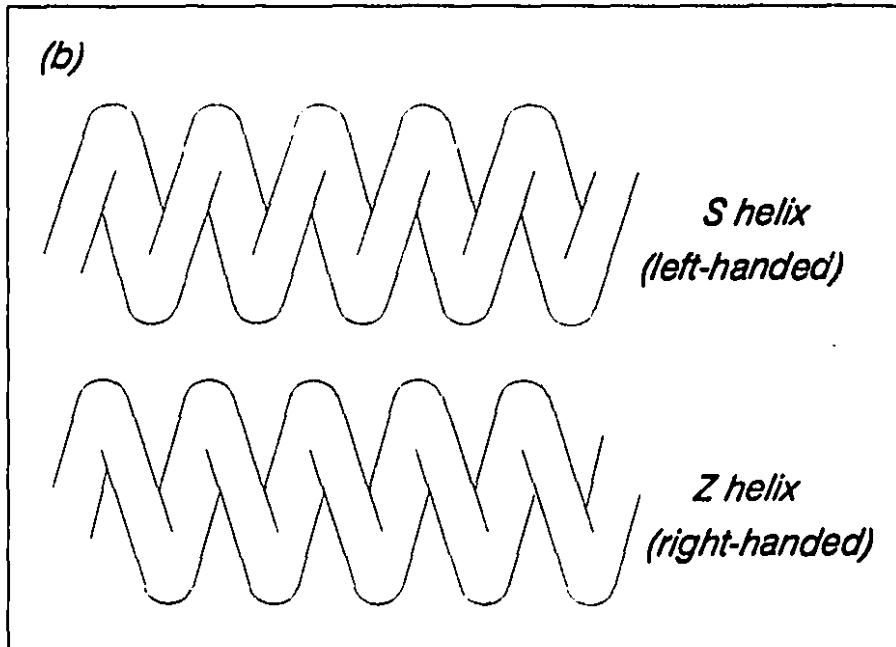
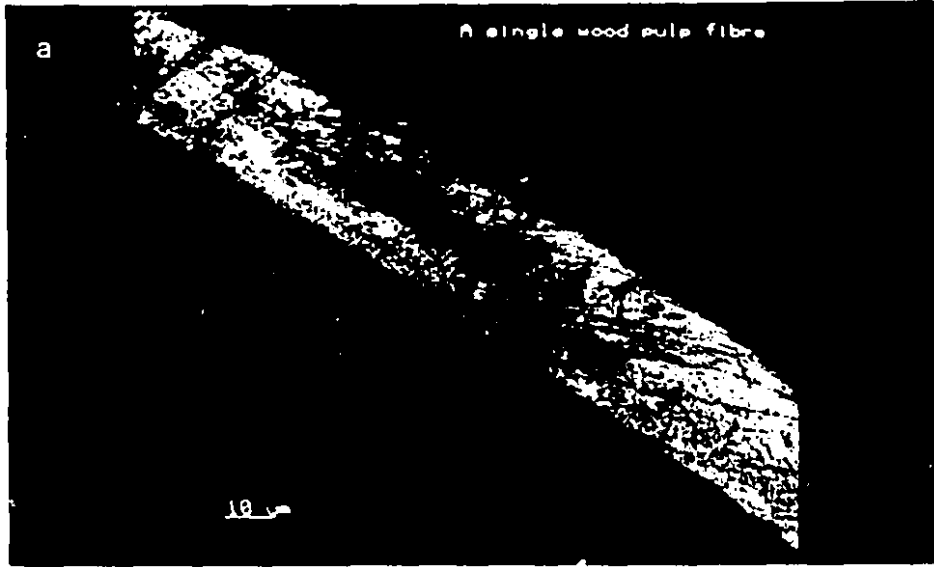


Figure 2.2: Different concepts of cell wall layers of a typical fibre or tracheid, showing fibrillar and/or microfibrillar directions: (a) from Wardrop and Bland [284]; (b) from Harada *et al.* [108]; (c) from Forgacs [79].

among the cellulosic fibrillar structures of the primary and secondary walls in varying concentrations [87, 106, 107, 235].

The layers in the wood cell wall have relative thicknesses of 7–14% for the primary wall, 5–11% for the S_1 layer, 74–84% for the S_2 layer and 3–4% for the S_3 layer [77].

Figure 2.3: A confocal laser scanning micrograph of a wood pulp fibre depicting the helical fibrillar orientation (a), along with a schema of the latter (b), of the S_2 layer of the cell wall.



2.1.3 The Physical Nature of Cell Wall Structure

Notwithstanding the individual molecular architecture natural cellulosic fibres have, there are several organisational features that are generally found in all such fibres. This bears significance when considering approaches to study the mechanical behaviour of wood fibres. (An *in extenso* discussion of the latter is presented in Chapter 4.) Thence, taking cognisance of the various concepts of cell wall constitution becomes of the essence.

Four composite views of the cell wall organisation of a typical fibre or tracheid according to different authors are depicted in Figures 2.2 and 2.4. A careful examination leads to the detection of slight differences amongst the four models. In some cases, the authors have subsequently modified their views. For example, Harada *et al.* [108] do not show a crossed fibrillar structure in S_1 whereas the others do. However, later work by Harada [106] recognised that there were two counter-rotating helical directions in S_1 . Another example is the designation "T" (for tertiary wall), used in entirely different senses by Forgacs [79] and Harada *et al.* [108]. The former used "T" to designate the layer referred to by the others as S_3 . The "T" includes the warty substance deposited on the inner wall as the cell loses its cytoplasmic contents at the conclusion of wall development. However, Harada *et al.* used T for the warty material only. Wardrop [283] concurred with Harada *et al.* that thin laminae of intermediate orientation were formed between the S_1 and S_2 , and the S_2 and S_3 layers, respectively. Earlier work by Wardrop and Bland [284] did not exhibit such characterisation. Moreover, the organisation of the S_3 was shown in one case as a single helix opposite in sense to that of the S_2 (Figure 2.4) and in another to have crossed S and Z helices (Figure 2.2a). Hosoi *et al.* [122] have indicated that S_3 has a single helix whose sense is identical to that of S_2 . Differing views among authors notwithstanding, the general outline of wall organisation is as evident as it is well established. Undoubtedly, the differences may be attributed to variations between species and individual trees [172]. Furthermore, pit cavities that pass through the cell walls at various points cause local deviations in the fibrillar structure. Figure 2.5 illustrates pinoid pitting in *pinus banksiana* (jack pine) pulp fibres. A general view of

the layer-by-layer orientation of microfibrils near pits is shown in Figure 2.6, adapted from Harada *et al.* [108].

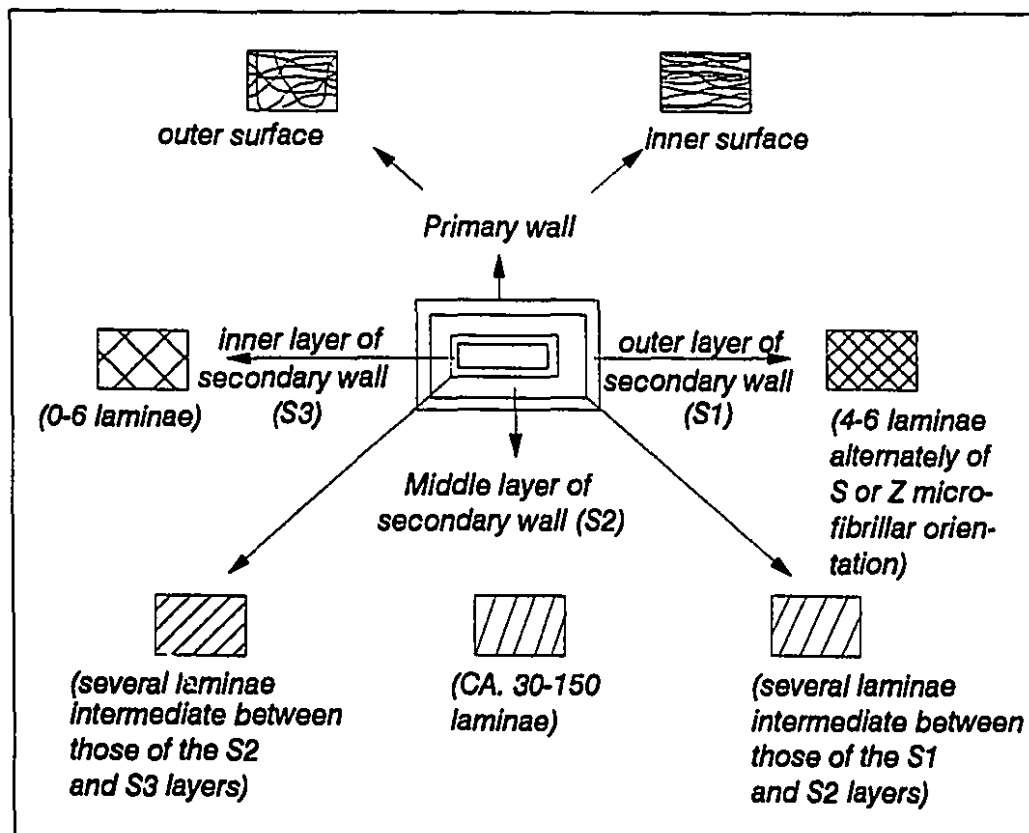


Figure 2.4: Cell wall organisation of a typical fibre or tracheid, showing fibrillar and/or microfibrillar textures [283].

The supermolecular arrangement of the polymer chains within the fibrillar and sub-fibrillar structure of the wall has been the subject of various theories. Some of these are depicted in Figure 2.7. From chemical and X-ray data it has become widely recognised that the cellulose chains were packed partially or wholly into crystalline regions termed “micelles”, also at times referred to as “crystallites” (see among others [172, 233]).

Early works spanning over the first quarter of this century proposed that micelles were brick-like in structure and were arranged in a geometric or random fashion. This view, as well as other similar theories for chain-packing were subsequently abandoned in favour of the “fringed micellar hypothesis” [118], for expounding the structure of

Figure 2.5: A confocal laser scanning micrograph of a *pinus banksiana* (jack pine) pulp fibre showing pinoid pitting.



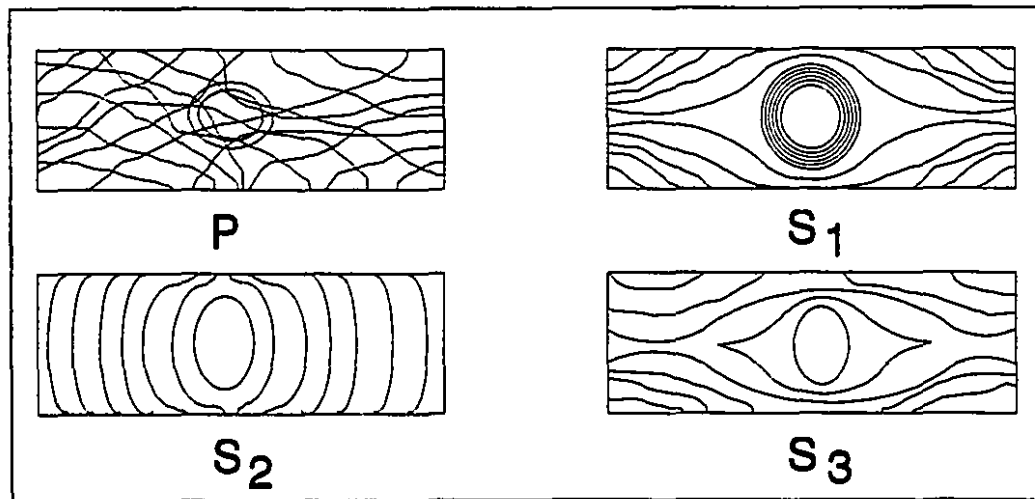


Figure 2.6: Orientation of microfibrils around pits in different layers [108].

cellulose in cell walls. According to this hypothesis, cellulose chain molecules pass through crystalline regions and then anastomose with other chains, becoming part of other crystallites. A different formation, based on extended chain conformations of native cellulose, was later proposed by Frey-Wyssling [84], which considered that there were several pure crystals of cellulose within a microfibril, each discrete, with no crossing over of chains from one crystallite to another. Furthermore, it was posited that a “paracrystalline” embedment cortex surrounded the long pure crystals; i.e., areas containing polymer chains having sugar residues other than glucose encapsulate the crystalline core. Along alternative lines to the above crystalline-with-order-defects system, researchers, for example [119, 231], postulated that chemical and/or physical irregularities in polymer structure would occur at intervals along the length, rather than the width, of the microfibril; that is: rod-like crystallites were thought to be strung together with irregular links possibly containing non-glucose monomers.

Frey-Wyssling and Mühlethaler [89] subsequently advanced an extended-chain model, thanks in many respects to discoveries made with electron microscopy. Hither, they came to realise that perfectly crystalline elementary fibrils were fasciated to make microfibrils, which must *a priori* be crystalline. During the early sixties, with burgeoning evidence adduced by novel scientific methods, an attempt to accommodate “older” concepts within the boundaries of this framework has resulted in the pro-

posal of a "fringed fibril" structure of fibres and polymers by Hearle [110] (refer to Figure 2.7). Gradually, the latter effected a departure from the concept of a fringed micelle in plant fibrils; whereupon concepts for regenerated celluloses and for synthetic polymers in general started to gain momentum in a rather fresh approach. Suffice it to say that it became vogue to propound "chain-folding" within the microfibrils of cellulosic plant walls, particularly after having observed folded-chain crystals in cellulose triacetate and triethyl cellulose crystallised from dilute solution [167, 168, 232]. (A chain-folding conformation is the progeny of motley developments in polymer research. It essentially suggests that when polymers are crystallised from dilute solution or the melt, the molecular weights—shown by the measurable dimensions of these structures and chain orientations therein—are too great for the chains to exist [whether in spherulites or single crystals] in other than a folded-chain conformation [135, 136, 262].)

In conclusion to the above discussion, few words in so far as the mechanical properties of cellulose and cellulosic cells are concerned seem appropriate. Microfibrils constituted of extended chains, folded chains, fringed fibrils, or fringed micelles vary rather significantly in strength and elastic properties from one another. It thus becomes crucial, in order to understand the cell wall mechanics, to ascertain what the nature of microfibrillar constitution is. Why, if stress analysis shows that stresses closely approach the ultimate values for crystalline cellulose, may there not be a disorganised, amorphous, or folded configuration of the chain [172]?

Another concept, that Page *et al.* [216] have utilised as their underlying theme when determining the elastic modulus of single wood pulp fibres, was enunciated by Freudenberg [83] over six decades ago. He observed that the cell walls of xylem were analogous to reinforced concrete and further remarked that: "The micelle series of cellulose may be compared with the iron rods, and the lignin together with the hemicellulose with the concrete in reinforced concrete. It is astonishing to see how nature has here made use of two of the best principles of rigidity which the human mind has independently discovered only in our own time." Bernal [31], among others, has re-iterated the sound physical underpinning behind this analogy of the composite.

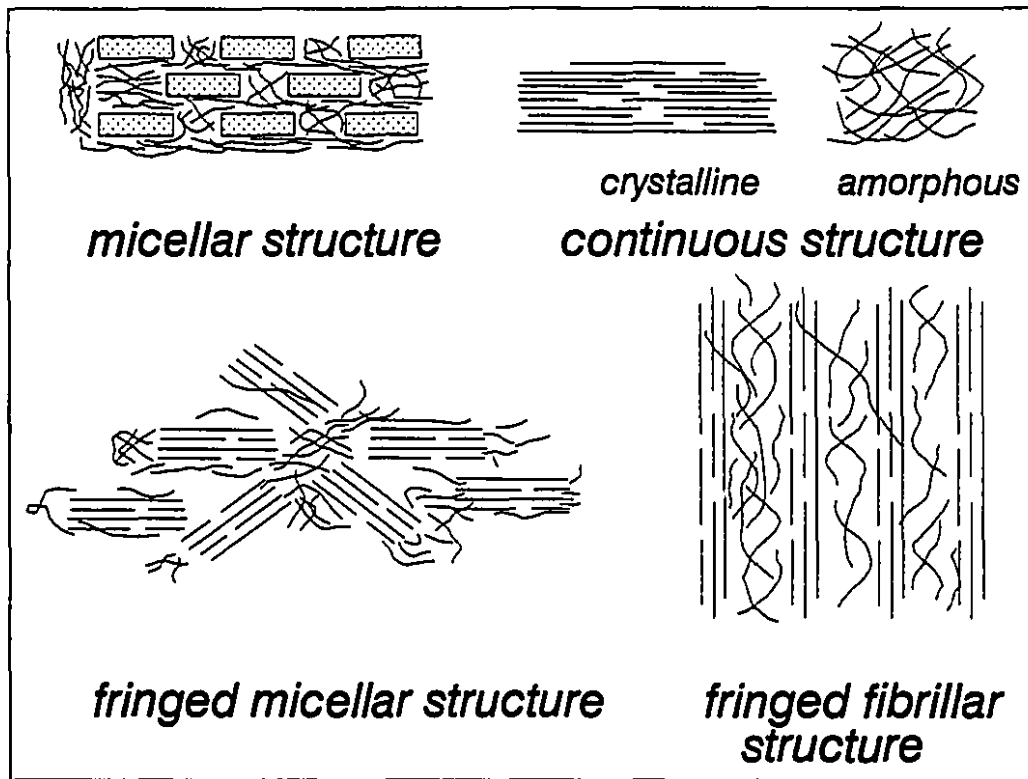


Figure 2.7: Schematic representation of several theories of component structures in fibres (adapted from [233]).

2.2 Chemical Constituents of Wood Fibres

The chemistry of the cell wall of wood fibres is highly complex. This is due mainly to the variety of chemical components making up the fibre wall as well as the heterogeneous nature of wood. It is not unlikely that the wood of each species has a different chemical make-up [285].

The components of the cell wall can principally be divided into four groups: cellulose, hemicellulose, lignin and extractives [77]. In most softwoods, these components make up $42 \pm 2\%$, $27 \pm 2\%$, $28 \pm 3\%$ and $3 \pm 2\%$ of the fibre mass, respectively [241]. The three major components: cellulose, hemicellulose and lignin are high-molecular-weight materials. Cellulose and hemicellulose are carbohydrates, while lignin is a phenolic-based polymer. In Figure 2.8 is an organisation chart of the principal substances of wood (after Browning [37]). A succinct exposition of the prime aspects of each component follows; for a more comprehensive treatment of the chemistry of the molecular constituents in wood, the reader is referred to [37, 241].

2.2.1 Cellulose

Cellulose, or poly(anhydro- β -1, 4-glucopyranose), exists in nature as a linear, crystalline macromolecule of high molecular weight having a high degree of polymerisation [95, 181]. The monomer is believed by some authors to be the dimer of glucose and cellobiose [16, 17], as illustrated in Figure 2.9. Cellulose is essentially invariant with tree species [77]. For an organic polymer, cellulose is remarkably resistant to chemical attack. Fairly severe conditions of acidity, alkalinity or temperature are usually required before degradation can take place [285]. In nature, cellulose exists as microfibrils of varying dimensions [169, 275]. These are aggregates of parallel chains of cellulose macromolecules which are held together by hydrogen bonding. However, as in all crystalline polymers, there are amorphous regions within cellulose which occur when the chains are not oriented parallel to one another.

Cellulose, the principal structural component of wood — a consequence of the superior mechanical strength resulting from its high crystallinity and molecular weight — is an oriented long-chained, unbranched polymer which is packed into a crystalline

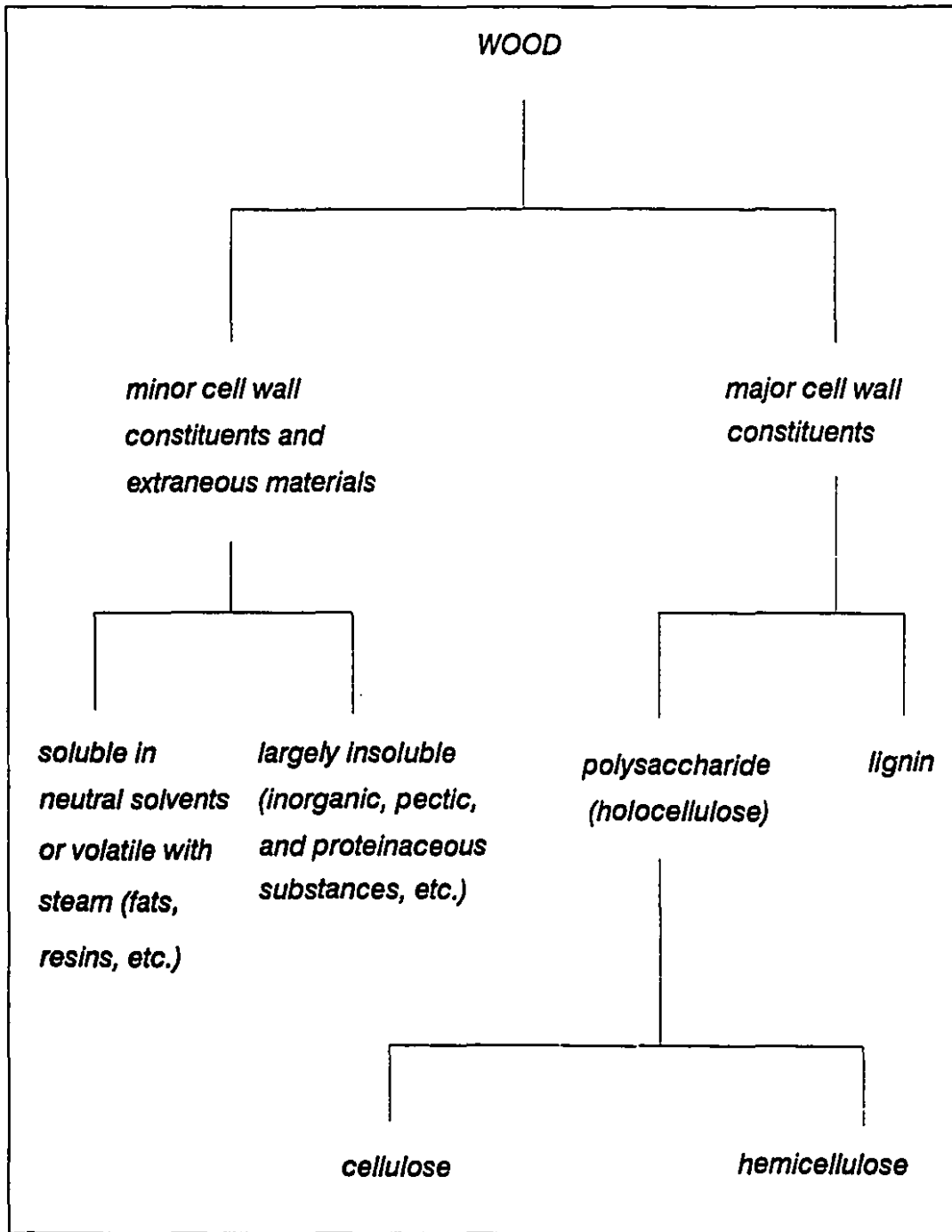


Figure 2.8: Constituents of wood (adapted from reference [37]).

lattice over much, if not all, of its length [172]. The chains in the lattice are rather strongly attracted laterally by secondary bonds, since infra-red data have indicated that almost all the hydroxyl groups in cellulose are engaged in hydrogen bonding [170, 183, 241]. This secondary bonding is of particular importance in determining the anisotropic elastic and strength properties of cellulose. Various concepts of crystallites as they exist within microfibrils have already been canvassed in Section 2.1.3. The lateral forces holding crystallites together internally account for several structurally important features of the cellulose framework. For one thing, a perfect cellulose crystallite itself is impenetrable to water and solvents—water can only be adsorbed on the outer surfaces between microfibrils or on the associated hemicelluloses if lignin protection is removed [124, 259]. Another feature is that large plastic deformations under stress are highly improbable because the inter-molecular forces of attraction prevent any extensive relative movements [187]. It was indicated by Klau-ditz [143] that cellulose was primarily but not exclusively the load-bearing material of the cell wall; moreover, a lack of an appreciable stabilising matrix does prevent the helically-wound cellulose chains from exerting their full structural capacity. Thus it appears that Freudenberg's original concept [83] (discussed above) of the cell wall as a composite of structural reinforcing materials in a cementing matrix is indeed valid.

2.2.2 Hemicellulose

The polysaccharide components of the cell wall other than cellulose are called the hemicelluloses. They are amorphous, branched polymers composed of two or three monosaccharide residues and have much lower degrees of polymerisation than cellulose. The structure and composition of hemicelluloses vary with tree species, and two major groups exist in gymnosperms: xylans and glucomannans [275].

Hemicelluloses in wood have often been described as cementing agents that bind microfibrils together and prevent splits as wood fibres are twisted, bent and/or stretched in service. Swollen in water, they render the surfaces of fibres tacky during paper formation and seem to form strong bonds upon drying [172, 241]. The greater the amount of these hemicelluloses in delignified fibres, the more pronounced is the

degree of fibre swelling. Hemicelluloses are less resistant to chemical attack than cellulose. They are usually soluble in aqueous alkali and are readily degraded by acid hydrolysis [285]. These polymers are thus recognised as being important with respect to swelling, beating and bond formation of fibres in the pulping and papermaking processes [275]; in the cell wall, they are oriented parallel to the cellulose chains [171].

2.2.3 Lignin

The third major component of wood, lignin, is a complex, three-dimensional, cross-linked network composed of phenyl propane-type monomers [33, 94, 251]. Since lignin is produced as a by-product of plant metabolism, it is located both within and between wood fibres [217]. The tough, amorphous nature of lignin serves to reinforce wood fibres by increasing the rigidity of the cell wall [77]. Studies have shown that lignin exists between the carbohydrate constituents of the cell wall in a lamellar-type of structure [140]. Lignin, which is generally insoluble in neutral solvents, can, however, be degraded under acidic or alkaline conditions [34, 94].

2.2.4 Extractives

The various minor constituents of wood which are soluble in organic solvents are collectively classified as extractives [77]. Two major categories exist, viz., wood resins and polyphenols. The former includes resin acids such as abietic acid, rosin, terpenes, diterpenes, fats, fatty acids such as oleic and stearic acids, triglycerides, long chain alcohols and sterols. On the other hand, the polyphenols are comprised of lignans, or dimeric phenyl propane compounds, tannins, flavones, catechins and stilbene derivatives. The variety and types of extractives differ considerably from one species to another.

2.2.5 Distribution of Chemical Components in Wood Fibres

The heterogeneity of wood stems not only from its structure and the litany of components making up the cell wall, but from the distribution of these components within the cell wall, as well. Over 50% of the lignin in wood is located in the S_2 layer of the

fibre wall. In contrast, only approximately 20% of the lignin in wood is located in the compound middle lamella (middle lamella + primary wall). However, this layer contains the highest concentration of lignin as a result of the thinness of the compound middle lamella in comparison to the S_2 layer. Cellulose, on the other hand, is found in all layers of the cell wall, but most prominently in the S_2 layer. Moreover, the highest concentration of hemicelluloses is found in the S_1 layer [77]. Whereas the extractives are predominantly found in the parenchyma cells and the resin canals in the wood structure. More recent microscopic studies have shown that the extractives were also present within the fibre and the tracheid cell wall [77]. Table 2.1 summarises the distribution of cellulose, hemicellulose and lignin in the cell wall of spruce tracheids—as per calculations performed by Fengel [76] from data obtained via ultra-violet microscopy [158, 186].

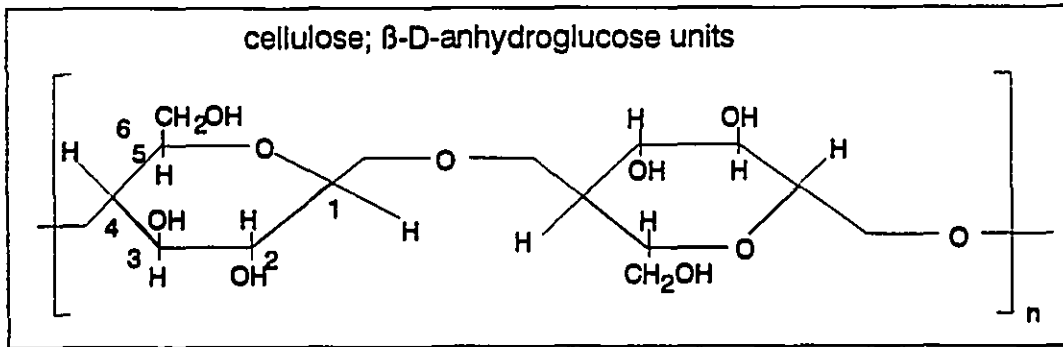


Figure 2.9: Cellobiose, the monomer of cellulose.

Table 2.1: Calculated distribution of the components in the cell wall layers of spruce tracheids (adapted from reference [77]).

Region	Wall Layer	Cellulose	
		% of wall layer	% of total cellulose
Earlywood	ML+P	13.9	4.1
	S ₁	36.4	8.9
	S ₂ + S ₃	58.5	87.0
Latewood	ML+P	13.7	2.5
	S ₁	34.6	5.2
	S ₂ + S ₃	58.4	92.3

Region	Wall Layer	Hemicellulose		Lignin	
		% of wall layer	% of total hemicellulose	% of wall layer	% of total lignin
Earlywood	ML+P	27.1	20.6	59.0	26.8
	S ₁	36.4	23.2	27.2	10.4
	S ₂ + S ₃	14.4	56.1	27.1	62.8
Latewood	ML+P	27.4	15.0	58.9	18.4
	S ₁	34.6	15.6	30.8	7.9
	S ₂ + S ₃	14.5	69.4	27.1	73.7

Chapter 3

Pulping Processes

3.1 What is Pulping?

Pulping is essentially the defibrising of wood [241], i.e., the process by which wood is reduced to a fibrous mass. Processes during which the bonds holding the fibres together in wood are broken to such an extent that individual fibres can be liberated from the wood structure. Table 3.1 summarises the range of pulping processes which are used to produce pulp fibres [33, 77].

Inter-fibre bonds can be weakened to the point of fibre liberation using chemical, thermal and mechanical treatments. These treatments can be applied individually, or in combination, to produce pulp of desired yield and quality. In all cases, an important step is the disruption of the middle lamella, thermally and/or mechanically, or by degrading the lignin chemically [47]. The process by which lignin is broken down and dissolved during pulping is referred to as delignification.

The pulping process used will define the end use of the pulp fibres produced. Fully delignified, low-yield chemical pulp fibres are flexible and are characterised by a highly fibrillated surface. These fibres are, thus, ideal for papermaking where a high degree of conformability and inter-fibre bonding are required. The kraft chemical pulping process, for example, produces fibres which are good for making strong papers such as those used in bags, cardboard and linerboard. When bleached, low-yield chemical pulps such as kraft are used for fine paper products. Alternatively, pulps

of very high yield that are produced mechanically are usually weak and have a layer rich in lignin on the surface of the fibres. Such pulps are also used in inexpensive paper where strength is not a pre-requisite, as in newsprint. Moreover, mechanical pulps contain large quantities of fine material which imparts opacity to the newsprint. High-yield chemimechanical pulping, however, is an intermediate process where a combination of chemical and mechanical treatments are applied. They are inexpensive pulps that have the advantage of having strength properties almost equivalent to chemical pulps. For these reasons, high-yield chemimechanical pulps are becoming increasingly popular for use in newsprint furnishes. A succinct description of the main pulping processes follows.

Table 3.1: Survey of pulping processes (adapted from reference [77]).

Process	Pulp type	Chemical Treatment	Mechanical Treatment	Wood ¹	Yield %	
• Mechanical pulping					80-99	
Stone grinding ²	o Groundwood (SGW)	None	Grindstone	S	93-99	
	o Steamed groundwood	Steam	Grindstone	S	80-90	
	o Pressure groundwood ³	None	Grindstone (pressure)	S		
Refiner pulping	o Refiner mechanical pulp (RMP)		None	Disc refiner	S	93-98
	o Pressurised refiner mechanical pulp (PRMP) ³		None	Disc refiner (pressure)	S	
	o Thermo-mechanical pulp (TMP)		Steam	Disc refiner (pressure)	S	91-98
	o Asplund pulp		Steam	Disc refiner	S	80-90

cont'd./...

Table 3.1 (cont'd.): Survey of pulping processes (adapted from reference [77]).

Process	Pulp type	Chemical Treatment	Mechanical Treatment	Wood ¹	Yield %	
• Chemi-mechanical and chemi-thermo-mechanical pulping					65-97	
Stone grinding ²	o Chemi-ground-wood (CGW)	Neutral sulphite	Grindstone	S/H	80-92	
		acidic sulphite		S/H	80-90	
		$Na_2S + NaOH$		S/H	85-90	
Refiner pulping	o Chemi-refiner mechanical pulp	$NaOH$ or $NaHSO_3$	Disc refiner	S/H	80-90	
		Steam +		Disc refiner (pressure)	S/H	65-97
		$Na_2SO_3 + NaOH$			(CTMP)	
• Semi-chemical pulping					65-92	
	o Neutral sulphite	$Na_2SO_3 + Na_2CO_3$	Disc refiner	H	65-90	
	o Cold soda	$NaOH$		Disc refiner	H	85-92
	o Alkaline sulphite	$Na_2CO_3, Na_2S, NaOH$	Disc refiner	H/S	80-90	
	o Sulphate	$NaOH + Na_2S$		Disc refiner	H/S	75-85
	o Soda	$NaOH$	Disc refiner	H	65-85	
	o Green liquor	$Na_2S + Na_2CO_3$		Disc refiner	H	65-85
	o Non-sulphur	$Na_2CO_3 + NaOH$	Disc refiner	H	65-85	
• High-yield chemical pulping					55-70	
	o Kraft	$Na_2S + NaOH$	Disc refiner	S/H	55-65	
	o Sulphite	Acidic sulphite		Disc refiner	S	55-70

cont'd./...

Table 3.1 (cont'd.): Survey of pulping processes (adapted from reference [77]).

Process	Pulp type	Chemical Treatment	Mechanical Treatment	Wood ¹	Yield %
• Full chemical pulping					30-60
Alkaline pulping	o Kraft (+AQ)	$NaOH + Na_2S$ (+AQ)	Mild to none	S/H	40-55
	o Kraft	$(NaOH + Na_2S)_x$	None	S/H	45-60
	o Soda	$NaOH$	None	H	40-55
	o Soda-AQ	$NaOH + AQ$	Mild to none	H	45-55
	o Soda-oxygen, two-stage	$NaOH$, oxygen	Disc refiner	H	45-60
Sulphite pulping	o Acidic sulphite	Acidic sulphite	Mild to none	S	45-55
	o Bisulphite	Bisulphite	Mild to none	S/H	45-60
	o Neutral sulphite	Neutral sulphite	Mild to none	S/H	45-60
	o Magnephite	Mg-bisulphite	Mild to none	S/H	45-60
	o Multi-stage sulphite	$Na_2SO_3 +$ $NaHSO_3/SO_2$	None	S/H	45-55
	o Alkaline sulphite ³	$Na_2SO_3 + NaOH$	None	S/H	
Dissolving pulping	o Acidic sulphite	Acidic sulphite	None	H/S	35-42
	o Pre-hydrolysis kraft	$Na_2S + NaOH$ (after pre- hydrolysis)	None	H/S	30-35

Notes:

1. S:softwood, H:hardwood.
2. Wood used in the form of bolts. All the other processes use chips.
3. Not commercially established.

3.2 Chemical Pulping

Kraft and sulphite pulping are the two most important commercial chemical pulping processes [217, 241]. Several other methods exist whereby lignin is solubilised to produce chemical pulps [2]. For chemical pulps the yield typically ranges from 30–60%. The primary goal of chemical pulping is the dissolution of the lignin with a minimum degradation of the carbohydrate components. However, for both kraft and sulphite pulping, substantial quantities of carbohydrates are dissolved in addition to lignin [88]. The first step which occurs during chemical pulping is the penetration of the cooking liquor into the chips. This process essentially takes place through the lumens which are exposed at the edges of the chips. From the lumens, the liquor penetrates the pits and finally the pores of the cell wall, to completely permeate the wood chip. The penetration which has been shown to be 50 to 100 times more rapid in the fibre direction than in the transverse direction [263], must be complete in order to effect efficient and thorough cooking. Upon heating, the solubilisation and degradation reactions are initiated. At the inception of the cooking procedure the lignin is dissolved more rapidly than the carbohydrate under acidic conditions; the reverse is obtained under alkaline conditions. However, after 50% delignification, the reactions which occur in acidic media favour the degradation of cellulose and lignin equally [264].

Furthermore, chemical pulping is fairly stronger in strength and lower in yield than mechanical pulp. It also produces a more compact sheet with lower opacity; and chemical pulps can be used in the unbleached state for such items as linerboard, wrapper or bag paper and can further be bleached to substantially higher brightness for use in a variety of products. In addition, the bleached brightness is considerably more stable than what can be obtained from mechanical pulps.

A fairly recent innovation in chemical pulping is the addition of catalytic quantities of anthraquinone to alkaline cooks. This process has resulted in more rapid rates of delignification with the simultaneous conservation of hemicelluloses and celluloses [121]. The pulps produced from the addition of anthraquinone have higher yields with strength properties equivalent to kraft pulps.

3.3 Mechanical Pulping

The process whereby wood is defibred by solely mechanical means is called mechanical pulping. The key difference between mechanical and chemical pulping processes is that the former does not destroy the lignin [47]. Because of the mixed nature of the particles in the pulp and because the lignin is not removed, the pulp has properties which render it desirable for use in certain types of paper. These properties include a small average particle length and a relatively stiff fibre which prevents packing and, hence, tends to give a sheet of paper high bulk and good opacity. The bulkiness gives a cushioning effect in sheets made this way, since the fibres tend to re-gain their shape when compressed and then released. This property — plus the fact that mechanical pulp absorbs ink easily, rapidly and uniformly — gives paper produced from this pulp excellent printability.

The two most common techniques in mechanical refining are: stone grinding and refining [77]. Stone-ground pulp, having a yield range of 93% to 99% [77], is produced from softwoods by pressing longitudinally debarked logs against the surface of a rotating grindstone. At the same time, water is sprayed on the grinding zone, where the temperature can range from 150° to 190°C as a result of friction. At these temperatures, lignin is plasticised allowing fibres, fibre bundles and fibre fragments to be readily removed from the wood. The fibre bundles are reduced to smaller units by the refining action of the grindstone grits [12, 38, 52]. Refining, however, differs from grinding in that chips (mainly softwood) are defibred between two metal refining discs, at least one of which rotates. The wood fibres are separated by the action of the grooves and the bars on the surfaces of the two discs. In essence, two steps occur: the defibrisation of wood to fibre bundles and fibres, followed by the fibrillation of the fibre surface. Pulp yields usually range from 91% to 98% [77]. The quality of the pulp produced is highly dependent on the designs of the disc and the refiner, as well as the number of refining stages [57].

These two types of mechanical pulps are significantly different. The ground-wood pulp has a higher content of fine material owing to the abrasive action of the stone, whereas the refiner pulp, which has a smaller content of fine material and long fibres,

tends to be more ribbon-like. The principle of ground-wood pulping is simple. However, the efficient production of a uniform, good-quality pulp requires careful control of stone surface roughness, pressure, shower water temperature and flow rate. While the mechanism governing refining is more complicated, it can produce a uniform quality of pulp and is more suitable for automation and computer control. Furthermore, refiner pulp can use sawdust or hardwood—though not as easily as softwood—as raw material, and has as a result been gaining growing popularity over the last few years.

Lastly, thermomechanical pulping, in which chips are penetrated and preheated with steam prior to refining under pressure, is an important and rapidly growing technology in mechanical pulping [91, 180].

3.3.1 Characteristics of Refiner Mechanical Pulping

In the early 1930's a novel pulping process, which used mechanical forces for defibrating chips that had been softened with the aid of water and high temperature, was developed [8]. The process was named after its inventor, Asplund, or after the defibriser, *defibrator*: a single-disc, semi-precision refiner, operating under pressure. The first commercial production of refiner mechanical pulp (RMP) was initiated in the 1960's. The process usually incorporated the use of two refining stages—operating in series, and producing longer fibrous pulp than the conventional groundwood. Pulp thus produced is characterised as being stronger, freer, bulkier but somewhat darker in colour than stone-ground [159]. Around the same period, development work on the thermal mechanical pulping (TMP) process began. TMP uses a pressurised, first-stage refiner at atmospheric pressure. The resultant pulp was stronger than RMP, contained fewer shives and had a lower bulk. The search for high-quality, high-yield pulps led the development of a number of modified TMP systems which could include a mild chemical treatment. An account of some critical aspects of refining is pithily dealt with below.

The core of RMP or TMP systems is the disc refiner, which is a double-revolving unit, with two discs rotating in opposite directions. Other combinations of disc design

and operation do exist: a rotating disc opposite to a stationary one, or a rotating double-sided disc [14, 189, 190, 261]. Figure 3.1 illustrates a schema of the three most common refiner configurations.

The principle upon which a disc refiner works is not comprehensively understood. It is, however, speculated that the mechanism of refining presents a simile to grinding—though there are some essential differences between the two methods. For instance, in grinding the lignin is softened by compression–decompression, and by the friction of wood to wood and metal to wood between stone and wood logs. Whereas in refining, the individual chips are *unravalled* into smaller entities and finally into fibres. Generally, refining plates—which constitute a significant parameter in the functioning of the refining process—are classified into two categories: first-stage and second-stage refiner plates (depicted in Figure 3.2). The former have widely spaced and wide breaker bars close to the eye of the refiner. The bars shred the chips and permit the development of centrifugal forces which move and align the wood particles for optimum results in the refining zone—the latter consisting of progressively narrower bars and grooves where the coarse material is converted to pulp. The plates are usually tapered slightly (by 0.01 mm/mm or less [260]) to ensure that the pulp moves evenly towards the periphery. Some plates are developed with dams to block the grooves at intervals and force the pulp to move over the bars. Plates may also be made with a peripheral rim to increase the retention time of pulp between the plates [75]. Second-stage refiner plates, on the other hand, have a shorter breaker bar section and a larger portion of refining surface. The breaker bars are necessary to align and impart centrifugal forces to the partly refined pulp.

In conclusion to this segment, an *exposé* of the forces involved during the refining process is deemed necessary. Espenmiller [74] deduced that the refining process is one in which mechanical and hydraulic forces are applied to the fibre network. These forces could generate two major types of stresses which result in desirable structural changes to the fibres. The shear stress is caused by rolling, twisting, tensile action between the bars and the grooves of the refiner; and normal stress (either tensile or compressive) is caused by bending, rolling, twisting, crushing, pulling and pushing actions on the fibre clumps caught between the bar-to-bar surfaces. Some fibre shortening or cutting

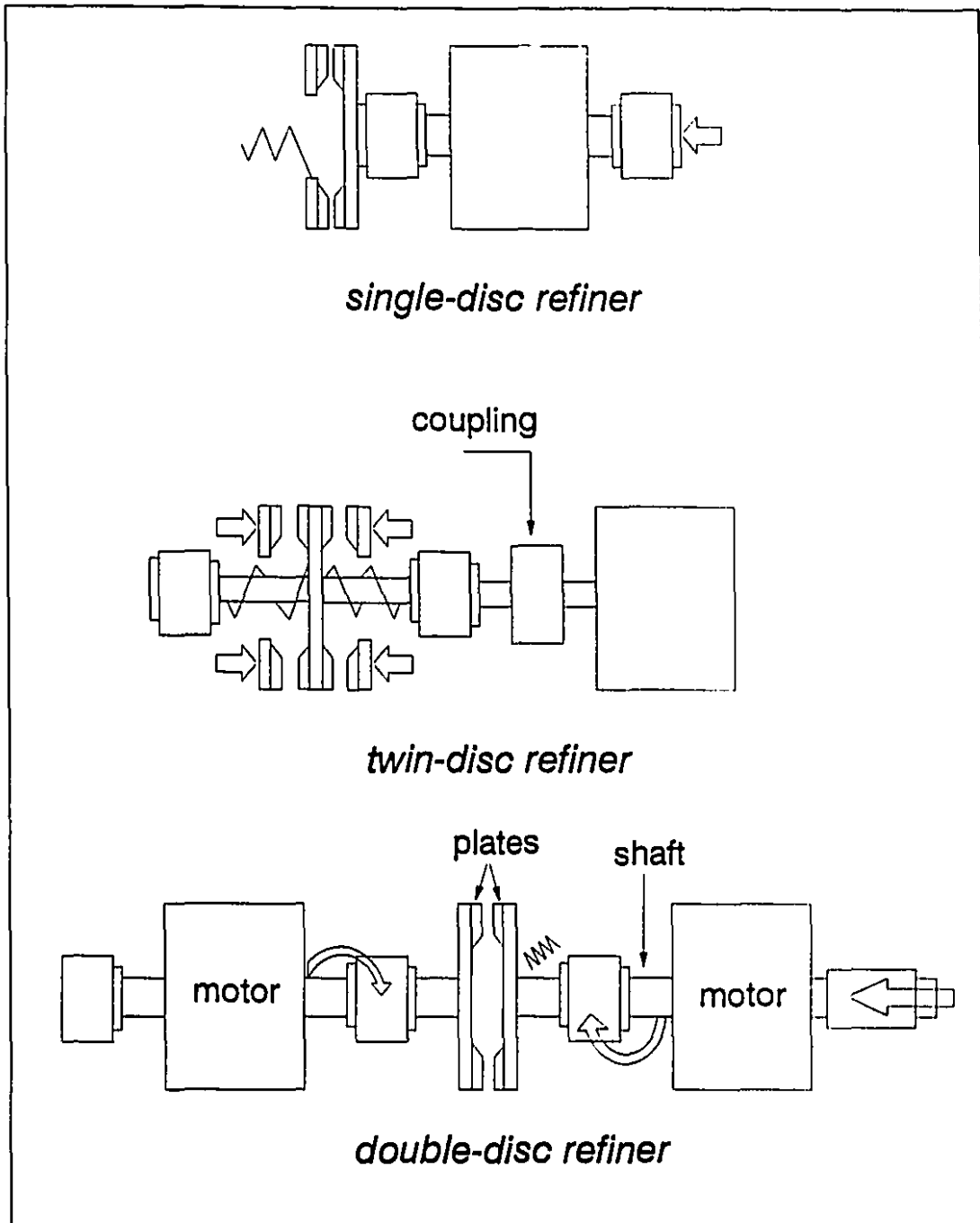
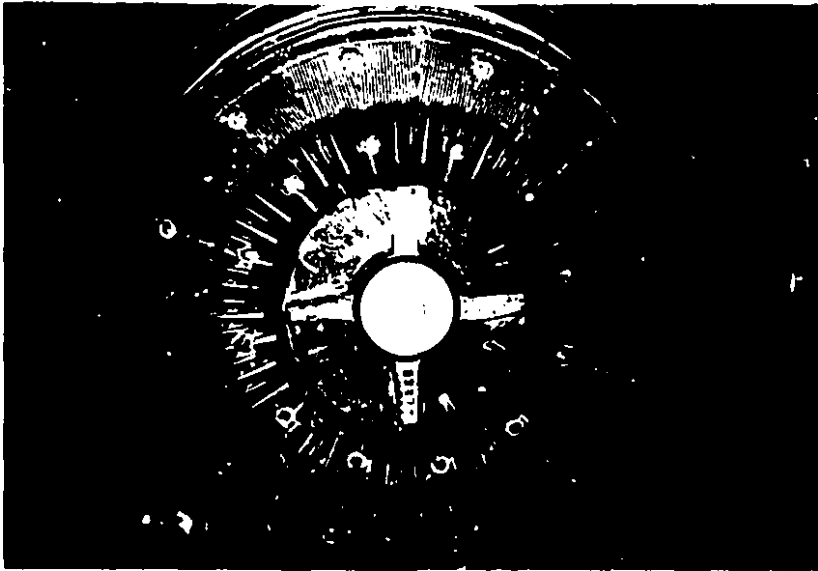


Figure 3.1: A schematic representation of the three most common refiner configurations [47].

Figure 3.2: Typical refiner plate designs illustrating beater bar sections and refining sections (*courtesy of Dr. A. Karnis, Paprican, Pointe Claire, Canada*).



↪ Refiner disc



← fine bar section

← intermediate bars

← breaker bars

almost always occurs during refining owing to the shearing action of the bar crossings. All different explanations of the refining process lead to diverse interpretations of the refining mechanisms and, therefore, there is *no* one generally accepted theory of refining that would exclusively expound what happens in the refining process.

3.4 Chemimechanical Pulping

As may be surmised from Table 3.1, a wide variety of processes exists between mechanical and full chemical pulping. Refining high-yield pulps has been shown to soften the fibres considerably, rendering them more flexible [160]. Alternatively, it is possible to make mechanical pulps more flexible by a post-refining or post-grinding chemical treatment [52, 81].

Chemimechanical pulping is the process whereby chips are given a mild chemical treatment followed by defibrisation in refiners [51]. The yield of the pulp produced can range anywhere from 65% to 97% [77]. The sulphonation of the lignin which occurs during the sulphite chemical pre-treatment has been indicated to irreversibly soften the lignin within the wood, resulting in a high-yield pulp being produced with strength properties comparable to those of full chemical pulps—however requiring less chemicals and shorter treatment times [11, 28, 116]. Newsprint furnishes could thus be produced more efficiently.

Chapter 4

Fibre Physics

4.1 Solid Mechanics of Cell Wall Components

It follows from the discussion of Chapter 2 that any given layer in a cellulosic (plant) fibre may be described as a filamentary composite. Since the fibre is composed of several such layers, whose microfibrils are differently oriented, it itself may be regarded as a *laminated composite*. A discussion of the organisation of a cellulosic fibre from the stand point of the mechanical functions of the structural components and how these components act together as a composite material is thus deemed of paramount relevance.

As is done with industrial materials and structures, structural functions may be assigned to each of the components found in a typical unit volume of fibre wall. This, in essence, would largely be made possible once experimental evidence—direct or indirect—would avail. Hence, in particular, the *à posteriori* deduction from experience with industrial multi-phase materials as to the fact that specific components of the fibre cell wall act as the bulking and stiffening matrix in which the reinforcement is embedded. In fibres and other plant cell walls, the microfibrils provide the structural reinforcement; and because the former are principally if not exclusively composed of cellulose, their mechanical properties are chiefly determined from those of the crystalline substance. Moreover, in some fibres—especially those of coniferous woods—some of the glucomannan hemicellulose is intimately associated with the na-

tive cellulose in the microfibril and, therefore, must also be considered as part of the reinforcing phase, or framework, of the fibre wall. Nevertheless, calculations of the cell wall elastic constants and other physical and mechanical properties of the solid-state have hitherto eschewed the presence of hemicellulose and dealt with the microfibrillar entity as being solely composed of cellulose, and as being defects-free (reference is made, among others, to [90, 173, 248, 288] concerning the latter approach).

4.1.1 Composite Characteristics of Wood fibres

The matrix phase in a cellulosic fibre cell wall consists of relatively unoriented or amorphous, short-chained or branched polymers of various molecular species, i.e., lignin and hemicellulose and any other polymers such as pectopoluronides that might be present in a given layer, plus all of the tiny voids and gases and adsorbed water associated with them [179]. In other words, everything else that surrounds the microfibrils in their local environment. An important feature of the crystalline structure of cellulose I (native cellulose) — a monoclinic crystal structure characterised by a repeat distance of 1.034 nm in the chain direction [179] — from the stand point of mechanical, electrical and other properties concerns the pattern of hydrogen bonding, since there are no inter-chain primary bonds. Lateral hydrogen bonds provide a mechanism for stabilising the crystal against relative displacement of the chains in response to imposed physical forces. One may thus think of the hydrogen bond network as a sort of cross-bracing. These bonds significantly inhibit any tendency for translation of the chains within the crystalline microfibrils.

In general, the microfibrils are not aligned with the fibre axis; therefore, a small element of the cell wall layer — such as shown in Figure 4.1 — has a filament alignment that differs by some angle α from the axial direction of the fibre. The two components of a submicroscopic element of the cell wall: the approximately rectangular reinforcing filaments (microfibrils), and the matrix that surrounds the microfibrils are depicted in Figure 4.1. The latter shows, too, the microfibrils in relation to their individual elastic co-ordinates (X, Y, Z) and the geometric co-ordinates of the fibre wall (1,2,3). A basic unit of cell wall material, containing a single anisotropic microfibril surrounded by

isotropic matrix material, which repeatedly produces the cell wall layer, is illustrated in Figure 4.2.

Some researchers [173, 174, 178] have adduced that cellulose I in the microfibril obeys Hooke's law very closely, hence the assumption that both the matrix and framework can be treated as linear, elastic materials. Victor [280], however, indicated that the wood cell could not be described by a linear theory at all stress levels; and further remarked that observed deformations were non-linear with respect to stress above certain stress levels. In fact, he made use of the place-exchange theory to explain non-linear rheological behaviour.

The physical and mechanical behaviour of the matrix is dependent upon the distribution of its molecular components and the presence or absence of moisture. Since the distribution of hemicelluloses, lignin, void space, and so forth is non-uniform, there is point-to-point variation in the matrix elastic constants. Regions of dense molecular aggregation will have high local moduli of elasticity and rigidity, and the more open regions where air and/or water is present in the cell wall voids will have small, perhaps insignificant, moduli [179]. The moduli will mostly take some sort of average values but deformations will take place preferentially in the regions of lower aggregate macromolecular packing density. It is worthwhile noting that work is required to deform the matrix molecular structure even if the matrix components are not bonded to each other or to the microfibrils. The physical location of the constituent polymer molecules between microfibrils requires that these molecules deform along with the microfibrils.

4.1.2 Anisotropy of the Fibre Wall

In the intact, wet or dry plant fibre, it may reasonably be assumed that the cell wall layers will deform together without relative slippage under applied load. Equivalently, one can adequately apply the same assumption for a dry pulp fibre subjected to small deformations, however, the same would unlikely hold for delignified wet fibres or fibres subjected to large deformations [179].

Several models, with varying motifs, have been applied by researchers when study-

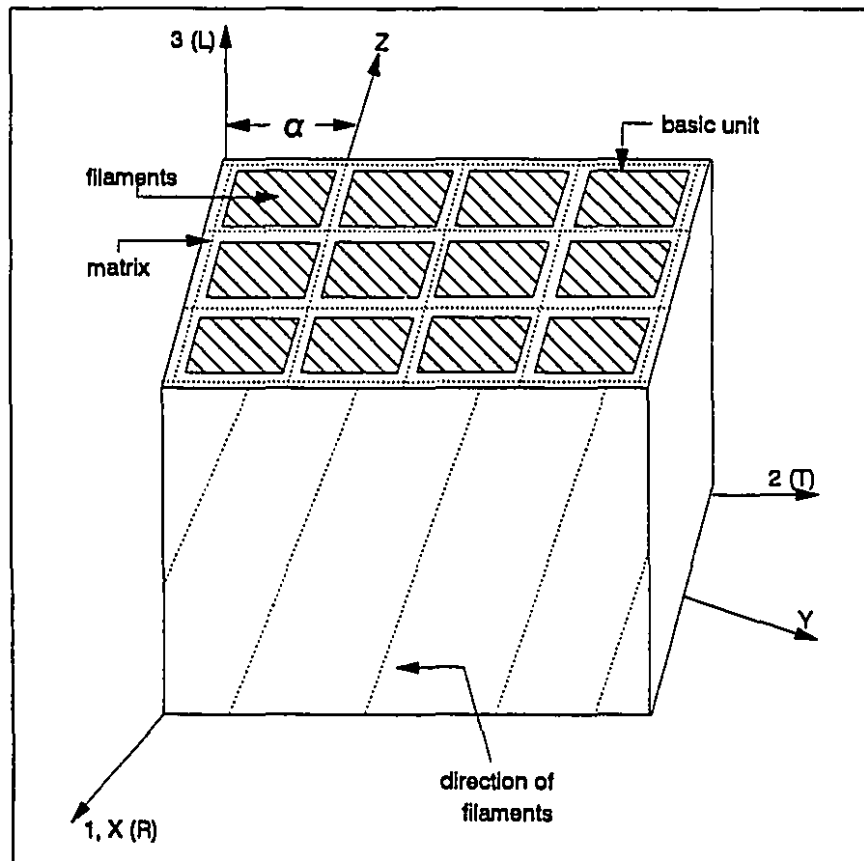


Figure 4.1: A model of a sub-microscopic element in a layer of a fibre wall (adapted from reference [273]).

ing the effects of structure on the mechanical properties of fibres. In the category of two dimensional models there have basically been four types:

1. A model for the fibre wall which assumes that the latter can undergo extensive torsional distortion in response to an axial load [172].
2. A model that assumes complete shear restraint in the fibre wall by virtue of complete contact and bond to other fibres, thus preventing twisting and also having uniform circumferential strains both radially and tangentially [249].
3. A model similar to that in 2, however allowing different circumferential strains in the radial and tangential directions—the “two wall” analysis model [177].
4. A model that is also similar to the one in 2, but which permits limited circumferential displacement (imperfect shear restraint) by virtue of a deformable bond between fibres [257].

Modifications of the above models have often included the simplifying assumption that the fibre only has an S_2 layer, either with a constant fibril angle [216], or with a statistical distribution of the microfibrillar reinforcement [48, 49]. A careful reading of the literature is thus imperative, especially when relating the various models to properties calculated from experiments. For instance, Page *et al.* [216] used experimental data to compute the values for the compliance and stiffness tensors on the basis of a single-layered model. From the stiffness tensor was derived a set of elastic moduli of single wood pulp fibres exhibiting an anisotropy of approximately 10:1. In this particular case the fibre was modelled as a collapsed, flattened structure—as the case may be for paper whose fibres are thin-walled. This conclusion markedly differed from what was presented by other authors [92, 172, 174]. Mark and Gillis [179] sought to make a comparison between the single-layered model and a collapsed fibre having the actual three-layered structure. They used in their comparison the following constants (refer to Figure 4.1 for orientation):

- E_L, E_T : moduli of elasticity of a cell wall lamina parallel and perpendicular to the mean fibrillar direction of the lamina = 177 GPa, 6.8 GPa respectively;

- G_{LT} : shear modulus of rigidity of the lamina in the plane of the lamina = 2.6 GPa; and
- ν_{LT} : Poisson's ratio for cell wall lamina, giving ratios for contraction in the direction indicated by the 2nd subscript to extension under stress in the direction indicated by the 1st subscript, in the plane of the lamina = 0.10.

(N.B. The value for the shear modulus was obtained from single-fibre torsional experiments by Kolseth and de Ruvo [146].)

Table 4.1 contains the values for both: the single- and three-layered models, for a range of fibril angles. It is clearly evident that the anisotropy when the fibril angle, θ , of the S_2 layer equals 10° is roughly 9:1 for the single layer model, but only 2.5:1 for the three-layer one. Moreover, the axial and transverse fibre moduli are reported to be approximately equal when $\theta = 20^\circ$ for the three-layer case, however, different over three-fold when considering the single-layer model. The predicted Poisson's ratios for the three layer model are seemingly more reasonable. It is important to note that for the comparison of both models an assumption of zero in-plane shear strain ($\epsilon_{LT}=0$) was made on the basis that the angular orientation(s) of the wall of the fibre balance the angular orientation(s) of the opposite wall, since the bisector of the two angles lies along the fibre axis. Also assumed: a state of plane stress; the wall layers, plies and regions all deform under the applied stress, i.e., no slipping; each layer is orthotropically elastic and is homogeneous.

It is deemed necessary in our opinion to re-examine the review proffered by Mark and Gillis [179] from another perspective in the hope of better explaining the source of apparent discrepancy which occurred in some of the reported results. The choice of a fibre model consisting of only the S_2 layer does not seem unreasonable, since the S_2 layer comprises such a large part of the cell wall material that the layers may have an insignificant effect on the fibre modulus. However, one important aspect concerning the determination of the fibre extension experimentally was neglected by Mark and Gillis when criticising the reported results. When measuring the strain of the fibre *in situ*, the displacement reading is not precisely what the fibre actually experienced

¹As per the experimental set-up of Page *et al.* [216]

Table 4.1: Calculated elastic constants for a collapsed pulp fibre assumed to only have an S_2 layer versus a typical three-layered fibre (adapted from reference [179]).

θ angle	Single-layer					Three-layer				
	E_L (GPa)	E_T (GPa)	G_{LT} (GPa)	ν_{LT}	E_L/E_T	E_L (GPa)	E_T (GPa)	G_{LT} (GPa)	ν_{LT}	E_L/E_T
0°	177.0	6.8	2.6	0.10	26.0	132.7	18.7	2.7	0.07	7.1
10°	60.0	6.7	2.8	0.44	9.0	46.7	18.5	2.8	0.16	2.5
20°	21.7	6.5	3.5	0.53	3.3	18.7	18.3	3.3	0.19	1.0
30°	11.9	6.5	4.7	0.52	1.8	11.4	18.1	4.3	0.19	0.6
40°	8.3	6.9	6.2	0.47	1.2	8.6	18.4	5.4	0.19	0.5

due to two factors: “First, the displacement given by the recorder include[d] the extension of the load cell and deformation of the jaws and other linkages. Second, the fibre [was] attached to glass tabs [for mounting purposes] by a glue that was itself extensible” [216]. Whilst the first error is a constant of the apparatus and could easily be accounted for, the extension of the glue could less easily be dealt with. As Page *et al.* correctly pointed out: the extension of the glue varies with the setting time of the glue and the cross-sectional area of the fibre. We feel that this presents a dilemma that cannot be resolved without a certain degree of uncertainty which could very well confound final results. (We have therefore opted — as will be explained in detail in Chapter 7 — for using a novel, precise, mechanical fixation mechanism for securely mounting single wood pulp fibres in position. Thus, at least, inaccuracy regarding stiffness and extensibility of the gluing material is omitted.)

Besides, after analysing ciné films of the fibres under strain, Page *et al.* [216] attributed the large differences — which are far greater than would be expected from mere experimental errors — to: the presence of crimps, nodes, micro-compressions, dislocations, or other irregularities in the structure. These effects tend to lower the modulus, whereupon fibres with high moduli are expected to be uniform in structure and generally free from irregularities. The important conclusion of their study was that for fibres free from defects, the modulus depended on fibril angle according to

orthotropic elasticity theory; moreover, the modulus in the fibril direction was one order of magnitude larger than the transverse and shear moduli, indicating the high anisotropy of the cell wall material. This result is expected from the high orientation of cellulose molecules in the fibrils and the high orientation of fibrils in the S_2 layer of the cell wall. Therefore, it is perhaps rather cynical that numerical values are fully trusted — or even disregarded — without taking cognisance of the aforesaid.

In closing it seems appropriate to enunciate examples of physical effects that result from the multi-layered structure of plant fibres. It has been shown by Cave [50] that layers other than the S_2 play a significant role in, for example, the longitudinal shrinkage calculations for wood fibres. He reported that when a model with all the layers accounted for was compared with a structural model of only an S_2 layer with a variable fibril angle, the variance in calculated longitudinal shrinkage is reduced by a factor of 2. Another example, illustrating the significant influence of the S_1 and S_3 layers on the fibre properties is proffered by El-Hosseiny and Page [69] basing their proof on optical observations. A fact — generally considered in Chapter 2 — which requires further elaboration concerns the angular orientations of the S_1 , S_2 and S_3 layers on one wall of a collapsed three-layered fibre, which are balanced by the same orientations of opposite sign on the other wall. In wood pulp fibres, the layers that balance one another — resulting from the complete collapse of the lumen — are neither contiguous (except for S_3) nor truly symmetrical through the thickness (albeit they are symmetrical with respect to the fibre axis) [179]. The asymmetry is rather significant for thin-walled laminates, however, it may be somewhat accentuated in the case of thick walls.

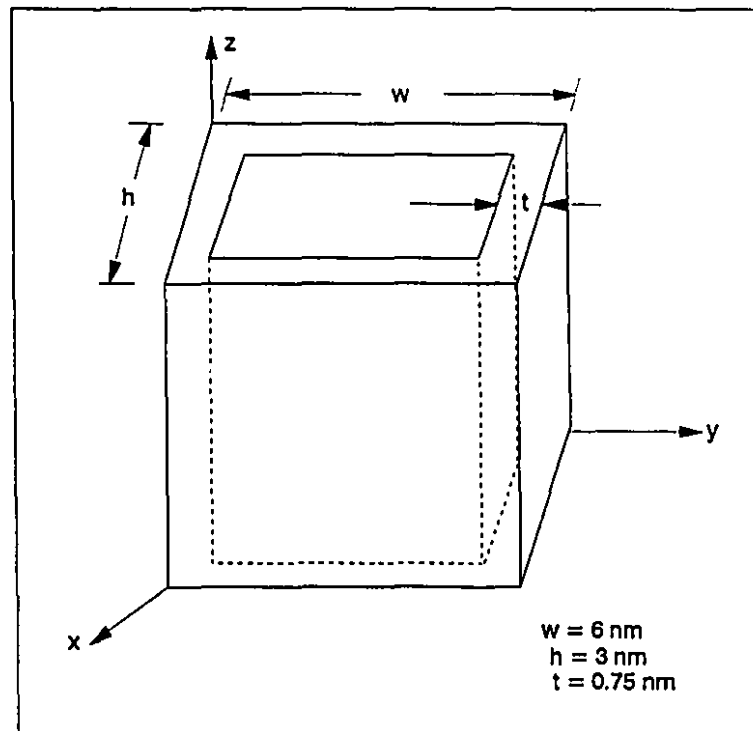


Figure 4.2: A model of a basic unit cell wall. The unit contains a single rectangular anisotropic filament surrounded by a matrix of thickness, t (adapted from reference [175]).

4.2 Mechanical Properties of Single Wood Fibres

A prelude to a more thorough understanding of paper properties would constitute an in-depth investigation of the mechanical behaviour of single wood pulp fibres. Early work has mostly been exploratory; henceforth, success in establishing some semblance of an order of magnitude for fibre strengths was yet to be realised. As the technological gap in Pulp and Paper research became narrower — with the advent of novel, sophisticated methods of determining stress and strain on such minute specimens — studies were made of the effects on fibre properties of: species, wall thickness, fibre type, pulping process, yield, chemical composition, refining, drying conditions, humidity and a sundry of other variables (refer to, among others, [279, 215, 70, 142, 210, 216, 212, 214, 211, 109, 250] and [272, 258, 249, 60, 128, 161, 68, 269, 270, 139, 271, 62]). Nonetheless, a comprehensive understanding of the fibre properties was not achieved in spite of a glut of data obtained from the various analyses: experimental and theoretical. This surfeit, in some respect, added to the confusion of an already complex and intricate task; some researchers [215], following a cautious re-evaluation of a large number of previous results while adopting a new approach altogether, endeavoured to rationalise the underlying causes for these conflicts. Basically two possible explanations were proffered: One is that some of the previous work has suffered from not-an-insignificant bout of inattention to the meticulous care necessary at all stages in the preparation and testing of samples — indeed, fibres must not be damaged or subjected to any appreciable mechanical stress during preparation, if accurate and precise results are to be obtained. Two, it is possible that the data are essentially correct, however, a sound understanding of the parameters affecting fibre properties has not been realised due chiefly to a lack of appreciation of the significance of some of these factors — most notably, the fibril angle — when performing experiments and analysing their findings. Clearly, no *one* definite answer could be offered to resolving the riddle. At any rate, a thorough, meticulous, *multi-faceted* approach to investigating the mechanics of cellulosic fibres remains of the essence. A summary of some of the well-established and widely-referred-to work is presented along thematic lines in the sections below.

4.2.1 Fibre Strength

Recall the structure of a wood fibre: A softwood fibre, consisting of long, substantially crystalline cellulosic microfibrils embedded in an amorphous matrix of hemicellulose and lignin, is a hollow tube made up of concentric layers. Since the P , S_1 and S_3 layers are much thinner and their microfibrils are transversely wound, the tensile behaviour of single fibres would be expected to be largely related to the behaviour of the S_2 layer [215]. An analogy may thence be drawn between the structure of the fibre, or rather the S_2 layer, and that of a helically-wound, fibre-reinforced, composite tube [70]: in which the cellulosic fibrils represent the fibre reinforcement and the amorphous hemicellulose and lignin, the composite matrix. Accordingly, the strength of the fibre is expected to depend on the fibril angle. Indeed, Page *et al.* [215] found that the tensile strength of a fibre was at a maximum when the fibril angle was zero, and diminished with increasing angle—irrespective of the fibre type (springwood or summerwood) or species (black or white spruce). They further adduced that failure was often initiated at defective regions: natural such as pits, or induced, such as nodes or wrinkles. The more severe the defects, the weaker is the fibre—to which the wide scatter of fibre strength results may be attributed. From the foregoing and in accordance with orthotropic elasticity theory, fibres free from obvious defects would be expected to fall on an upper bound of a strength versus fibril angle plot; as indeed experimental data corroborate [215].

The state of strain of a pulp fibre subjected to axial stress needs some elaboration. A helically-wound structure tends to rotate when axially stressed; the cell wall undergoes both: axial and shear strains. To ensure against rotation, El-Hosseiny and Page [70] prepared and tested their samples between non-rotatable tabs; hence, the fibre would experience an axial strain, but no shear strain. A shear stress, proportional to the axial stress, would however be induced in the cell wall by the restraining tabs of a magnitude sufficient to maintain zero shear strain. This condition of shear restraint had formerly been acknowledged by Cave [48] and Schiewind and Barrett [249] for fibres in longitudinally stressed wood.

The single-layer (fibrils in matrix of S_2) composite may, based on orthotropic

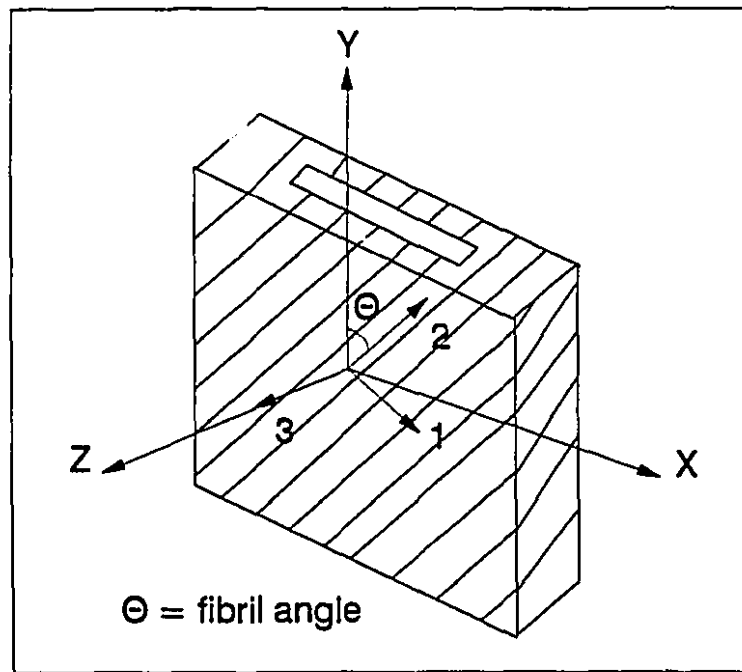


Figure 4.3: A wood fibre in its flattened form, defining the principal axes 1, 2, 3 of the S_2 layer and the fibre axes X, Y, Z (single-layer model concept after [70]).

elasticity theory [93], be considered to have orthotropic symmetry, i.e., the cell wall has three mutually perpendicular axes of symmetry, one in the fibril direction and the other two in the radial and tangential planes of the wall (see Figure 4.3). The stress-strain behaviour of the fibre could be related mathematically to the elastic constants of the cell wall material and fibril angle—an approach already undertaken by Mark [172] and to whose work the avid reader is referred for further details.

An important recent finding that we wish to make some mention of pertains to the elastic constants evaluation of cellulose (cf. Section 4.1.2 of this thesis). Tashiro and Kobayashi [274] have theoretically determined the three-dimensional elastic constants of cellulose crystalline form I, native cellulose, (as well as of form II, regenerated cellulose). The authors utilised lattice dynamical equations for calculating the constants and reported on the anisotropy associated with the latter. The calculated Young's modulus along the chain axis was found to be 167.5 GPa for native cellulose which was consistent with X-ray data previously obtained by the same authors (120–140 GPa). It was further found that Young's modulus was not affected by inter-molecular inter-

actions but by intra-molecular hydrogen bonds along the chain axis.

4.2.2 Fibre Strain Behaviour

Interest in stress-strain properties of single wood pulp fibres and tracheids has been tremendous, because of what they impart onto the properties of paper, board and other composite structures.

The phenomenon illustrated in Figure 4.4, which shows a fibre before and after straining, was observed in many fibres [214]. The figure clearly evinces fibre twisting under the influence of axial strain, even though its ends have remained firmly glued to their non-rotatable supports.² The development of this twisted appearance may be explained in terms of the structure of wood fibres and the theory of buckling of orthotropic shells: buckling theory predicts that the critical buckling stress is a function of the principal elastic constants of the fibre wall, the angle of the spiral winding and the fibre wall thickness. Furthermore, recall the analogy of wood fibres to spirally-wound, fibre-reinforced composite tubes (see Sections 4.1.1 & 4.1.2). Detailed studies of the properties of such tubes have been carried out and their stability under axial tensile strain was considered [236]. It was shown that, because of the development of shear stresses, buckling could occur. Along similar lines, Page *et al.* [214]—in the light of analysing ciné films and stress-strain records—had demonstrated that the shape of the fibre stress-strain curve was influenced by the onset of buckling. Fibres which exhibited no observable buckling had substantially linear stress-strain relations, but fibres that buckled gave sigmoidal curves.

Moreover, the stress-strain curve of single wood pulp fibres was found to depend on the fibril angle [212]: for low fibril angles, the curve is steep and substantially linear; for high fibril angles the curve shows a marked yield point followed by plastic deformation and a stretch-to-break as high as 20%. The mechanism of deformation of high-fibril-angle fibres was recognised to be the flow of the inter-fibrillar matrix under the induced shear stress. For fibres of 0° fibril angle, the load is borne as tensile load in the linearly elastic fibrils. However, for fibres of finite fibril angle, as the tensile

²Page *et al.* [214] provided scanning electron micrographs to support the latter statement.

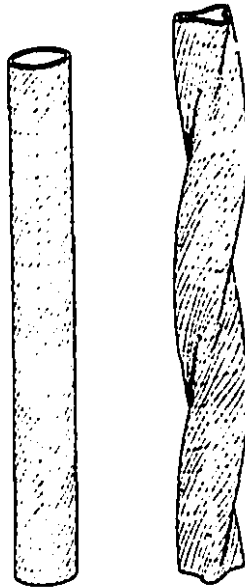


Figure 4.4: A schematic representation of the tension buckling phenomenon. Left, spirally-wound tube which, according to theory, buckles under axial strain to the form indicated on the right (adapted from reference [214]).

stress in the fibres rises, the coupled shear stress in the inter-fibrillar matrix increases as depicted in Figure 4.5.

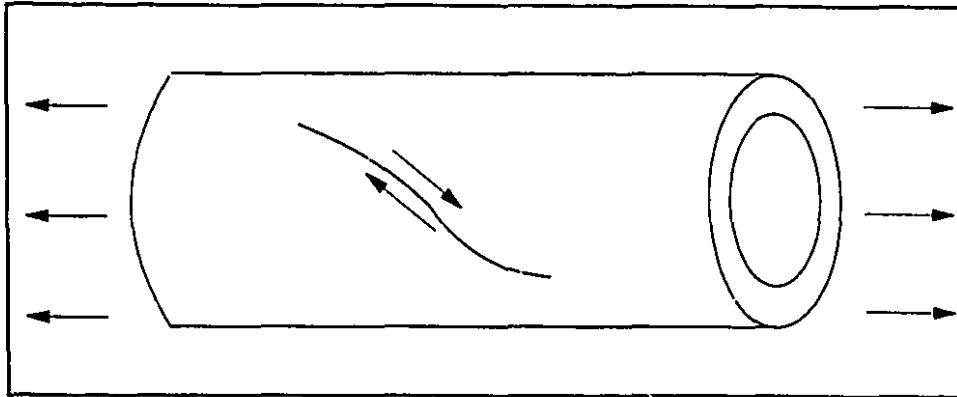


Figure 4.5: The direction of coupled shear stress in a fibre of high fibril angle, due to tensile strain (adapted from reference [212]).

Attention is drawn to the fact that when a fibre is subjected to tension, its cross-sectional shape changes [214]. This is a natural consequence of the application of tensile loading to a helically-wound hollow tube—referred to as tension buckling. It is worthwhile noting, too, that buckling under tension was primarily observed with thin-walled fibres; thick-walled fibres resist buckling because the critical buckling stress depends on the response of the fibre to bending stresses in the cell wall [212].

4.3 Mechanics of Fibrous Structures

In certain classes of fibrous structures the mechanical response to external loads largely depends on the loading behaviour between fibres. In, for example, sheets made of cellulose and viscose, in which fibres are randomly arranged, the hydrogen bond (hereafter H-bond) dissociation is one of the most significant parameters in their strength characteristics; albeit other factors such as humidity (water adsorption), temperature, etc. may contribute to the overall mechanical response behaviour.

Our aim is to concisely present a qualitative account of the mechanics of randomly-structured fibrous materials. However, we elected to elide any detailed mathematical manipulation, but rather concentrate on outlining the necessary background pertaining to the probabilistic approach to the mechanics of fibrous structures of cellulose sheets, in order not to get off course; viz.: An endeavour to set forth a modality for quantifying the outcome of our fundamental study on the fracture and fatigue characterisation of single wood pulp fibres, via *linking* the microstructural details to the macroscopic behaviour of the material. The probabilistic path naturally lends itself to the essence of the subject at hand, broadly stated: the modelling of crack initiation and propagation, as well as the formulation of the mechanisms of failure, in a multi-layered composite tube, i.e., the fibre.

The behaviour of single fibres and the effect of bonding between them at a fibre cross-over within a fibrous network may be modelled in light of the conceptual basis of probabilistic mechanics of discrete media — reference is made to some recent work dealing with a variety of materials, however, employing similar conceptual underpinnings; see, for instance, [19, 20, 22, 23, 150, 239, 240]. The deformational behaviour of a fibrous network may thence be assessed on three spacial levels, i.e., microscopic, mesoscopic and macroscopic, diagrammatically illustrated in Figure 4.6. Regarding field quantities as random variables or functions of such variables necessitates the use of the mathematical theory of probability, measure theory and topology, too. In accordance with the aforesaid, (mesoscopic) material operators need be established and, hence, for a domain in the material sample, the internal stress distribution could be found. In contrast to the continuum mechanics formulation which only leads to macroscopic stress values, the contribution due to the fibres and bonding between them results in the actual stress distribution.

4.3.1 Molecular Properties of Hydrogen Bonds

Generally, an H-bond occurs, if one hydrogen atom is bonded to more than one atom, say X, Y. If the two bonds H to X and Y have different strengths, the stronger is written as X-H (normal X-H bond), whilst the weaker one is designated by H....Y and

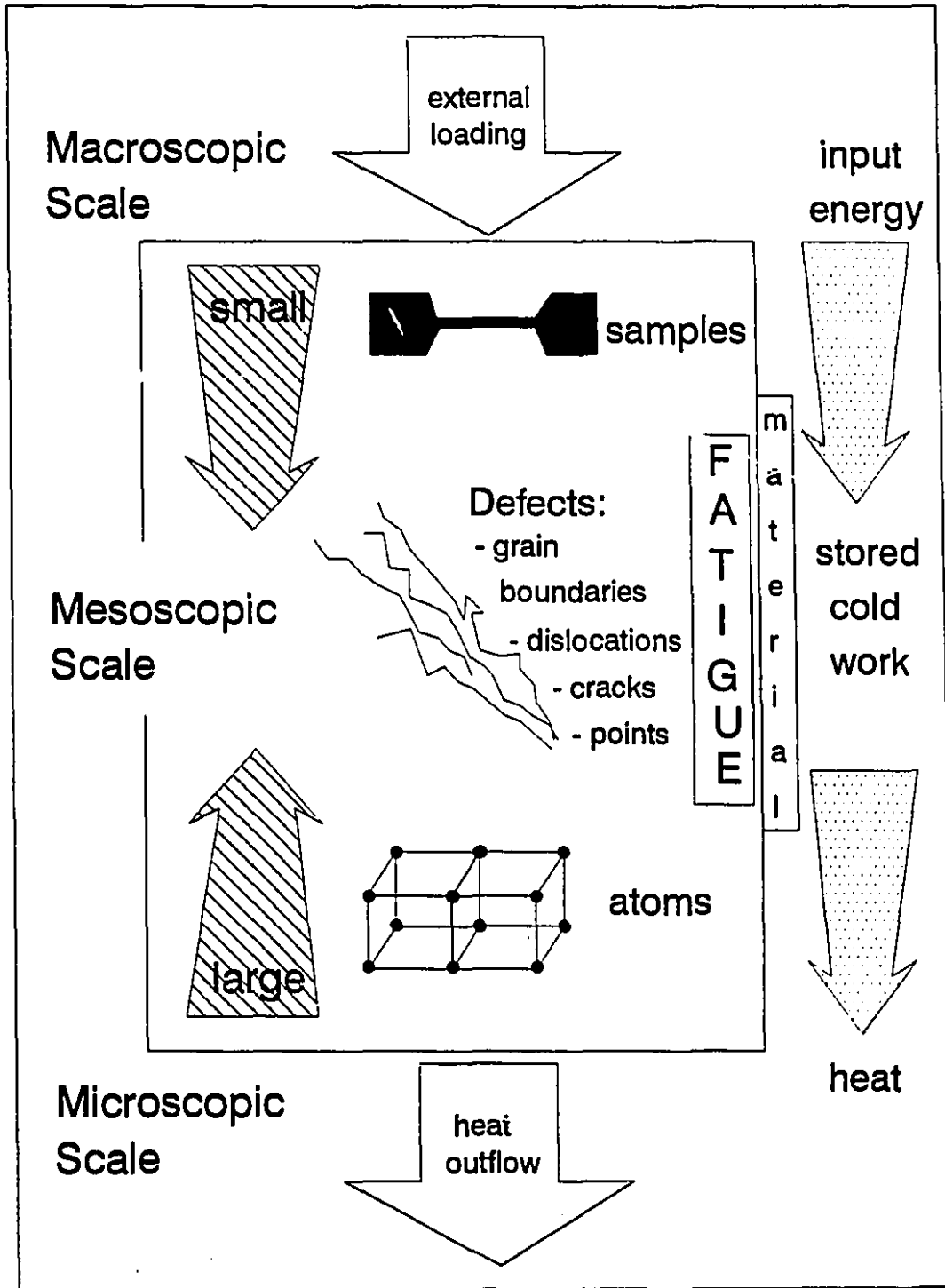


Figure 4.6: Three distinct length scales in which materials may be considered.

termed hydrogen or H-bond [252]. (For a comprehensive coverage on the theory of hydrogen bonding, the reader is referred to the aforementioned reference, from which the description below is derived unless otherwise stated.) In this case, the strength of H...Y can be associated with the "dissociation energy" of the complex X-H...Y. The H-bond forming the complex can either be symmetrical or asymmetrical depending on whether the surface energy for the proton between atoms X and Y is symmetric or not. The H-bond is intra-molecular or inter-molecular, depending on whether the atoms X and Y belong to the same molecule or not — the term molecule is thus understood in the chemical sense. From a physical stance, each inter-molecular bond forms a larger molecule or complex that exhibits its own force constants, chemical reactivities, etc. If the complex forming molecules are of the same type as, for instance, water, the inter-molecular association is referred to as "self-association". However, if the molecules are of different type then the association is called "mixed association".

The typical molecular structure of cellulose is illustrated in Figure 4.7 below. Apart from the inter-molecular bonding present in this type of bond, intra-molecular bonding must also be considered in order to account for the spacial configuration of the bond [21]. X-ray data [85, 103] on cellulosic systems show that cellulose in natural fibres partially or completely crystallises with the fibres in such a manner that "unit cells" are formed. These cells are repeated in form of a chain.

Referring to Figure 4.7, the unit cell is composed of two (β -D) glucose residues which are linked by the oxygen bridge to adjacent residues and are also rotated with respect to one another about a screw-axis so that they form continuous chain segments. In addition, there is an intra-molecular bond between the hydroxyl group of one glucose residue and the oxygen ring of the next residue. In order to form a bond, it is necessary for the neighbouring glucose units to be rotated around the glucose linkage resulting in a "bent" conformation [218].

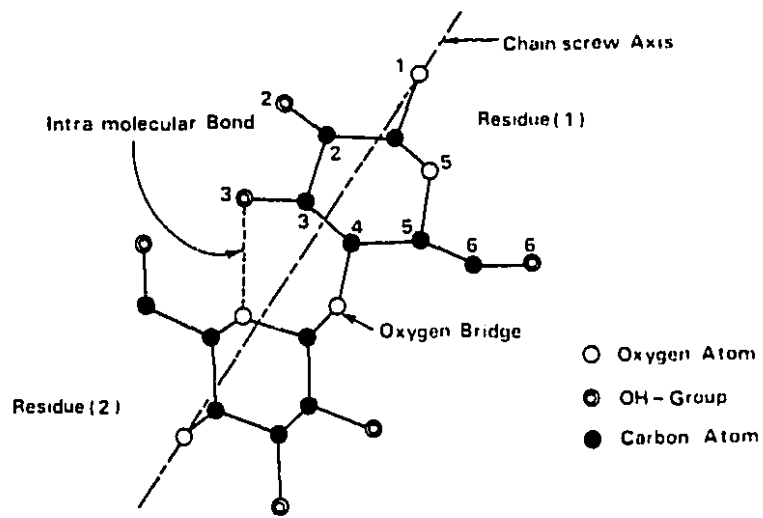


Figure 4.7: A structural model of repeating unit cells of natural cellulose (adapted from reference [123]).

Chapter 5

Fatigue of Wood

5.1 Fatigue Characterisation in Refining

The mechanical degradation of wood in the form of chips or logs into a pulp suitable for papermaking is a highly specialised attrition process whose principal objective is to separate the fibres while retaining their integrity.¹ This process consumes significant amounts of energy [244]; however, only a small portion of the energy input into the system is actually utilised in the separation of fibres [13, 157, 277]. Furthermore, if the fibres produced are to be suitable for papermaking, it is necessary to induce a certain amount of mechanical flexing and surface fibrillation into these fibres [265]. This may be accomplished by the cyclic deformations to which the wood or chips are subjected — while between the discs of mechanical refiners — during the fibre separation process: the former ranging from small viscoelastic to large plastic deformations [245]. The viscoelastic deformations, by definition [7], only produce heat in the system, whereas it is the plastic deformations that are basically responsible for making the fibres flexible.

Fatigue may hence be regarded as a process whereby the cumulative breakdown of the structural components takes place, as a consequence of the cyclic mechanical treatment. This structural breakdown is believed to be related to the fibrillation and flexibilisation of the fibres. It is further thought to occur in the refining zone

¹Refer to Chapter 3, Section 3.3.1 for details on aspects of mechanical refining.

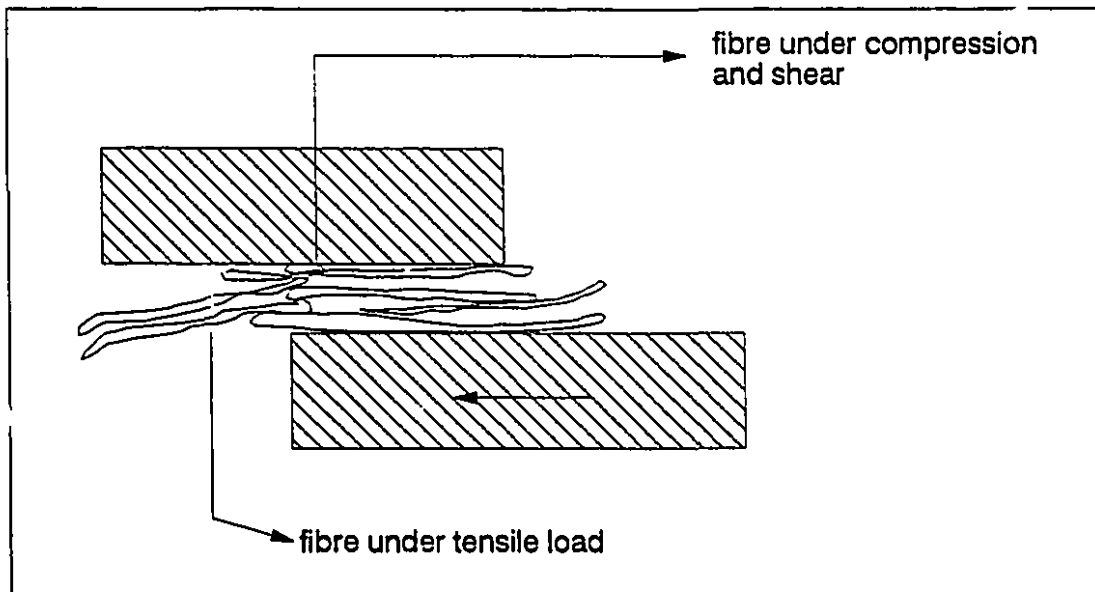


Figure 5.1: A schema illustrating an impression of fibres trapped between the passing stator and rotor bars of a disc refiner. The stresses that the fibres experience under these conditions are responsible for the cumulative fatigue damage phenomenon.

of a mechanical refiner [132]. Essentially three principal, cyclic-type forces are in action (see Figure 5.1), viz.: *uniform shear*, *radial* (i.e. across the fibre) *compression and tension*. The structural breakdown of wood is reflected in changes in its elastic modulus, thereupon, *fatigue* may be defined as *the total permanent change in the elastic modulus in the loading direction as a function of the cyclic loading* [246].

Basic studies on the mechanical behaviour of wood with reference to defibrisation have mostly been focussed on rupture properties [13, 18, 147], or on the viscoelastic properties of wood [243, 244, 245, 246, 247]. Earlier work had concentrated on examining the influence of the softening temperature of the wood, and the efficiency of the process of defibrisation was attributed to the position of this transition. The softening of the wet wood largely reflected, as it was suggested, the softening or glass transition of the wet lignin. This softening would thus play an important role in fibre separation and, consequently, the surface characteristics of the fibre [25, 147]. However, no direct linkage between the softening temperature or viscoelastic properties

of wood and the latter's behaviour under mechanical action, was proposed. In order to be able to better expound how wood would behave when defibrated, it would be essential to study the wood material under plastic deformations, i.e., to understand the cycle-by-cycle variation in the stress-strain behaviour of the wood material at the most highly strained region. In other words, to study the fatigue life characteristics of wood. Salmén and Fellers [245] were first to make use of this concept: studying the fatigue properties of wood under environmental conditions emulating defibration.

5.2 Fundamentals of Energy Consumption and Mechanical Deformation of Wood

Salmén *et al.* [247] defined fatigue in wood as *the relative loss in elastic modulus*. From the foregoing, it becomes evident — as it is characteristic of classical fatigue-type behaviour — that the higher the stress amplitude, the lower is the number of cycles needed to cause failure, i.e., to reach a given relative loss in modulus. Indeed, the latter was corroborated by a series of tests performed by Salmén *et al.* [243, 244, 245, 246, 247] on dumb-bell shaped samples of wood² subjected to cyclic compression — both along and across the grain — under water-saturated steam conditions at temperatures varied between 20° and 160°C.³ Moreover, the fatigue process may be characterised by decrease in the elastic modulus with the number of cycles; the higher the stress amplitude, the higher is the efficiency of the process. Upon relating the relative loss in elastic modulus to the energy absorbed by the wood in the fatigue process, it was realised [247] that the efficiency of the fatigue process, i.e., the breakdown of wood, was greater for the first cycles and that the decrease was inversely proportional to (a power of) the energy absorbed in wood.

When a viscoelastic material like wood is subjected to a loading-unloading cyclic action, at small deformations, the material follows a hysteresis loop when examin-

²Heartwood of Norwegian spruce, *Picea abies*, with necks of cross-section 10x15 mm for tests along the grain and 15x50 mm across the grain.

³Mechanical defibration in refiners and grinders generally takes place at temperatures between 100° and 160°C [12, 29].

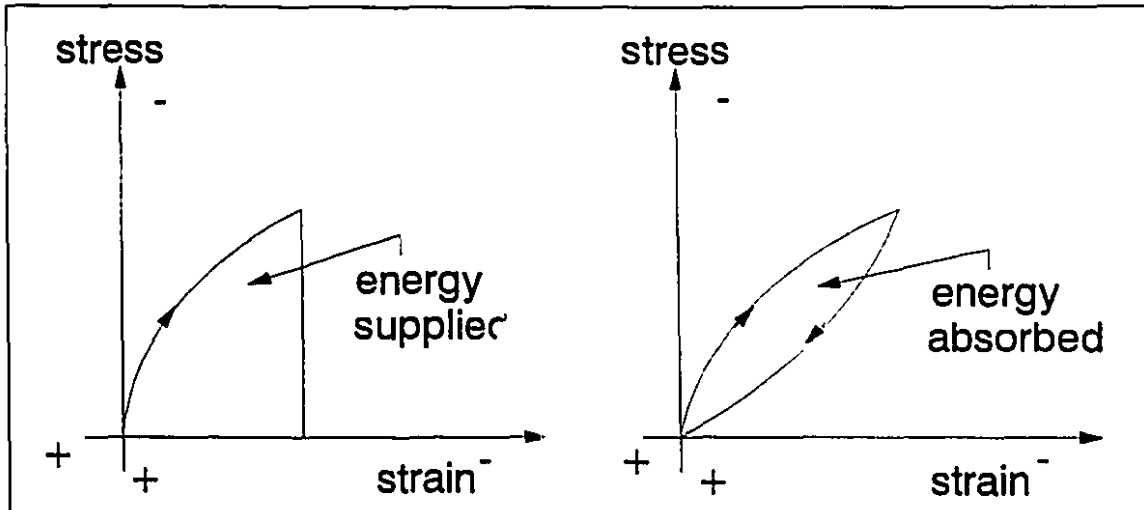


Figure 5.2: A diagrammatic depiction of the energy supplied to a sample of wood in cyclic compression, and the energy absorbed in one cyclic compression (adapted from reference [247]).

ing its stress-strain behaviour. The energy taken up by the material is represented by the area under the loading part of the stress-strain curve of the cyclic deformation, schematically depicted in Figure 5.2. During unloading of the wood, energy is given back to the system, the extent of which is dependent on the process concerned. Therefore, to remove any process-dependency, Salmén *et al.* [247] prudently related the deformation of wood only to the energy absorbed within the wood — represented by the area within the stress-strain curve described in cyclic loading and unloading (refer to Figure 5.2). The energy is only partly consumed in processes that structurally change the wood, since the largest portion is lost as internal frictional heat due to viscoelastic deformation.

To offer a suitable reasoning for the viscoelastic behaviour in wood, Salmén and Fellers [245] suggested, based on their experimental findings, the following: Along the grain, the reinforcing cellulose microfibrils diminish the role of lignin as a load-bearing component and hence reduce the energy losses in the lignin. In the perpendicular direction, however, the stress is transferred through the middle lamella making the energy losses in the lignin much more pronounced.

If cycling is further carried out to larger deformations, the material will thence

experience plastic deformation. In this case, there will still be a viscoelastic component, and it may thus prove exceedingly difficult to relate any area under the cyclic stress-strain curve to the consumed plastic energy. Salmén and Fellers [245] concluded from their tests that a large portion of the non-linear part of the stress-strain curve was reversible and must therefore be attributed to non-linear, viscoelastic deformation. This then demonstrated the almost "impossibility" of determining the amount of plastic energy input to the system. Energy absorption could only be inferred from the material changes: structural changes in the lignin or structural breakdown in the microfibrillar structure making the lignin a more important load-bearing part. The influence by a litany of factors on the mechanical response of wood subjected to cyclic loading is briefly explicated below.

5.2.1 Temperature Dependence

Temperature is one of the parameters which varies between different mechanical defibrisation processes and affects the produced pulp. Salmén *et al.* [247] suggested that, generally speaking, the higher the treatment temperature of the fatigued wood, the more efficient is the structural breakdown. (Refer to Section 5.2 for details on testing conditions.) This behaviour is indeed not dissimilar to other polymer materials [42, 227, 228]. It was further shown experimentally that the most efficient mode of loading, i.e., along or across the grain, was dependent on the treatment temperature [247]. At 80°C, mechanical loading across the grain seemed to be more effective than loading along the grain, whereas at 100°C the opposite was true. Contrariwise, when examining the situation globally, loading along the grain at high temperatures seemed to be the most effective treatment. This could largely be attributed to the fact that at temperatures above 100°C the lignin feebly buttresses the fibre wall and hence the latter easily buckles along the grain, thereby reducing its modulus at a low energy input level.

5.2.2 Frequency Dependence

Owing to the viscoelastic nature of wood, its mechanical behaviour will be dependent on the frequency of the mechanical action. Also, the softening temperature of wood increases with frequency—a recognised fact in refining [29]. Frequencies at which mechanical defibrisation in refiners occurs are in the kilo-Hertz (kHz) range [12, 29]; appreciably higher than what could be achieved in laboratory studies of the controlled mechanical deformation. Thereupon, to recognise structural changes in fibres at relevant frequencies, viz.: fibre flexibilisation during refining, it becomes necessary to generalise the data from the frequency-dependent fatigue-testing of wood into functions spanning large frequency ranges. This may be accomplished by constructing what is termed as “master curves” in order to facilitate the extrapolation of results at low frequencies to the relevant (much higher) ones of mechanical pulp production. This concept is not novel, and has widely been used in research dealing with viscoelastic materials, e.g., polymers (see, for instance, [100]). The construction of master curves means that a property is obtained as a function of frequency at various temperatures; the curves thus obtained are shifted with respect to the frequency axis to form a single curve at a reference temperature which spans a large frequency range.

For completely-saturated woods, viscoelastic properties could, too, be generalised into the form of a master curve which follows the laws of viscoelastic polymers [242]. Salmén [243] pursued an investigation of the effects of frequency of a mechanical treatment of the fatigue of water-saturated wood (under conditions previously described in Section 5.2), along identical lines to what has been canvassed hereinbefore. He concluded, having studied the influence due to temperature variation from 80° to 140°C at frequency values of: 0.1, 0.5 and 5 Hz, that the fatigue of wood was elevated by higher temperatures and lower frequencies. This is indeed similar to the fatigue behaviour of polymers, where the *crack growth rate*—which is a measure of the specific structural breakdown along a crack [229]—decreases with increasing frequency at a given stress amplitude (see, for instance, [255, 154, 223, 155, 148, 149, 156, 151] and [192, 24, 130, 228, 164, 165, 35, 291, 104, 7]). Concomitantly, temperature–frequency equivalence typifying fatigue characterisation of wood makes possible the extrapo-

lation of low frequency measurements so as to predict higher frequency behaviour (refining frequency occurring in the innermost zone of the breaker bars corresponds to around 3000 Hz [29]). Hereupon, it could be anticipated that an increased temperature and a reduced frequency might lower energy consumption in the production of mechanical pulp.

5.2.3 Effects of Loading Mode

What is the most effective loading mode? If a comparison is to be made between the effects of mechanical loading along and across the grain at a particular energy input, available experimental evidence [246] demonstrates that temperature has a considerable influence. At 80°C, mechanical loading across the grain seems to be more effective than loading along the grain, whereas at 100°C the reverse holds. Nonetheless, examination of the overall picture reveals that loading along the grain at high temperatures seems to be the most effective treatment.

5.2.4 Effects of Sulphonation

Wood chips are normally treated with sulphite prior to refining in order to lower the softening temperature of the wood, this will, in turn, result in producing more fully separated fibres. Consequently, chemimechanical pulps contain more long fibres and less shives than those of mechanical refining produced from untreated chips. On the other hand, the energy requirements for producing chemimechanical pulps is roughly similar to that for mechanical pulps—considering chemimechanical pulps with a degree of sulphonation below 1.2% SO_3^- based on dry wood [10]. For such pulps, the strength and density are also about the same as those of the corresponding refiner mechanical pulps. It is only when chips are sulphonated to sulphonate contents above 1.2% that tensile strength and density increase, and the energy requirements become lower than that needed to produce comparable mechanical pulps [10].

In this respect, changes in the properties of the pulp with increasing sulphonation may partially be ascribed to the fact that the secondary wall lignin behave differently in terms of how the viscoelastic properties influence the fibre separation process and

achievable fibre flexibility under different conditions of sulphonation [244]. In light of the aforesaid, a difference might expectedly be observed in the viscoelastic properties of wood measured along and across the grain. Therefore, based on this reasoning, Salmén [244] proceeded, using mechanical spectroscopy to test unsulphonated and sulphonated wood samples both along and across the grain, to study the structural properties in order to explicate the relationship between viscoelastic properties and sulphonation. This approach is deemed necessary, if a better understanding of the mechanisms involved in refining is sought. The conclusions arrived at may be summarised as follows. Below 1.2% SO_3^- , the relative reduction in elastic modulus, i.e., fatigue, is the same as that of untreated wood; whereas above 1.2%, the fatigue is much higher at a given number of cycles. For the latter case, the sulphonation has resulted in reducing the energy requirement for the material degradation of wood to take place. In examining the viscoelastic properties of sulphonated wood it is recognised that, apart from lowering the softening temperature, there is a large reduction in modulus for high degrees of sulphonation, too. It may well be that the latter which is the prime contributor to influencing the energy requirements in refining.

5.2.5 Fibre Flexibility

Fibre flexibility is an important pulp property in the manufacture of paper. It is known to influence the behaviour of the pulp suspension from which paper is made, the drainage characteristics of the sheet forming process, the strength of the wet fibre network, and the strength and optical properties of the final paper [269]. The flexibility of any solid body, such as a pulp fibre, may be defined as the inverse of its stiffness, EI , where E is Young's modulus of elasticity — a material property, and I is the area moment of inertia — a geometrical property.

The development of fibre flexibility and other fibre properties during refining occurs through the conversion of mechanical energy into work done on fibres. A number of hypotheses have been proposed to explain this energy transfer from refiner to refiner, but the exact mechanism has *never* been conclusively confirmed by experiment.

One way to examine the flexibility of single pulp fibres, is to perform small-

amplitude, transverse bending, i.e., flexing, of fibres. By measuring the changes in the fibre flexibility caused by this type of loading, an insight into the role of beating may be gained.⁴ Tam Doo and Kerekes [269, 270] devised a simple experimental method to measure the absolute flexibility of wet pulp fibres. They concluded, from a series of tests on several pulp species, that there was a consistent decrease in stiffness with cyclic, small-amplitude flexing, suggesting an important role in beating and refining.

Pondering all that has been canvassed thus far, one *à fortiori* deduces that: the structural changes during cyclic loading of wood indicate a process whereby fibres are believed to become more flexible due to the breakdown of the internal fibre structure. The succeeding chapters will treat in detail the fundamental task of testing single wood pulp fibres under cyclic loading, and the pertinent conclusions derived thereof.

⁴N.B. Beating is the older term reserved for the mechanical treatment of pulp at low consistencies, but beating and refining have now become synonymous.

Chapter 6

Scope and Aims of Thesis

It has been tersely stated in Chapter 1 that the crux of this research endeavours to determine and characterise the fatigue-failure mechanisms and morphological behaviour of wood pulp fibres subjected to cyclic mechanical action. Bearing in mind the gist of what has been canvassed throughout the preceding five chapters — while emphatically re-iterating the fact that the structural breakdown of the fibres is thought to occur in the refining zone of a mechanical refiner, where essentially three principal cyclic-type forces are active: uniform shear, radial compression and tension — we shall indulge hereunder in thoroughly enunciating the specific objectives to be pursued.

1. Because of their premier role in papermaking, the current study focuses on establishing the fundamental material property degradation characteristics of single wood pulp fibres subjected to the application of cyclic action. In this regard, the following particulars need be elucidated:
 - (a) What are the forms in which material damage takes place and the relation, if any, between these forms; and how is the extent at which damage accumulates related to wood species, pulping type, refining energy, or number of cycles?
 - (b) Based on the engendered forms, one needs to expound the underlying theme(s) responsible for material degradation, i.e.: the recognition, first, of the regions where damage occurs (viz., regions of high localised deformation) and, subsequently, the form of crack growth as well as the general

weakening of the material, due to structural damage or chemical degradation. This will determine whether there is indeed *true* fatigue-failure; in retrospect, we will have specifically elucidated the micro-mechanism(s) of damage accumulation and failure in accord with the chemical composition and physical structure of those filamentary-wound, composite tubes.

It is important in studying fatigue to try and sort out which of these various factors are effective, and not to necessarily require all the results to be explained by a single mechanism. Our first task must therefore be to see how this group of motley effects can be recognised: We shall then be in a position to examine experimental data and see how indeed the initiation stage commences, and any other subsequent stages, before failure actually materialises.

2. In pursuance of determining a detailed anthology of the aforementioned, a comprehensive experimental methodology must be instated, whose characteristics are:
 - (a) The capability to perform either displacement- or load-controlled, constant-amplitude fatigue-testing. However, the minute dimensions of the fibre specimens in question impose restrictions on the size of the device to be designed, the *single-fibre tensiometer*. It should be stated, for clarity's sake, that *no* other such device exists, whether commercially or solely for research purposes, for fatigue-testing of single wood fibres. Moreover, to test the single fibre under cyclic shear, radial compression and tension, a mechanism unique for each mode of loading need be designed as part of the tensiometer assembly, so as to ensure satisfying the loading condition while maintaining easy adaptability of the set-up. A reliable, secure and robust modality must, too, be integrated into the loading mechanism for the purpose of mounting these delicate, minute fibres.
 - (b) It is mandatory, for reasons of proper and accurate coordination and control of the fatigue-testing process, that the entire set-up be automated.

3. In order to obtain information on the morphology and structural behaviour of fatigued fibres, a microscopical study must be performed if answers to the questions raised in (1) are to be provided. Our opting for a state-of-the-art technique, *confocal laser scanning microscopy*, is necessary for the following reasons:

- (a) While notions of surface morphologies are required for explaining some of the questions raised hereinbefore, knowledge of what happens inside the fatigued fibre—i.e., changes in cross-section as well as along the interior layers of the fibre cell wall—is of equal significance. That is to say, sectioning of the fibre need be done, which may only be achieved non-destructively using confocal scanning microscopy. In this manner, it will be possible to construct a three-dimensional image of the fibre by adding two-dimensional scans. This will, as attested to later on, accrue tremendous information in abetting the analysis of the morphology and structural integrity of the fatigued fibres.
- (b) The fact that we need to test pulp fibres in conditions similar to refining, i.e., in saturated form and at high temperature, would exclude the utilisation of scanning electron microscopy for *in situ* observations and acquisition of micrographical images—owing to the necessity to place specimens inside of a vacuum chamber.¹

4. In parallel with the experimental developments, a theoretical analysis need be performed to qualitatively assess the effectiveness of the proposed mounting-fixation and loading mechanisms. This necessitates the three-dimensional geometric modelling of the fibre, and the choosing of a suitable numerical technique—finite-element analysis. The latter has the distinct advantage of enabling to

¹Although we are aware of the fact that the fibres could be treated with substances such as glycerol before being placed in the SEM, we can, at this stage, make no learned judgment as to what effects the glycerol has on the chemical composition, or structural breakdown, of the fatigued fibre. Hence, any such adoption without first recognising all possible effects, would only confound an already complex issue.

garner knowledge of the strain behaviour — which may only be qualitatively examined at this stage; however, may subsequently be improved upon to undertake full-fledged quantification of the material property degradation phenomena.

5. At the completion of all of the aforesaid and once a comprehensive analysis of the experimental outcome is accomplished, contribution, based on microscopic considerations, to advancing the theory of fibre development may thence be realised.

Chapter 7

Experimental Methodology

7.1 Prelude

Let us recall that, while between the discs of mechanical refiners, wood pulp fibres are subjected to the repeated loading action of the refiner bars. This loading action can be classified into three principal cyclic-type force actions, viz.: uniform shear, radial compression and tension (refer to diagrammatic representation in Figure 5.1 of Chapter 5). Each case shall be studied individually and pertinent conclusions accordingly made. Specifics of the modality, design and performance of the components of the novel experimental technique are detailed in succeeding sections. However, before doing so, it is deemed essential to indulge in a terse exposition of the meaning of fatigue-failure *vis à vis* fatigue-testing.

A necessity arises to clearly distinguish what phenomena are involved when studying fatigue of materials; indeed, to discover whether there is anything that can properly be called fatigue. This is more than a mere quibble; for the word fatigue has been rather loosely utilised, by some aloof to the field, whenever discussing the behaviour of materials—be them polymeric or otherwise. A useful distinction would be: fatigue-testing covers a variety of experimental procedures, whereas fatigue-failure implies a specific mechanism of rupture. An elaboration follows.

Fatigue-testing may primarily be defined as the subjection of specimens to cyclically varying stress or strain ultimately leading to breakage. This definition excludes

dynamic tests which do not cause breakage, and eliminates, too, the failure of a specimen after some time under a constant load. The latter type of testing is often referred to as a creep test ultimately leading to the breaking extension, with the breaking extension as well as the nature of the breakage being perhaps dependent on the type of test, and may be taken as a function of the time to break [36, 111, 268].

On the other hand, deformation and damage imparted on an imperfectly-elastic material during fatigue-testing may be classified into two sorts. Firstly, there could be effects which are incidental to fatigue-testing, in the sense that they can, in principle, be predicted from a knowledge of the stress-strain-time and recovery properties obtained in other simple tests. Such effects may include: (i) continuing deformation resulting from imperfect recovery in successive cycles; (ii) continuing creep and stress relaxation effects; (iii) rise in temperature, and its effects, resulting from the loss of energy in cyclic deformation. Secondly, there may be effects which are peculiar to the fact that stress is repeatedly applied and removed. These may include: (i) true fatigue-failure due to some form of crack growth, often limited to regions of highly localised deformation; (ii) general weakening of the material, due to structural damage or chemical degradation. This study concerns this latter type, as the results of the next chapter shall vindicate.

7.2 Philosophy of Experimental Approach

Owing to the properties of cellulosic fibres subjected to varying stress, namely, imperfect recovery due to viscoelastic and plastic deformations, constant-amplitude, displacement-controlled fatigue-testing is the methodology selected to characterise the fatigue fracture mechanism(s) of wood pulp fibres. The choice is apposite since, in this way, the force reactions of the specimens — whose magnitude is rather vague to us at this stage — will continuously be monitored, while feeding into the system the appropriate displacement imposed on the fibre specimens, which is precisely delivered via the computerised control set-up. Referring to Figure 7.1, the fully-automated experimental set-up may be divided into two groups: the *in situ* apparatuses and the accompanying electronic hardware. The former comprises the *single-fibre tensiometer*,

designed and built in-house, in conjunction with the *confocal laser scanning microscope (CLSM)*; whereas the electronic hardware include the controller of the testing procedure, the *microcomputer*, along with the necessary periphery to operate devices and to convert and adjust signals; others for the purpose of data acquisition.¹

Prior to commencing the manufacture of the principal fatigue-testing apparatus, the single-fibre tensiometer, it was necessary to engage in a thorough study of the most efficient way to securely mount fibres without inducing unnecessary stresses which could cause localised damage. Moreover, since there were only intuitive deductions, from indirect experimental evidence, as to what the fibres actually experience whilst between the discs of mechanical refiners (refer to Chapters 3 and 5), it is deemed paramount to perform a conceptual analysis of what to anticipate; hence, be better equipped to design the necessary gadgets and, furthermore, be able to project an approximate modality for fibre behaviour under cyclic loading emulating conditions of a mechanical refiner. With the aforesaid in mind, three-dimensional, finite-element modelling and analysis of a single fibre subjected to uniform shearing action were initiated. The model consists of a quarter fibre (due to geometrical symmetry), clamped from one end, and whose surface is subjected to simultaneous, uniform tangential displacements.² The linear finite-element analysis reveals that highly strained regions occur at surface areas where shear contact is instigated, and the former are oriented longitudinally, i.e., along the fibre axis — refer to Figure 7.2.

The model is fairly sophisticated in the sense that careful consideration is made of the composite nature of the fibre wall material, and special provisions are included in the model to simulate wall layer separation. The engendered results indicate that if mounting of the single fibre is to be performed meticulously, then, strictly speaking, *no* significant (unnecessary) stresses will be induced in the fibre body due to mounting. Hence, with extreme care during each step of preparation and testing, one would be

¹The electronic periphery has principally been inherited from past research projects at the Fracture and Fatigue Control Laboratory, however, essential, significant modifications were carried out to make it conform to the needs of the current research. It should also be noted that all the components, except for the microcomputer, were built in-house.

²The full scope of the finite-element modelling, analysis and results is discussed in Appendix A.

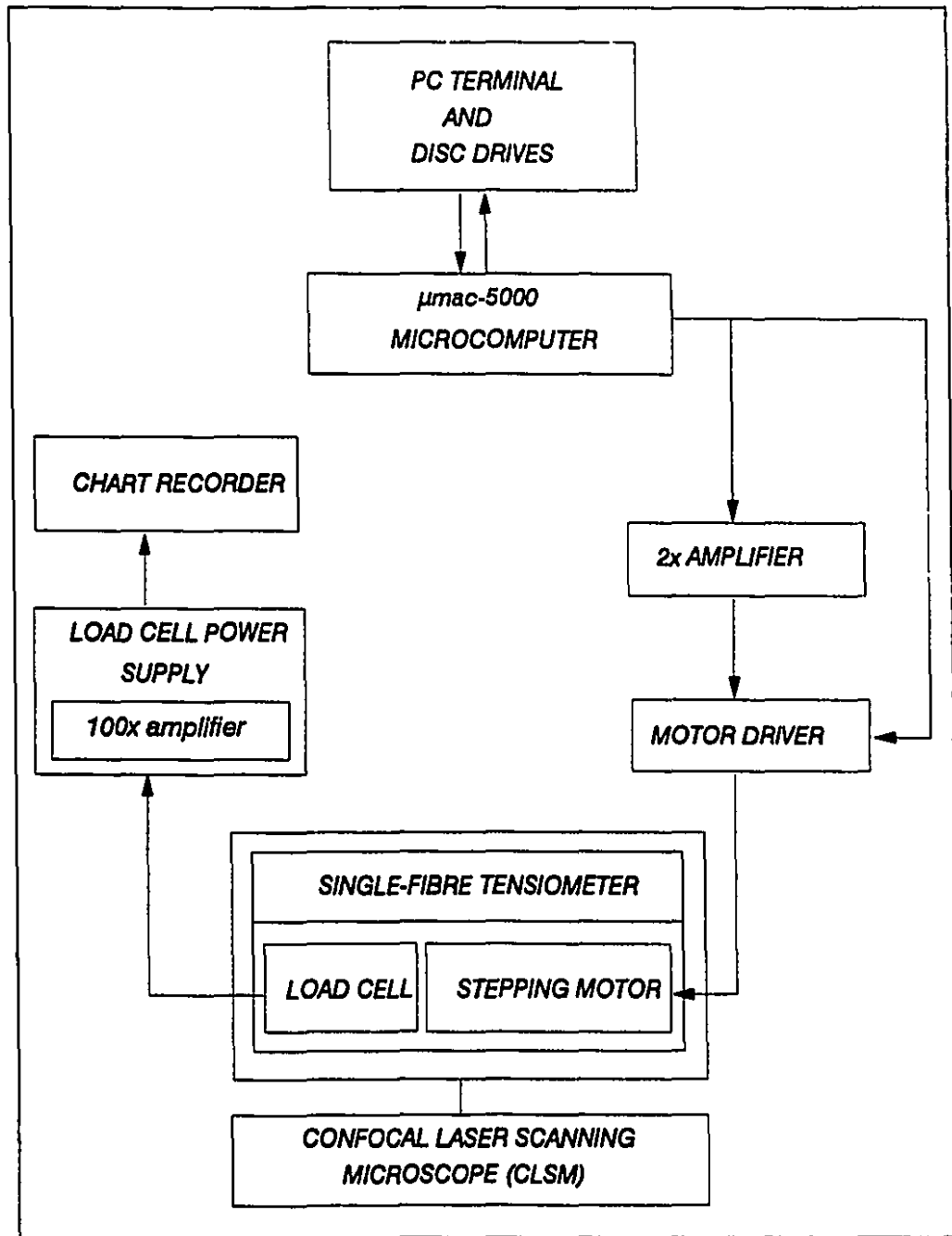


Figure 7.1: Testing system block diagram.



Figure 7.2: Strain distribution of a two-layered wood fibre subjected to uniform tangential displacement (5% of the fibre length), and has a fibril angle of 20° . The picture shows one-quarter of the fibre owing to geometrical symmetry of the structure (for further details, refer to Appendix A).

safe to assume that structural and material changes imparted on the fibre are wholly a consequence of applying the cyclic loading.

Henceforth, we proceed, while taking cognisance of the above, to discuss *in extenso* the functional determinants, design parameters and operation of each of the experimental constituents.

7.3 The Single-Fibre Tensiometer

The philosophy behind designing this device, whose prime characteristic is its miniature size,³ is dictated by both the minute size of the fibre specimens and the fact that it has to partly fit under the CLSM. The device has the capability to perform under displacement or force control, manual or automatic operation. It is essentially designed and constructed to specifically correspond to the needs of the current research; nonetheless, fairly straightforward adaptability to testing different materials and geometries is ensured by constructing the device in compartments which can be mechanically disassembled.

The tensiometer, depicted schematically and pictorially in Figures 7.3 and 7.4, respectively, is structured in such a way as to have an *observation compartment*,⁴ so to speak, which accommodates the loading jaws and load cell; and a *peripheral compartment* in which the stepping motor is situated, with the latter being connected to the load cell and the jaws via a shaft (13.5 cm long). The (horizontal) structural format is partly necessitated by the geometry of the microscope in use (see Figure 7.14), and by the need to have a support/stage mechanism in which the motor resides (details pertaining to the support/stage mechanism is found in Section 7.4.2). Furthermore, the observation compartment is characterised by having an open space, providing easy access to the components therein, and, needless to say, a must for allowing observation of the fibre specimen during testing. (This is also advantageous for any future modifications, for example, the inclusion of a humidifying mechanism to control the ambient moisture content within the immediate vicinity of the fibre.)

In what follows, a thorough description of each of the prime constituents of the tensiometer is provided.

³Actual dimensions are: 28 cm x 4.7 cm x 1.6 cm, and the material from which the tensiometer is made is steel.

⁴Whose dimensions are: 8.6 cm x 4.7 cm x 1.6 cm.

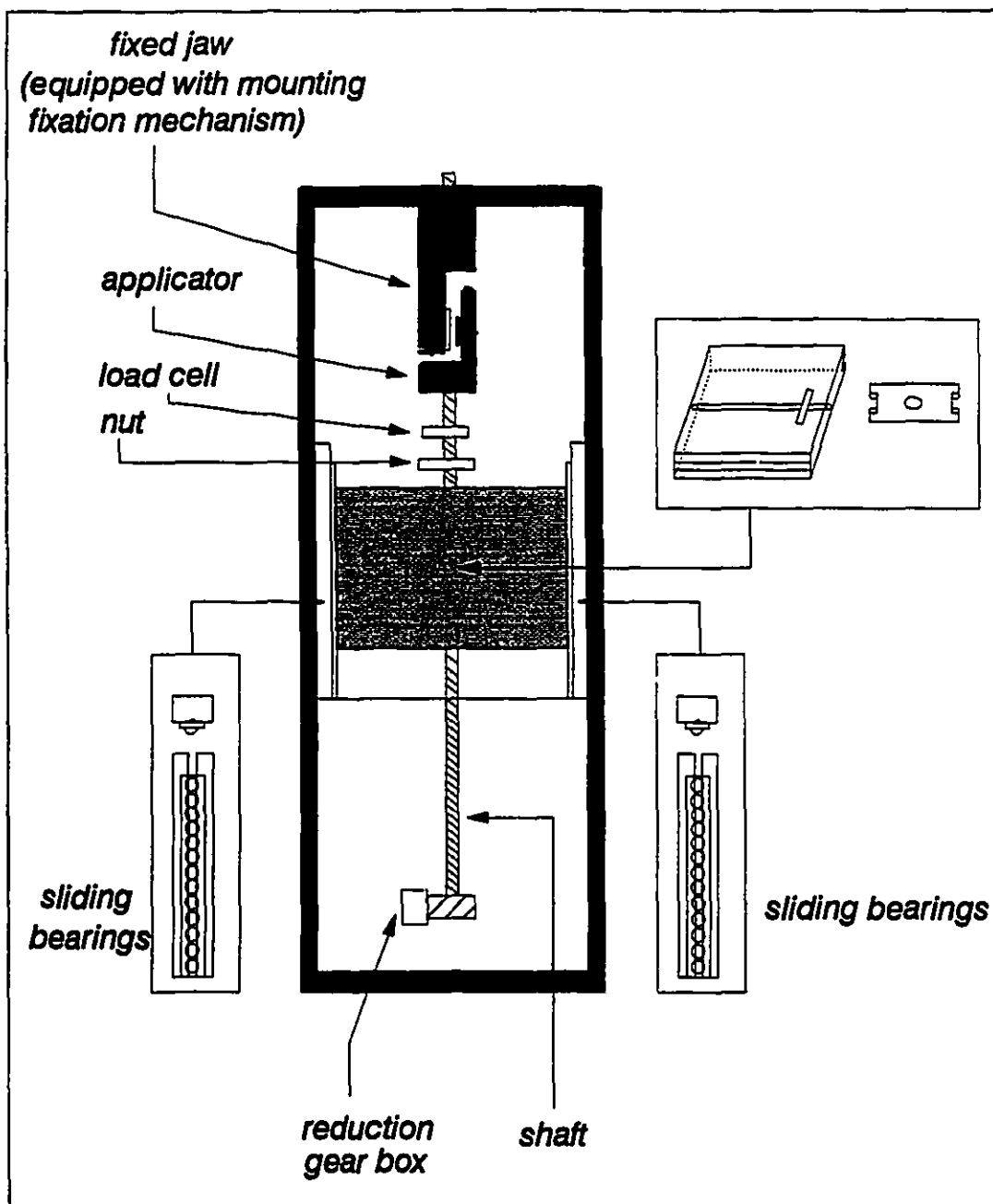
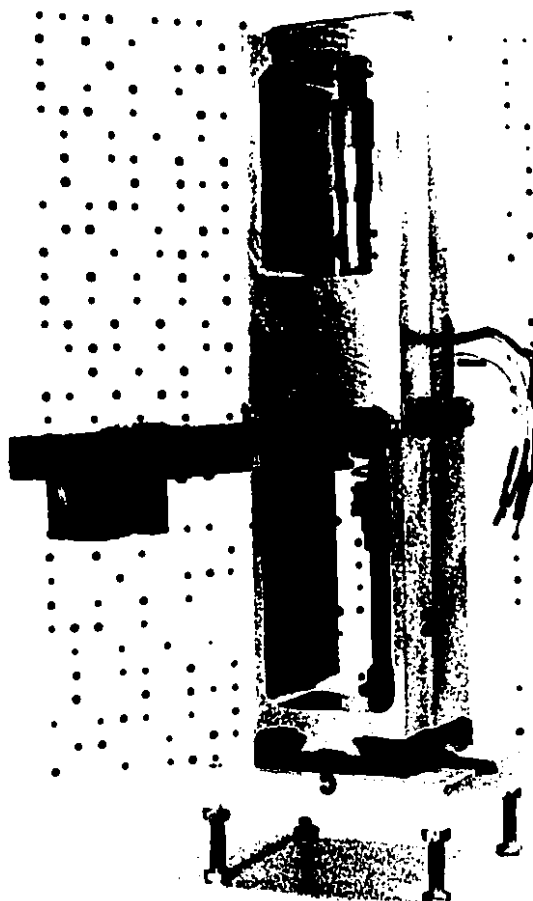
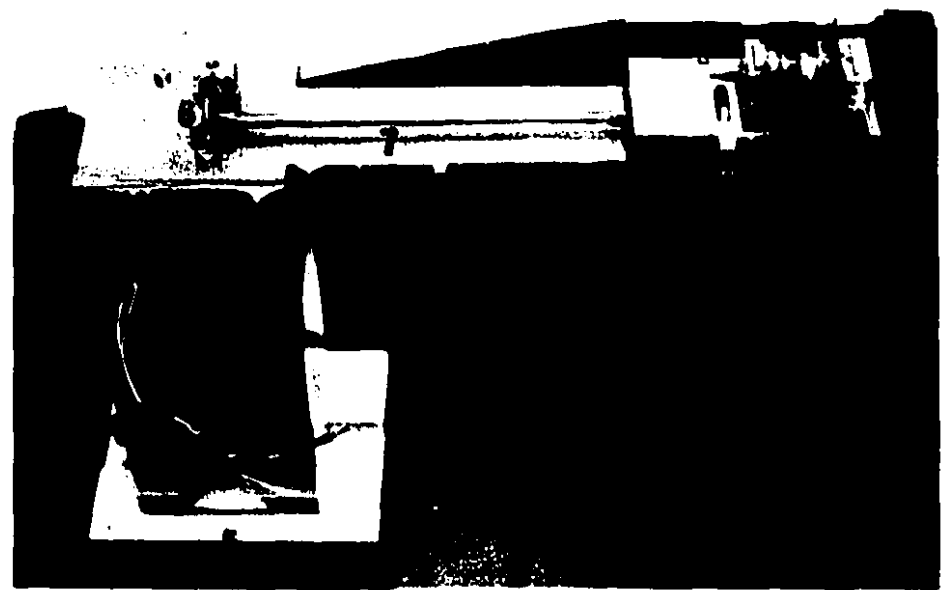


Figure 7.3: A schematic diagram of the single-fibre tensiometer used for fatigue-testing wood pulp fibres.

Figure 7.4: A photograph showing the single fibre tensiometer residing in the support/stage mechanism, specifically designed to allow movement in the horizontal plane, and vertically, accurate to 1 μm using a sensitive micrometer screw-head.



1. Single-fibre tensiometer
2. Support/stage mechanism
3. Stepping motor (inside)
4. Micrometer screw head
5. X-Y stage
6. Reduction gear box
7. Shaft
8. Observation compartment



7.3.1 Loading Jaws

The principal components of the tensiometer, and the ones that require both, an insight into the proposed modes of testing, and extraordinary care in design and manufacture, are the loading jaws. Since the tensiometer operates in just one mode,⁵ i.e., the shaft, connected from one end to the stepping motor and reduction gears, solely advances and recedes upon operation, then to emulate whatever loading action, it is necessary to design jaws, one fixed and the other connected to the end of the shaft — i.e., it, too, advances and recedes along with the shaft. As a consequence, three pairs of jaws, each consisting of an applicator and a fixed jaw, are specifically designed to simulate each mode of loading to be investigated, namely: uniform shear, radial compression and tension. For each pair, the fixed jaw is equipped with a novel, mechanical fixation mechanism for securely mounting the fibre specimen in place. Diffidence in using a gluing material, owing to incertitude arising from the extensibility of the glue in relation to the extension of the fibre, led to the choice of a mechanical mechanism for mounting single fibres. At any rate, if the mechanism is to be designed and manufactured to a high level of precision, two important attributes will have been achieved. (1) Elimination of inaccuracy germane to the stiffness and extensibility of the gluing material, and subsequent influence of the glue-fibre interface on the strength of the tested fibre. Hence, compounded ambiguity regarding final morphological and structural results is removed. (2) Relatively easier handling of the components, and more systematic control over each at every step of the experimental methodology, from start to finish.

It must be realised that this approach is part and parcel of our design philosophy to mechanise and automate wherever and whenever feasible, hence, in this manner subjective factors — individual adroitness and personal temperament may adversely influence the smooth running of the experiment, thereby considerably biasing reliability — are significantly minimised. It must also be noted, at this stage, that the applicator and the fixed jaw, each resides in a jacket⁶ that is fixed (via a screw)

⁵It is so designed to make efficient use of the stepping motor, while maintaining the universal utilisation of the tensiometer under any mode of loading.

⁶Made of brass in order to minimise friction between the steel jaws and the jacket. Physical

in the observation compartment of the tensiometer (see Figures 7.6, 7.8 and 7.10). Each jacket is U-shaped, and the jaw simply slides in it to the desired depth and held in place by tightening a screw on the side of the jacket. This is necessitated by two reasons. (1) To maintain perfect alignment of the jaws, which was performed using a photonic probe sensor,⁷ it is easier and more certain — experience has shown — to work with such a set-up, rather than the jaws fixed directly to the tensiometer. (2) Peculiar to the geometry of the microscope in question, the extra depth was required to bring the specimen as close as possible to the objective lens. The jaws, and parts thereof, are made of stainless steel, polished to a high degree of smoothness and machined to the utmost (achievable) precision — 1 thou for all surfaces in contact with the fibre.

7.3.1.1 Shear-Loading Jaws

The jaws, fixed and moving, are depicted schematically and pictorially in Figures 7.5 and 7.6, respectively. The fixation mounting mechanism principally consists of a block⁸ residing in an appropriate house inside of the fixed jaw, whereby motion in the horizontal plane is maintained via two adjustable springs, and out-of-plane motion is prevented by controlling a screw (and a nut) connecting the back of the block to the rear of the fixed jaw. Prior to mounting a fibre, the distance (in the y-direction) between the block and the jaw is adjusted so that the former smoothly slides to and fro. Moreover, the gap between the applicator and the fixed jaw is tuned to the desired distance by sliding the T-shaped block (which is part of the applicator) in and out.⁹ Recall that the jaws reside in the U-shaped jackets, so once distances are adjusted and alignment is performed, the whole set-up is precise and robust. It should further be mentioned that all components are placed on a vibration-damped table, all steps

dimensions are: 0.9 cm x 2.3 cm x 3.2 cm.

⁷Appendix B details, in part, the principle of operation, and the procedure for calibration, of a photonic probe sensor. This choice is made to ensure high-precision alignment of the components — a requirement of crucial import, considering the sensitivity of the task undertaken.

⁸Whose dimensions are: 7 mm x 3 mm x 10 mm.

⁹Note that the applicator itself is activated by the stepping motor, that is controlled via the computer algorithm — described in Sections 7.3.3 and 7.5, respectively.

are performed under an ordinary optical microscope, and meticulous care is a must at each and every step.

In this manner, the fibre mounting procedure is made facile since all that needs to be done is to: (i) slightly slide the block back; (ii) insert the fibre in place; (iii) slowly release the block to hold the fibre in position, and (iv) finally tighten the screw. To aid in making certain that the fibre resides as close to the top of the surface of the fixed jaw as possible,¹⁰ a channel is engraved in the block (see Figure 7.6) leaving a border of only 1 mm from the top surface as a guide to positioning the fibre.

While the fibre could have been fixed from both ends and shearing action accordingly applied, it is reckoned that the current design bears more resemblance to the actual physical situation inside of a refiner — the fibre (or fibre bundle) is seldom fixed from both ends. Furthermore, the procedure, utilised in the course of this research, is adopted in order to permit the application of the shearing action to a sufficiently large area of the fibre surface from which detailed morphological and structural information could be ascertained, while keeping reasonably away from the clamped end — in order to exclude any effect instigated by the clamp itself.

Last but not least, it is worthwhile noting that when cyclic testing is carried out, a point-to-point contact between the fibre surface and the applicator is most essential for any material degradation to take place. (More will be said about this aspect when discussing the experimental results in Chapter 8.)

7.3.1.2 Radially-Compressive-Loading Jaws

As for radial compression testing, the overall technique is similar, however not identical, to the one just described. The objective is basically to apply a compressive force across the fibre, while ensuring that the latter experiences the same frequency as that of the applicator, i.e., there is *no* impact action. The minute dimensions, however, preclude the placing of any form of attachment on the fibre that would allow it to flex at the applicator's frequency — refer to the schematic diagram of both jaws presented in Figure 7.7. An apt manoeuvre would therefore constitute the following.

¹⁰This is necessary to ensure that the fibre will be within the depth-of-field of the objective lens.

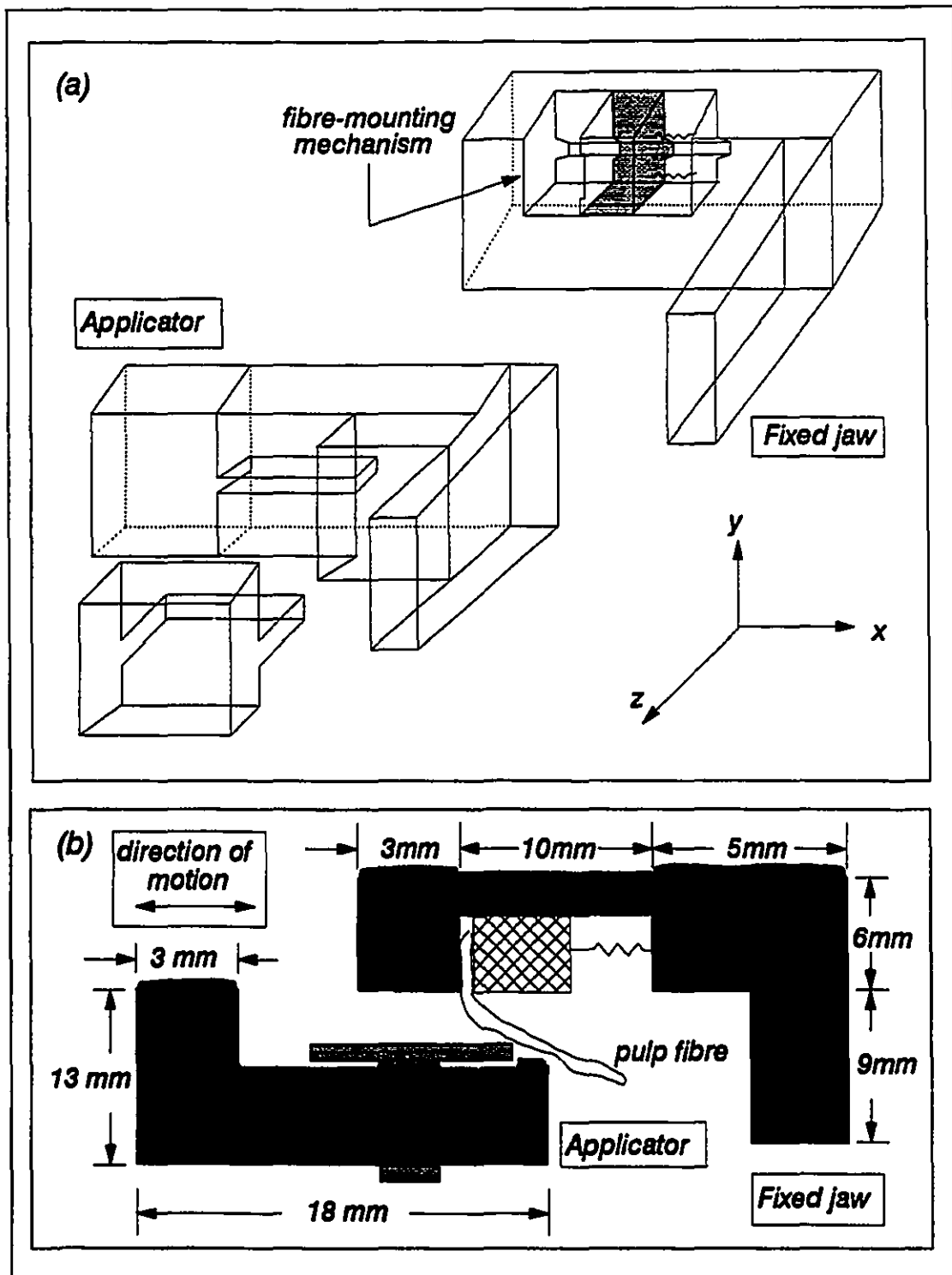
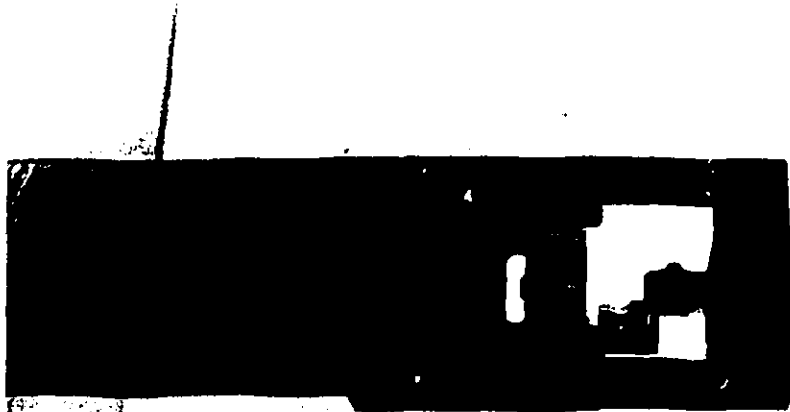


Figure 7.5: A schema of the loading jaws used for fatigue-testing fibres under uniform, cyclic shear: (a) a three-dimensional representation of the jaws; (b) a two-dimensional profile.

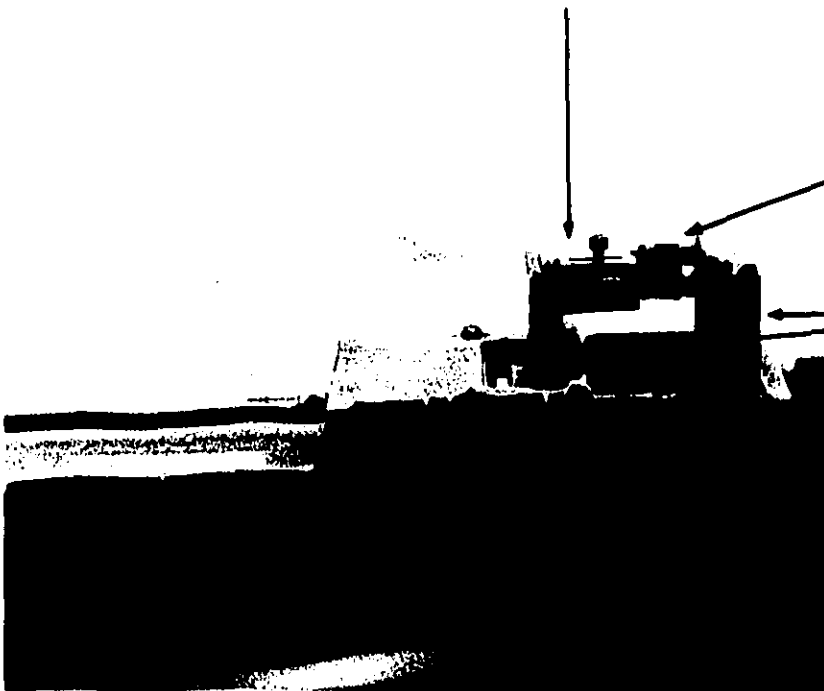
Figure 7.6: A photographic depiction of the shear-loading jaws residing in the jackets.



applicator

fixed jaw

brass jackets



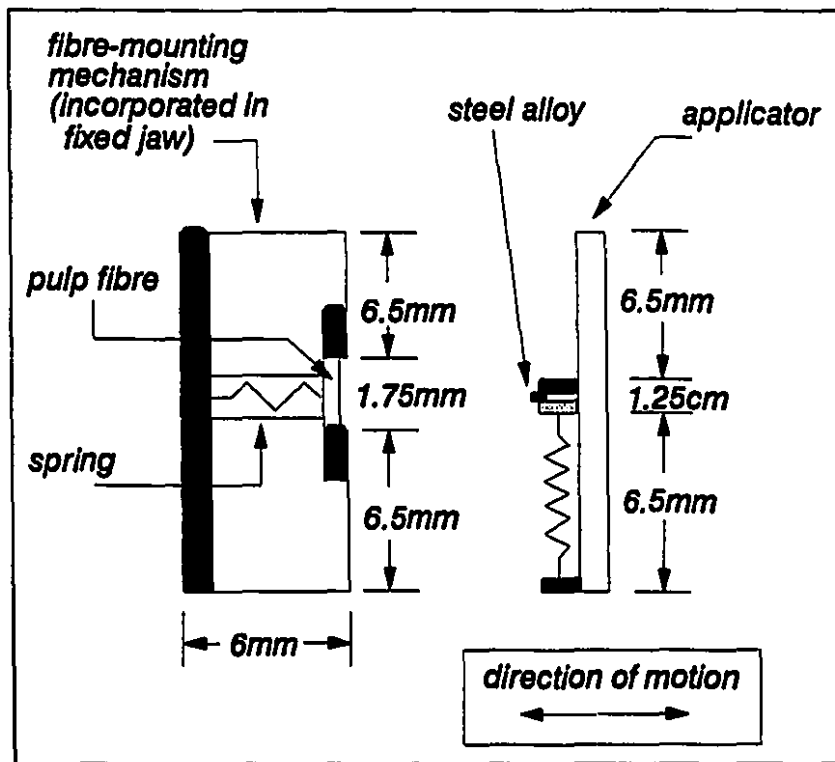


Figure 7.7: A schema of the loading jaws used for testing fibres under cyclic radial compression.

The fibre is clamped from both ends in a fixation mechanism consisting of a U-shaped bar attached to an adjustable spring, pictorially shown in Figure 7.8. The compressive load is applied via a steel-alloy wire (whose diameter is comparable to that of the pulp fibre) securely clamped in a fixation mechanism housed in the applicator. The steel-alloy wire is positioned so as to form a semi-circular shape, thus, upon contact with the fibre, a direct point-to-point correspondence is established at the centre of the straight fibre—henceforward referred to as the “neutral position”. Upon operation, at the neutral position, the applicator advances a specified distance¹¹ causing the fibre to flex in the middle; when the applicator recedes, the fibre returns to neutral position. Of course, depending on the flexibility of the fibre and the number of cycles, the fibre will undergo some permanent deformation. Whenever this occurs,¹² operation is halted and the applicator advanced to re-establish a point-to-point contact between the steel-alloy wire and the fibre; running is then resumed. Precise movements are made possible by controlling the entire set-up through a computer algorithm, specifically written for the present methodology. In this manner, flexing of the fibre is ensured to occur at the frequency of the applicator and that no impact action is introduced.

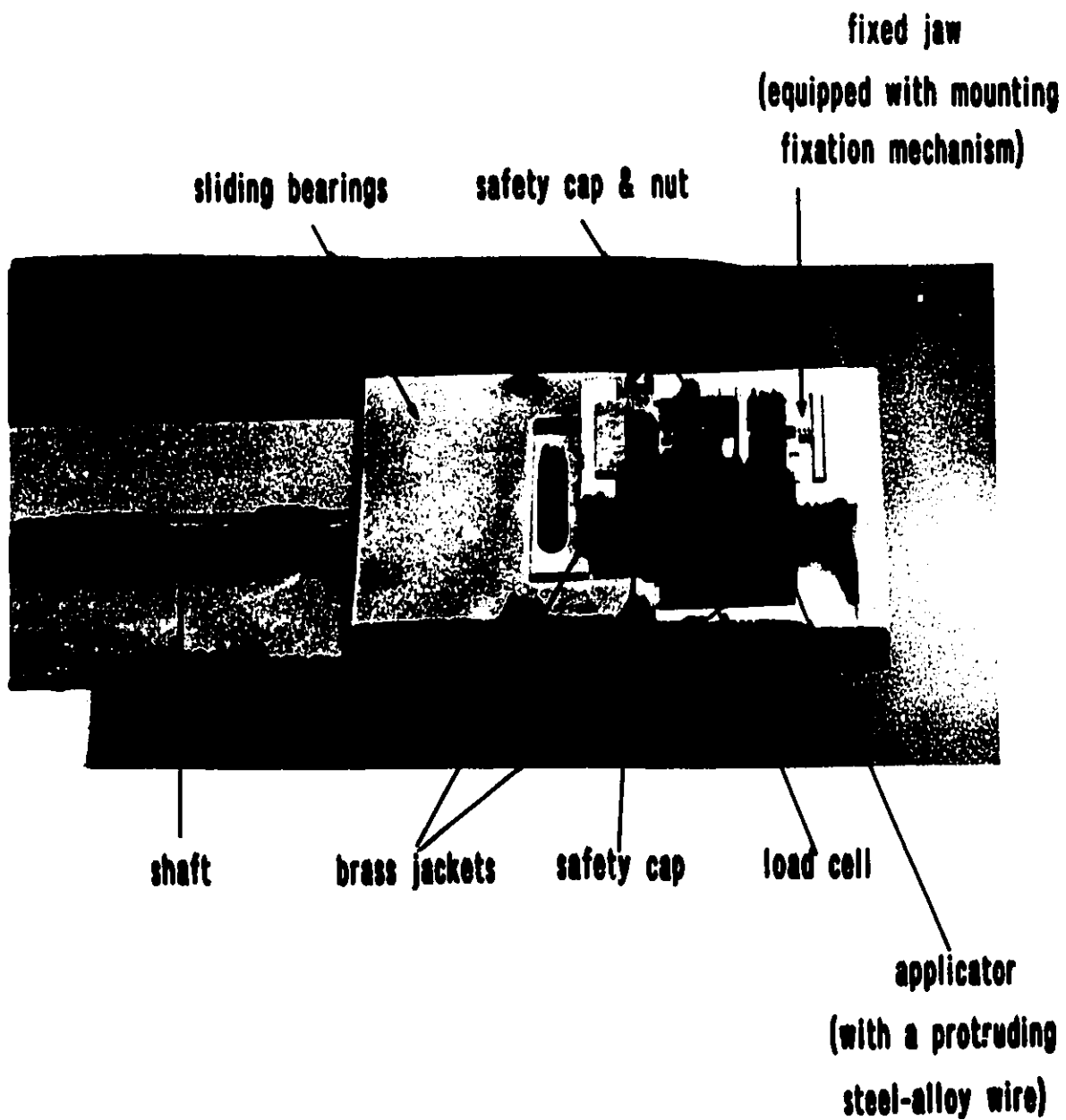
7.3.1.3 Tensile-Loading Jaws

The loading jaws used for cyclic tensile testing are somewhat simpler in operation than either of the two previous sets. A fibre is mounted in the fixation mechanism, housed in both: the applicator and the fixed jaw, by clamping both ends, as depicted schematically in Figure 7.9, and the clamp housed in the applicator is subjected to a cyclic change of position. Prior to initiating fatigue-testing, the applicator is moved until the fibre specimen is taut. This is the “neutral position” for cyclic tensile testing. Cycling commences by instructing the applicator to alternately move, in tension, a specified stroke (35 μm is the optimal magnitude). One unavoidable difficulty with this method, nevertheless, is that the fibre becomes slack owing to imperfect recovery

¹¹35 μm is the optimal distance, taking into consideration the frequency (refer to Chapter 8 for details).

¹²It is to be borne in mind that the fibre is continuously monitored.

Figure 7.8: A photographic illustration of the radially-compressive-loading jaws set-up.



and, henceforth, is not under tension. This situation may however be remedied in the manner discussed below.

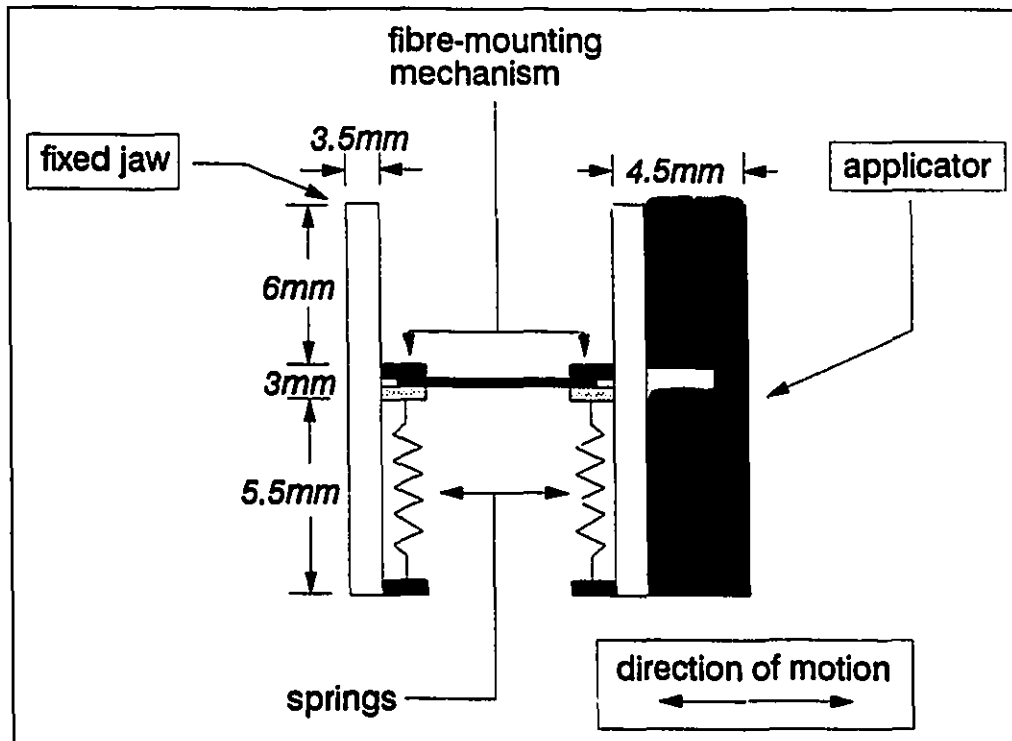
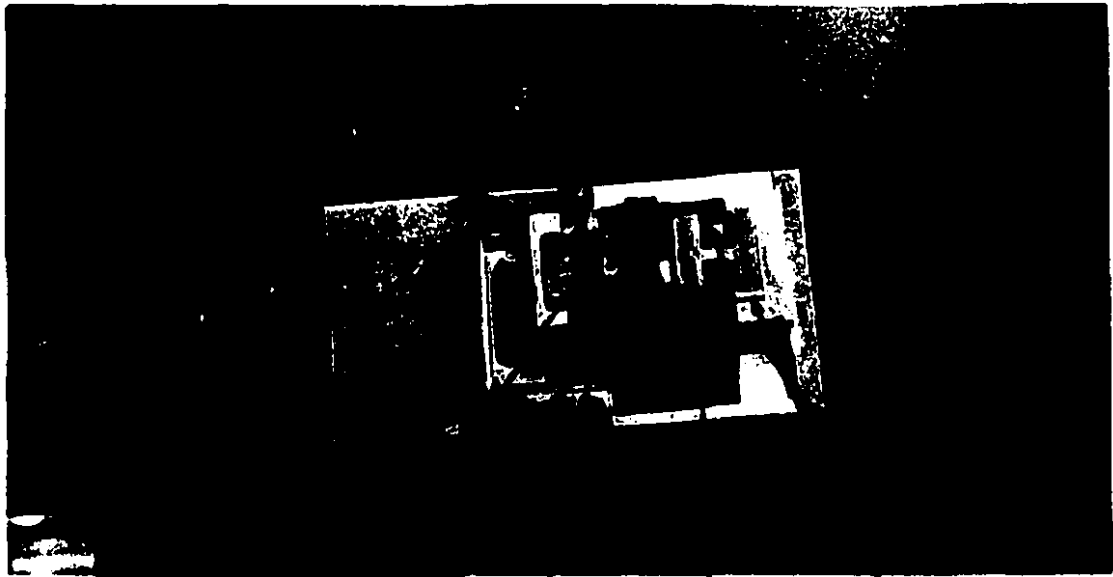


Figure 7.9: A schematic diagram of the tensile-loading jaws.

During testing, the response of the fibre specimen is continuously recorded by the load cell and subsequently output on a chart recorder. Any discrepancy, e.g. fibre slackening, would thence be easily spotted since there will be irregularities in the load cell output, whereupon testing may be interrupted. A given extension stroke is then imposed on the fibre specimen which is once again taut. This may be referred to as *cumulative extension testing*.

Most critical in the whole process is the *accurate* alignment of the jaws, which is highly dependent on the precision of machining as well. Prior to mounting, alignment is methodically checked using a photonic probe sensor to precision of $\pm 1\mu\text{m}$. (See actual depiction of the jaws in Figure 7.10.)

Figure 7.10: A photographic representation of the tensile-loading jaws, *in situ*.



safty cap & nut

load cell

applicator

fixed jaw

7.3.2 Load Cell

The load cell used in the current research is an *Entran*^R ultra-miniature device, model type: ELF-TC500-1, capable of measuring tensile as well as compressive axial loads in the range of ± 1 lb—which is the most sensitive in this series. The load cell is a typical active transducer with a force input, electrical excitation input of 15 Volts DC and electrical output. The transducer employs a fully active Wheatstone bridge consisting of semi-conductor strain gauges. The latter are bonded to a thin circular diaphragm which is clamped along its circumference and which contains a load button at its centre. Load applied to the button presents a distributed load to the diaphragm, which in turn provides bending stresses and resultant strains to which the strain gauges react. This stress creates a strain proportional to the applied load which results in a bridge imbalance. With an applied voltage, this imbalance produces a milli-Volt (mV) deviation at the bridge output, which is proportional to the load acting upon the load button.

As may be seen from, for example, Figure 7.10, the load cell is installed between two nuts, which are tightened—when the entire set-up is completed—to prevent any accidental torsional load, as the latter may prove damaging to the load cell. Moreover, the load response of each fibre specimen may continuously be monitored through the load cell voltage output (which may be read from a chart recorder). The load cell output offers a useful, qualitative guideline of the progress of fatigue-testing in the sense that it helps in monitoring the crack propagation and other material changes. Moreover, it serves as a warning in case of, for instance, fibre slackening, or any other discrepancy that may occur during the course of testing.

The sensitivity of the load cell used in the current set-up is found to be 7.52 V/lb when the signal is fed into a 100x amplifier located in the load cell power supply, otherwise it is 75.21 mV/lb.¹³ Calibration is performed by comparing the load cell output with a known static load, details of which are found in Appendix B.

¹³The manufacturer's calibration certificate shows 75.68 mV/lb.

7.3.3 Stepping Motor

A unipolar (model: AIRPAX K82430) stepping motor is used in conjunction with a 25:1 reduction gear box; the combination provides exact displacement strokes in the cyclic loading of the specimen. When a voltage pattern is applied in a correct sequence, the rotor (permanent magnet) is forced to rotate clockwise or anti-clockwise a precise number of steps, or to stop in a given exact position. The rotation is comprised of discrete, repeatable steps, requiring digital techniques for control—which makes coupling with a computer an ideal option.

The stepping motor is directly controlled by the motor driver (refer to Figure 7.1). The driver, essentially consisting of an LM555 oscillator,¹⁴ basically translates the signal relayed by the microcomputer into different current signals. These currents are sent into various coils of the motor, so that it moves in a given direction for a specified time or a defined number of steps. Moreover, the driver is capable of operating the stepping motor either uni-directionally (tension or compression) or cyclically. A 2x amplifier is included in the set-up in order to transform the 5 V digital output of the $\mu\text{mac-5000}$ microcomputer into a 10 V signal necessary to trigger the stepping motor whenever the internal oscillator of the motor driver is bypassed—as in the case of step-by-step operation (see below, and refer to Section 7.5 for more details).

The stepping motor in the current experimental system functions in two modes: continuous and step-by-step. Since the experiments are highly dependent on the stepping motor calibration, the latter is performed with a great deal of care using a photonic probe sensor carefully calibrated beforehand. (Full description of each calibration is given in Appendix B.) For both modes of operation, the optimal results for the stepping motor calibration are: 13.1 μm per second for the continuous mode, and 0.04 μm per step for the other.

¹⁴Schematics of the interior of the motor driver is available in Appendix C.

7.4 Confocal Laser Scanning Microscopy

The confocal laser scanning microscope (CLSM) complements the *in situ* testing apparatuses. It is an example of a sequential imaging system, i.e., it functions by scanning a diffraction limited spot of light relative to the specimen in a raster-type scan [287]. In this way, the image is built up point by point, as in a domestic television set,¹⁵ and may be displayed on a Visual Display Unit (VDU) or stored in a computer for future processing. Furthermore, the CLSM has a distinct advantage in its ability to rapidly generate non-destructive optical sections of thick translucent specimens, such as wood fibres. The CLSM, used to monitor the fibre during fatigue-testing, facilitates the gathering of qualitative information on the structural behaviour of the fatigued fibres; and provides accurate visual records of the history of crack propagation until fracture. It has also been extensively used, in the course of this research, to provide qualitative interpretations of the morphology of fractured surfaces.

In what follows, a concise exposition of the theoretical aspects of confocal scanning microscopy, together with basic information on the system utilised in the course of this research, is provided.

7.4.1 Fundamentals of Optical Image Formation

The key difference between the confocal scanning microscope and the conventional instrument is that the confocal uses a point detector rather than a large-area detector; in all other respects, the optical systems are identical.¹⁶ As all the considerable advantages of confocal microscopy directly follows from the use of a point detector, it is important to know how small a practical detector must be in order to approximate, as closely as possible, a true point detector. It is usual to form a "point" detector by placing a circular pinhole in front of a suitable photodetector; and is reasonable, in general, to try to use as small a detector as possible, although in many applications,

¹⁵Although the scanning rate is usually significantly slower than the 25 or 30 frames per second of a conventional video.

¹⁶The contents of this section are broadly derived from two recent, comprehensive books on the subject [286, 287], to which the interested reader is referred for further details.

the freedom to do so may significantly be curtailed because of signal-to-noise problems. (This is particularly true, for example, in the imaging of weakly fluorescing objects — as the case may be with wood fibres.)

A typical arrangement of a scanning optical microscope is shown in Figure 7.11. The system operates well in the brightfield and fluorescence modes, and it is possible, in principle, to operate these systems in transmission. The essential components are some form of a mechanism for scanning the light beam (usually from a laser) relative to the specimen, and appropriate photodetectors to collect the reflected or transmitted light. Most of the early systems were analogue in nature; however, owing to the serial nature of the image formation, digital devices are nowadays used both to drive the microscope and to collect and display the image.

An inevitable consequence of the progressive research in confocal microscopy is the capability that the image is obtained in an electrical form. This permits many forms of image enhancement and processing to be undertaken, the simplest example being probably contrast enhancement. Both linear and non-linear techniques such as histogram equalisation and homomorphic filtering are used to allow full use to be made of the dynamic range of display. A further advantage of the scanning approach is that the processing is done on data from an ordinary image. Thus, there is no need to modify the optical system to increase contrast by, for instance, stopping down the collector lens or using dark-ground techniques — since these latter techniques modify the resolution of the image formation, whereas electrical processing does not.

The optical sectioning or depth discrimination property has become a major motivation for using confocal microscopes; and has consequently become the keystone of many of the novel imaging modes of these instruments. The underlying principle may easily be understood from examining Figure 7.12, where a reflection-mode confocal microscope imaging a rough surface specimen is shown. The full lines show the optical path when an object feature lies in the focal plane of the lens. At a later scan position, the object is supposed to be located in the plane of the vertical dashed line. In this case, simple ray tracing shows that the light reflected back to the detector pinhole arrives as a defocussed blur, only the central portion of which is detected and contributes to the image. In this manner, the system discriminates against features

which do not lie within the focal region of the lens.

Before closing the discussion on the theoretical underpinnings of confocal microscopy, fluorescence-mode confocal microscopy merits particular consideration: It underlies the theme used in the current research to obtain images of the fracture morphology of wood pulp fibres. Briefly, the image formation properties of fluorescence microscopes are completely different from those of the brightfield instruments (for a detailed discussion refer to the aforementioned references). This essentially results from the nature of the fluorescence generation mechanism. The fluorescence generation process is principally modelled by assuming that the fluorescence in the object destroys the coherence of the illuminating radiation and produces an incoherent fluorescent field proportional to the intensity of the incident radiation.

Referring to the conventional scanning microscope of Figure 7.13(a), and imagining that suitable filters are present such that only fluorescence radiation is detected. It is immediately recognised that the resolution results from the primary, incident radiation and not from the longer wavelength fluorescence: the collector lens essentially converges fluorescence radiation onto a detector. In a conventional non-scanning microscope, Figure 7.13(b), this is not the case. Here, the primary radiation excites the fluorescence, which is then imaged by the objective lens. Thus, in this case, the resolution results essentially from the longer wavelength fluorescence radiation. This leads to the important, conclusive affirmation that scanning microscopes are capable of producing superior fluorescence images. If these advantages of confocal microscopy are combined together with optical sectioning, it may be fathomed as to why the technique has become so useful.

7.4.2 The CLSM: System Description

A Leitz FLUOVERT-FS CLSM assembly, optimised for low-level fluorescence measurements, has been used for the present study; along with a 50 Watt, high pressure mercury vapour lamp for incident light fluorescence. The light source is an argon ion laser with laser output power of 2-50 mV and excitation wavelengths of 488 and 514 nm. Excitation and suppression filter types BP530-560 and LP580, respectively;

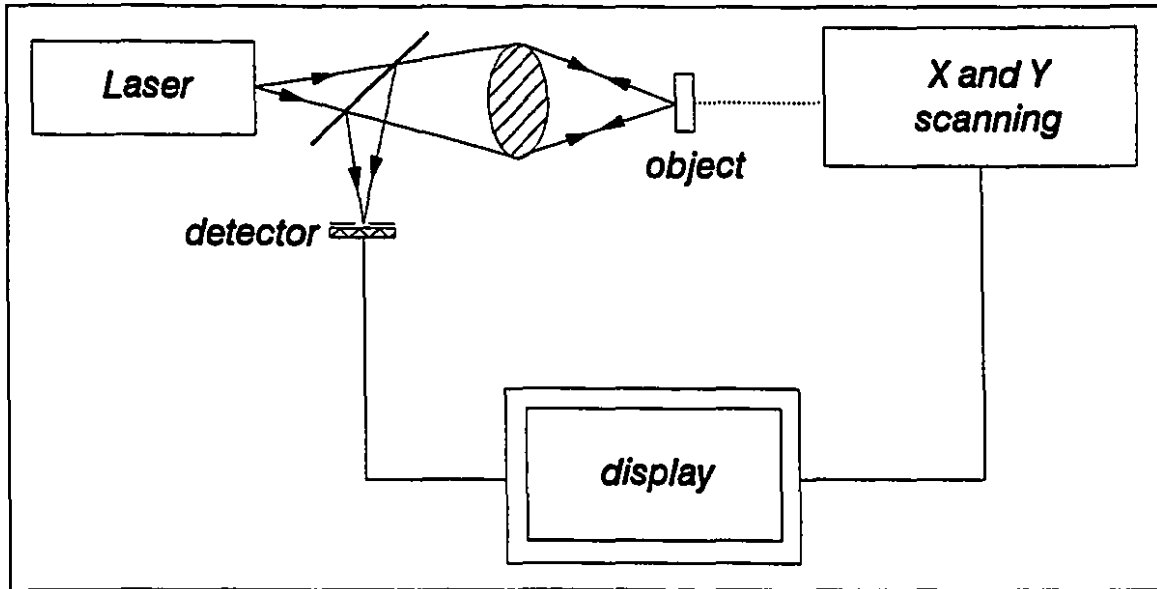


Figure 7.11: Schematic arrangement of a reflection mode scanning optical microscope (adapted, however with slight modifications, from reference [286]).

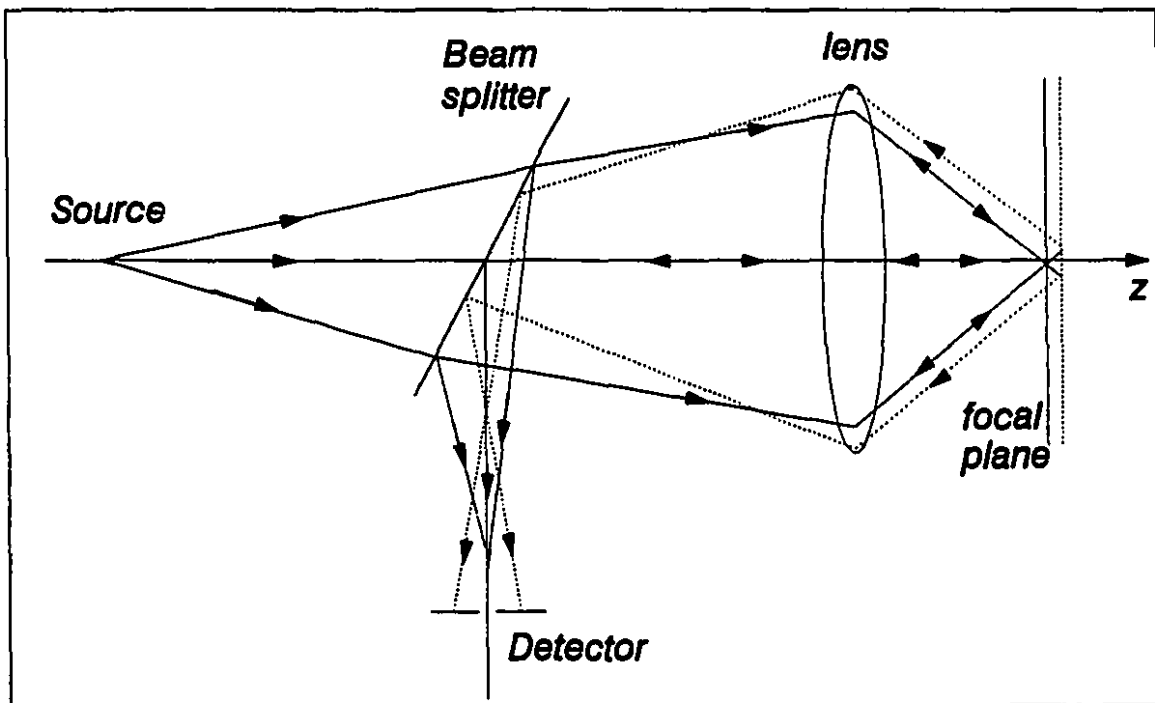


Figure 7.12: The origin of depth discrimination or optical sectioning property of confocal optical systems (adapted from reference [286]).

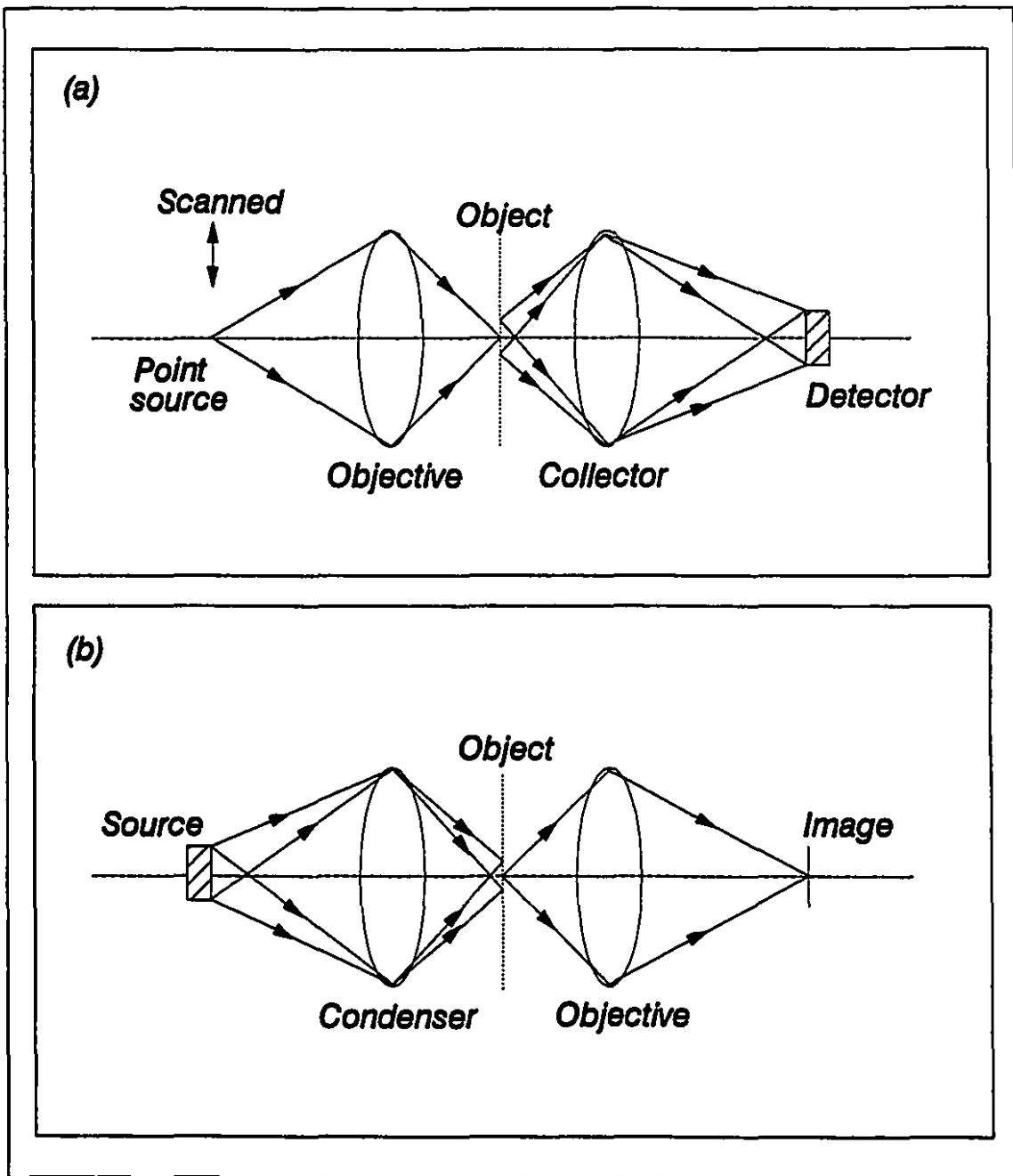


Figure 7.13: The optical arrangement of various forms of scanning optical microscopes. (a) A form of conventional scanning microscope. (b) Conventional microscope. (After reference [286].)

and dichromatic mirror RKP580 are used to attain the desired intensity of the laser. Figure 7.14 illustrates the entire CLSM assembly.

The configuration is an inverted Leitz *Diaplan*^R microscope stand, which is equipped with a special intermediate tube for coupling the argon ion laser with the scanning and detection unit. The microscope is typically equipped with a high-precision focussing stage, responsible for vertical movements. However, in our case, the weight of the tensiometer exceeds what is normally permitted by the manufacturer to be placed on the stage. It was then necessary to design a substitute: the *support/stage mechanism*, in order to scan the fibre *in situ*—see Figure 7.4. This mechanism, in which the tensiometer resides, is capable of moving in the horizontal plane as well as vertically in 1 μm increments—using a high-precision micrometer screw-head. A powerful computer system¹⁷ controls the entire CLSM and processes the images. An optical disc (800 MByte) with a storage capacity of 12000 images in 256 x 256 pixel format is utilised for image archiving. The system is operated by means of digital potentiometers and trackball for the most important microscope adjustments, and by a terminal with numerous programmed functions (cf. Figure 7.14)—using multi-tasking, real-time operating system OS9. The system is also equipped with 4 MByte RAM (Random Access Memory) and 2 MByte frame storage.

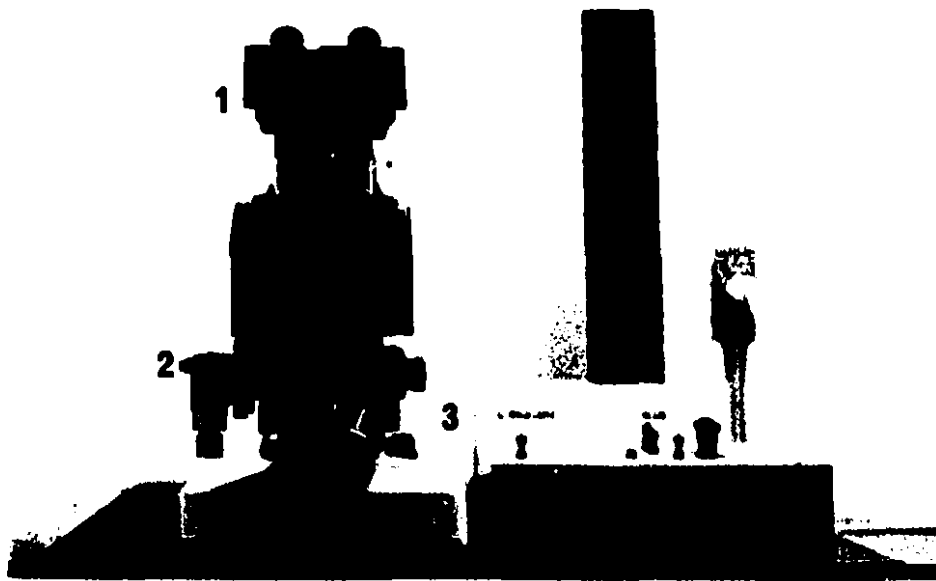
7.5 Electronic Hardware and Software

The automation of the fatigue-testing methodology may be realised through the incorporation of the μmac -5000 microcomputer. The latter, which is a programmable stand alone measurement and control system, is a single-board microcomputer with: an INTEL 8088 CPU; 80 KBytes of ROM (Read Only Memory) in which the μmac -BASIC, the resident programming language, is stored; 32 KByte of battery backed-up RAM (12 KBytes used by the compiler and the remainder reserved for the programmer's use); 8 digital output channels; 12 analogue input channels, a 14-bit resolution analogue-to-digital convertor; and two serial input/output communication ports.¹⁸

¹⁷The Motorola CPU 68020/68881 based on VME bus and running at 20 MHz.

¹⁸Block diagram of the interior of the μmac -5000 is available in Appendix C.

Figure 7.14: The Leitz FLUOVERT-FS CLSM assembly.



1. Classical microscope (with confocal unit)
2. Z-scanning stage
3. Argon ion laser
4. Excitation, barrier & dichroic filter slides
5. Image monitor
6. Data monitor with status display
7. Interactive operator console
8. Keyboard with programmed functions
9. Vibration-damped table

The capacity of the μ mac-5000 to handle a wide range of analogue and digital input/output tasks, together with its powerful real-time BASIC language, the μ mac BASIC, render the microcomputer a versatile tool in the measurement and control of the fatigue-testing experiment. The role of the μ mac-5000 in the present investigation may be summarised as follows:

1. To control the stepping rate and displacement amplitude by transmitting to the motor driver outputs of 0 V and 5 V through its digital output channels, either directly or via a 2x amplifier.¹⁹
2. To host and run the interactive control routine (discussed later in this section).
3. To record and display the number of cycles executed during fatigue-testing through interfacing, via an RS-232C²⁰ serial data link, with an AT-IBM compatible personal computer: the PC, in other words, functions as a terminal. The conversion into a terminal is made possible using a communication software, TELIX, having the following configuration: baud rate = 9600, data bit = 8, stop bit = 2, parity = none.

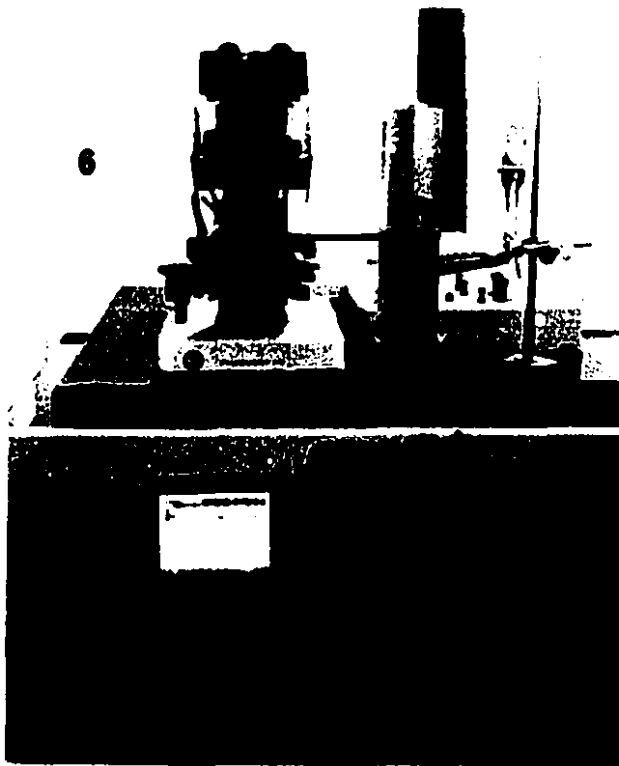
Load data acquisition is, on the other hand, carried out by feeding the load cell output signal—which is usually small—into a 100x amplifier located in the load cell power supply; the latter is, in turn, connected to a chart recorder. In this way, a permanent, continuous record of the specimen load response is obtained.

On the software front, a computer program has specifically been developed to control the automated fatigue-testing operation. The algorithm, written in μ mac-BASIC, regulates, on a real-time basis, the μ mac-5000's control of the functioning of the stepping motor, number of cycles performed and positioning of the applicator, in response to the interactive command of the user. Its structure is such that it includes two modules: the *interrupt* and *fatigue* modules. The former primarily enables testing interruption at any juncture. The *fatigue* module, on the other hand, consisting of

¹⁹The 2x amplifier is used to trigger the stepping motor whenever the internal oscillator of the motor driver is bypassed (cf. Section 7.3.3).

²⁰It is worthwhile noting that 2 jumpers were added to the DB25 connector on the PC side.

Figure 7.15: Complete experimental set-up for fatigue-testing of single wood pulp fibres.



1. mac-5000 microcomputer
2. PC terminal & disc drives
3. 2x amplifier
4. Motor driver
5. Chart recorder
6. In situ apparatuses:
Tensiometer & CLSM assembly



three principal routines, forms the core of the software.²¹ It principally controls two operations: the positioning of the applicator and the application of cyclic loading to the specimen. In the former case, the algorithm regulates the functioning of the stepping motor to control the uni-directional movement (tension or compression) of the applicator according to a specified displacement. This movement is realised by continuously alternating the digital output (of channel 3) of the μ mac-5000 until the specified number of steps is reached. Contrariwise, the actual cyclic loading may be applied in one of two modes: continuous or step-by-step. The continuous mode instructs the stepping motor to operate at its maximum speed without stalling, by activating the internal oscillator of the motor driver. The other mode performs a similar function, however, at a slower rate—since the internal oscillator is bypassed.

²¹Full listing of the fatigue-testing software is given in Appendix D.

Chapter 8

Experimental Results: Discussion and Analysis

8.1 General Remarks on Functional and Procedural Considerations

Before broaching the intricacies of the results obtained, it is appropriate to succinctly indicate the prime considerations involved in preparing the pulp samples for testing, and for microscopic observations. As well, pulp types need be clarified at the inception, along with the modality of testing.

Wood pulp fibres are separated by adding a few drops of water and using gentle agitation. With the aid of fine tweezers to grip one end, single fibres are transferred from a slurry to a drop of water on a glass slide. (An endeavour has been made to choose as straight and defect-free fibres as possible.) The fibre is then transferred to the mounting fixation mechanism, in the manner canvassed earlier on (refer to Section 7.3.1 in its entirety). The entire procedure is performed under an ordinary optical microscope and, needless to say, scrupulous care and patience are necessary pre-requisites throughout each step of the process. It is all but impossible to eliminate the element of subjectivity when handling the fibres, however, dexterity is developed through experience. This, it must be noted, is one prime source of uncertainty; nevertheless, it could be mitigated as long as microscopic observations are carried out

at each step of handling and mounting to ensure that *only* “healthy” fibres reach the mounting mechanism. Henceforth, the set-up is controlled and operated via the fatigue-testing algorithm; while bearing in mind the alignment of the jaws are performed beforehand.

At this juncture, it is deemed helpful to elucidate immanent aspects of the computer algorithm. In Chapter 7 it is mentioned¹ that the optimal distance for moving the applicator in the cases of radial compression and tension testing is 35 μm : How is it arrived at? The functional parameters of the stepping motor, viz., rates of operation obtained from calibration: 13.1 μm per second and 0.04 μm per step, are integrated into the logic of the algorithm. That is to say, recalling that our methodology is displacement-controlled, the displacement of the applicator is precisely governed by the functioning (capability) of the stepping motor in both continuous and step-by-step modes. It is worthy of note that these values are obtained on the basis of numerous trial tests by varying the voltage, and hence the stepping rate, of the motor driver — for details refer to Appendix B. Moreover, now that the rate of operation of the stepping motor has been determined, the ceiling of the frequency may be ascertained: The frequency² of testing is a function of both the (continuous mode) rate of operation and the minimum, precise displacement the stepping motor can deliver. The latter’s value is 5 μm . (We could actually go as low as 1 μm , however, noise becomes a significant factor below 3 μm and this, therefore, might call into question the very accuracy of the displacement imparted on the specimen. Hence the decision to choose 5 μm as the minimum, precise, permissible displacement, x_{min} .) Based on the manner in which the experimental set-up and computer algorithm are designed, the frequency, f , is defined as:

$$f = \frac{\text{optimal rate of operation of stepping motor, } \Omega}{\text{total to — and — fro movement of applicator, } \delta},$$

the maximum frequency, f_{max} , consequently becomes:

$$f_{\text{max}} = \frac{\Omega}{x_{\text{min}}} = \frac{13.1 \mu\text{m}/\text{sec}}{5 \mu\text{m}} = 2.62 \text{ Hz}.$$

¹Sections 7.3.1.2 and 7.3.1.3.

²Of course, the mode in question here is the continuous — the one at which testing is carried out.

This then brings us to the point of enunciating the specifics germane to each mode of loading.

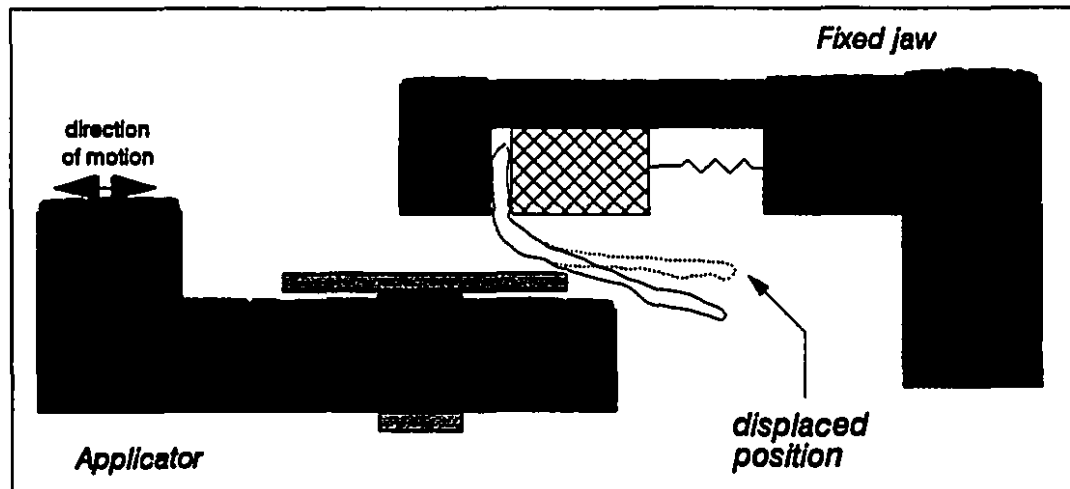


Figure 8.1: Schematic representation of the fibre posturing as the applicator prods, to and fro, along the fibre specimen during shear-mode testing.

Shear loading It has been mentioned earlier on (refer to Sections 7.2 and 7.3.1.1 of Chapter 7) that point-to-point correspondence between the applicator and the pulp fibre specimen is of the essence, if damage accumulation due to fatigue is to take place. Figure 8.1 illustrates schematically how the fibre flexes as the applicator prods along the fibre; the latter returns to original posture as the applicator recedes—and so forth repeatedly. It is also mentioned that there is a need to cover as large an area as possible away from the clamped end. The fact that the mounting-fixation mechanism, surfaces *et al.* are designed and machined in such a manner as to absolutely minimise any (possible) extraneous damage may be corroborated by examining Figure 8.2(a), which depicts the clamped end of a pulp fibre residing in the fixation mechanism of the fixed jaw of the shear-loading set. Moreover, the other consideration, i.e., the need to examine a large area of the fibre surface, dictates that we reconcile with much lower frequencies.

Examination of Table 8.1 casts some light on appreciating that long, continuous hours are required to run each test at such low frequencies. It is also revealed that

Figure 8.2: Fluorescence confocal micrographs of the clamped end of fibres mounted in the fixation mechanism (after the completion of testing): (a) shear-mode testing; (b) radial compression; and (c) tension.



three different species, three ranges of refining specific energies and a wide range of fatigue life (i.e. number of cycles) are investigated in order to draw comprehensive conclusions on the morphological and structural behaviour of single wood pulp fibres subjected to fatigue loading; *in extenso* discussion of the findings will ensue.

Radially-compressive loading The optimal distance the applicator advances (from neutral position to cause the fibre to be radially compressed³) is determined through a series of trials at a broad range of fatigue cycles. The essence here is to induce a low deflection compared to the length of the fibre, such that the percentage ratio is below 5%.⁴ While taking cognisance of what has been canvassed earlier regarding frequency and minimum, precise displacement, an average fibre length, l_{av} , of 1500 μm and a deflection at the fibre centre, y , of 35 μm , result in a ratio of deflection to fibre length of 2.3%—refer to Figure 8.3. It is worthy of note, however, that the value of the deflection, y , corresponds to the amplitude of cycling. That is to say, the to-and-fro movement of the applicator identically equals twice the amplitude—refer to Figure 8.4 for clarification.

At the risk of being repetitive, after a large number of cycles (>1000 cycles) the fibre, depending on its flexibility, undergoes permanent deformation; thenceforth, the applicator is advanced to establish a point-to-point contact with the fibre, and cycling is resumed at the same frequency (which is equal to: $\frac{13.1\mu\text{m}/\text{sec}}{2(35)\mu\text{m}} = 0.187 \text{ Hz}$). Furthermore, careful mounting and superb surface finishing of the fixation mechanism may be attested to by examining the micrograph in Figure 8.2(b).

The fibre species, refining energies, etc. for the particular tests under radial-compression loading are summarised in Table 8.2.

Tensile loading The rationale for selecting 35 μm as the amplitude for cyclic testing

³Cf. Section 7.3.1.2 of Chapter 7.

⁴This is mainly imposed to conform with the basic assumption of 'low deflection theory'. Although we make no use of this theory in our study, we however endeavoured to generalise the experimental configuration and computer algorithm so as some benefit may be acquired for other purposes, such as determining the stiffness of pulp fibres. This set-up overcomes many of the difficulties (and hence over-simplifying assumptions) peculiar to fluid mechanics methods used to determine the fibre stiffness; or incertitude with older methods—based on solid mechanics—owing to the unreliability of fibre-mounting procedures, monitoring and measuring load response.

Table 8.1: Specifications concerning wood-pulp fibre samples used in shear-loading mode fatigue-testing. (The author acknowledges Dr. A. Karnis, Mechanical Pulping Division, PAPRICAN, Pointe Claire, for supplying all the pulp samples.)

Sample No.	Wood Species	Pulping Process	Refining Energy (GJ/t)	A* (μm)	Frequency (Hz)	Number of Cycles
1 [†]	Jack pine	RMP [‡]	4.4	500	0.0262	350
2	Jack pine	RMP	6.5	500	0.0262	1050
3	Jack pine	RMP	6.5	500	0.0262	1200
4	Loblolly pine	CTMP*	6.4	500	0.0262	1200
5	Black spruce	RMP	8.5	500	0.0262	1200
6	Jack pine	RMP	8.7	500	0.0262	1200
7	Jack pine	RMP	6.5	500	0.0262	1750
8	Jack pine	RMP	6.5	500	0.0262	2100
9	Jack pine	RMP	6.5	10	1.31	36000

* A = Distance along the fibre surface at which point-to-point contact is established with the applicator, as the latter prods to and fro.

[†] Pulp fibre was washed using acetone to remove extractives.

[‡] RMP = Refiner mechanical pulp; one-stage refining at 1200 rpm.

* CTMP = Chemi-thermomechanical pulp; two-stage refining: 1st stage at 1800 rpm (high intensity), 2nd stage at 1200 rpm. Also pulp is treated with 2% Na_2SO_3 .

• All pulps are fractionated at P-14/R-28.

◦ Ambient environment testing conditions: Temperature = $23 \pm 1^\circ\text{C}$; relative humidity = $60 \pm 5\%$.

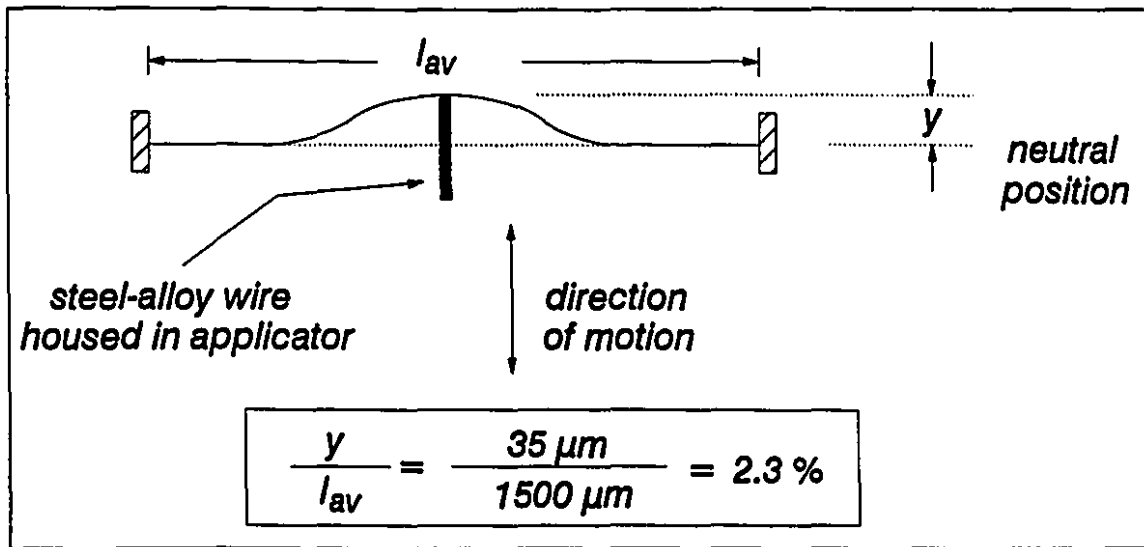


Figure 8.3: Schematic illustration of fibre deflection under radial compression testing.

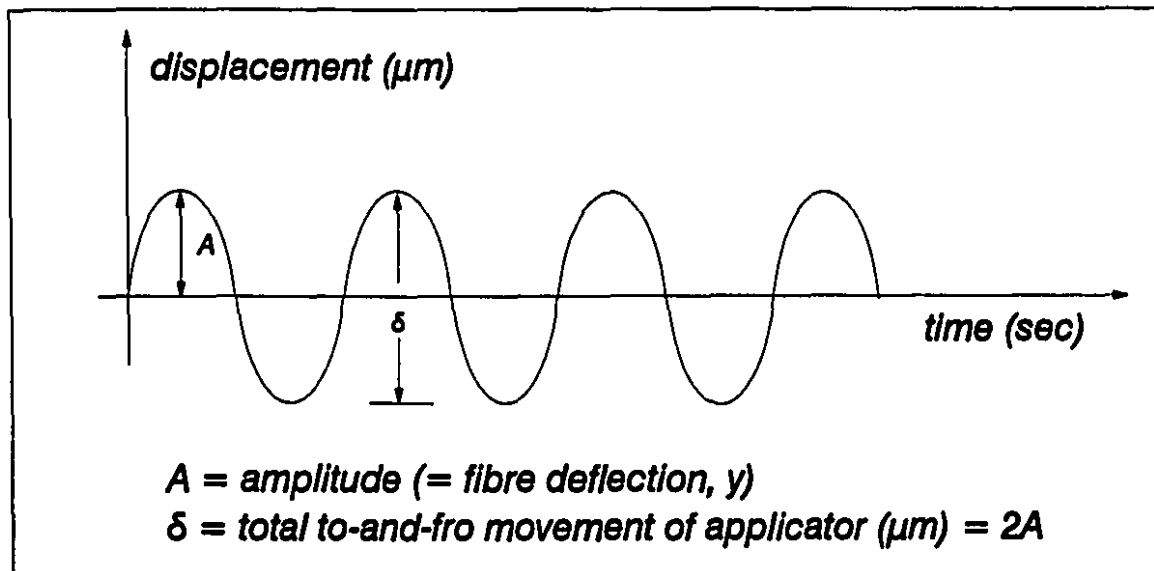


Figure 8.4: Graphical depiction of the applicator movement and fibre deflection, as incorporated in the fatigue-testing algorithm.

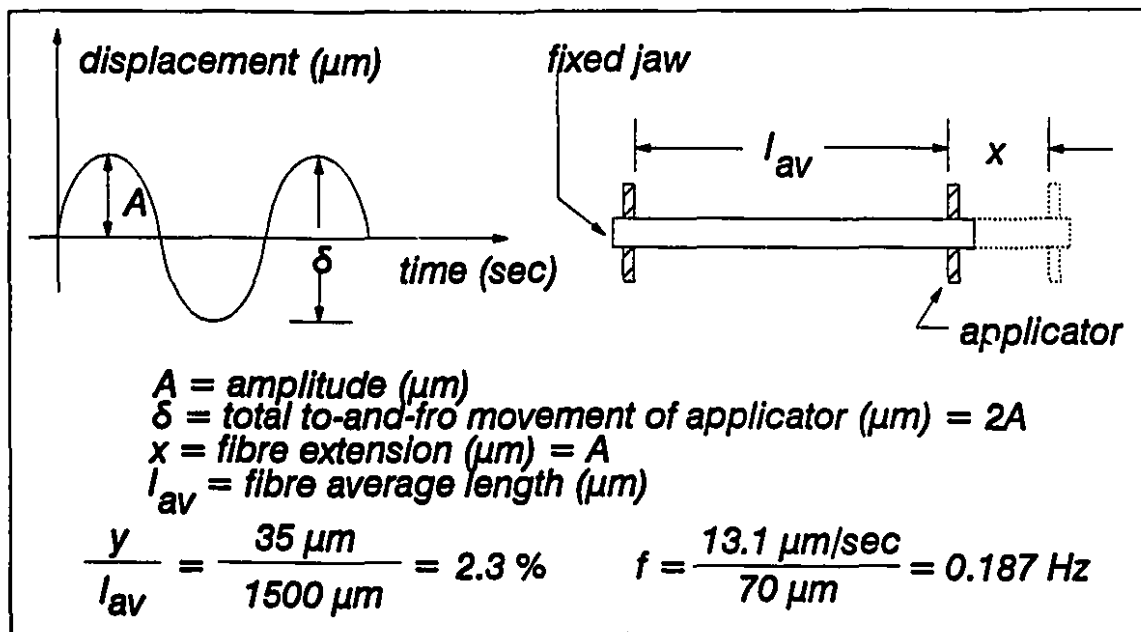


Figure 8.5: Diagrammatic representation of the relationship between fibre extension and the amplitude of cycling in tensile-mode fatigue-testing.

is similar, in principle, to that for radial-compression testing. However, the tensile extension — rather than the deflection — is, in this case, related to the amplitude, and thence to the total to-and-fro movement of the applicator. Figure 8.5 diagrammatically depicts the aforementioned relationship.

Particulars of specimen types *et al.* are provided in Table 8.3; and pictorial proof of the good condition of the clamped ends of a fibre is presented in Figure 8.2(c).

Table 8.2: Specifications concerning wood-pulp fibre samples used in radial-compression fatigue-testing.

Sample No.	Wood Species	Pulping Process	Refining Energy (GJ/t)	Frequency (Hz)	Number of Cycles
1	Loblolly pine	CTMP [†]	6.4	0.187	350
2	Jack pine	RMP [‡]	6.5	0.187	600
3	Jack pine	RMP	6.5	0.187	2700
4	Jack pine	RMP	6.5	0.187	3400
5	Jack pine	RMP	4.3	0.187	3600
6	Jack pine	RMP	8.5	0.187	5000
7*	Jack pine	RMP	4.4	0.187	5000
8	Black spruce	RMP	8.5	0.187	5400

[†] CTMP = Chemi-thermomechanical pulp; two-stage refining: 1st stage at 1800 rpm (high intensity), 2nd stage at 1200 rpm. Also pulp is treated with 2% Na_2SO_3 .

[‡] RMP = Refiner mechanical pulp; one-stage refining at 1200 rpm.

* Pulp fibre was washed using acetone to remove extractives.

• All pulps are fractionated at P-14/R-28.

◦ Ambient environment testing conditions: Temperature = $23 \pm 1^\circ C$; relative humidity = $60 \pm 5\%$.

Table 8.3: Specifications concerning wood-pulp fibre samples used in tensile-mode fatigue-testing.

Sample No.	Wood Species	Pulping Process	Refining Energy (GJ/t)	Frequency (Hz)	Number of Cycles
1	Jack pine	<i>RMP</i> [†]	6.5	0.187	5700
2	Black spruce	RMP	4.3	0.187	6000
3	Jack pine	RMP	8.5	0.187	6100
4	Loblolly pine	<i>CTMP</i> [‡]	6.4	0.187	6500
5*	Jack pine	RMP	8.7	0.187	6500

[†] RMP = Refiner mechanical pulp; one-stage refining at 1200 rpm.

[‡] CTMP = Chemi-thermomechanical pulp; two-stage refining: 1st stage at 1800 rpm (high intensity), 2nd stage at 1200 rpm. Also pulp is treated with 2% Na_2SO_3 .

* Pulp fibre was washed using acetone to remove extractives.

• All pulps are fractionated at P-14/R-28.

◊ Ambient environment testing conditions: Temperature = $23 \pm 1^\circ C$; relative humidity = $60 \pm 5\%$.

8.2 Image Analysis

Extensive treatment of the theory of confocal microscopy has already been presented in the previous chapter. However, it may be useful to recall some aspects that are specifically related to image analysis. The image in a CLSM, whose resolution is essentially determined by the diffraction-limited laser beam size, is built up point by point (i.e., pixel by pixel) by scanning either the laser beam or sample. The CLSM has a distinctly better lateral resolution than the conventional optical microscope [287]; furthermore, digital image processing may be used to improve the image signal-to-noise (S/N) ratio and contrast.

Raw images engendered from the CLSM are two-dimensional; however, optical sectioning (or slicing) enables, by means of software,⁵ two forms of image construction from a three-dimensional image data block⁶ of a stack of two-dimensional images acquired over the depth of the thick translucent object, the pulp fibre. In the first form of image construction, which is most useful in terms of producing hardcopies, the image slices in the three-dimensional image data block are added to give a two-dimensional image that is in focus throughout the entire depth of the original block.⁷ Whereas, using a suitable visualisation software, these two-dimensional images may be rotated, manipulated and displaced on a (VDU) monitor as a three-dimensional structure.

In the course of this research, two kinds of images were generated: (1) surface images indicating the morphology of the fatigued fibres; and (2) cross-sectional images to gain insight into the structural collapse of the fibre wall. In order to scan the image plane—in both cases—through the depth of the fibre, with the focal plane of the

⁵In the course of this research, we have endeavoured to expand manoeuvrability with available graphics capabilities on the system by writing macros—based on the OS9 operating system. However, these macros are specific to this operating system and already-existing basic graphics manipulation routines (of the Leitz system); which unfortunately render them incompatible with other CLSM systems.

⁶Recall that images are converted to digital form using the computer system controlling the CLSM (see Section 7.4 of Chapter 7 in its entirety).

⁷This, it must be noted, cannot easily be generated with a conventional optical microscope.

CLSM being fixed relative to the optics, the object itself must be moved along the optical axis. However, while the modality of scanning is similar for both cases, the particulars for obtaining surface and cross-sectional images are somewhat different. Surface images, i.e., x-y images (refer to Figure 8.6), are obtained from a series of horizontal line scans acquired while stepping the sample stage vertically along the depth of the fibre (i.e., fibre diameter). This is in the case if the fibre is on a glass slide; however, when *in situ*, that is during fatigue-testing, the vertical movement is controlled via the micrometer screw-head of the support/stage mechanism. It should emphatically be enunciated that *in situ* scanning is not a means for obtaining detailed morphological micro-images of the fibre for two reasons: (i) limitation to using only low-magnification objectives (at most 10x), would result in significant details being overlooked; and (ii) while *in situ*, the fibres cannot be placed in a proper mounting medium,⁸ thus contributing to the distortion of the images by increasing the optical aberration of the system. Therefore, *in situ* imaging is solely used for *monitoring* the fibres during fatigue-testing.

On the other hand, to generate cross-sectional images, the fibre must first be oriented perpendicular to the direction of scanning — along the y-axis of Figure 8.6 — and images are constructed by scanning in the x-z plane at a specified point along the y-axis. Typically, the smallest step size available, 0.16 μm , is used, and a maximum of 64 scans per step are averaged to increase the S/N ratio. Similarly for surface images, except that a range from 0.16–1 μm is used for the step size. In all cases, moderate laser power is made use of — through utilising a neutral density filter. Observations are made as follows: 100x and 63x semi-apochromatic objectives with numerical apertures of 1.20 and 1.30 (both oil immersion), respectively, are utilised for obtaining cross-sectional images; whilst principally 25x, 32x and 40x objectives with numerical apertures of 0.35, 0.40 and 1.30, respectively, for the surface images.

As alluded to above, detailed confocal images, both cross-sectional and of the surface morphology, are obtained after the completion of fatigue-testing: fibres are dismantled and placed on a glass slide for *post mortem* examination. Since pulp fibres

⁸Refer to the discussion below on the importance of a suitable mounting medium for reducing optical aberration.

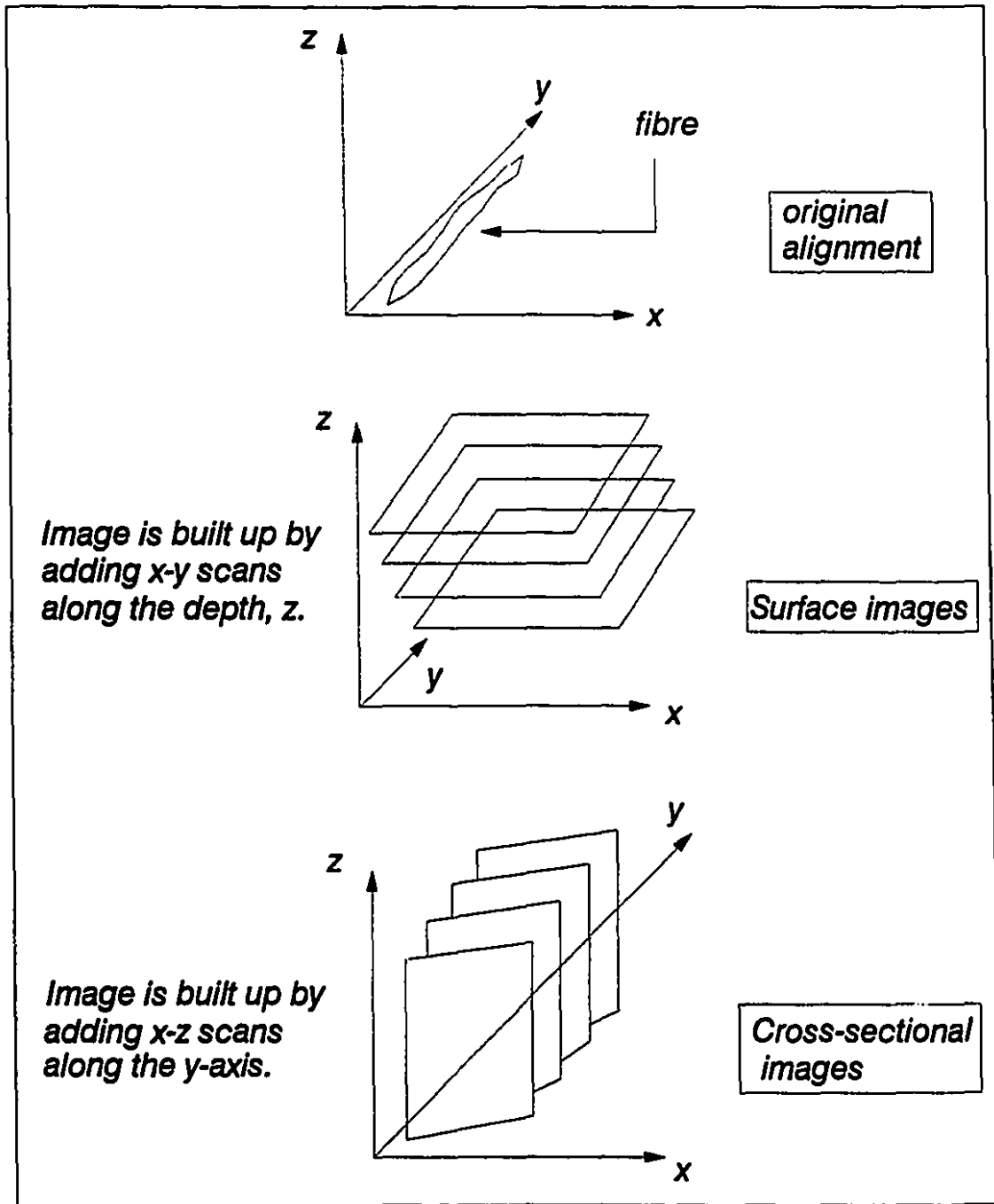


Figure 8.6: Schematic illustration of surface and cross-sectional image scanning in a Leitz CLSM system.

are only weakly fluorescent, they need to be dyed with fluorochrome dye in order to obtain a good image in fluorescence mode. After removing excess dye, through washing the fibre with water, the fibre is mounted in Zeiss immersion oil 518C, and covered with a cover glass (#1, thickness=0.169 mm), which is then sealed with nail polish. The immersion oil is used because its refractive index ($n_e=1.518$ at 23°C) is close to that of the fibre, microscope slide and cover slip. This conclusion, i.e., suitability of immersion oil as a mounting medium, was reached after having experimented with various mounting media: oil immersion gave the best defined images especially in the case of xz-images, since distortion is significantly increased if an inappropriate mounting medium is chosen — as shall be explained below.

These findings were corroborated by those of Leung [162] who concluded from his experimental investigation with $9\ \mu\text{m}$ fluorescent beads that, “distortion of the xz-image varied inversely with the refractive index of the mounting medium.” He had experimented with various mounting media (from Zeiss immersion oil to PBS, $n_e=1.333$) and found that undistorted images of the fluorescent beads were only observed when immersion oil was used to mount them. Furthermore, he investigated the influence of the thickness of cover glass on induced spherical aberration in confocal images. His findings revealed no noticeable difference in resolution when using either #0 (thickness=0.125 mm) or #1 cover glasses, however, distortion was apparent when the image was collected from #2 (0.216 mm) cover glass. The rationale will follow in a rather straightforward manner if it is recognised that objective lenses are designed to be optimally corrected for objects located immediately below the cover glass; hence, the necessity to mount the specimen as close to the cover glass as possible — by removing excessive mounting medium. This also minimises the amount of spherical aberration caused by unmatched mounting media. All of the aforesaid may easily be understood from the basic principle of optics, as shown in Figure 8.7.

Lastly fluorescence images, in the course of this work, could be obtained with two sets of excitation filters: 488 nm (FITC) and 514 nm (Rhodamine). The strongest fluorescence signals are, however, acquired with fibres weakly dyed in a very dilute solution of Fluorine-ruby (2% in saline solution at room temperature with dyeing times of 2–5 minutes) and the FITC filter set. (All confocal micrographs presented

in this thesis were obtained using this combination.) It should further be noted that signals rapidly deteriorate through the thickness of a fibre, if the latter is strongly dyed.

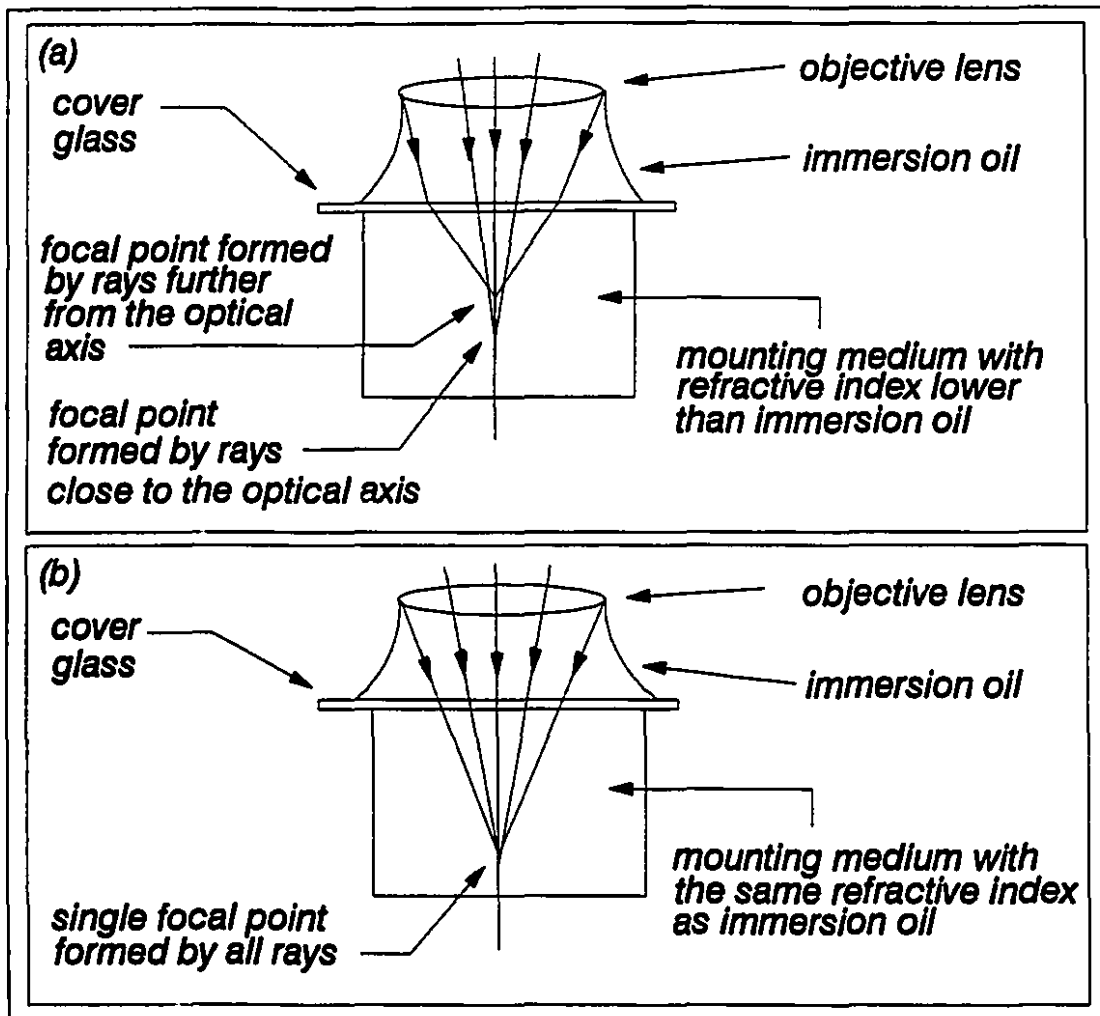


Figure 8.7: Light refraction in media of identical and different refractive indices to expound effects of mounting media on the spherical aberration of confocal images, when using oil-based objective lenses: (a) When passing through a mounting medium of low refractive index, rays from the periphery of the objective lens converge to a focal point different from the one formed by rays closer to the optical axis, thus inducing spherical aberration. (b) However, if the refractive indices of both, the immersion oil and mounting medium, are the same, rays from all parts of the lens are focussed on the same focal plane. (N.B. In both cases, the thickness of the covering glass is assumed to be very small, hence causing no change in the path of the rays.)

8.3 Morphological Features of Fibres: A Cumulative Fatigue Damage Analysis

There may be several ways in which the results of this research, which are *suis generis*, may be presented. When considering a comprehensive study that endeavours to expound the fundamental aspects of material formulations — under mechanical action — of a complex system such as wood-pulp fibres, it is paramount that no detail is overlooked even though some of the present tools may prove inadequate to explicate each and every phenomenon. Moreover, odd or contradictory occurrences should not be eschewed: on the contrary, they may instigate the adoption of a novel modality to understanding existing phenomena. The prime purpose is to underscore the necessity to objectively present the outcome of the present work, provide a cogent analysis of the results, set forth the path for future considerations, and finally seek to contribute to advancing scientific knowledge with the broad prospects of transcending conventional models merely relying on macroscopic interpretations.

In what follows, the results are presented in a progressive manner, i.e., crack propagation, structural changes, failure mechanism, etc., in relation to each mode of testing. Along with offering a rudimentary interpretation of each phenomenon according to the level at which it occurs — i.e., microscopic, mesoscopic and macroscopic.

At this juncture, it is deemed of import to precisely elucidate what is meant by the three scales at which materials may be grouped. For starters, recall that the fibre specimens in question are of minute dimensions: 1–3 mm long and 20–40 μm in cross-section — this is the macroscopic scale. The fact that a microscope is used to view the intact specimens should not confound the issue of scaling; small dimensions notwithstanding, they represent the *macroscopic* frame of reference — in global terms — from which other scales are gauged. Hence, the scale at which such phenomena as cracks, dislocations, delaminations, volumetric expansion, etc., is referred to as the *mesoscopic* scale. Explanations emanating from consideration of the atomic structure fall within the *microscopic* scale, which are, strictly speaking, deduced, at this juncture, from mesoscopic observations. The aforesaid is in agreement with the rationale of Figure 4.6 of Chapter 4. Hereinafter, we shall adhere to the scaling

system described above.

8.3.1 Crack Formation and Propagation

The initiation of cracks at the atomic level cannot, at this stage, be conclusively ascertained; however, the current results will tremendously help in elucidating the phenomena at the macroscopic scale—and consequently make appropriate conclusions—as well as significantly *contributing* to formulating a comprehensive theory at the microscopic level. It is thus deemed apposite to try and understand the genesis of crack formation in accord with the structural changes occurring in the fibre being subjected to cyclic loading as a function of the number of cycles, and further examine this relation in the light of other relevant parameters, such as: refining energies, wood species and pulp type. With this in mind, the results acquired from cyclic-shear testing are first examined.

Shear testing From the samples that have been tested under cyclic shear—refer to Table 8.1—no influence on the rate of crack growth, crack initiation and propagation may be attributed to species variation (jack pine, loblolly pine or black spruce) as the results, which will momentarily be canvassed, shall attest.

A litany of tenuously-oriented microcracks coalesce to form a dominant macrocrack which, upon referring to Figure 8.8(a), may clearly be seen to propagate along the fibre length. It is also evident that some macrocracks do span across the fibre (Figure 8.8(b)); others form interesting geometrical shapes (Figures 8.8(c) and 8.11(a)) which may easily be understood by delving deeper into the particular species and its characteristics. As pertains to the latter point, it is common knowledge that wood fibres contain naturally-existing defects such as pits, and in the case of jack pine, they may take up shapes as the ones shown in Figure 2.5 of Chapter 2. These natural defects are locations of stress concentration, hence, it is to be expected that microcracks actually initiate at such weak points and consequently propagate in their proximity. If the number of cycles is increased to less than 15%—i.e., from 1050 to 1200 cycles—, while considering another fibre with identical characteristics, namely, wood species, refining energy, pulping method and frequency, no significant effect on the degree of

Figure 8.8: Fluorescence confocal micrographs of a jack pine (*Pinus banksiana*) subjected to 1050 cycles in shear (sample #2 in Table 8.1) depicting: (a) dominant longitudinal macrocrack; (b) occurrence of transversely-oriented macrocracks; and (c) geometrical orientations of the macrocracks peculiar to this species type.

a



maturation of the cracks or orientation of propagation is noticed.⁹ Similar remarks may be made if the characteristics are, however, changed to: loblolly pine, CTMP, 6.4 GJ/t refining energy, while retaining the same frequency, 0.0262 Hz, and the same fatigue life, 1200 cycles—Figure 8.9 clearly shows the propagation of a dominant, longitudinal macrocrack.

Expanding the latter discussion to two more different species (black spruce and jack pine, sample Nos. 5 and 6, respectively, in Table 8.1) obtained from a rather higher refining energy, while maintaining the same fatigue life, leads to concluding the following: the initiation and propagation of cracks (initially microcracks coalescing to form dominant macrocracks) are principally governed by the number of cycles¹⁰ the fibre specimen undergoes. While pulp fibres obtained from higher refining energies indicate a higher susceptibility to undergoing overall damage, i.e., material property degradation (which we will further explore in the succeeding section), an *indirect* relationship may be deduced as to the influence of refining energy on increasing (or decreasing) the rate at which the crack propagates and its degree of maturation: The higher refining energies indicate a larger period of exposure to external actions (i.e., cyclic forces), thereby enhancing the structural damage imposed on the fibre. The latter provides fertile ground for cracks to form and subsequent degradation characteristics to materialise.

Furthermore, examining Figure 8.10, which depicts a jack pine pulp fibre engendered from a much lower refining energy (4.4 GJ/t), and experienced a mere 350 cycles, reveals that: an inchoate macrocrack slightly deviating from its dominant longitudinal path distinctly appears at this stage. It should be remembered that this particular fibre had the extractives removed, thus clarifying the dependence of crack propagation and maturation on the structural deformation of the fibre structure with respect to the fatigue life. Moreover, the developed, longitudinal macrocrack will, as

⁹See Appendix E for more results.

¹⁰Frequency is also expected to influence the rate of crack growth, particularly when dealing with a viscoelastic material; however, the frequency has been kept constant with respect to each mode of testing since it was our intention to establish the fundamental behaviour of pulp fibres under cyclic loading in order to set the ground upon which further studies may be based.

Figure 8.9: Propagation of a dominant longitudinal macrocrack in a loblolly pine subjected to 1200 cycles in shear at 0.0262 Hz (refining energy = 6.4 GJ/t; CTMP).

Figure 8.10: A fluorescent confocal micrograph depicting the crack propagation at an early stage of the sample fatigue life. The sample is: jack pine RMP (washed); refined at 4.4 GJ/t and experienced 350 cycles in shear at 0.0262 Hz.



the number of cycles increases, act as the region where eventual peeling-off of some of the material of the external layer of the fibre cell wall occurs. The slow crack growth, which seems characteristic of the fatigued pulp fibres, is symbolised by the opening of the cracks with increasing fatigue life—refer to Figure 8.11(b).

Upon a thorough re-examination of Figures 8.8 - 8.11, one is to deduce that initiation occurs at the fibre surface leading to the formation of motley microcracks which coalesce to form a dominant macrocrack that tends to orient itself longitudinally. This occurs in unison with transverse macrocracks which may sharply be deflected from the radial direction to run at a slight angle to the axial direction. The atomic structure around the initiation point seemingly determines the direction in which the macrocracks propagate; moreover, cases where there is no natural bias, the crack tends to propagate along the fibre in an unabated fashion. The crack formation and propagation pay tribute to the fact that the microfibrils—which are mainly made up of cellulosic chains—are *not* aligned with the fibre axis (refer to Section 4.1 of Chapter 4 in its entirety): The macrocracks propagate in a manner parallel to the orientation of the (mechanically-superior) cellulose chains. The cohesion and, hence, strength of the filamentary composite tube, i.e., the fibre, are largely dictated by the strength of the cellulosic microfibrils: once the latter become structurally degraded, i.e., the crystalline structure is re-arranged, then the amorphous hemicellulose-and-lignin matrix can no longer hold the layers of the laminated tube together; subsequently leading to the delamination of the external wall layer, and the complete peeling-off of cell wall material—as we shall see in a short while. Furthermore, if we recognise the higher (global) anisotropy of the fibre cell wall in the longitudinal direction, then it becomes clearer as to why the macrocracks take a dominant path longitudinally—if no natural defects deviate the crack direction.

In the preceding chapter, the necessity of establishing a point-to-point contact between the fibre specimen and the applicator was alluded to. A jack pine pulp fibre (sample No. 9 in Table 8.1) was subjected to 36000 cycles, however, with the applicator being in superficial contact with the fibre surface: Because the latter is naturally uneven, under this arrangement, *no* point-to-point correspondence can be established. *Post mortem* examination revealed absolutely no (developed) crack

Figure 8.11: (a) Mature macrocracks as well as evidence of cracks taking the shape of bordered pits (regions of high stress concentration) in a jack pine RMP (6.5 GJ/t) which experienced 1750 cycles in shear at 0.0262 Hz. Clearly illustrated in the micrograph as well, is the phenomenon of peeling-off of parts of the external layer of the cell wall material. (b) Slow crack growth leading to the opening of the macrocracks as the number of cycles is increased by about 20% (i.e., to 2100 cycles) for a pulp fibre of identical properties as that in (a).



formation, or the occurrence of other phenomena indicating structural damage in the fibre body, which can only be attributed to the fact that no effective shearing action was actually applied to the fibre specimen. This presents an important practical implication: The edges of bars of the refiner disc are responsible for imposing external actions on the pulp fibres, which, in turn, translate into structural re-arrangement of the fibre cell wall.

Radial-compression testing Turning our attention to the results engendered from cyclic radial compression testing, one overwhelming factor comes to the fore: a significantly higher number of cycles is required to effect permanent material damage in the fibre cell wall. For fibres—refer to Table 8.2—tested at below 3000 cycles, no developed cracks are observed; nor do we notice any significant structural changes in terms of internal and external fibrillation or collapsibility of the fibre cell wall (see Appendix E for some of the results). However, as the number of cycles approaches ten-fold the lower limit at which inchoate macrocracks form in a fibre subjected to cyclic loading, the fibre in question—i.e., the one being radially compressed—begins to experience the coming together of microcracks into a dominant longitudinal macrocrack. Figure 8.12 depicts the manner in which these macrocracks propagate, which is strikingly similar to the case of shear testing. In the confocal micrograph of Figure 8.12(a) the macrocrack continues to span the length of the fibre until it is rather sharply deflected—as in Figure 8.12(b)—owing to the presence of natural deformities in the fibre cell wall. Within the vicinity of the deformity, a region of high stress concentration, a litany of microcracks combine into another dominant macrocrack which, in turn, propagates longitudinally. The dominant cracks mature rather prominently as the fatigue life is increased by about 50% (from 3400 to 5000 cycles), regardless of the wood species used—refer to Figure 8.13. It is worthy of note that the refining energy of the fibres in Figure 8.13 is roughly one-third higher than that of the fibre presented in Figure 8.12. Besides, a fibre having its extractives removed, that is cycled 5000 times, shows no variation in so far as the behaviour enunciated above is concerned. (N.B. consult Appendix E for further results.)

Tension testing Carrying the discussion further to consider testing under cyclic extension, it is to be recognised that even though the global mechanisms of crack

Figure 8.12: Fluorescence confocal micrographs of a jack pine pulp fibre (RMP, refining energy = 6.5 GJ/t) subjected to radial compression, 3400 cycles at 0.187 Hz: (a) Depicts the apparent volumetric expansion resulting from internal fibrillation in the fibre cell wall. Also shown is the propagation of a dominant longitudinal crack. (b) The crack from (a) continues until it is sharply deflected owing to natural bias. Another macrocrack (the upper of the two shown) is formed in this region of high stress concentration which also propagates longitudinally.

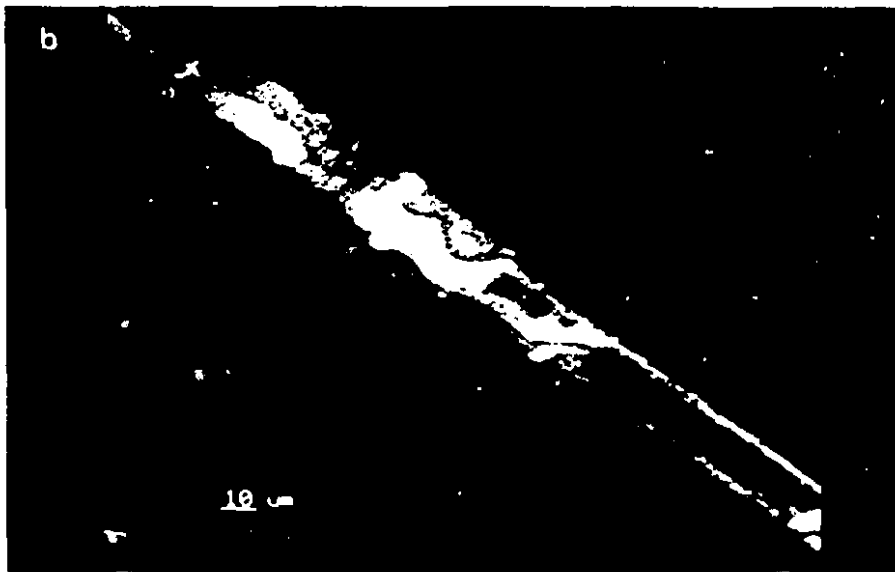
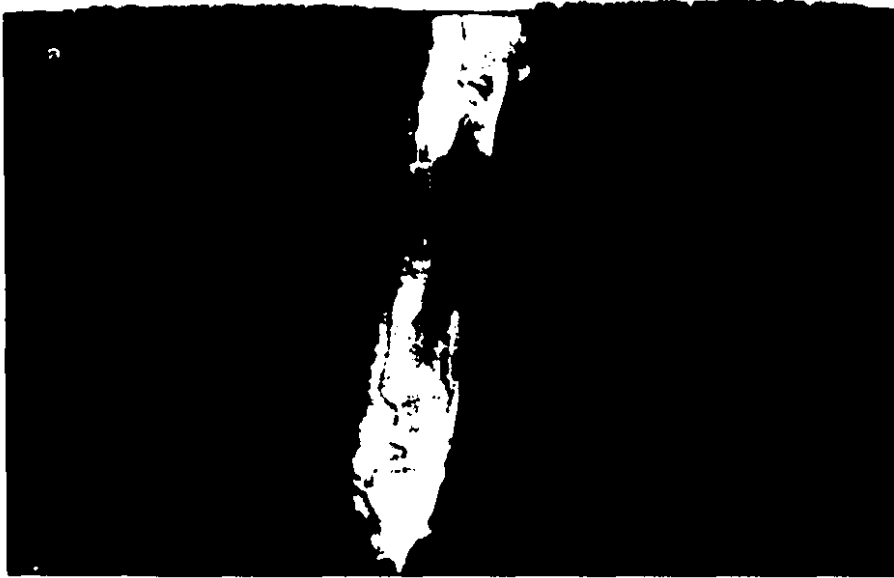
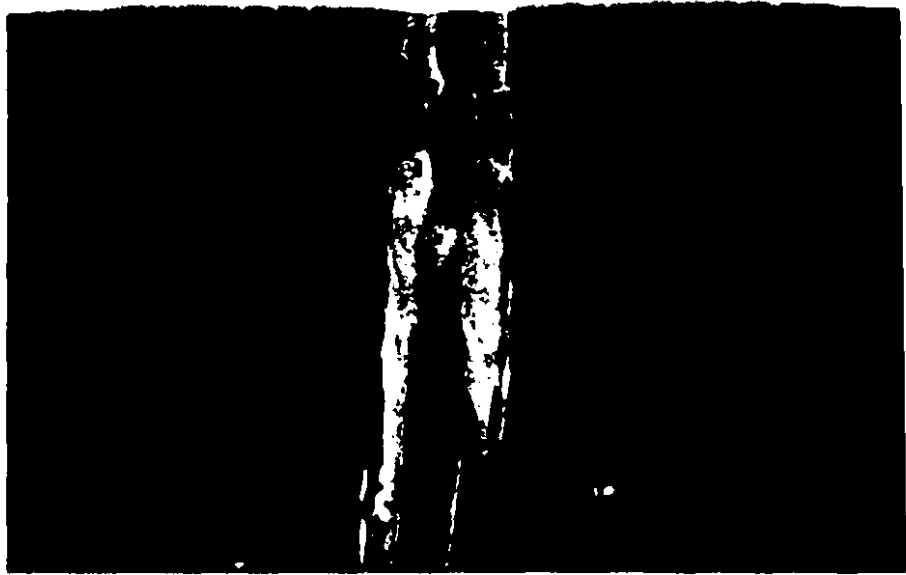


Figure 8.13: Fluorescence confocal micrographs depicting developed longitudinal macrocracks in pulp fibres subjected to cyclic radial compression, for two cases: (a) jack pine RMP (8.5 GJ/t) subjected to 5000 cycles at 0.187 Hz; and (b) black spruce RMP (8.5 GJ/t) subjected to 5400 cycles at 0.187 Hz. Also shown here is the volumetric expansion of the filamentary composite fibre.



propagation (as well as other structural changes, which will be considered later on) present a simile to what has been canvassed for both shear and radial compression testing, they are nonetheless extremely feeble in effect and degree of development. For all the fibres tested in this category, fatigue life of (in excess of) three-fold the maximum adopted for cyclic shear testing has to be reached before any semblance of material damage accumulation could be observed. Figure 8.14 depicts a sample cycled 6500 times in tension, in which inchoate longitudinal macrocracks are weakly apparent. Further indications on the insignificant effects of cyclic tension on pulp fibres shall be proffered in succeeding sections.

Figure 8.14: Inchoative crack formation in a loblolly pine fibre (CTMP, 6.4 GJ/t) cycled 6500 times in tension at 0.187 Hz.



8.3.2 Characteristic Material Degradation Properties

The recognition of any fatigue material degradation requires the systematic portrayal of the particular morphological phenomena conspicuous in pulp fibres subjected to cyclic loading. Concurrently, to fathom the causes of the general structural weakening of the material, it is significant to first comprehend the genesis of crack growth. While the latter has methodically been dealt with hereinbefore, the moment seems opportune to further the discussion to encompass the phenomenological behaviour and structural damage in fatigued fibres. From the discussion of the preceding section, crack initiation and propagation in regions of highly localised deformation are clearly most pronounced in fibres subjected to cyclic shear; whereas those undergoing cyclic radial compression and tension exhibit a much less significant formation, thus unequivocally tipping the balance to conclude the prominence of shear-loading effects relative to the others. The aforesaid chiefly assists in foretelling how the phenomenon of crack formation is intimately linked to the conspicuous structural and morphological changes in the body of the fibre. In what follows, an endeavour to carefully collate the engendered results is made.

The wall of the wood fibre of Figure 8.11(a), which consists of concentrically layered composite shells, is clearly seen to have had parts of the external layer being peeled off. The delamination of adjacent layers has occurred after the development of dominant macrocracks in this highly-strained region in the individual layer. With continued subjection to cyclic shear-loading, the chemical degradation of the cellulosic microfibrils and the ensuing inability of the amorphous matrix to withstand further straining, in effect, result in destabilising the interaction between the framework and matrix components; subsequently, the latter's disintegration, partial to regions of highly-localised deformation. This explains why the removal of (roughly) ovally-shaped parts of the cell wall layer material was also detected. This occurs in locations where natural deformities characterised by high stress concentration — previously alluded to in the discussion of the preceding section — are predominant. It is to be noted that this characteristic disintegration and internal changes in the wall structure take different forms; peeling-off of part of the cell wall material being only

one such form. Figure 8.15, showing confocal micrographs of jack pine pulp fibres subjected to 1050 and 1200 cycles in shear (refer to sample Nos. 2 and 8 in Table 8.1, respectively), prominently depicts the external fibrillation in, and partial removal of, the fibre cell wall material. The inchoate internal changes in the wall structure result in partly delaminating the external wall layers while keeping them still attached to the fibre body.¹¹

Furthermore, pulp fibres subjected to cyclic loading poignantly depict a propensity for volumetric expansion, i.e., swelling. They however differ in their propensity for swelling depending on the extent of material property degradation and damage accumulation, which are intrinsically associated with the mode of loading (i.e., cyclic shear, radial compression or tension). Figure 8.16 superbly illustrates two such occurrences. The development of macrocracks in the highly-strained regions of the cell wall (see Figure 8.16(a)) principally contributes to such formations as the strength of the matrix is expected to be significantly decreased with increasing fatigue life—as the number of cycles increases, the crystalline structure of the cellulosic microfibrils is successively re-arranged then, at a particular level of damage accumulation, the microfibrils may wholly degrade leaving the matrix in an unstable state—, thus allowing a faster rate of cell wall breakdown under mechanical action. Moreover, the random breakage of the cross-links in the inter-fibrillar matrix during the cyclic variation of shear action on the fibre, causes a loosening of the laminated structure that results in the volumetric expansion of the fibre body. It is crucial to further note that, at times, large macrocracks—which are caused by the coherent breakage of the inter-fibrillar matrix (most likely) in planes—induce complete separation of whole chunks of the fibre cell wall material, which may clearly be seen in Figure 8.16(b).

In light of the foregoing discussion and what has been canvassed in the preceding section regarding crack evolution in fibres subjected to cyclic radial compression, it is to be expected that the phenomena characteristic to cumulative material degradation become apparent after the fatigue life of the fibre has reached a high enough level. This

¹¹Many more supporting evidence is proffered in Appendix E. It should further be noted that in excess of 7000 confocal images were compiled; however, it would be impractical to append them in full: the gist of the discussion is, nonetheless, strictly uncompromised.

Figure 8.15: The prominent partial delamination of the external wall layers, while leaving parts still attached to the fibre body, is a consequence of the cycle-dependent damage accumulation in the fibre cell wall which translates into destabilising the framework-matrix interaction of each layer of the laminated composite tube—externally first, then, successively inwards. A concomitant consequence of material degradation and immanent structural changes is the occurrence of fibrillation in the external (as well as internal) cell wall layers. These morphologies are illustrated in the fluorescence, confocal micrographs of: (a) jack pine pulp fibre (RMP, 6.5 GJ/t) subjected to 1050 cycles in shear at 0.0262 Hz; and (b) a fibre similar to (a), however subjected to 2100 cycles.

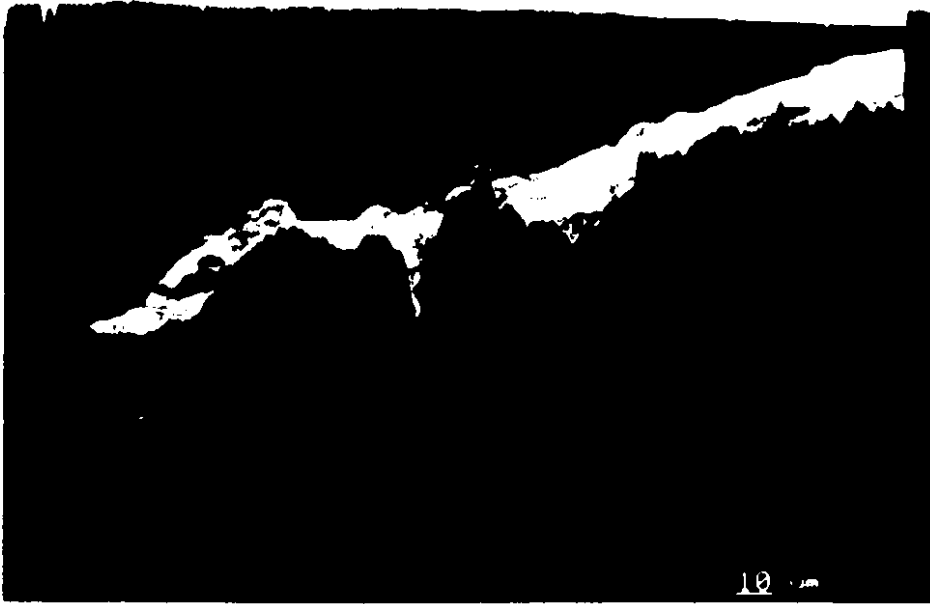


Figure 8.16: A significant consequence of the internal fibrillation of, and the maturation of macrocracks in, the fibre cell wall material is the occurrence of volumetric expansion: (a) Developed macrocracks in the external layer of the cell wall — which are, in this case, oriented along the helical micrographs of the S_2 layer — allow a faster rate of cell wall breakdown owing to the resulting structural instability of the framework-matrix interaction. (Fibre sample: jack pine RMP, refined at 6.5 GJ/t, subjected to 2100 cycles in shear at 0.0262 Hz.) (b) The loosening of the structure of the laminated composite fibre resulting from random degradation of the inter-fibrillar matrix, induce the complete separation of whole chunks of cell wall material. (Fibre sample: jack pine RMP, refined at 6.5 GJ/t, subjected to 1050 cycles in shear at 0.0262 Hz.)



level ensures the presence of highly-strained regions where developed macrocracks will progressively undermine the framework-matrix interaction within each layer of the laminated composite fibre so that the latter's structure is ultimately destabilised. These phenomena are quintessentially represented by: volumetric expansion, internal and external fibrillation of the cell wall material; and the partial delamination, and eventual, gradual peeling-off, of the material of the layers comprising the fibre cell wall. Figure 8.17 photomicrographically depicts the latter statement.

According to the aforesaid, a mild occurrence of the above described phenomena is expected, in so far as fibres subjected to cyclic tension are concerned. At the highest attained fatigue life, a fibre subjected to cyclic tensile stroke (while removing any slack developed with the number of cycles) could only exhibit (very limited) partial delamination; and some semblance of fibrillation of the external layer of the cell wall—as shown photomicrographically in Figure 8.18. The reasoning for the latter should follow from foregoing discussions and, hence, shall not be repeated.

Figure 8.17: Fluorescence, confocal micrographs of a wood pulp fibre (jack pine, RMP, refined 6.5 GJ/t) subjected to 3400 cycles in radial compression (at 0.187 Hz) illustrating the characteristic material degradation phenomena due to the cumulative damage after a large-enough number of cycles: (a) developed, longitudinal macro-cracks contributing to the general weakening of the framework-matrix interaction symbolised by the partial delamination and extensive internal fibrillation of the cell wall material, which also results in the local volumetric expansion of the fibre; and (b) the unravelling (peeling-off) of parts of the external layer material while leaving the remainder of the layer still attached to the fibre body.



Figure 8.18: Pulp fibres tested under cyclic tensile stroke only show insignificant degree of damage accumulation represented by partial delamination, and weak external fibrillation, of the external layer of the cell wall. This fluorescence confocal micrograph is of a loblolly pine (CTMP, refined at 6.4 GJ/t) cycled 6500 times at 0.187 Hz.



8.3.3 Structural Integrity of the Fibre Wall

A deeper insight may be gained into the global integrity of the laminated composite structure by examining the fibre collapse behaviour. The latter may be indicated by examining optical (transverse) cross-sections of the fibre, which can non-destructively be obtained through utilising confocal scanning microscopy techniques — discussed in detail in Sections 7.4 of Chapter 7, and 8.2 of the current. In this way, not only is a relationship between fibre collapse, on the one hand, and the fibre wall thickness and cross-sectional area, on the other, formulated, but a reliable tool is made use of to corroborate (or refute) current findings germane to the cumulative damage phenomena. While taking cognisance of antecedent discussions regarding the latter's relation to such factors as: fatigue life, specific refining energy, etc., as per each mode of loading, the treatment of the subject of fibre collapsibility shall proceed in a manner that is entirely morphological.

Incipient degradation of the fibre cell wall material, even though conspicuous on the surface of the external layer — cf. Figure 8.10, does not yet present itself in any destabilising form: whether in terms of effects on the inter-laminar interaction between the cell wall layers or the global rigidity of the fibre cell wall — as may be surmised from Figure 8.19. As the number of cycles increases, material (chemical) degradation cumulates and subsequently translates in a more limpid fashion in so far as cell wall collapsibility is concerned. Furthermore, when juxtaposing the micrographs of Figures 8.20 and 8.21, it is recognised that, as expected, the collapse behaviour somewhat varies depending on the refining energy of the engendered pulp fibre; however, no influence *per se* is detected when modifying species or pulp type. Above this level of fatigue life, the number of cycles outweighs, in influence, the refining energy of the pulp, as the continued damage accumulation in the cell wall and the latter's progressive structural degradation become solely dependent on the number of cycles to failure. Of equal import, is the fact that at higher number of cycles the extent of material degradation is significantly enhanced: The confocal micrographs of Figure 8.22 illustrate, for jack pine (RMP) pulps of the same refining energy (6.5 GJ/t) and cycled in shear to 1750 and 2100, respectively, the morphological consid-

Figure 8.19: Fluorescence confocal micrographs of fibre cross-sections, 30 μm apart, indicating global structural integrity of the cell wall at incipient levels of fatigue damage accumulation — 350 cycles in shear. (Cf. the surface morphology of the same fibre shown in Figure 8.10.)

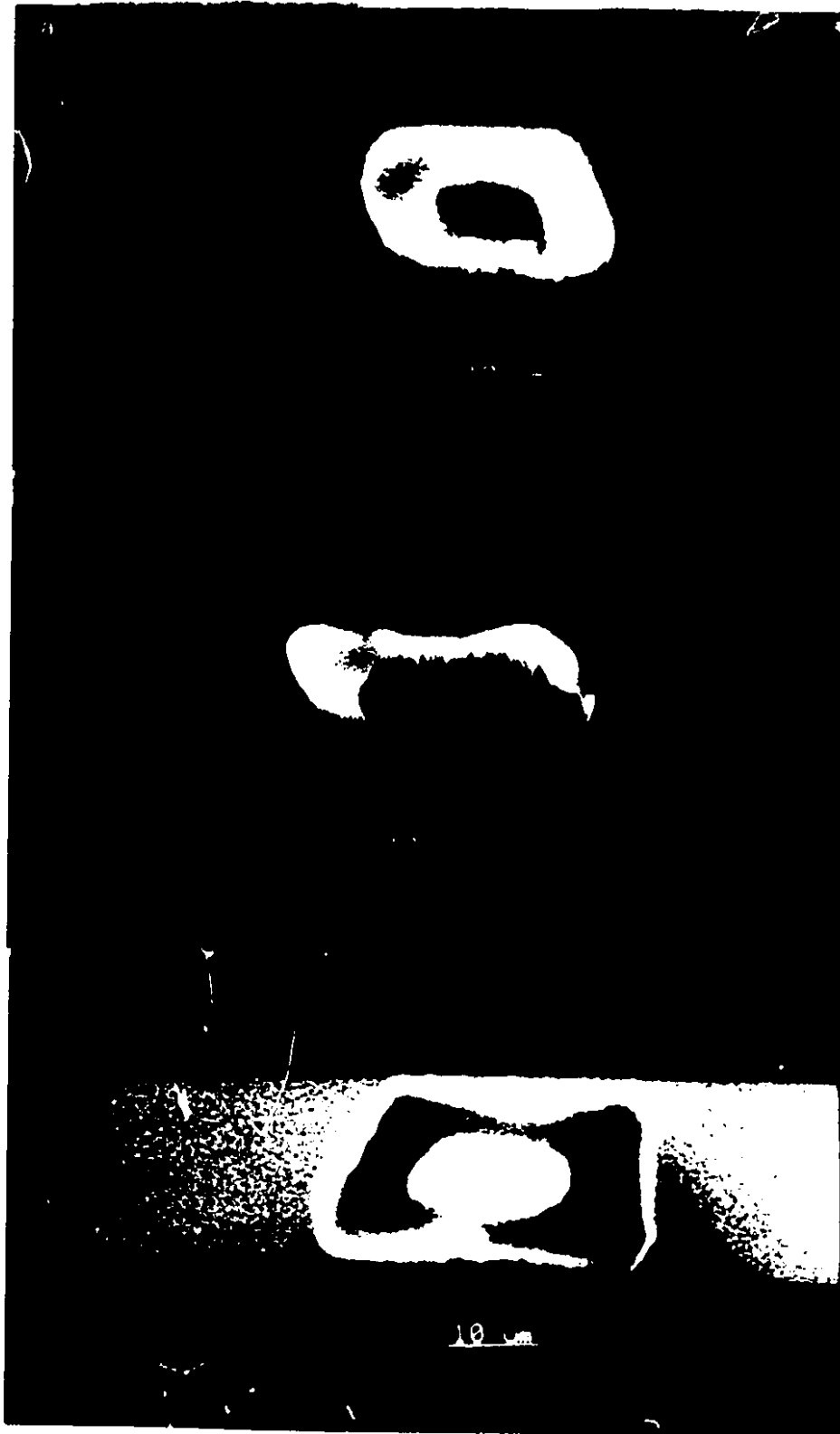
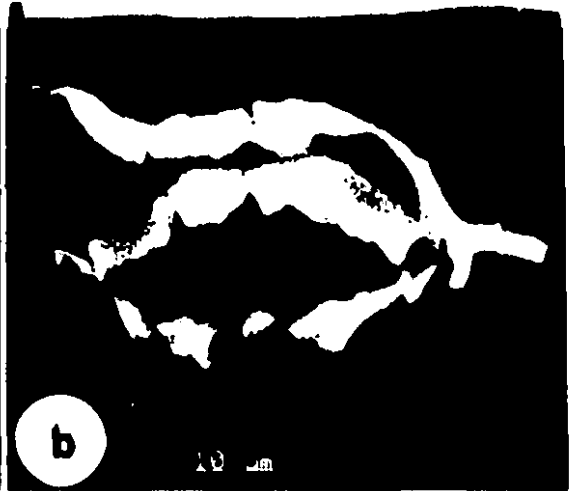
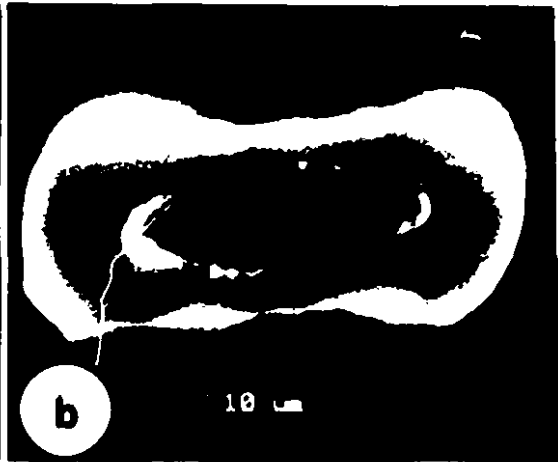
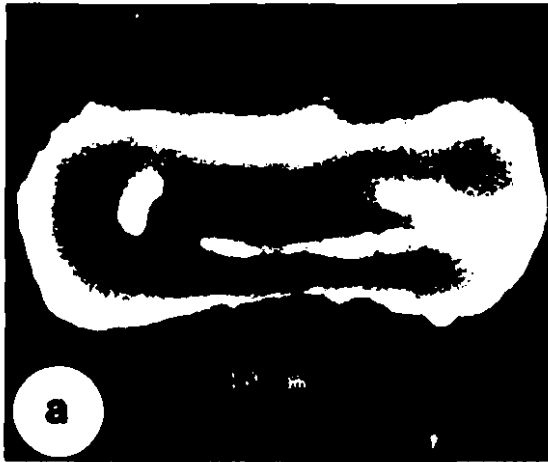


Figure 8.20: Cross-sectional fluorescence confocal images, 30 μm apart, of a loblolly pine CTMP (refined at 6.4 GJ/t) subjected to 1200 cycles in shear at 0.0262 Hz. Moderate structural collapse of the fibre cell wall is noticed, characteristic material degradation of the surface morphology notwithstanding.

Figure 8.21: In contrast to the above figure, a higher-refining-energy pulp fibre (8.7 GJ/t, jack pine RMP) cycled to the same number of cycles in shear exhibits more degradation of the fibre cell wall material characterised by more pronounced inter-laminar separation and cell wall collapse. Clearly evident, too, is the presence of slip planes and micro-compressions in the cell wall, and partial delamination of the external layer of the laminated composite tube.



erations of the cell wall (viewed in cross-section). It is rather evident from examining the aforementioned figures that the whole gamut peculiar to the fatigue damage accumulation, we have become accustomed to seeing in the course of prior illustrations, poignantly depicts itself in terms of: reduction in the cell wall thickness (i.e., thinning) due to peeling-off of cell wall material, random macrocracks traversing the cell wall thickness, inter-laminar separation, presence of micro-compressions and slip planes in the cell wall, and cell wall collapse due to reduced structural integrity of the laminated composite fibre (itself a consequence of the aforesaid material degradation phenomena).

Exploring the morphology of fibres subjected to cyclic radial compression reveals that by comparison to cyclic shear tests, the extent of overall progressive damage accumulation is ostensibly less pronounced: Consequently, the loss in structural integrity of the fibre cell wall is expectedly lower. The response of the laminated composite fibre to cycles of radial compression relative to the fatigue life, refining energy, etc., has previously been canvassed *ad infinitum*; the cross-sectional images shown hereunder seek to complement the aforesaid.

Figure 8.23 depicts confocal cross-sections, 30 μm apart, of pulp fibres (of three different species, two ranges of refining energy) at four limits of fatigue life. The trend that is clearly indisputable is the fact that material damage cumulates at a rate that is seemingly far too low to effect any basic structural collapse in the fibre cell wall; indeed, as witnessed in the preceding sections, crack formation and material degradation phenomena are confined to localised, highly-strained regions of the external layer of the laminated cell wall. Degradation of the inter-fibrillar matrix, while distinct in the external layer, does not seem to progress across the cell wall thickness even though the particular specimen is cycled to over twice the maximum level attained in shear-mode testing. This is unequivocally attributed to the influence rendered by the largely undegraded cellulosic fibrils which, at this juncture, oversee that the framework-matrix interaction is still coherent enough not to permit the collapse of the cell wall structure.

Confocal images obtained from pulp fibres subjected to cyclic extension stroke strike a resemblance with the above trend, as seen in Figure 8.24. Bearing in mind

Figure 8.22: Material damage accumulation in pulp fibres, after a certain fatigue life limit (around 1200 cycles), seems to be solely dictated by the number of cycles to which the fibre is subjected; moreover, damage rapidly cumulates as cycling exceeds this level. The above cross-sectional confocal micrographs are of two different fibres: (a)–(c) belong to a jack pine RMP, refined at 6.5 GJ/t and cycled to 1750 in shear at 0.0262 Hz; whereas (d)–(e) refer to a fibre only different from the above in that it is cycled to 2100 times in shear. The micrographs attest to the developed stage of the material chemical degradation, and subsequent loss of structural integrity, of the cell wall. (All optical cross-sections are obtained 30 μm apart.)

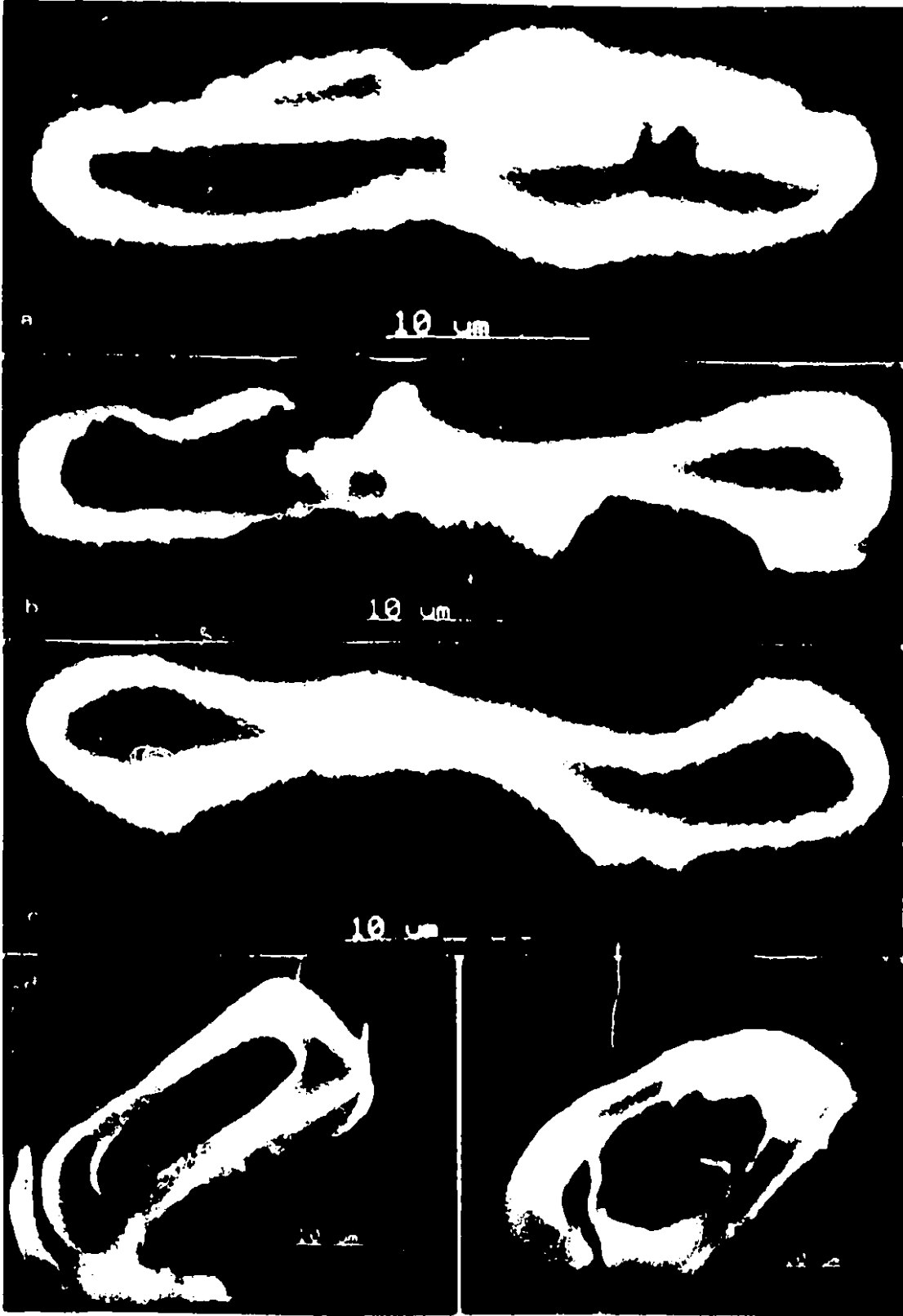
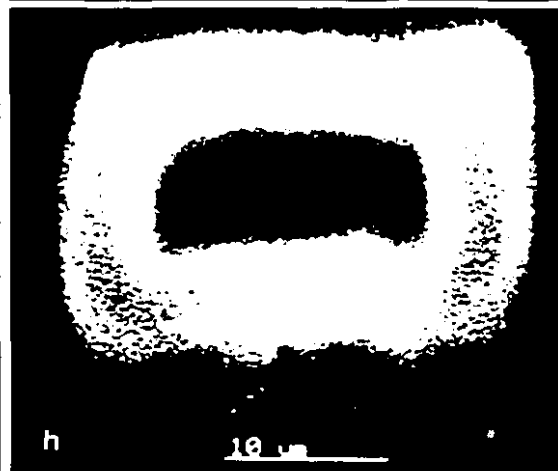
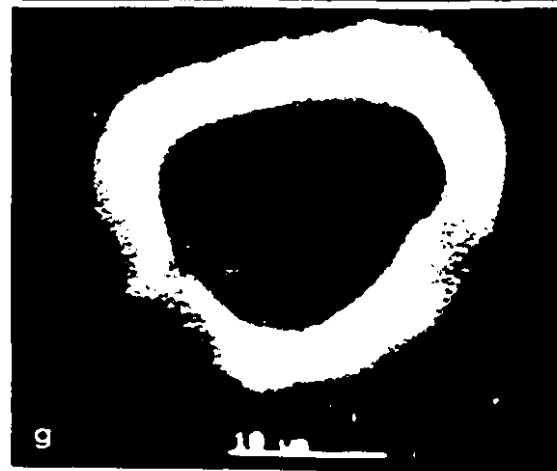
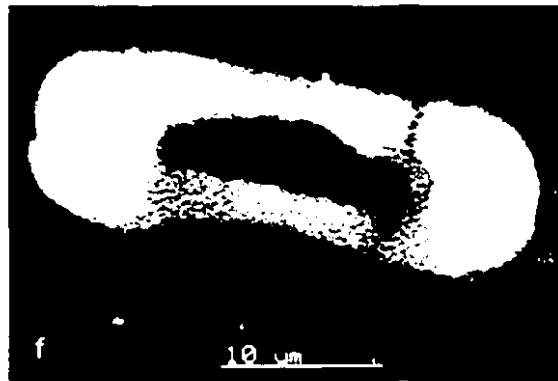
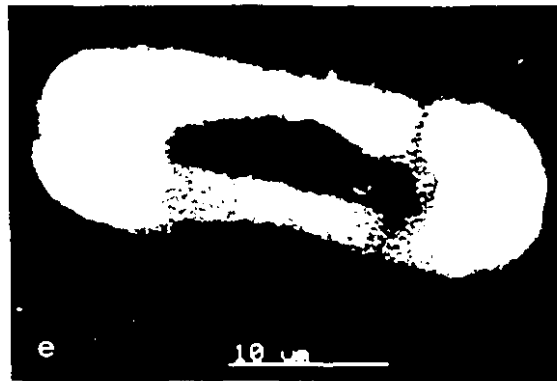
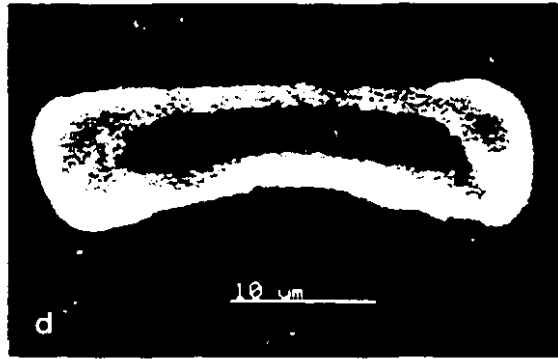
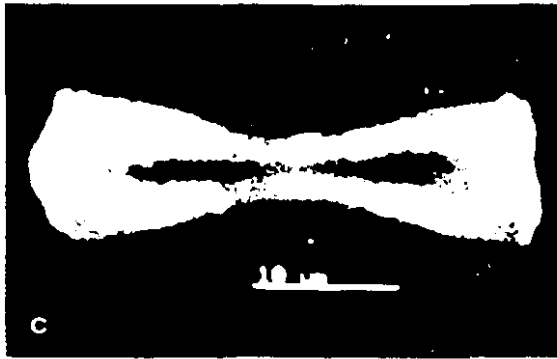
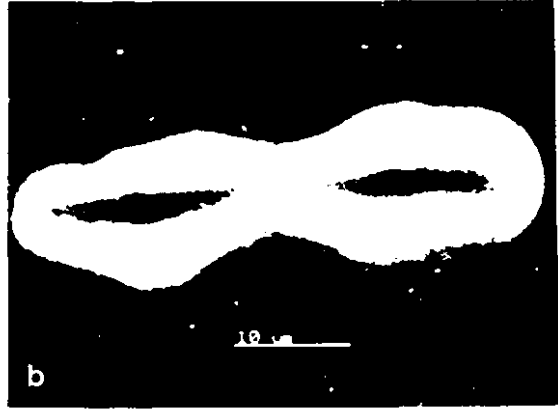
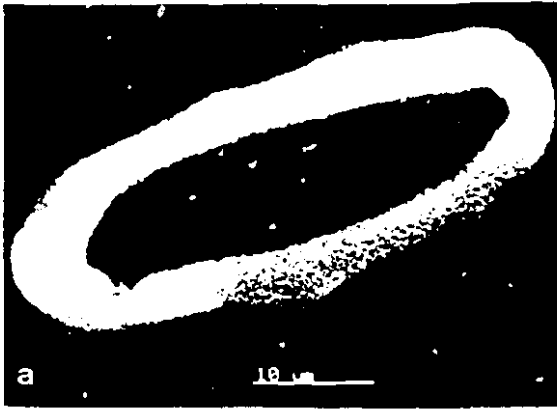


Figure 8.23: The cell wall structural integrity of fibres subjected to cyclic radial compression testing is hardly affected since the material damage accumulation occurs at an insignificant rate to cause the collapse of the inter-fibrillar matrix. The above confocal micrographs illustrate the cross-sections, $30\mu\text{m}$ apart, of a motley combination of pulp fibres: (a)–(b) refer to loblolly pine CTMP, refined at 6.4 GJ/t , cycled 350 times at 0.187 Hz ; (c)–(d) to jack pine RMP, refined at 6.5 GJ/t , cycled 600 times at 0.187 Hz ; (e)–(f) to jack pine RMP, refined at 6.5 GJ/t , cycled 2700 times at 0.187 Hz ; and (g)–(h) to black spruce RMP, refined at 6.5 GJ/t , cycled 5400 times at 0.187 Hz .



what is now known about the progressive damage accumulation due to cyclic tensile action, and in light of the discussion hereinbefore, the trend seen in the cross-sectional confocal micrographs of Figure 8.24 needs no further elaboration.

The last words must touch upon the recognition of non-uniformity in the cross-sections along any one pulp fibre—cf. Figures 8.21–8.24. Intact fibres, whose cross-sections are shown in figure 8.25, naturally exhibit this non-uniformity, which is varied depending on the rate of cell wall development within the tree.¹²

¹²For more cross-sectional confocal images of fatigued and intact pulp fibres consult Appendix E.

Figure 8.24: The localised material degradation in the external layers of pulp fibres subjected to cyclic tensile stroke becomes effaced as we traverse the cell wall cross-section: A trend strikingly similar to cyclic radial compression. The above confocal micrographs depict cross-sections, $30\ \mu\text{m}$ apart, of fibres whose characteristics are as follows: (a)–(b) refer to black spruce RMP, refined at $4.3\ \text{GJ/t}$, subjected to 6000 cycles in tension at $0.187\ \text{Hz}$; and (c)–(d) to jack pine RMP, refined at $8.7\ \text{GJ/t}$, subjected to 6000 cycles in tension at $0.187\ \text{Hz}$ (extractives, in this case, are removed from the cell wall).

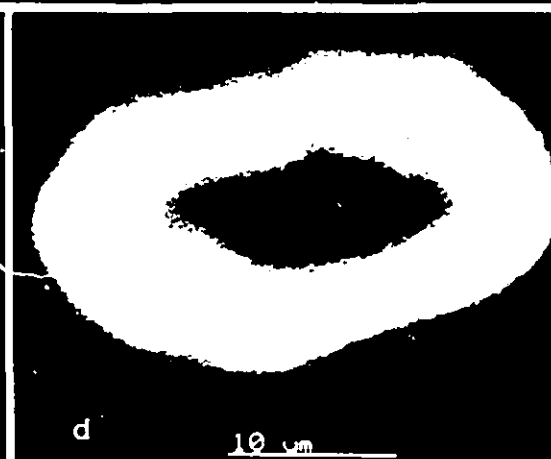
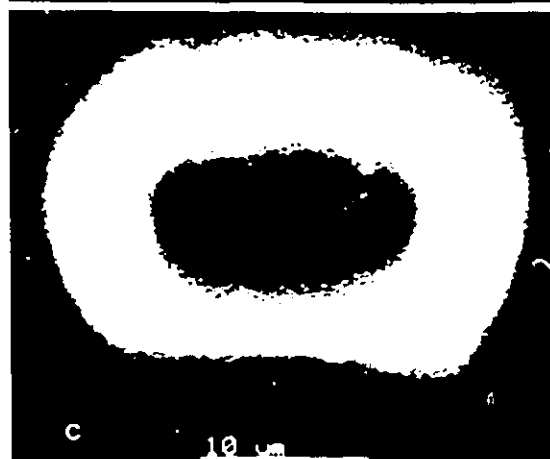
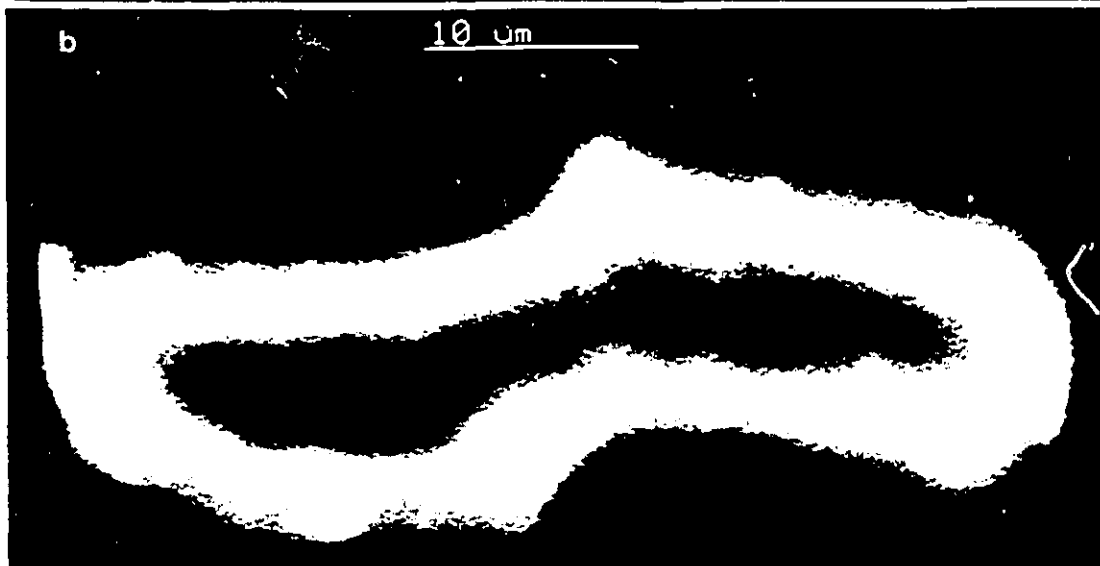
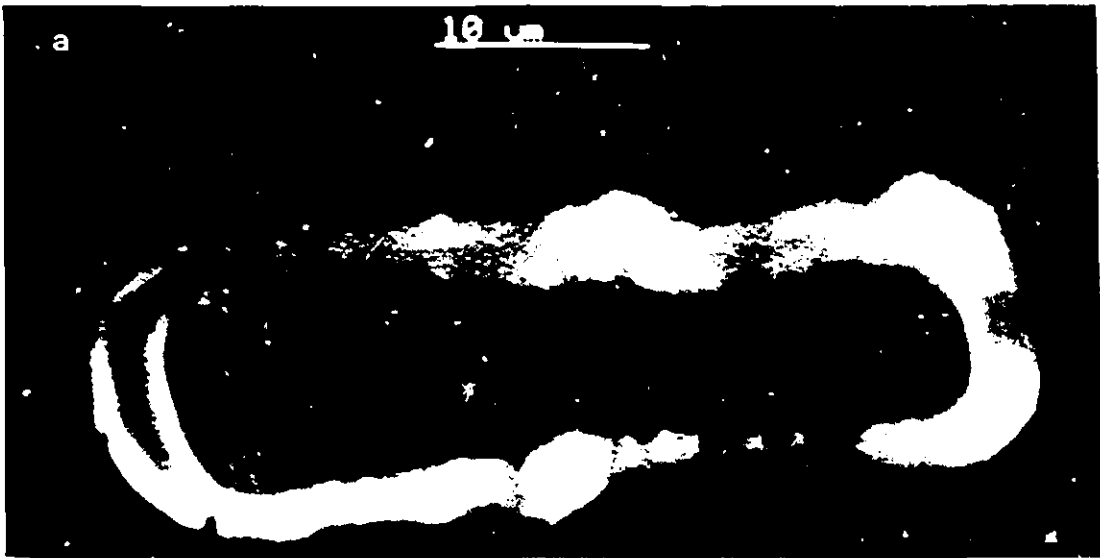
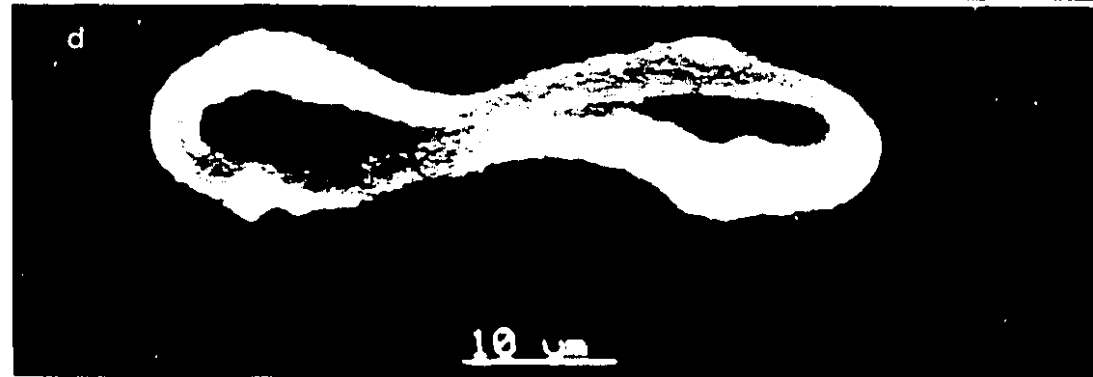
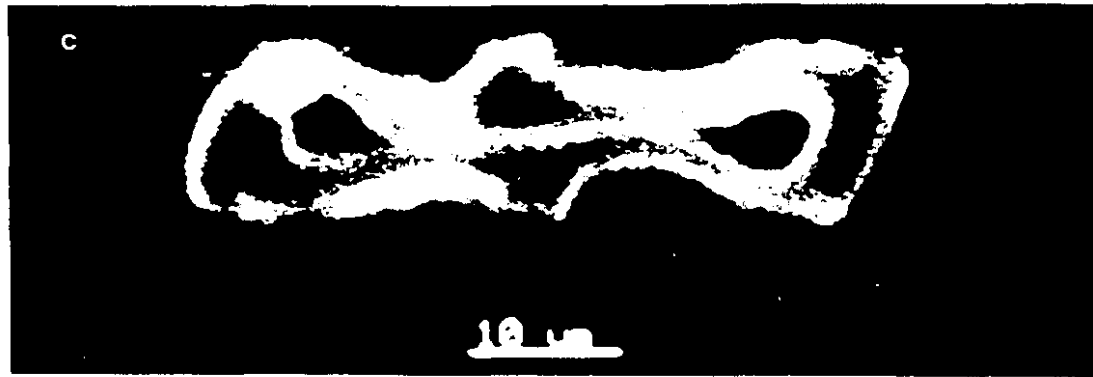
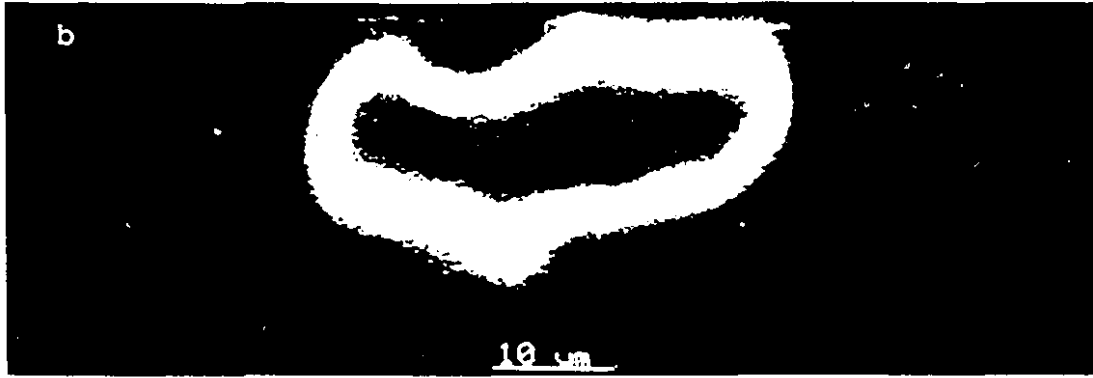
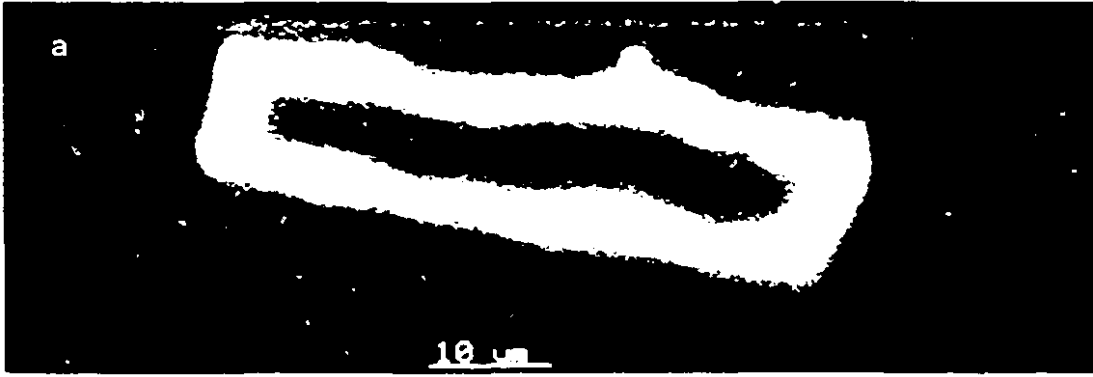


Figure 8.25: Intact fibres of whatever species exhibit natural non-uniformity in cross-section owing to differing rates of cell wall development. Confocal micrographs show cross-sections, 30 μm apart, of: (a)–(b) intact black spruce RMP, refined at 8.5GJ/t; and (c)–(d) intact jack pine RMP, refined at 8.7 GJ/t (whose extractives have been removed).



8.4 Micro-mechanisms of Fibre Fatigue-Failure: A Theory

The in-depth exposition of the preceding pages detailed the morphological forms which pulp fibres typically undergo while being subjected to fatigue loading (shear, radial compression and tension). The given description of what, in essence, causes the damage accumulation phenomena raises a number of challenging questions, which will now be answered at the level of crack formation, and where possible, in terms of the known atomic structure of the cellulosic fibrils and characteristic interaction between the amorphous hemicellulose-and-lignin matrix, on the one hand, and the micro-fibrillar framework, on the other. It is to be recalled that for each particular phenomenon, e.g., volumetric expansion, delamination, etc., a succinct analysis at the level which the former takes place, i.e., mesoscopic or microscopic, was proffered hereinbefore. Furthermore, it must clearly be recognised that the aforementioned effects are specifically due to the fact that stress is repeatedly applied and removed as evinced by the true fatigue-failure due to a specific form of crack growth—limited to regions of highly-localised deformations, and by the general weakening of the cell wall material due to structural damage and chemical degradation of the fibrillar framework. Those challenging questions are, viz.:

1. What is (are) the micro-mechanism(s) of initial crack formation?
2. Why does the crack then propagate along the fibre?

Methodical answers to the above questions require a systemic treatment. First, recall one relevant structural function of cellulose,¹³ which is primarily but not exclusively the load-bearing component of the cell wall: the lateral forces holding the crystallites together account for an important structural feature of the cellulose framework; namely, that large plastic deformations under stress are highly improbable because the inter-molecular forces of attraction prevent any extensive relative movements [187]. Acknowledging—as it must, by now, be unequivocal—the cell wall

¹³Refer to Sections 2.1.3 and 2.2.1 of Chapter 2 for a comprehensive review of the structure of cellulose, and that of the overall cell wall.

as a composite of structural reinforcing materials in a cementing matrix necessitates accommodating an appropriate theoretical approach for deciphering the framework-matrix interaction. From the consideration of the “law of mixtures” of physics [129], wherein a hard phase is dispersed within the soft phase of a composite material: in this sense, the ‘hard’ phase refers to a material of high elastic modulus and strength embedded in a ‘soft’ matrix with weaker mechanical properties; considering this law one recognises that the matrix serves to stop propagation of (inchoate) microcracks and distributes stresses to the reinforcement. This can be accomplished by a plastic or elastic-plastic deformation of the matrix that causes a well-distributed elastic deformation in the hard phase because of the adhesion of the two phases.

The scanning confocal microscope has enabled a close examination of the fracture surfaces to be made and ideas of crack development to be garnered: slow crack growth, plastic deformation, and the opening of crack have been shown to be characteristic of many fibres under cyclic-loading conditions involving uniform shear, radial compression or tension. The stable tearing, i.e., layer slippage, depicted in Figure 8.26,¹⁴ is typically seen when the fibre is subjected to a large number of cycles in shear. This type of crack propagation leading to rupture may be explained in terms of: the time-dependence behaviour of the viscoelastic wood-pulp material, and the concomitant stabilisation effects of plastic deformation around the crack tip. The anisotropy of both the cell wall structure and the material properties of the fibre, is clearly reflected in the latter statement — as well as by the plethora of confocal micrographs depicting crack formation and propagation at high localised deformation, and the subsequent evolution of material cumulative damage phenomena. The transverse and longitudinal confocal images of various fatigued fibres reveal the underlying reasons for crack initiation as follows: Slip plane, micro-compressions, dislocations and (natural or induced) deformities, which we shall group together under the term *strain bands*, develop in the (laminated) fibre cell wall under periodic deformation; failure subsequently occurs along these bands. The surface lamina of the fibre—in direct point-to-point contact with the applicator, as in the case of shear testing—goes into compression principally owing to the presence of (tenuous) inhomogeneities, experiences fatigue

¹⁴See Appendix E as well.

Figure 8.26: Fluorescence confocal micrographs illustrating the cumulative build up of plastic deformation as microcracks propagate along the cell wall layer. The gradual formation of developed macrocracks in any one layer ultimately leads to the slippage of layers, or what may be termed as *tearing action*—clearly depicted in (d). (Fibre sample: Jack pine RMP, refined at 6.5 GJ/t, subjected to 1200 cycles of shear displacement at 0.0262 Hz.)



growth of micro-voids and surface damage which individually and collectively give rise to stress concentrations; and eventually cracks develop.¹⁵ Confocal observations unequivocally show that initial crack growth is widespread on the surface of the material: many cracks in various stages of growth may be found in a fatigue specimen. Once an initial macrocrack has formed, there is high shear stress just ahead of the tip of the crack, as indicated in the schema of Figure 8.27. *This* hypothesis is fully supported if we recall from foregoing discussions the analogy between the pulp fibre and a laminated, fibre-reinforced composite tube: in such a material the matrix provides lines of weakness preferentially arranged in the direction of the (helical) cellulosic microfibrils of the dominant S_2 layer—whose fibril angle is normally low, i.e., the microfibrils are more closely oriented along the axis of the fibre. Hence, automatically follows the explanation as to why longitudinal crack propagation is favoured in the fatigued fibres. It is now necessary to explicate the mechanism(s) via which these cracks develop (and deflect).

Referring to Figure 8.27(b), the turning of the crack would relieve the shear stress and so the propagation would be in only one direction. In some circumstances, presumably when there is no local bias favouring one direction, the shear stress would initially lead across the end of the initial notch: this would then propagate in both directions (Figure 8.27(c)). Once the crack has turned, the continuing propagation along the fibre would be a result of the stress distribution shown in Figure 8.28. The shear stress which is needed to transfer load from the whole cross-section below the crack to the reduced cross-section alongside the crack, would generate continued crack propagation—refer to the confocal micrographs of Figure 8.29.

It is important to note that the load cell voltage output, which is continuously monitored during the course of testing, varies in such a manner as to indicate reduced load response at the inception of crack initiation and propagation. This may simply be

¹⁵It is worthwhile noting that, in the case of radial compression and tension, a *gradation* of properties from the external layer to the inner ones could result in the latter being able to recover more than the outer parts of the fibre, which could then be put into compression. This recovery is clearly evinced by confocal micrographs showing the cell wall retaining its structural integrity—even though the surface experiences some damage accumulation.

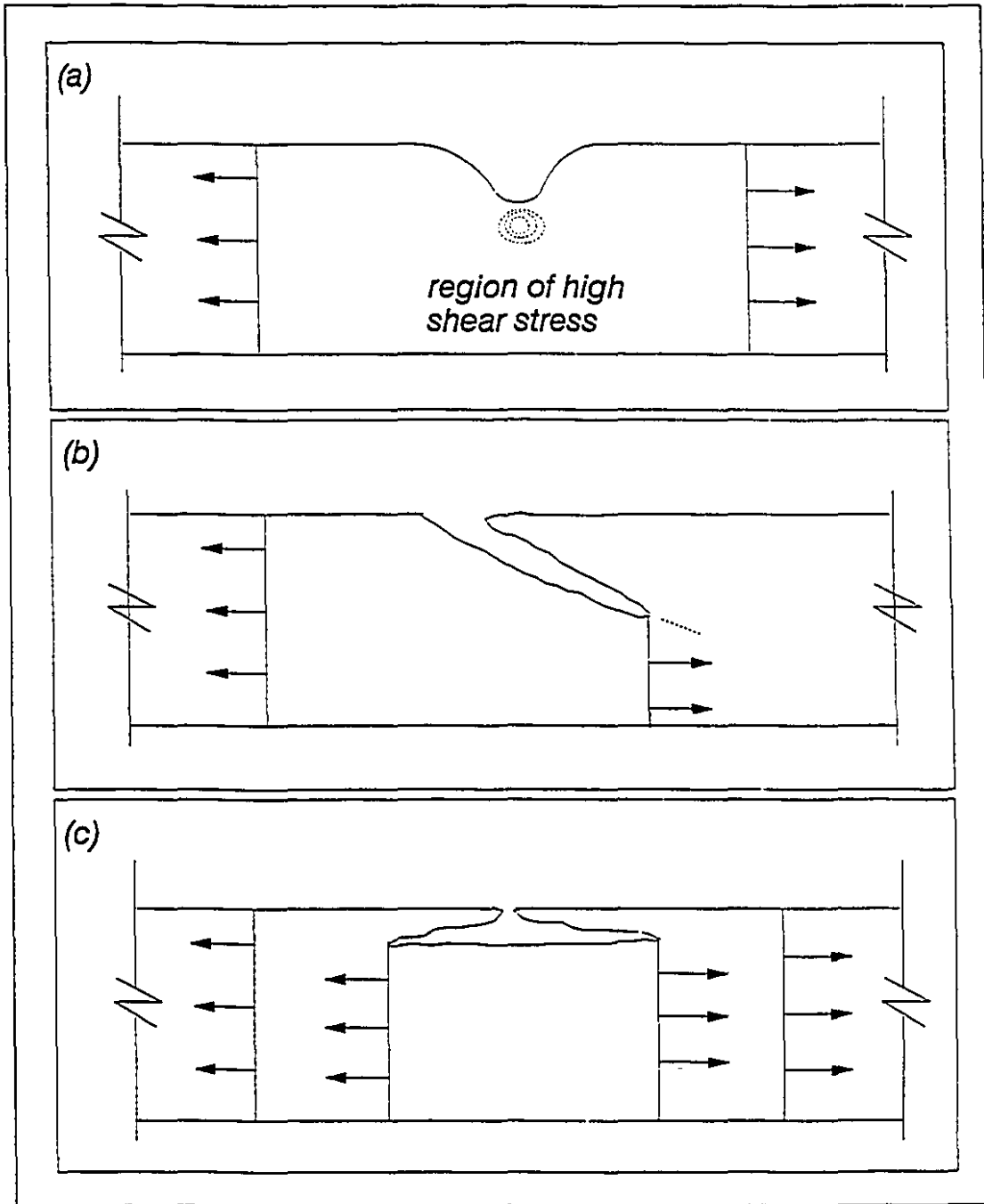


Figure 8.27: Schematic representation of the model describing inchoate fatigue crack growth in pulp fibres (subjected to cyclic shear, radial compression or tension) under the influence of shear stress.

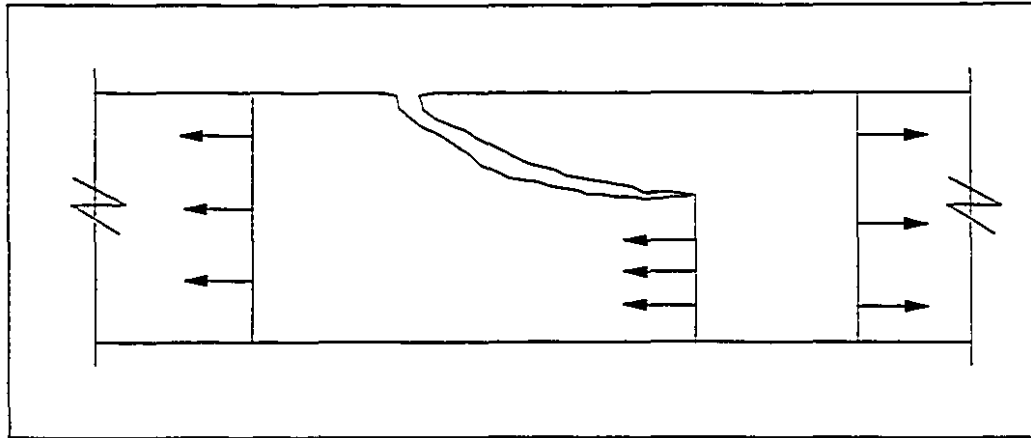
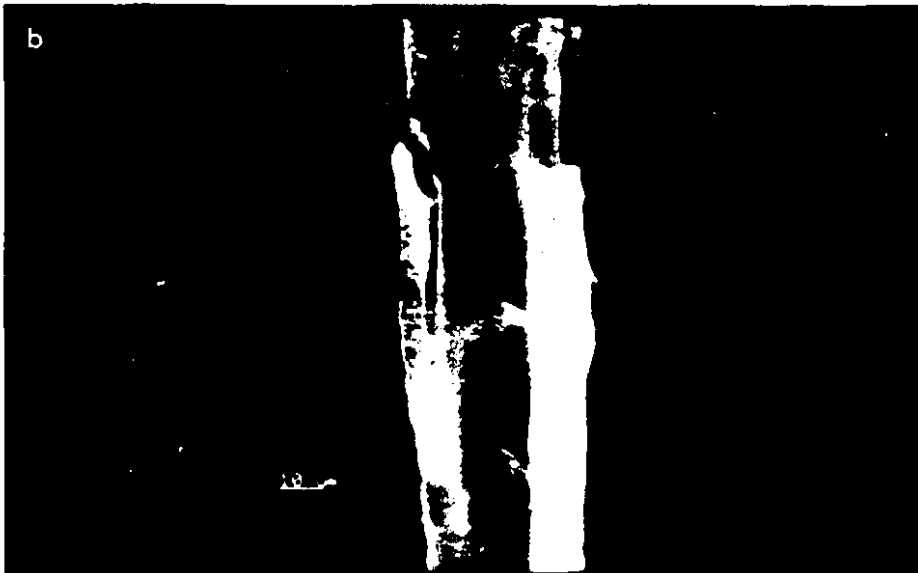


Figure 8.28: A schema of the stress distribution with developed longitudinal crack growth.

attributed to the effects of hysteresis brought on by the strain-induced crystallisation in the cell wall fibre under cyclic-loading conditions where the material is continually being stressed and recovering: The mechanical hysteresis giving rise to structural changes, may, drawing upon polymer research terminology [7], be referred to as a “frozen stress-field”. The interaction of the successive cycles with this frozen stress-field also contributes to crack growth by a fatigue mechanism. The latter association seems apt in the light of the severe structural changes and material degradation (at each cycle) in the fatigued fibres.

Last but not least, it is particularly relevant to realise that—having recognised that microcracks initiate from deformities or inhomogeneities in the fibre cell wall—once the macrocrack has been deflected, the high anisotropy of the fibre would promote fracture preferentially along the axial direction.

Figure 8.29: Supportive evidence of the proposed stress-distribution hypothesis shown in Figure 8.28. Depicted above are fluorescence confocal images of: (a) jack pine RMP, refined at 8.7 GJ/t, subjected to 1200 cycles in shear at 0.0262 Hz; (b) black spruce RMP, refined at 8.5 GJ/t, also cycled 1200 times in shear.



Chapter 9

Rheological Aspects of Papermaking Fibres

9.1 Towards a Microscopic Theory of Fibre Development

Fibre development is a term commonly used in mechanical pulping to infer (and refer to) changes occurring in the fibre properties during refining. In line with the results presented in the preceding chapter, the characterisation of such properties must stem from a basic understanding of the morphological phenomena intimately associated with the structural behaviour of pulp fibres under cyclic loading. These properties are, hence, intrinsically inter-dependent, and their formation is principally influenced by the fatigue crack growth evolution. In relation to general mechanical pulping practice, *mutatis mutandis*, the approach developed in this investigation seeks to characterise phenomenological aspects via a systematic modality based on microscopic considerations of the fibre structure¹: Macroscopic changes in fibre properties such as, length, coarseness, width, flexibility, cell wall thickness and degree of collapsibility can be categorised once a pellucid analysis of cumulative material degradation is undertaken. Hence the direct association of fibre development to the latter.

¹Proof of what actually occurs in refining, see for instance the very recent work by Karnis [131], corroborates our viewpoint, as we shall detail below.

As evidenced from the multitude of results (refer to Chapter 8 and Appendix E), the cumulative fatigue damage of the cell wall material conclusively and fundamentally presents itself in the coalescence of a litany of tenuously-oriented microcracks into a dominant macrocrack spanning along the fibre, unless and until deflected by natural bias. Further aspects of the material property degradation phenomena centre around: volumetric expansion, at regions of high localised strain, owing to the internal fibrillation of the cell wall material; as well as the apparent intensive external fibrillation of the latter. As the extent of material degradation builds up with continued cyclic loading, structural disintegration is quintessentially designated by the inter-laminar separation between the cell wall layers as well as the partial peeling-off of the external layer material. Our study, all and sundry, indicates that the effectiveness of cumulative material damage and structural breakdown is greatest in pulp fibres subjected to cyclic shear — as contrasted with radial compression and tension — in the first several hundred cycles,² and are steadily promoted with the number of cycles irrespective of wood species or pulp type.

In light of the aforesaid, a direct analogy may then be drawn between the fatigue damage accumulation of wood pulp fibres subjected to cyclic loading, mainly shear and radial compression, and the physical process predominant in mechanical refiner pulping: In refining operations, wood pulp fibres are subjected to variable loading situations accompanied by complicated treatments that occur simultaneously [11, 12, 15]. The energy applied in refining disintegrates wood chips at the entrance of the refining zone to produce coarse fibres and fibre bundles [15]; primary fines and wood dust are also produced [131]. These fines constitute part of the lint candidate material in the final pulp. As seen in Figure 9.1, the fibre separation and development regions can overlap in the refining process. Rejects are mostly reduced to long fibres, nevertheless, fibre bundles (shives and minishives), short fibres and fines are also produced. Subsequently, short fibres and fines are primarily produced from long fibres by the peeling-off mechanism, which contributes to improving bonding — see Figure 9.2.

²As for radial compression and tension, fatigue life, at which inchoate damage materialises, borders ten-fold and twenty-fold, respectively, that for shear.

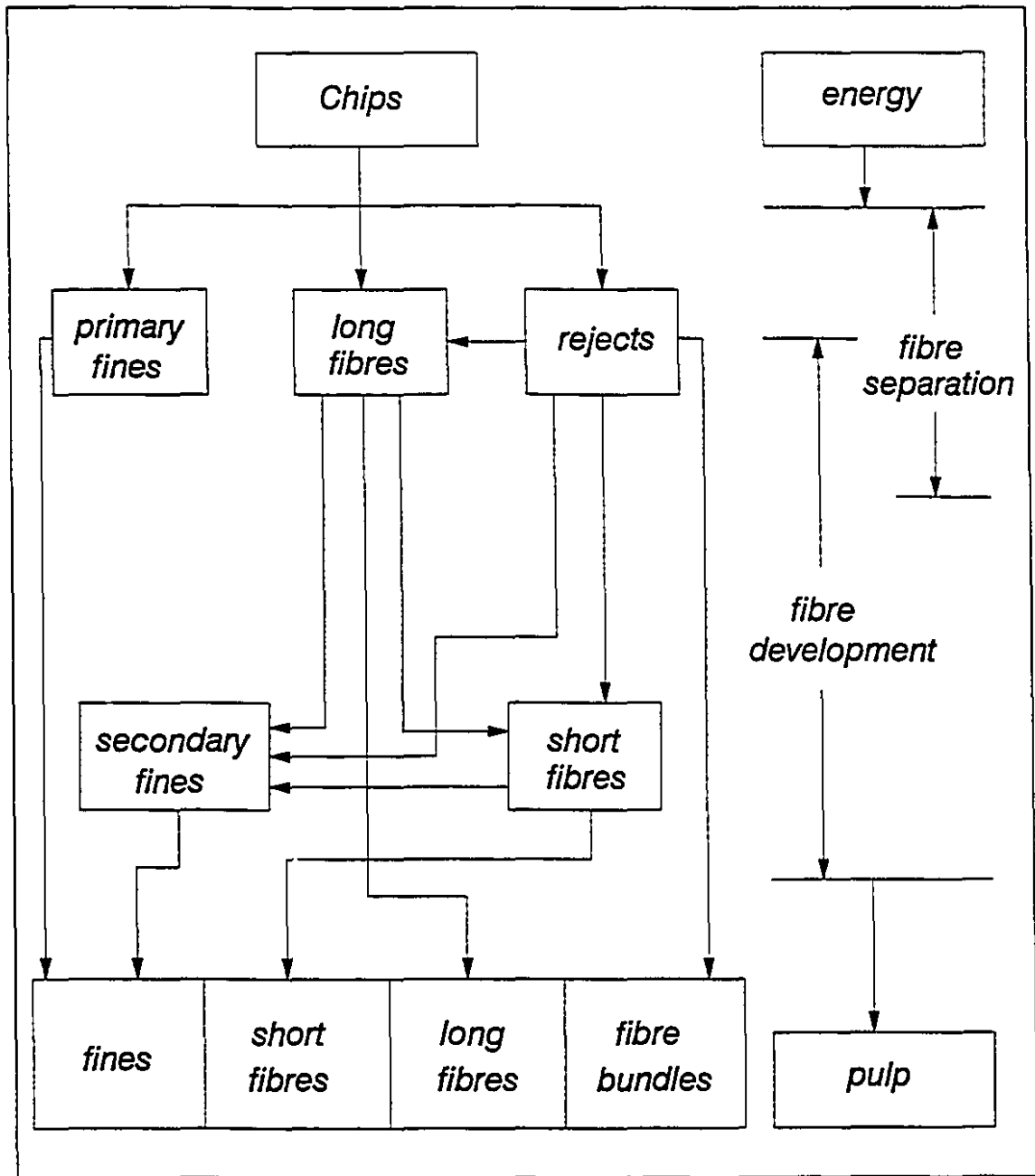
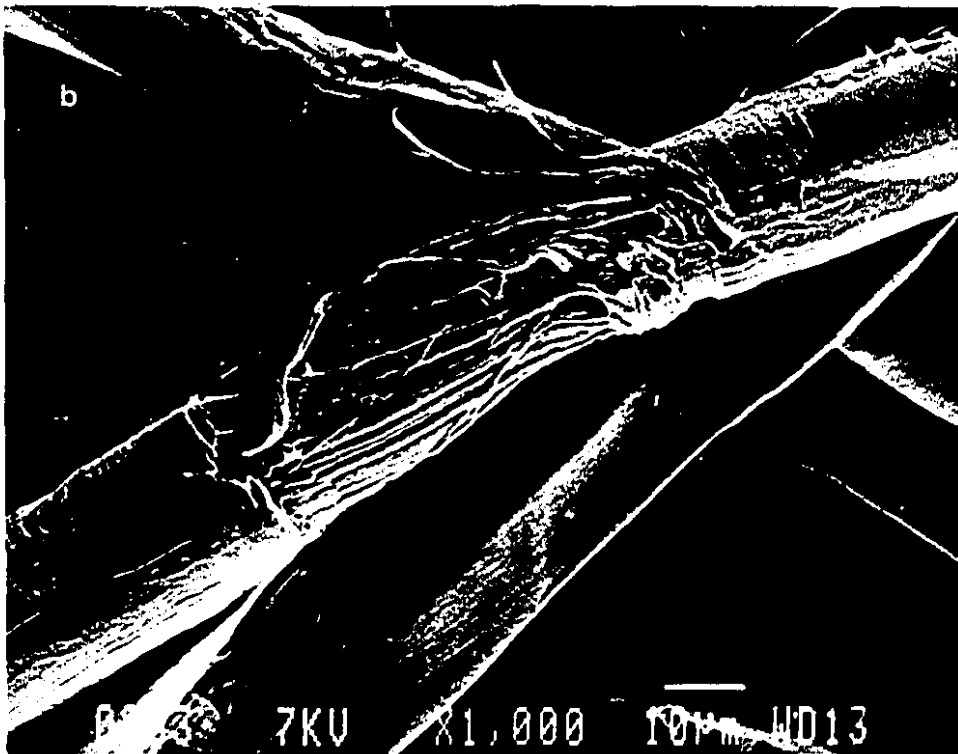
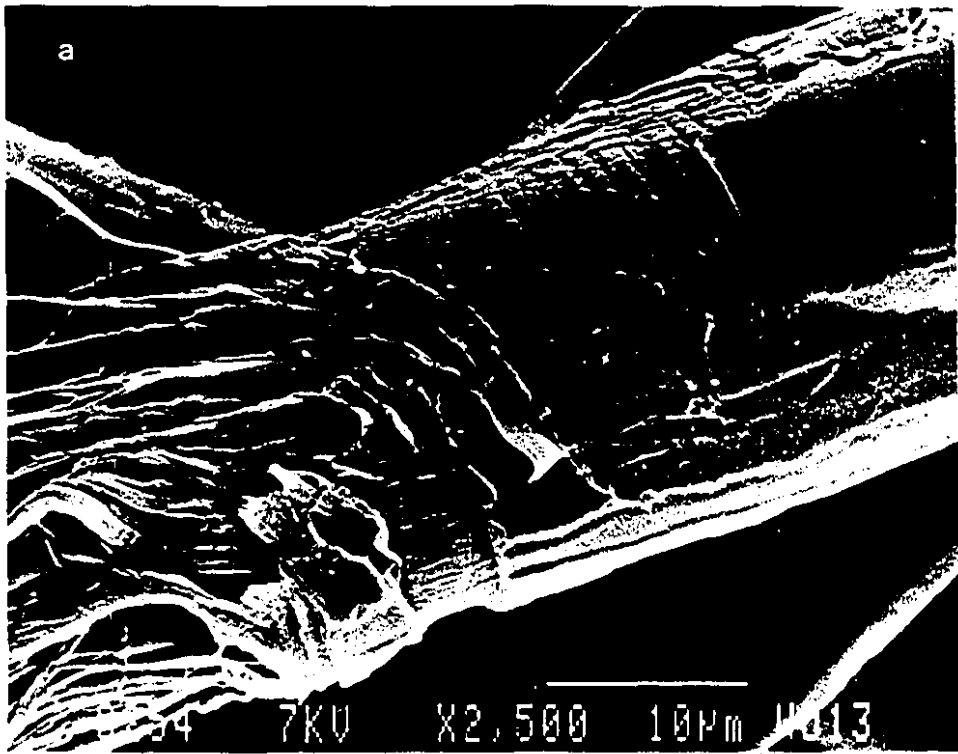


Figure 9.1: A schematic representation of the chip reduction process and stages to produce a papermaking pulp (adapted from reference [131]).

Figure 9.2: Scanning electron micrographs of a pulp refined at 7.0 GJ/t depicting: (a) the partial removal of P and S_1 layers (mag. 2500x); and (b) exposure and disruption of the S_2 layer (mag. 1000x). (*Courtesy of Dr. A. Karnis, PAPRICAN, Pointe Claire, Canada.*)



The (macro)mechanism of fibre development may *à fortiori* be explicated in terms of the cumulative (fatigue) material property degradation process—in all of its previously described facets: inter-laminar separation (delamination) and peeling-off being the more prominent contributors. Karnis [131] has recently carried out a study methodically detailing the practical considerations involved in the actual process of refining: His findings remarkably corroborate, on the practical level, and are comprehensively explained by, the material degradation phenomena and structural changes begotten from the cumulative fatigue damage mechanisms—elucidated *in extenso* in the course of the preceding pages. Karnis suggested a mechanism of fibre development other than the comminution models, which assume that the size reduction proceeds through a breakdown of chips and shives, then to individually intact fibres where further size reduction and production of fines mostly occur by fibre breakage. This mechanism, schematically illustrated in Figure 9.3, indicates that the initial breakdown of chips into shives and coarse intact fibres takes place in the fibre separation stage; furthermore, fibre development proceeds by delamination and gradual peeling-off of the external cell wall layers—namely, P and S_1 layers—and the subsequent exposing of the S_2 layer (cf. Figure 9.2, on the one hand, and for example, Figures 8.15–8.17, on the other).

The fundamental mechanism responsible for fibre development postulates the following particulars:

1. The length of the fibre is (almost entirely) preserved.
2. Fibre coarseness, defined as mass per unit fibre length [253], is reckoned to decrease since, according to the above mechanism, material is removed—through peeling-off and delamination—from the fibre cell wall. Moreover, coarseness has been reported to decrease with decreasing fibre length [131] as a result of the peeling-off of cell wall material. (It is however not unlikely that, in refining, long fibres are occasionally shortened at the same time that cell wall material is being removed.)
3. Owing to the peeling-off of cell wall material, the weight, rather than the length, of a fibre is reduced; consequently effecting a decrease in the content of long

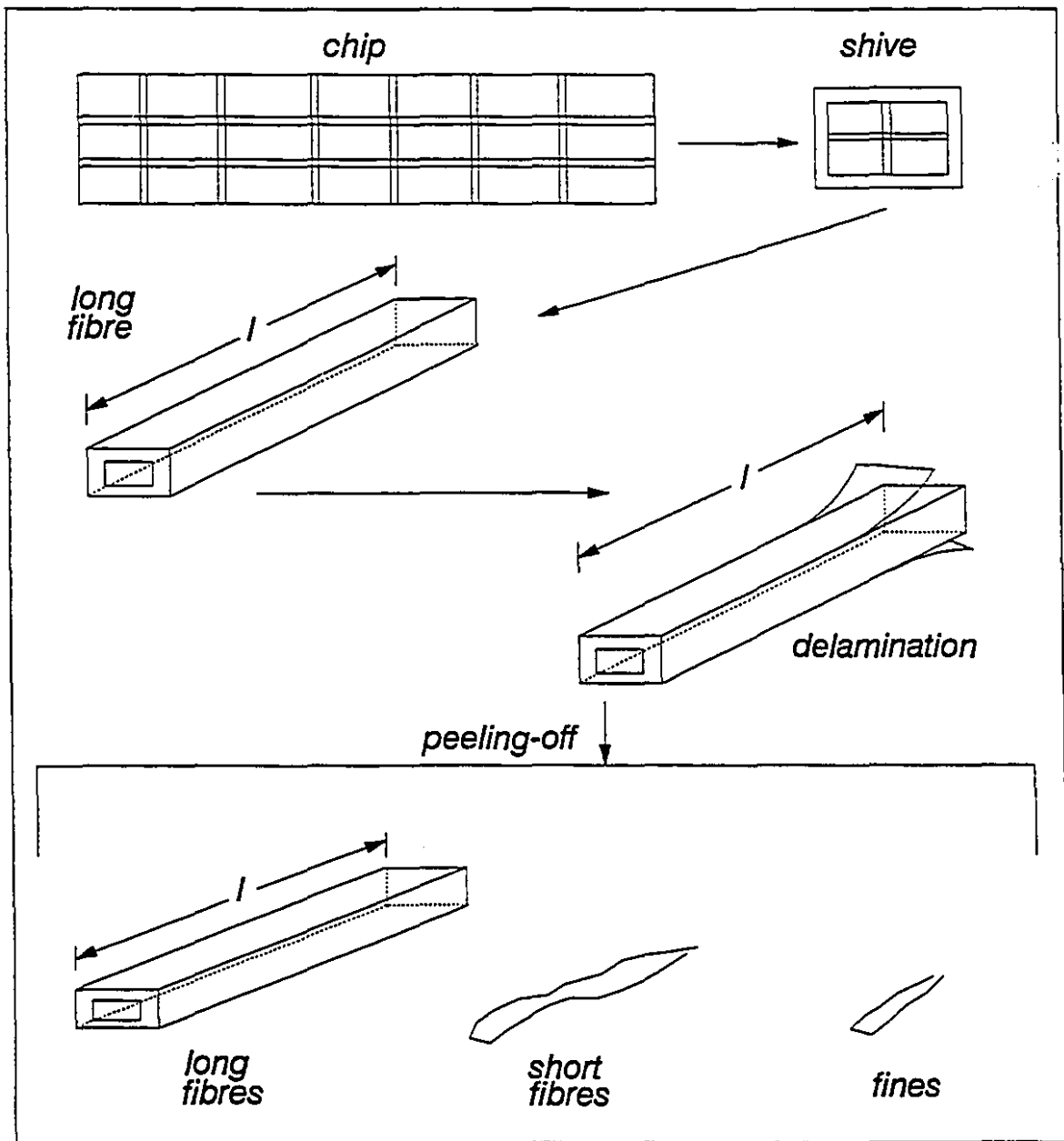


Figure 9.3: A schema illustrating the mechanism of fibre development, that is characterised by: (i) the fibre separation stage, in which the chips are reduced to shives and long intact fibres; and (ii) the peeling-off stage, where parts of the fibre cell wall material are eventually removed to form short fibres and fines. (Adapted with modification from reference [131].)

fibres expressed as weight fraction.

4. Material peeled-off of the external cell wall layer forms short fibres and fines — that are oft-found in refining.
5. The width of a fibre is intrinsically affected by the phenomena of inter-laminar delamination and partial peeling-off of cell wall material, albeit in somewhat different manners. In cases where there is an insignificant degree of fibre collapse — refer to the cross-sectional images of Chapter 8 and Appendix E —, the removal of cell wall material *à priori* decreases the fibre width. Furthermore, the complete delamination and peeling-off of the external layers, P and S_1 , effectively result in exposing the S_2 layer. This, accompanied by intensive internal fibrillation of the fibre cell wall, may increase the fibre width (i.e., causing the fibre to swell) — cf. Figures 8.16(a) and 9.2(b).
6. While it has been observed that delamination and partial peeling-off of cell wall material are rather more pronounced for pulp obtained from higher refining energies, the basic mechanism is intrinsically influenced by, and must hence be directly related to, the accumulated material degradation micro-mechanisms due to cyclic loading (see Section 8.4). Thence, we must only *cautiously* remark that fibre thickness decreases with increasing refining specific energy.
7. Extensive material damage accumulation, especially in shear-mode loading, results in destabilising the structural integrity of the fibre cell wall — owing to the combined effects of inter-laminar separation, partial peeling-off and development of macrocracks across the fibre diameter — which subsequently leads to the collapse of the fibre wall. The more severe the material damage³ is, the greater is the degree of fibre collapsibility.

³Which is a function of principally the number of cycles and mode of loading.

9.2 Practical Implications of Current Findings: A Synopsis

As it must be clear from foregoing discussions, when wood pulp fibres are mechanically treated, significant changes occur in the morphological behaviour of these fibres. These changes are, in essence, effected as a consequence of the cumulative (fatigue) material property degradation phenomena which, in turn, result in modifying the structural behaviour of these fibres and, hence, the properties of the paper to be produced. This so-called *degradation* of material properties *does* indicate a variation on the previous set of material properties; and *does* indeed imply the possible debonding of molecules and the subsequent formation of new alignments of fibrous aggregates. Notwithstanding, this degradation is *beneficial* rather than detrimental, when ultimately considering the material improvements that are enhanced in the papermaking fibres.

The proposed fibre development model, based on the micro-mechanisms of fatigue damage accumulation, provides a novel insight into the rudimentary operations of the refining process: The findings are indeed instrumental in expounding the fundamental causes responsible for producing suitable pulp for paper production; they could definitively be implemented to revolutionise the design of mechanical refiners as the century draws to a close.

It has been documented in the course of this research that external fibrillation of the fibre cell wall has a predominant occurrence in the fibres subjected to all modes of cyclic loading. Considerable economic advantage may accrue from the action promoting external fibrillation rather than fines: The pulp would have yield retention properties, good strength, and would make a sheet in which the distribution of the fine material throughout the sheet thickness was uniform [208]. Furthermore, the presence of micro-compressions and slip planes is important for many properties of paper and board products; notably extensibility and dimensional stability. The structural changes occurring during the application of cyclic action to wood pulp fibres reflect a process whereby the fibres are believed to become more flexible due to the breakdown of internal fibre structure. A comparison between the structural changes

introduced during fatigue of single fibres (as presented in Chapter 8 and Appendix E) and those which are produced in the refining process may further elucidate the global effects of some of the fundamental mechanisms at work.

Fibre flexibility, which is the inverse of stiffness, EI , is reported by Karnis [131] to behave asymptotically: it initially increases with increasing refining energy, then reaches a plateau. Since the moment of inertia,⁴ I , is a function of the fibre cross-section (i.e., diameter), it follows from the aforesaid, that the fibre flexibility increases with decreasing elastic modulus and decreasing fibre diameter. Moreover, differences reported [131] in fibre flexibility in relation to thermo-mechanical and refiner mechanical pulps may be attributed to the fact that the elastic modulus tends to decrease at higher temperatures [247]; since the higher the treatment temperature, the more efficient is the structural breakdown process. Consequently, for a given fibre width — i.e., same moment of inertia —, thermo-mechanical pulp fibres are expected to attain higher flexibility.

The internal fibrillation and flexibilisation are of great import to enable the production of strong paper: Essentially, the bonding is enhanced by the greater ability of the fibres to conform to each other. It is thus apposite to conclude that most of the changes within the fibre cell wall structure, introduced by the cyclic-loading action, are fundamentally ascribed to the same intrinsic micro-mechanisms responsible for the development of cumulative fatigue damage phenomena — refer to Chapter 8 in its entirety.

⁴If we assume a cylindrical cross-section, $I = \pi(d_o^4 - d_i^4)/64$; where d_o and d_i are outer and inner diameters of the fibre, respectively.

Chapter 10

Conclusions

10.1 Concluding Remarks

As with any fundamental scientific investigation, this study raised new questions as it sought answers to many others. In the foregoing chapters, an endeavour has been made to methodically set forth the underlying concepts germane to the mechanics of pulp fibres subjected to cyclic loading. In the following pages, a conspectus is presented of what has been canvassed, with particular emphasis on the contextual material of the last three chapters.

The wall of a wood fibre or tracheid can structurally be considered as a layered composite shell, shaped like a very elongated, somewhat polygonal spindle with a hollow interior. Each layer consists of strong reinforcing filaments (microfibrils) that are primarily composed of cellulose, together with embedding matrix of amorphous and/or polycrystalline polymers that bulks, links and stabilises the microfibrillar framework. The interaction of these framework and matrix components is analogous to that of anisotropic composite shell structures of reinforced concrete or fibrous glass reinforced plastics. (Refer to Chapters 2 and 4.)

The bonds which hold the fibres together in wood are broken, in refining, to such an extent that individual fibres can be liberated from the wood structure. Inter-fibre bonds can be weakened to the point of fibre liberation using chemical, thermal and mechanical treatments, or a combination thereof (refer to Chapter 3). In refining,

softwood chips are defibrised between two refining discs, at least one of which rotates. Essentially, two steps occur: the defibrisation of wood to fibre bundles and fibres, followed by the fibrillation of the fibre surfaces. When fibres are being mechanically refined, it is suspected that they get fatigued by the repeated loading action of the refiner bars. This loading action can primarily be classified into three principal cyclic-type force actions on the pulp fibres, viz.: uniform shear, radial compression and longitudinal tension. A novel experimental methodology has been introduced to investigate the fatigue and fracture characteristics of single wood pulp fibres under mechanical cyclic loading. The apparatuses, *suis generis* in contexture, comprise the in-house designed and built *single-fibre tensiometer* in conjunction with the confocal laser scanning microscope (CLSM), on the one hand, and computer hardware and periphery, on the other, and are fully automated to perform displacement-controlled fatigue-testing. Mechanical fixation mechanisms, incorporated into the loading jaws of the tensiometer, are used to securely mount the single fibres in position — where the jaws are specifically designed to simulate what pulp fibres actually undergo while between the discs of mechanical refiners (refer to Chapter 7). Confocal scanning imaging, whose principal feature is that detection is strictly limited to what is in focus — out-of-focus regions appear bleak — thus eliminating all unwanted glare, provides a powerful tool to monitor the fibre during fatigue-testing and to obtain qualitative information on the morphology and structural behaviour of the fibre being tested (see Section 8.2 of Chapter 8).

When wood fibres, or any other material for this matter, are mechanically treated, energy is consumed in the process. The viscoelastic character of wood means that the energy may be absorbed both in large plastic deformations and small reversible viscoelastic effects (see Chapter 5). Damage phenomena characteristic of fatigued fibres are consequences of the cumulative material chemical degradation and subsequent structural breakdown of the cellulosic fibrils, the primary — however, not exclusive — structural load-bearing framework component of the tracheid wall. Fatigue damage accumulation qualitatively manifests itself in the formation of cracks which may be characterised by three distinctive stages: (i) the initiation stage, followed by (ii) the micro-propagation stage of the crack, then (iii) the macro-propagation stage; includ-

ing the transitory modes linking them. A myriad of tenuously-oriented microcracks initiate from the fibre surface and coalesce to form dominant macrocracks, spanning the high deformation regions along the fibre, which sharply deflect once confronted by natural bias, such as the presence of pits — that are considered as points of high stress concentration. (Three-dimensional modelling and finite-element analysis qualitatively confirm the longitudinal regions of high deformations.) Commensurate with the successive application of cyclic action, the extensive cumulative material degradation takes the forms: (i) internal changes in, and fibrillation of, the fibre cell wall structure causing the volumetric expansion at localised regions; (ii) extensive external fibrillation and inter-laminar delamination of the cell wall layers which effectively lead to the partial peeling-off (i.e. removal) of the cell wall material, leaving it still attached to the body of the fibre; and (iii) as a further consequence of the latter point, complete removal of parts of the fibre wall materialises in the production of fines. Rupture ultimately occurs via one of two mechanisms, viz.: (i) the branching, at points of high stress concentration, of the dominant, longitudinal macrocrack to form transverse macrocracks that propagate to cause eventual failure; or (ii) the inter-laminar separation materialises, owing to intensive material degradation and structural breakdown, in effecting the slippage of the cell wall layers which leads to fracture.

From the comprehensive examination of the morphologies of fibres tested under different modes of loading, cyclic shear, relative to radial compression and tension, is found to be unequivocally the most significant, since the extent of material damage accumulation is distinctly more pronounced. Moreover, confocal optical imaging of the fibre cross-sections indicates a much more prominent degree of fibre collapsibility, as well as development of macrocracks, slip planes and micro-compressions, in so far as shear-mode testing is concerned. Radial-compressive loading only occupies a secondary position, in terms of material chemical degradation and structural breakdown, since almost ten-fold the fatigue life under shear-loading, i.e., roughly 3000 cycles, is necessary before any noticeable macrocracks are formed; damage thenceforth cumulates at a similar rate to shear. However, tensile-loading, even at thrice the maximum fatigue life due to shear-loading (roughly 6000 cycles), effects insignificant damage

accumulation that is primarily manifested in the formation of (infirm) macrocracks; thereupon, one may confidently discard effects due to cyclic tension as being inconsequential on the fatigue and fracture characterisation of pulp fibres in mechanical refiners.

In each mode of loading, higher energy pulp depicts more susceptibility to undergoing fatigue damage accumulation. However, beyond a certain level (around 1200 cycles for shear; 3400 for radial compression), the motley damage phenomena become principally dependent on the rate of chemical degradation and structural breakdown of the cellulosic fibrils and subsequent breakage of the inter-fibrillar matrix—which leaves the latter unstable. No difference is discerned, either in the extent or form of cumulative fatigue damage phenomena, betwixt chemi-thermomechanical (CTMP) and refiner mechanical (RMP) pulps. The aforementioned micro-mechanisms of fatigue cumulative material property degradation (refer to Section 8.4 of Chapter 8) formulate the basis for our proposed theory of fibre development—corroborated to a large extent by recent findings germane to refining—reference is made to [131].

10.2 Proposals for Future Research

Having determined the fundamental morphology and structural behaviour of single wood pulp fibres under fatigue-loading, the quantification of the pertinent parameters becomes of the essence. In this regard, the theoretical undertaking to be pursued is outlined hereinbelow. Concomitantly, further experimental examinations are necessitated to clarify the extent of significance of several factors enunciated hereunder. With the aforesaid in mind we proceed to elucidate the particulars of each approach:

1. Theoretical Approach: To realistically model the physical mechanisms that lead to material failure and best emulate the fatigue damage accumulation in wood pulp fibres, an analysis of the progressive failure in the laminae comprising the fibre cell wall must be performed. In this approach one first identifies the possible modes of material failure by incorporating the consequences of each type of failure on the subsequent behaviour of the damaged laminae. This may be

done by appropriately modifying the material or structural properties in regions where failure is deemed to have occurred. The entire process, it must be recognised, is highly *stochastic*: caused by the random nature of the very failure phenomena themselves. Hence, this author proposes that a simulation, via fractal modelling, of the growth of fatigue defects in pulp fibres be undertaken, so as to have an intrinsic model based on the microscopical observations discussed in the course of this thesis: A novel approach in the area as a whole. These random quantities may directly be integrated into the finite-element procedure we have developed — an approach referred to as stochastic finite-element analysis, based on perturbation theory [188].

2. Experimental Investigation: Our findings have hitherto been successful in expounding the essence of fatigue evolution and damage accumulation in pulp fibres. It is now required to further investigate the influence of the following important parameters: temperature and moisture variation, frequency and sulphonation. The first two parameters entail designing a mechanism, incorporated into the single-fibre tensiometer, to regulate, *in situ*, the ambient environment around the vicinity of the fibre by continuously supplying a fully-saturated steam jet. Furthermore, characteristic of our design is the fact that the frequency of testing is directly linked to the shearing action, which is, in turn, associated with the heat generated. The temperature of the fibre surface may henceforth be coordinated with the frequency of the test. Last but not least, the effect of sulphonation on the effectiveness of the fatigue process is required for correlating the former with the energy consumption in mechanical pulping.

Statement of Originality and Contributions to Knowledge

The author of this thesis claims to have made the following contributions to the fields of fibre physics and experimental mechanics:

1. A novel, fully-automated experimental methodology has been developed for the fatigue-testing of single wood pulp fibres, which represents a distinct contribution to experimental mechanics. The methodology principally includes the following new features:
 - (a) The design and construction of a single-fibre tensiometer specifically suited for testing small-dimension specimens.
 - (b) The introduction of a novel mechanical mechanism for securely mounting single fibres.
 - (c) The automation of the set-up via a fatigue-testing computer algorithm, in conjunction with the electronic hardware.
2. The utilisation of confocal laser scanning microscopy and image analysis to obtain longitudinal and transverse optical sections of the translucent pulp fibre, which are used in constructing three-dimensional images of the fibre. This technique has been most instrumental in detailing the morphology and structural changes in the fatigued fibres.
3. It has been shown in this thesis, for the first time, in a methodical and comprehensive manner that fatigue-failure owing to the chemical degradation in, and structural breakdown of, the fibre cell wall material, is a predominant occurrence when pulp fibres are subjected to cyclic loading — as in refining.
4. Unequivocally enunciating a thorough microscopic anthology of all forms of material property degradation phenomena of fatigued pulp fibres. Moreover, the realisation of the significant and superior effect of cyclic shear action, on the fatigue damage accumulation in pulp fibres, relative to radial compression and tension.

5. The contribution to advancing the theory of fibre development on the basis of microscopic analysis: The peeling-off mechanism and developed longitudinal macrocracks being responsible for creating long, slender fibres (rather than short ones) — a remarkable advantage to producing “better” papermaking fibres.
6. Nascent three-dimensional, finite-element modelling and analysis have been carried out, which may pave the road for further rigorous quantification based on the engendered results of this research.

Bibliography

- [1] Aboudi, J., 'Micromechanics Prediction of Fatigue Failure of Composite Materials,' *Journal of Reinforced Plastics and Composites* 8:150-166 (1989).
- [2] Ahlgren, P. A. V., *Chloride Delignification of Spruce Wood*, Ph. D. Thesis, McGill University, Montréal, Québec, Canada (1970).
- [3] Alinec, B., 'Mechanism of TiO₂ pigment retention on pulp fiber with polyelectrolytes,' *Colloids and Surfaces* 23:199-210 (1987).
- [4] Amiri, R., Görres, J., Grondin, M., and Wood, J. R., 'Fibre Collapse and Sheet Structure,' *PPR 964*, 18 pgs., Sept. (1992).
- [5] Amiri, R., May, W. D., and Miles, K. B., 'Design and Construction of an Apparatus for Measuring the Dynamic Compressive Stress-Strain of Pulp Samples,' *PPR 962*, 18 pgs., Sept. (1992).
- [6] Andersson, H., and Bergkvist, H., 'Analysis of a non-linear crack model,' *J. Mech. Phys. Solids* 18:1-28 (1970).
- [7] Andrews, E. H., *Fracture in Polymers*, American Elsevier, New York (1968).
- [8] Asplund, G., *Svensk Papperstid.* 55:505 (1952).
- [9] Asunamaa, S., *Svensk Papperstidn.* 58:308 (1955).
- [10] Atack, D., Heitner, C., and Karnis, A., 'Ultra-high yield pulping of eastern black spruce, Part 2,' *Sven. Papperstidn.* 83(5):133 (1980).
- [11] Atack, D., Heitner, C., and Karnis, A., *Pulp & Paper Mag. Can.* 82:T103 (1981).

- [12] Atack, D., and May, W. D., *Pulp & Paper Mag. Can.* 63:T10 (1962).
- [13] Atack, D., May, D., Morris, E. L., and Sproule, R. N., 'The energy of tensile and cleavage fracture of black spruce,' *TAPPI* 44(8):555 (1961).
- [14] Atack, D., and Stationwala, M. I., 'On the measurement of temperature and pressure in the refining zone of an open discharge refiner,' *Transactions of The International Mechanical Pulping Conference*, San Fransisco, California, June 16-20, pp.1-6 (1975).
- [15] Atack, D., Stationwala, M. I., and Karnis, A., 'What happens in refining,' *Pulp & Paper Mag. Can.* 85(12):T303-T308 (1984).
- [16] Atalla, R. H., *ASC Adv. Chem. Ser.* 181:55 (1979).
- [17] Atalla, R. H., Ranna, J., and Malcom, E. W., *TAPPI* 67(2):96 (1984).
- [18] Atalla, R. H., and Wahren, D., *TAPPI* 63(6):121 (1980).
- [19] Axelrad, D. R., *Micromechanics of Solids*, Polish Academy of Sciences, Warsaw and Elsevier Publ. Co., Amsterdam, Holland (1976).
- [20] Axelrad, D. R., *Probabilistic Mechanics of Structured Solids*, PWN and Elsevier Publ. Co. (1977).
- [21] Axelrad, D. R., 'Theory of bond failure in hydrogen bonded solids,' *Advances in Molecular Relaxation and Interaction Processes* 15:51-69 (1979).
- [22] Axelrad, D. R., Atack, D. and Provan, J. W., 'Microrheology of fibrous systems,' *Rheo. Acta* 12:170 (1973).
- [23] Axelrad, D. R., Rezai, K., and Atack, D., 'Probabilistic mechanics of fibrous structures,' *Journal of Applied Mathematics (ZAMP)* 35(4):497-513 (1984).
- [24] Azzi, V. D., and Tsai, S. W., 'Anisotropic strength of composites,' *Experimental Mechanics*, pp. 283-288, Sept. (1965).
- [25] Back, E. L., and Salmén, N. L., *TAPPI* 65(7):107 (1982).

- [26] Barnet, A. J., Bedard, J., and Shaw, A. C., *Pulp & Paper Mag. Can.* 76:T185 (1975).
- [27] Baxevanakis, C., Jeulin, D., and Valentin, D., 'Fracture statistics of single fibre composites specimens,' *Int. Conf. on Microphenomena in Advanced Composites*, 34 pp. (Reprints), July (1992).
- [28] Beatson, R. P., Heitner, C., and Atack, D., *J. Pulp Paper Sci.* 10:J12 (1984).
- [29] Becker, H., Höglund, H., and Tistad, G., 'Frequency and temperature in chip refining,' *Pap. Puu* 59:123 (1977).
- [30] Berlyn, G. P., 'Recent advances in wood anatomy,' *For. Prod. J.* 14(10):467-476 (1964).
- [31] Bernal, J. D., Concluding Remarks on 'A discussion of new materials,' *Proc. Roy. Soc. London A* 282:147-154 (1964).
- [32] Birchon, D., *Optical Microscope Technique*, George Newnes Ltd., London (1961).
- [33] Bolker, H. I., and Brenner, H. S., *Science* 170:173 (1970).
- [34] Brauns, F. E., and Brauns, D. A., *The Chemistry of Lignin*, Suppl. Vol., Academic Press, New York (1960).
- [35] Broberg, K. B., 'Crack-growth criteria and non-linear fracture mechanics,' *J. Mech. Phys. Solids* 19:407-418 (1971).
- [36] Broek, D., *Elementary Engineering Fracture Mechanics*, The Hague; Boston: Martinus Nijhoff Publishers (1986).
- [37] Browning, B. L., 'The composition and chemical reactions of wood,' In *The Chemistry of Wood*, Browning, B. L. (ed.), Interscience, New York, pp. 57-101 (1963).
- [38] Bruun, H., Gadda, L., and Vartiainen, H., *TAPPI* 62(12):110 (1979).

- [39] Bucher, H., 'Discontinuities in the microscopic structure of wood fibres,' In *Fundamentals of Papermaking Fibres*, Bolam, F. (ed.), Brit. Pap. Bd. Assoc., Surrey, pp. 7-26 (1958).
- [40] Bunsell, A. R., 'Fibre failure and fatigue,' *Chem. Tech.* 4:292-299 (1974).
- [41] Bunsell, A. R., and Hearle, J. W. S., 'A mechanism of fatigue failure in nylon fibres,' *J. of Materials Science* 6:1303-1311 (1971).
- [42] Bunsell, A. R., and Hearle, J. W. S., 'The fatigue of synthetic polymeric fibers,' *J. Appl. Polym. Sci.* 18(1):267-291 (1974).
- [43] Bunsell, A. R., Hearle, J. W. S., and Hunter, R. D., 'An apparatus for fatigue testing of fibres,' *Journal of Physics E: Sci. Instrum.* 4:868-872 (1971).
- [44] Bunsell, A. R., Hearle, J. W. S., Konopasek, L., and Lomas, B., 'A preliminary study of fracture morphology of acrylic fibres,' *J. of Applied Polymer Science* 18:2229-2242 (1974).
- [45] Burgel, B., Perry, A. J., and Schneider, W. R., 'On the theory of fibre strengthening,' *J. Mech. Phys. Solids* 18:101-114 (1970).
- [46] *Canadian Pulp and Paper Association*, 1985 Reference Tables, December 1985.
- [47] Casey, J. P. (ed.), *Pulp and Paper: Chemistry and Technology*, Wiley Interscience, New York (1980).
- [48] Cave, I. D., 'The anisotropic elasticity of the plant cell wall,' *Wood Sci. Tech.* 2:268-278 (1968).
- [49] Cave, I. D., 'The longitudinal Young's modulus of *Pinus radiata*' *Wood Sci. Tech.* 3:40-48 (1969).
- [50] Cave, I. D., 'Modelling the structure of the softwood cell wall for computation of mechanical properties,' *Wood Sci. Tech.* 10:19-28 (1976).
- [51] Cayoutte, D. J., Morey, L. P., Fournier, M., Dines, R. E., and Ford, M. J., *Pulp & Paper Mag. Can.* 85:T112 (1984).

- [52] Chang, H., Sinkey, J. D., and Yan, J. F., *TAPPI* 62(9):103 (1979).
- [53] Charuel, R., and Rueff, M., 'The Wood Behaviour during Wood Defibring,' In *Pulp, Paper and Board*, Hendry, I. F., and Hanssens, W. J. H. (eds.), pp. 10-17, Elsevier Applied Science, London and New York (1987).
- [54] Choi, H. J., and Thangjitham, S., 'Micro- and macromechanical stress and failure analyses of laminated composites,' *Composites Science and Technology*, 40:289-305 (1991).
- [55] Cholakara, M. T., Jang, B. Z., and Wang, C. Z., 'Deformation and Failure Mechanisms in 3D Composites,' 34th *Int. SAMPE Symp.*, vol. 34, book 2, pp. 2153-2160, May 8-11 (1989).
- [56] Clark, I. E., Hearle, J. W. S., and Taylor, A. R., 'A multi-station apparatus for fatiguing fibres in various environments,' *J. Phys. E: Sci. Instrum.* 13:516-519 (1980).
- [57] Collicutt, S. A., Frazier, W. C., Holmes, G. W., Joice, P., Mackie, D. A., and Torza, S., *TAPPI* 64(6):57 (1981).
- [58] Corte, H., and Kallmes, O., 'Statistical Geometry of a Fibrous Network,' *Trans. of the Oxford Symp. on the Formation and Structure of Paper*, Tech. Sect., B.P. & B.M.A., p. 14, London (1962).
- [59] Côté, W. A., Jr., and Day, A. C., 'Anatomy and ultrastructure of reaction wood,' In *Cellular Ultrastructure of Woody Plants*, Côté, W. A., Jr. (ed.), pp. 391-417, Syracuse Univ. Press (1965).
- [60] Cowdrey, D. R., and Preston, R. D., 'Elasticity and Microfibrillar Angle in The Wood of Sitka Spruce,' *Proc. Roy. Soc. London B* 166:245-272 (1967).
- [61] Cox, H. L., 'The elasticity and strength of paper and other fibrous materials,' *British Journal of Applied Physics* 3:72-79 (1952).
- [62] Dagan, S. J., and Gould, S. O., 'A practical approach for using fiber length data to monitor refiner performance,' *TAPPI*, pp. 69-73, April (1987).

- [63] Dalby, W. E., 'Researches on the elastic properties and the elastic extension of metals,' *Phil. Trans. Roy. Soc. London A* 221:117-138 (1921).
- [64] de Ruvo, A., Carlsson, L., and Fellers, C., 'Biaxial strength of paper,' *Proc. of The International Paper Physics Conference*, British Columbia, pp.23-30, Dec. 17-19 (1979).
- [65] Duckett, K. E., and Goswami, B. C., 'A multi-stage apparatus for characterizing the cyclic torsional fatigue behavior of single fibers,' *Textile Research Institute* 54(1):43-64.
- [66] Duffy, G. G., 'New uses for wood pulp fibres,' *TAPPI*, pp. 107-112, May (1987).
- [67] Dunlop, J. I., and Barker, A., 'Fatigue testing of fibres under compressive flexing,' *Textile Res. J.* 43(6):379-382 (1973).
- [68] Dunning, C. E., 'The Structure of Longleaf-Pine Latewood. I: Cell-Wall Morphology and The Effect of Alkaline Extraction,' *TAPPI* 52(7):1326-1345 (1969).
- [69] El-Hosseiny, F., and Page, D. H., 'The measurement of fibril angle of wood fibres using polarized light,' *Wood and Fiber* 5(3):208-214 (1973).
- [70] El-Hosseiny, F., and Page, D. H., 'The Mechanical Properties of Single Wood Pulp Fibres: Theories of Strength,' *Fibre Science and Technology* 8:21-31 (1975).
- [71] Emerton, H. W., and Goldsmith, V., *Holzforsch.* 10:108 (1956).
- [72] Eskilsson, S., *Svensk Papperstidn.* 75:397 (1972).
- [73] Eskilsson, S., *Svensk Papperstidn.* 77:165 (1974).
- [74] Espenmiller, H. P., 'The theory and practice of refining,' *Southern Pulp and Paper Mfr.*, April 10 (1969).
- [75] Fan, X., *Material Flow in Wood Chip Refiner*, M.Eng. Thesis, McGill University, Montréal, Québec, Canada (1987).

- [76] Fengel, D., *Wood Sci. Technol.* 4:15 (1970).
- [77] Fengel, D., and Wegener, G., *Wood: Chemistry, Ultrastructure, Reactions*, W. de Gruyter, Berlin & New York (1984).
- [78] Fergus, B. J., Procter, A. R., Scott, J. A. N., and Goring, D. A. I., *Wood Science Technology* 3:117 (1969).
- [79] Forgacs, O. L., 'The Characterization of Mechanical Pulps,' *Pulp and Paper Mag. Can.* 64(C):T89-T118 (1963).
- [80] Fredholm, B., Samuelsson, B., Wallis, A., Westfelt, A., and Westfelt, L., *Cell. Chem. Technol.* 17:245 (1983).
- [81] Fredholm, B., Samuelsson, B., Wallis, A., Westfelt, A., and Westfelt, L., *Cell. Chem. Technol.* 17:255 (1983).
- [82] Frei, E., Preston, R. D., and Ripley, G. W., 'The fine structure of the walls of conifers tracheid. VI. Electron microscopic investigations of setions,' *J. Exp. Botany* 8(22):139-46 (1957).
- [83] Freudenberg, K., 'The relationship of cellulose to lignin in wood,' *J. Chem. Edu.* 9(7):1171-80 (1932).
- [84] Frey-Wyssling, A., 'The fine structure of cellulose microfibrils,' *Science* 119:80-82 (1954).
- [85] Frey-Wyssling, A., *Biochem. Bio-Phys. Acta* 18:166-168 (1955).
- [86] Frey-Wyssling, A., 'The general structure of fibres,' In *Fundamentals of Paper-making Fibres*, Bolam, F. (ed.), pp. 1-6 (1958).
- [87] Frey-Wyssling, A., *Die Pflanzliche Zellwand*, Springer, Berlin, p. 17 (1959).
- [88] Frey-Wyssling, A., and Mühlethaler, K., *Makromol. Chem.* 62:25 (1963).
- [89] Frey-Wyssling, A., and Mühlethaler, K., *Ultrastructure Plant Cytology*, pp. 34-40, Elsevier, New York (1965).

- [90] Gardner, K. H., and Blackwell, J., 'The structure of native cellulose,' *Biopolymers* 13:1975-2001 (1974).
- [91] Gavelin, G., and Luden, L., *Svensk Papperstidn.* 83:416 (1980).
- [92] Gillis, P. P., 'Effect of hydrogen bonds on the axial stiffness of crystalline native cellulose,' *J. Polymer Sci. (A-2)* 7:783-794 (1969).
- [93] Goodier, J. N., and Hodge Jr., D. G., *Elasticity and Plasticity*, John Wiley & Sons, Inc., New York (1958).
- [94] Goring, D. A. I., *Polymer Properties of Lignin and Lignin Derivatives*, In *Lignins: Occurrence, Formation, Structure and Reactions*, Sarkanen, K. V., and Ludwig, C. W. (eds.), pp. 695-768, Wiley Interscience, New York (1971).
- [95] Goring, D. A. I., and Timell, T. E., *TAPPI* 45(6):454 (1962).
- [96] Gray, D. G., 'Chirality and Curl of Paper Sheets,' *Journal of Pulp and Paper Science* 15(3):J105-J109 (1989).
- [97] Griffith, A. A., 'The phenomena of rupture and flow in solids,' *Phil. Trans. Roy. Soc. London A* 221:163-198 (1921).
- [98] Griffiths, J. R., and Owen, D. R. J., 'An elastic-plastic stress analysis for a notched bar in plane strain bending,' *J. Mech. Phys. Solids* 19:419-431 (1971).
- [99] Haddad, Y. M., *Response Behaviour Of A 2-D fibrous Network*, Ph.D. Thesis, McGill University, Montréal, Québec, Canada (1975).
- [100] Halpin, J., 'Introduction to viscoelasticity,' In *Composite Materials Workshop*, S. W. Tsai, J. C. Halpin, and N. J. Pagano (eds.), Technomic Publ. Co. Inc., Stamford, Conn. (1967).
- [101] Hamad, W. Y., and Provan, J. W., 'On the fracture and fatigue characterisation of single wood pulp fibres,' *Proc. of the 5th Int. Conf. on Fatigue and Fatigue Thresholds*, Montréal, May 3-7, vol. III, pp. 1429-34 (1993).

- [102] Hamad, W. Y., and Provan, J. W., 'Confocal laser microscopy of the morphology of wood pulp fibres,' *Proc. of the 20th Annual Meeting of the Microscopical Society of Canada*, Toronto, June 3-5, pp. 136-7 (1993).
- [103] Hamilton, W. C., and Ibers, J. A., *Hydrogen Bonding in Solids*, Benjamin, New York (1968).
- [104] Hamilton, B., and Rawson, H., 'The determination of the flaw distributions on various glass surfaces from Hertz fracture experiments,' *J. Mech. Phys. Solids* 18:127-147 (1970).
- [105] Hanley, S. J., Giasson, J., Revol, J.-F., and Gray, D. G., 'Atomic force microscopy of cellulose microfibrils: comparison with transmission electron microscopy,' *POLYMER* 23(21):4639-4642 (1992).
- [106] Harada, H., 'Ultrastructure and organization of gymnosperm cell walls,' *In Cellular Ultrastructure of Woody Plants*, W. A. Côté, Jr. (ed.), pp. 215-234 (1965).
- [107] Harada, H., 'Ultrastructure of angiosperm vessels and ray parenchyma,' *In Cellular Ultrastructure of Woody Plants*, W. A. Côté, Jr. (ed.), pp. 235-250 (1965).
- [108] Harada, H., Miyazaki, Y., and Wakashima, T., 'Electron-microscopic investigation on the cell wall structure of wood,' *Bull. Govt. Forest Sta. (Japan)*, No. 104, 115pp. (1958) [in Japanese].
- [109] Hardacker, K. W., 'Cross-sectional Area Measurement of Individual Wood Pulp Fibers by Lateral Compaction,' *TAPPI* 52(9):1742-1746 (1969).
- [110] Hearle, J. W. S., 'The fine structure of fibres and crystalline polymers. I. Fringed fibril structure,' *J. Appl. Polymer Sci.* 7(4):1175-92 (1963).
- [111] Hearle, J. W. S., 'Fatigue in fibres and plastics (A Review),' *J. Mat. Sci.* 2:474-488 (1967).
- [112] Hearle, J. W. S., and Cross, P. M., 'The fractography of thermoplastic textile fibres,' *J. Mat. Sci.* 5:507-516 (1970).

- [113] Hearle, J. W. S., and Peters, R. H., *Fibre Structure*, The Textile Institute Butterworths, Manchester and London (1963).
- [114] Hearle, J. W. S., and Plonsker, H. R. 'Behaviour of fibre in cumulative extension cycling,' *J. Appl. Poly. Sci.* 10:1949-1971 (1966).
- [115] Hearle, J. W. S., and Wong, B. S., 'A fibre fatigue tester, based on rotation over a wire, for use in different environments,' *J. Phys. E: Sci. Instrum.* 10(5):448-450 (1977).
- [116] Heitner, C., Beatson, R. P., and Atack, D., *J. Wood Chem. Technol.* 2:169 (1982).
- [117] Hermans, P. H., *Physics and Chemistry of Cellulose Fibres*, Elsevier Publishing Co. Inc. (1949).
- [118] Herrmann, K., Gerngross, O., and Abitz, W., *Z. Phys. Chem.* B10:371-394 (1930).
- [119] Hess, K., Mahl, H., and gütter, E., *Kolloid-Z.* 155(1):1-19 (1957).
- [120] Hill, R., *The Mathematical theory of Plasticity*, The Clarendon Press, Oxford (1964).
- [121] Holton, H., *Pulp & Paper Mag. Can.* 78:T218 (1977).
- [122] Hosoi, H., Katahara, K., and Migita, N., 'Research on the swelling of fibres. III. Relationship between the morphological structure and the behaviour of swelling of fibres,' *J. Japan Wood Res. Soc.* 4(2):60-66 (1958) [in Japanese].
- [123] Jacobson, R. A., Wunderlich, J. A., and Lipscomb, W. N., 'The crystal and molecular structure of cellbiose,' *Acta Cryst.* 14:598-607 (1961).
- [124] Jane, F. W., *The Structure of Wood*, New York, p. 175 (1956).
- [125] Jane, F. W., *The Structure of Wood*, 2nd edition, revised by Wilson, K. and White, D. J. B., A. and C. Black Ltd., London (1970).

- [126] Jang, H. F., Robertson, A. G., and Seth, R. S., 'Transverse Dimensions of Wood Pulp Fibres by Confocal Laser Scanning Microscopy and Image Analysis,' *PPR* 876, 23 pp, July (1991).
- [127] Jeffery, G. B., 'Plane stress and plane strain in bipolar coordinates,' *Phil. Trans. Roy. Soc. London A* 221:265-293 (1921).
- [128] Jentzen, C. A., 'The Effect of Stress Applied During Drying On Some of The Properties of Individual Pulp Fibers,' *TAPPI* 47(7):412-418 (1964).
- [129] Johnston, T. L., Stokes, R. J., and Li, C. H., 'Fundamental mechanical behavior of composite crystalline mixtures,' In *Proc. Sixth Ordnance Materials Res. Conf.*, Syracuse Univ. Res. Inst., pp. 75-93 (1959).
- [130] Kanninen, M. F., Rybicki, E. F., and Brinson, H. F., 'A critical look at current applications of fracture mechanics to the failure of fibre-reinforced composites,' *Composites*, pp. 17-22, Jan. (1977).
- [131] Karnis, A., 'The mechanism of fibre development in mechanical pulping,' *Reprints of the IMPC Conference (Oslo)*, 26 pp., June 15-17 (1993).
- [132] Karnis, A., *Personal Communication*.
- [133] Ke-fu, C., and Shu-mei, C., 'The determination of the critical shear stress for fluidization of medium consistency suspensions of straw pulps,' *Nordic Pulp and Paper Research Journal* 6(1):20-22 (1991).
- [134] Kellogg, R. M., and Wangaard, F. F., 'Influence of Fiber Strength on Sheet Properties of Hardwood Pulps,' *TAPPI* 47(6):361-367 (1964).
- [135] Keller, A., 'A note on single crystals in polymers: Evidence for a folded chain configuration,' *Phil. Mag. (8th series)* 2:1171-75 (1957).
- [136] Keller, A., and O'Connor, A., 'Study of single crystals and their association in polymers,' *Disc. Faraday Soc.* 25:114-21 (1958).

- [137] Kelly, A., and Davies, G. J., 'The principles of the fibre reinforcement of metals,' *Metallurgical Reviews* 10:1-77 (1965).
- [138] Kenney, M. C., Mandell, J. F., and McGarry, F. J., 'Fatigue behaviour of synthetic fibres, yarns and ropes,' *J. Mat. Sci.* 20:2045-2059 (1985).
- [139] Kerekes, R. J., and Tam Doo, P. A., 'Wet fibre flexibility of some major softwood species pulped by various processes,' *J. of Pulp and Paper Science* 11(2):J60-J61 (1985).
- [140] Kerr, K. J., and Goring, D. A. I., *Cell. Chem. Technol.* 9:563 (1975).
- [141] Kerr, T., and Baily, I. W., 'The Cambium and Its Derivative Tissues. No. X: Structure, Optical Properties and Chemical Composition of The So-called Middle Lamella,' *J. of The Arnold Arboretum*, vol. XV, pp. 327-349 (1934).
- [142] Kim, C. Y., Page, D. H., El-Hosseiny, F., and Lancaster, A. P. S., 'The Mechanical Properties of Single Wood Pulp Fibres. III The Effect of Drying Stress on Strength,' *J. of Applied Polymer Science* 19:1549-1561 (1971).
- [143] Klauditz, W., *Holzforsch* 11(4):110-16 (1957).
- [144] Klauditz, W., Marschall, A., and Ginzel, W., 'Technology of lignified plant cell walls; determination of the tensile strength of pulp fibres obtained from *Pinus merkusii* wood,' *Holzforschung* 1:98 (1947).
- [145] Knox Jr., L. J., and Whitwell, J. C., 'Studies of breaking-stress distributions. Part I: The weak-link theory and alternate models,' *Text. Res. J.*, pp. 510-517, June (1971).
- [146] Kolseth, P., and de Ruvo, A., 'An attempt to measure the torsional strength of single wood pulp fibers.' In *General Constitutive Relations for Wood and Wood-Based Materials*, NSF Workshop Report, Syracuse Univ., Syracuse, New York, pp. 57-79 (1978).
- [147] Koran, Z., *Pulp & Paper Mag. Can. Trans. Sec.* 7(2):TR1 (1980).

- [148] Kortschot, M. T., Beaumont, P. W. R., and Ashby, M. F., 'Damage mechanics of composite materials. III: Prediction of damage growth and notched strength,' *Composites Science and Technology* 40:147-165 (1991).
- [149] Kortschot, M. T., and Beaumont, P. W. R., 'Damage mechanics of composite materials. VI: The effect of lay-up on damage growth and notched strength,' *Composites Science and Technology* 40:167-179 (1991).
- [150] Kozaczewski, P., Rybaczuk, M., 'Simulations of fractal fatigue process in fibrous composites,' *Proc. of the 5th Int. Conf. on Fatigue and Fatigue Thresholds*, Montréal, May 3-7, vol. II, pp. 1245-1250 (1993).
- [151] Krey, J., and Friedrich, K., 'Fracture toughness and fatigue crack propagation of single fibre-bundle reinforced model composites,' *J. of Materials Science Letters* 6:851-856 (1987).
- [152] Kulkarni, A. G., Satyanarayana, K. G., and Sukumaran, K., 'Mechanical behaviour of coir fibres under tensile load,' *J. Mat. Sci.* 16:905-914 (1981).
- [153] Labossière, P., and Neale, K. W., 'On the determination of strength parameters in the tensor polynomial failure criterion,' *Journal of Strain Analysis* 22(3):155-161 (1987).
- [154] Labossière, P., and Neale, K. W., 'A general strength theory for orthotropic fiber-reinforced composite laminae,' *Polymer Composites* 9(5):305-317 (1988).
- [155] Labossière, P., Neale, K. W., and Neglo, K., 'Damage accumulation in fibre-reinforced composite laminates,' *Journal of the CSME* 12(3):133-137 (1988).
- [156] Lai, J. S. Y., and Findley, W. N., 'Stress relaxation of nonlinear viscoelastic material under uniaxial strain,' *Trans. of the Soc. of Rheology* 12(2):259-280 (1968).
- [157] Lamb, G. E. R., 'Energy consumption in mechanical pulping,' *TAPPI* 45(5):364 (1962).

- [158] Lange, P. W., *Svensk Papperstidn.* 57:525 (1954).
- [159] Leask, R. A., *Pulp and Paper Manufacture*, vol. 2, 3rd ed. (1987).
- [160] Leask, R. A., MacDonald, J., and Shaw, A. C., *Pulp & Paper Mag. Can.* 75:T361 (1974).
- [161] Leopold, B., and Thorpe, J. L., 'Effect of Pulping on Strength Properties of Dry and Wet Pulp Fibers From Norway Spruce,' *TAPPI* 51(7):304-308 (1968).
- [162] Leung, H., 'The importance of mounting medium's refractive index and cover glass thickness for reducing optical aberration in a confocal laser scanning microscope (CLSM),' *bulletin of the Microscopical Society of Canada* 21(2):19-24 (1993).
- [163] Lubliner, J., *Plasticity Theory*, Macmillan Publishing Co., New York (1990).
- [164] Lyons, W. J., 'Fatigue in textile fibers. Part XI: Fatiguing by cyclic extension: Effects of temperature, stroke and frequency on life times,' *Text. Res. J.*, pp. 60-68, Jan. (1970).
- [165] Lyons, W. J., 'Fatigue in textile fibers. Part XII: Fatiguing by cyclic tension at constant force amplitude,' *Text. Res. J.*, pp. 836-843, Sept. (1970).
- [166] Makinde, A., and Neale, K. W., 'A general criterion for low-cycle multiaxial fatigue failure,' *J. of Engineering Materials and Technology* 111:263-269 (1989).
- [167] Manley, R. S. J., 'Growth and morphology of single crystals of cellulose triacetate,' *J. Polymer Sci.* A1:1875-92 (1963).
- [168] Manley, R. S. J., 'Hydrolysis of cellulose triacetate crystals,' *J. Polymer Sci.* A1:1892-99 (1963).
- [169] Manley, R. S. J., *J. Polym. Sci.* 9(A2):1025 (1971).
- [170] Mann, J., and Marrinan, H. J., 'The reaction between cellulose and heavy water,' *Trans. Faraday Soc.* 52:481-97 (1956).

- [171] Marchessault, R. H., 'Chimie et Biochimie de la Lignine, de la Cellulose et des Hémicelluloses,' *Actes du Symp. Intern. de Grenoble*, 287 (1964) [in French].
- [172] Mark, R. E., *Cell Wall Mechanics of Tracheids*, Yale University Press, New Haven, Conn., 310 pp. (1967).
- [173] Mark, R. E., 'Mechanical behaviour of cellulose in relation to cell wall theories,' *J. Polymer Sci.* C36:393-406 (1971).
- [174] Mark, R. E., 'Mechanical behavior of the molecular components of fibres,' In *Theory and Design of Wood and Fiber Composite Materials*, Jayne, B. A. (ed.), Syracuse Univ. Press, Syracuse, New York, pp. 49-82 (1972).
- [175] Mark, R. E., 'Molecular and cell wall structure of wood,' *Journ. of Educational Modules for Materials Science and Engineering* 2(2):251-308 (1980).
- [176] Mark, R. E. (ed.), *Handbook of Physical and Mechanical Testing of Paper and Paperboard*, vol. 1, Marcel Dekker Inc. Publ., New York (1983).
- [177] Mark, R. E., and Gillis, P. P., 'New models in cell wall mechanics,' *Wood and Fiber* 2(2):79-95 (1970).
- [178] Mark, R. E., and Gillis, P. P., 'The relationship between fiber modulus and S2 angle,' *TAPPI* 56(4):164-167 (1973).
- [179] Mark, R. E., and Gillis, P. P., 'Mechanical Properties of Fibers,' In *Handbook of Physical and Mechanical Testing of Paper and Paperboard*, Mark, R. E. (ed.), vol. 1, pp. 409-495 (1983).
- [180] Marton, R., Tsujimoto, N., and Eskelinen, E., *TAPPI* 64(8):71 (1981).
- [181] Marx-Figini, M., J., *J. Polym. Sci.* 28(C):57 (1969).
- [182] Mayhood Jr., C. H., Kallmes, O. J., and Cauley, M. M., 'The mechanical properties of paper. Part II: Measured shear strength of individual fiber to fiber contacts,' *TAPPI* 45(1):69-73 (1962).

- [183] McKenzie, A. W., and Higgins, H. G., 'The reactivity of cellulose,' *Holzforsch* 10(6):179-84 (1957).
- [184] McLaughlin, E. C., and Tait, R. A., 'Fracture mechanism of plant fibres,' *J. Mat. Sci.* 15:89-95 (1980).
- [185] McLaughlin, E. C., 'The strength of bagasse fibre-reinforced composites,' *J. Mat.Sci.* 15:886-890 (1980).
- [186] Meier, H., *J. Polymer Sci.* 51:11 (1961).
- [187] Meyer, K. H., *Natural and Synthetic High Polymers*, Interscience, New York, p. 395 (1950).
- [188] Michel, B., Winkler, T., and Sommer, J. P., 'Theoretical Concepts and Experiments in Fracture Mechanics—Macroscopic and Microscopic Aspects of Modelling,' *Plenary Lecture, 1st European Solid Mechanics Conference*, 16 pgs., Munich, Sept. 9-14, 1991 (published in the *European Journal of Mechanics* [Paris]).
- [189] Miles, K., 'Refining Intensity and Paper Quality in High-Consistency Refining,' *Paperi ja Puu* 72:508-514 (1990).
- [190] Miles, K. B., and May, W. D., 'The Flow of Pulp in Chip Refiners,' *Journal of Pulp and Paper Science* 16(2):J63-J72 (1990).
- [191] Morley, T. G., 'Strong fibres and fibre-reinforced metals,' *Proc. Roy. Soc. London* A 282:43-52 (1964).
- [192] Mu, E. M., 'Application of fracture mechanics to anisotropic plates,' *Trans. of The ASME Journal of Applied Mechanics*, pp. 967-974, Dec. (1967).
- [193] Mühlethaler, K., 'Growth theories and the development of the cell wall,' In *Cellular Ultrastructure of Woody Plants*, Côté, W. A., Jr. (ed.), pp. 51-59 (1965).
- [194] Mühlethaler, K., 'The fine structure of cellulose microfibrils,' In *Cellular Ultrastructure of Woody Plants*, Côté, W. A., Jr. (ed.), pp. 191-198 (1965).

- [195] Mukherjee, P. S., and Satyanarayana, K. G., 'An empirical evaluation of structure-property relationships in natural fibres and their fracture behaviour,' *J. Mat. Sci.* 21:4162-4168 (1986).
- [196] Nahas, M. N., 'Survey of failure and post-failure theories of laminated fibre-reinforced composites,' *Journal of Composites Technology and Research* 8(4):138-153 (1986).
- [197] Naito, T., Usuda, M., and Kadoya, T., 'Fatigue phenomena of single pulp fibres under repeated torsional stress,' *SEN-1 GAKKAISHI* 39(1):T8-T13 (1983).
- [198] Neale, K. W., and Labossière, P., 'Failure of composite laminae under biaxial loading,' *Polymer Composites* 10(5):285-292 (1989).
- [199] Ohad, I., and Danon, D., 'On the dimensions of cellulose microfibrils,' *J. Cell Biol.* 22:302-305 (1964).
- [200] Onogi, S., and Sasaguri, K., 'The Elasticity of Paper and Other Fibrous Sheets,' *TAPPI* 44(12):874-880 (1961).
- [201] Östberg, G., and Salmén, L., 'Effects of fibrillation of wood fibres on their interaction with water,' *Nordic Pulp and Paper Research Journal* 6(1):23-26 (1991).
- [202] Page, D. H., 'The axial compression of fibres, a newly discovered beating action,' *Pulp and Paper Mag. Can.* 67(1):T2 (1966).
- [203] Page, D. H., 'The Collapse Behaviour of Pulp Fibres,' *TAPPI* 50(9):449 (1967).
- [204] Page, D. H., 'A Method for Determining The Fibrillar Angle in Wood Tracheids,' *J. of Microscopy* 90(2):137-143 (1969).
- [205] Page, D. H. (ed.), *The Physics and Chemistry of Wood Pulp Fibers*, STAP No. 8 (1970).
- [206] Page, D. H., 'A note on the cell-wall structure of softwood tracheids,' *Wood and Fibre* 7(4):246 (1976).

- [207] Page, D. H., 'Mechanisms of strength development of dried pulps by beating,' *Svensk Papperstidn.* 88(3):R30 (1985).
- [208] Page, D. H., 'The beating of chemical pulps—The action and the effects,' *Miscellaneous Reports, MR 166*, 36 pp., July (1989).
- [209] Page, D. H., and De Grâce, J. H., 'Delamination of fibre walls by beating and refining,' *TAPPI* 50(10):489 (1967).
- [210] Page, D. H., and El-Hosseiny, F., 'The Mechanical Properties of Single Wood Pulp Fibres. Part IV: The Influence of Defects,' *Sven. Papperstid.* 14:471 (1976).
- [211] Page, D. H., and El-Hosseiny, F., 'The birefringence of wood pulp fibres and the thickness of the S_1 and S_3 layers,' *Wood and Fiber* 6(3):186-192 (1974).
- [212] Page, D. H., and El-Hosseiny, F., 'The Mechanical Properties of Single Wood Pulp Fibres. Part VI: Fibril Angle and The Shape of The Stress-Strain Curve,' *Jour. Pulp and Paper Sci.* 9(4):TR99-TR100 (1983).
- [213] Page, D. H., El-Husseiny, F., Bidmade, M. L., and Binet, R., 'Birefringence and the chemical composition of wood fibres,' *Appl. Polym. Symp.* 28:923 (1976).
- [214] Page, D. H., El-Hosseiny, F., and Winkler, K., 'Behaviour of single wood fibres under axial tensile strain,' *Nature* 229:252-253 (1971).
- [215] Page, D. H., El-Hosseiny, F., Winkler, K., and Bain, R., 'The Mechanical Properties of Single Wood-Pulp Fibres. Part I: A New Approach,' *Pulp and Paper Mag. Can.* 73(8):T198-T203 (1972).
- [216] Page, D. H., El-Hosseiny, F., Winkler, K., and Lancaster, A. P. S., 'Elastic Modulus of Single Wood Pulp Fibres,' *TAPPI* 60(4):114-117 (1977).
- [217] Pearl, I. A., *For. Prod. J.* 17:23 (1967).
- [218] Pedersen, B., *Acta Crystallogr. B* 30:289 (1974).
- [219] Peirce, F. T., 'Theorems On The Strength of Long and Composite Specimens,' *Jour. of The Textile Institute* 17:T355-T368 (1926).

- [220] Perkins Jr., R. W., 'A Theory of Mechanical Response of Fiber Networks,' *Wood and Fiber* 5(1):26-33 (1973).
- [221] Perkins, R. W., 'Mechanics of cellulosic and polymeric materials,' *Proc. of The 3rd Joint ASCE/ASME Mechanics Conference*, University of California-San Diego, La Jolla, California, July 9-12 (1989).
- [222] Plummer, G. M., *TAPPI* 61(3):45 (1978).
- [223] Poon, C., Scott, R.F., and Lee, S., 'Testing of new-generation carbon fiber/toughened resin epoxy systems,' *Polymer Composites*, vol. 9, No. 5, October (1988).
- [224] Porter, A. W., 'On The Mechanics of Fracture in Wood,' *Forest Products Journal* XIV(8):325-331 (1964).
- [225] Preston, R. D., 'The electron microscopy and electron diffraction analysis of natural cellulose,' In *The Interpretation of Ultrastructure*, pp. 325-348, Academic Press, New York (1962).
- [226] Preston, R. D., 'Interdisciplinary approaches to wood structure,' In *Cellular Ultrastructure of Woody Plants*, Côté, W. A., Jr. (ed.), pp. 1-31 (1965).
- [227] Prevorsek, D. C., and Lyons, W. J., 'Endurance of polymeric fibers in cyclic tension,' *Rubber Chemistry and Technology* 44(1):271-293 (1971).
- [228] Prevorsek, D., and Lyons, W. J., 'Fatigue fracture in fibrous polymers as a brittle, crack-nucleation process,' *J. of Applied Physics* 35(11):3152-3164 (1964).
- [229] Provan, J. W., 'An introduction to fatigue,' *J. Mater. Educ.* 11(1&2):1-104 (1989).
- [230] Provan, J. W., 'An introduction to fracture mechanics,' *J. Mater. Educ.* 10(4):325-430 (1988).

- [231] Rånby, B. G., and Grinberg, B., 'Sur la sorption de la vapeur d'eau par la cellulose hydrolysée et par les micelles isolées de cellulose,' *Compt. Rend.* 230(15):1402-04 (1950).
- [232] Rånby, B. G., and Noe, R. W., 'Crystallization of cellulose and cellulose derivatives from dilute solution. I. Growth of single crystals,' *J. Polymer Sci.* 51(155):337-47 (1961).
- [233] Rebenfeld, L., 'Morphological foundations of fibre properties,' *J. Polymer Sci.* C9:91-112 (1965).
- [234] Reifsnider, K. L., 'A Micromechanical Approach to Fatigue of Composite Material Systems,' *Proc. of the 5th Int. Conf. on Fatigue and Fatigue Thresholds*, vol. II, pp. 1219-21, Montréal, May 3-7 (1993).
- [235] Roelofsen, P. A., *The Plant Cell Wall*, Borntraeger, Berlin, p. 23 (1959).
- [236] Rosato, D. V., and Grove Jr., C. S., *Filament Winding: its development, manufacture, applications and design*, Interscience Publishers, New York (1964).
- [237] Ruel, K., Barnoud, F., and Goring, D. A. I., *Wood Science Technology* 12:287 (1978).
- [238] Ruhleman, F., *Papier Farikank* 24(1):1 (1962).
- [239] Rybaczuk, M., 'The fatigue evolution of fractal defects in metals,' *Proc. of the Conf. on Low Cycle Fatigue and Elasto-Plastic Behaviour of Materials*, K. T. Rie (ed.), pp. 733-738, Elsevier, London (1992).
- [240] Rybaczuk, M., 'The fractal growth of fatigue defects,' *Proc. of the 5th Int. Conf. of Fatigue and Fatigue Thresholds*, Montréal, May 3-7, vol. I, pp. 257-262 (1993).
- [241] Rydholm, S. A., *Pulping Processes*, Wiley Interscience, New York (1965).
- [242] Salmén, L., 'Viscoelastic properties of in-situ lignin under water-saturated conditions,' *J. Mat. Sci.* 19(9):3090 (1984).

- [243] Salmén, L., 'The Effect of the Frequency of a Mechanical Deformation on the Fatigue of Wood,' *Journal of Pulp and Paper Science* 13(1):J23-J28 (1987).
- [244] Salmén, L., 'Chip Refining: Influence of Mechanical and Chemical Treatments on the Energy Consumption during Fatigue of Wood,' In *Pulp, Paper and Board*, Hendry, I. F., and Hanssens, W. J. H. (eds.), pp. 18-24, Elsevier Applied Science, London and New York (1987).
- [245] Salmén, L., and Fellers, C., 'The Fundamentals of Energy Consumption during Viscoelastic and Plastic Deformation of Wood,' *Trans. Tech. Sect. (Can. Pulp Pap. Assoc.)*, pp. TR93-TR99, December (1982).
- [246] Salmén, L., Fellers, C., and Tigerström, A., 'The Effect of Loading Mode on the Energy Consumption during Mechanical Treatment of Wood,' *TAPPI Int. Mech. Pulping Conf. Proc.*, Washington, D.C., pp. 109-114, June, 13-17 (1983).
- [247] Salmén, L., Tigerström, A., and Fellers, C., 'Fatigue of Wood - Characterization of Mechanical Defibration,' *Journal of Pulp and Paper Science* 11(3):J68-J3 (1985).
- [248] Sarko, A., 'What is the crystalline structure of cellulose?' *TAPPI* 61(2):59-61 (1978).
- [249] Schniewind, A. P., and Barrett, J. D., 'Cell Wall Model with Complete Shear Restraint,' *Wood and Fiber* 1(3):205-214 (1969).
- [250] Schniewind, A. P., Nemeth, L. J., and Brink, D. L., 'Fiber and Pulp Properties. I: Shear Strength of Single-Fiber Crossings,' *TAPPI* 47(4):244-248 (1964).
- [251] Schuerch, C., *J. Amer. Chem. Soc.* 74:5061 (1952).
- [252] Schuster, P., Zundel, G., and Sandorfy, C., *The Hydrogen Bond, Recent Developments in the Theory and Experiments*, vols. I-III, North-Holland, Amsterdam (1976).
- [253] Seth, R. S., *MRS Symposium Proceedings 197*, Materials Research Society, Pittsburg, PA, pp. 143-161 (1990).

- [254] Seth, R. S., and Page, D. H., 'Fracture Resistance: A failure criterion for paper,' *TAPPI* 58(9):112-117 (1975).
- [255] Sih, G. C., Paris, P. C., and Irwin, G. R., 'On cracks in rectilinearly anisotropic bodies,' *Int. J. Fract. Mech.* 1(3):189-203 (1965).
- [256] Smook, G. A., *Handbook for Pulp and Paper Technologists* (1982).
- [257] Sobue, N., and Asano, I., 'Studies on the fine structure and mechanical properties of wood. On the longitudinal Young's modulus and shear modulus of rigidity of cell wall,' *J. Japan Wood Res. Soc. (Mokuzai Gakkaishi)* 22:211-216 (1976) [in Japanese].
- [258] Spiegelberg, H. L., 'The Effect of Hemicellulose on The Mechanical Properties of Individual Pulp Fibers,' *TAPPI* 49(9):388-396 (1966).
- [259] Stamm, A. J., *Wood and Cellulose Science*, Ronald Press, New York, p. 44 (1964).
- [260] Stationwala, M. I., Atack, D., and Karnis, A., 'Effect of refiner plate design on the development of pulp properties,' *PPR 605*, December (1986).
- [261] Stationwala, M. I., and Karnis, A., 'Pulp Grinding - a new method for producing mechanical pulp,' *TAPPI* 73(12):187-195 (1990).
- [262] Stein, R. S., 'Structural interpretations of mechanical properties of polycrystalline polymers,' *SPE Trans.* 4(3):178-86 (1964).
- [263] Stone, J. E., and Scallan, A. M., *Pulp & Paper Mag. Can.* 66:T407 (1965).
- [264] Stone, J. E., and Scallan, A. M., *Pulp & Paper Mag. Can.* 69:T288 (1968).
- [265] Stone, J. E., Scallan, A. M., and Abrahamson, B., 'Influence of beating on cell wall swelling and internal fibrillation,' *Sven. Papperstidn.* 71(19):687 (1968).
- [266] Stoves, J. L., *Fibre Microscopy: Its Technique and Application*, National Trade Press, London (1957).

- [267] Strelis, I., and Kennedy, R. W., *Identification of North American Commercial Pulpwoods and Pulp Fibres*, Univ. of Toronto Press (1967).
- [268] Suresh, S., *Fatigue of Materials*, Cambridge University Press (1991).
- [269] Tam Doo, P. A., and Kerekes, R. J., 'A method to measure wet fiber flexibility,' *TAPPI* 64(3):113-116 (1981).
- [270] Tam Doo, P. A., and Kerekes, R. J., 'The flexibility of wet pulp fibres,' *Pulp and Paper Canada* 83(2):T37-T41 (1982).
- [271] Tam Doo, P. A., and Kerekes, R. J., 'The effect of beating and low-amplitude flexing on pulp fibre flexibility,' *Jour. of Pulp and Paper Science* 15(1):J36-42 (1989).
- [272] Tamolang, F. N., Wangaard, F. F., and Kellogg, R. M., 'Strength and Stiffness of Hardwood Fibers,' *TAPPI* 50(2):68-72 (1967).
- [273] Tang, R. C., and Hsu, N. N., 'Analysis of the relationship between microstructure and elastic properties of the cell wall,' *Wood and Fiber* 5:139-151 (1973).
- [274] Tashiro, K., and Kobayashi, M., 'Theoretical evaluation of three-dimensional elastic constants of native and regenerated celluloses: role of hydrogen bonds,' *POLYMER* 32(8):1516-1526 (1991).
- [275] Timell, T. E., *Wood Sci. Technol.* 1:45 (1967).
- [276] Treloar, L. R. G., 'Physics of textiles,' *Physics Today*, pp. 23-30, Dec. (1977).
- [277] van den Akker, J. A., 'Energy consideration in the beating of pulp,' In *Fundamentals of Papermaking Fibres*, F. Bolam (ed.), Techn. Sec. B. P. & B. M. A., p. 435 (1958).
- [278] van den Akker, J. A., 'Structure and Tensile Characteristics of Paper,' *TAPPI* 53(3):388-400 (1970).
- [279] van den Akker, J. A., Lathrop, A. L., Voelker, M. H., and Dearth, L. R., 'Importance of fibre strength to sheet strength,' *TAPPI* 42(6):461 (1959).

- [280] Victor, V. J., 'Application of the molecular place-exchange theory to the cell wall rheology of wood,' *J. Indian Acad. Wood Sci.* 3(1):1-12 (1972).
- [281] Wardrop, A. B., 'Cell wall organization and the properties of the xylem. I. Cell wall organisation and the variation of breaking load in tension of the xylem in conifer stems,' *Aust. J. Sci. Res. Ser. B.4* (4):391 (1951).
- [282] Wardrop, A. B., 'Organisation of the primary wall in differentiating conifer tracheids,' *Australian J. Bot.* 6:229-305 (1958).
- [283] Wardrop, A. B., 'The structure and formation of the cell wall in xylem,' *In The Formation Of Wood In Forest Trees*, M. H. Zimmermann, ed., Academic Press, New York, pp. 87-134 (1964).
- [284] Wardrop, A. P., and Bland, D. E., 'The process of lignification in woody plants,' *In Proc. Fourth Intl. Congr. of Biochem.*, Pergamon Press, New York, 2, pp.76-81 (1959).
- [285] Willis, J. M., *The Leaching of Lignin And Carbohydrate From High Yield Pulp Fibres Suspended In Water*, Ph.D. Thesis, McGill University, Montréal, Québec, Canada (1984).
- [286] Wilson, T., *Confocal Microscopy*, Academic Press, London (1990).
- [287] Wilson, T., and Sheppard, C., *Theory and Practice of Scanning Optical Microscopy*, Academic Press, London (1984).
- [288] Woodcock, C., and Sarko, A., 'Packing analysis of carbohydrates and polysaccharides. II. Molecular and crystal structure of native ramie cellulose,' *Macromolecules* 13:1183-1187 (1980).
- [289] Woods, H. G., *Physics of Fibres: An Introductory Survey*, The Institute of Physics, London (1955).
- [290] Wyrick, D. A., and Adams, D. F., 'Damage sustained by a carbon/epoxy composite material subjected to repeated impact,' *Composites* 19(1):19-27 (1988).

- [291] Zweben, C., and Rosen, B. W., 'A statistical theory of material strength with application to composite materials,' *J. Mech. Phys. Solids* 18:189-206 (1970).

Appendix A

Finite-Element Modelling and Analysis

A.1 A Brief Overview

The finite-element method has long been a fertile research field: A tool for numerical experiments using the methods of discretisation and numerical approximation to solve scientific and engineering problems. The earliest evidence of the finite-element concept could probably be traced back to the geometric approximations of pyramids by the Egyptians some five millennia ago.

The finite-element method is an analysis method that idealises a continuous medium as an assemblage of a finite number of discrete elements interconnected at a finite number of nodal points. This idealisation is performed by an articulated system to which matrix methods are directly applicable, i.e., there are two approaches that are the dual of each other: the force or flexibility method, which assumes the internal forces to be the unknowns of the problem (the complementary energy approach); and the displacement or stiffness method, which assumes the internal displacements to be the unknowns of the problem (the energy approach). Moreover, the latter method is more desirable since its formulation is slightly simpler for the majority of stress analysis problems; hence, it is the approach undertaken here.

In the course of this research the geometrical modelling and finite-element anal-

ysis are performed using a commercial software package, I-DEAS (INTEGRATED DESIGN ENGINEERING SOFTWARE ANALYSIS). The latter is a complete, user-friendly, general-purpose, finite-element package capable of handling a large variety of engineering design and analysis problems. It supports a number of element and material types, such as: isotropic, anisotropic, orthotropic and laminate material properties. Furthermore, the software has a built-in, linear, finite-element solver that may be accessed, in ASCII mode, once the geometric modelling is performed and necessary material properties are assigned. All operations have been performed on a 700 series Hewlett Packard workstation network.

A.2 Modelling and Analysis

An appropriate model of a single fibre as a two-layered hollow tube of elliptical cross section is formulated. The latter stipulation is called for as fibres tend to flatten when beaten or refined [101]. Moreover, the approximations enunciated below are within reason, especially if we recall that the main purpose, at this stage, is to use this analysis as a qualitative tool for verifying certain aspects of the experimental technique. The middle lamella and the primary wall are easily destroyed when the fibres are mechanically treated [15, 132], and thus could be neglected. Also the S_1 layer has a rather negligible effect on the structural integrity and strength parameters of the pulp fibre when compared with the two other secondary layers due mainly to: (i) its thickness is considerably less than that of the S_2 layer; (ii) the S_1 being the outermost layer in the secondary wall and because of the large angle ($\sim 80 - 85^\circ$) of the cross fibrillar network with respect to the fibre axis.

The S_2 and S_3 layers are joined using springs whose stiffnesses (are arbitrarily defined at this stage); thus enabling the model to simulate the inter-laminar separation between the layers. Only one quarter of the fibre is modelled due to the geometrical symmetry of the problem and the boundary conditions are accordingly set. It should be noted that, in light of the discussions in the main body of the thesis regarding the significance of the various modes of loading, analysis is *only* performed for the shear mode. Needless to say, the model is perfectly applicable to any case, while appropri-

ately changing the boundary conditions for different runs. The pertinent boundary conditions for a fibre subjected to a uniform tangential displacement along with a schematic of the three-dimensional, finite-element model are depicted in Figure A.1.

As regards the type of element utilised, thin-shell, quadrilateral, laminate elements are used to model each of the two layers; and spring elements to join the layers. The geometric model and the finite element mesh are illustrated in Figure A.2.

Specific runs of the model are performed using material parameters analytically determined, by Mark and Gillis [179], for a three-layered fibre and for different fibril angles.¹ An assumption of zero in-plane shear strain is made on the basis that the angular orientation(s) of the wall of the fibre balance those of the opposite wall, since the bisector of the two angles lies along the fibre axis. Also assumed: a state of plane stress; the wall layers, plies and regions all deform under the applied stress, i.e., no slipping; each layer is orthotropically elastic and is homogeneous. The various executions indicated a similar strain-distribution pattern, characterised by high localised deformation *along* the fibre surface. In terms of magnitude, the deflection of the fibre was least at 0° fibril angle and more pronounced for larger angles. Figure A.3 shows the strain distribution for a 30° fibril angle, in which a uniform tangential displacement of 5% of the fibre length resulted in maximum strain values of slightly above 60%. (Also refer to Figure 7.2, Chapter 7.)

¹See Table 4.1, Chapter 4.

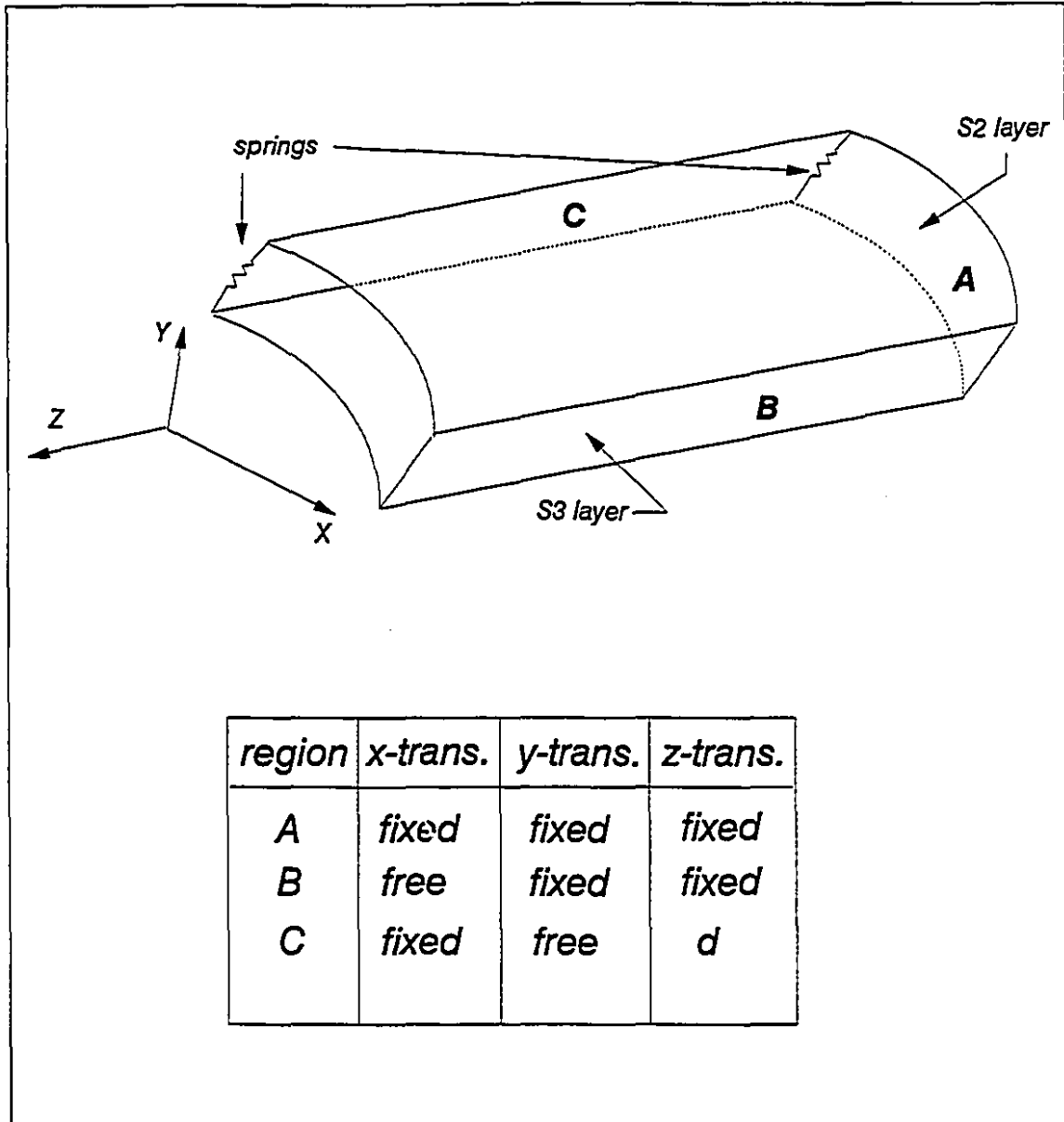


Figure A.1: Schematics of the three-dimensional, finite-element model of a single pulp fibre, along with the boundary conditions for the application of a uniform tangential displacement.

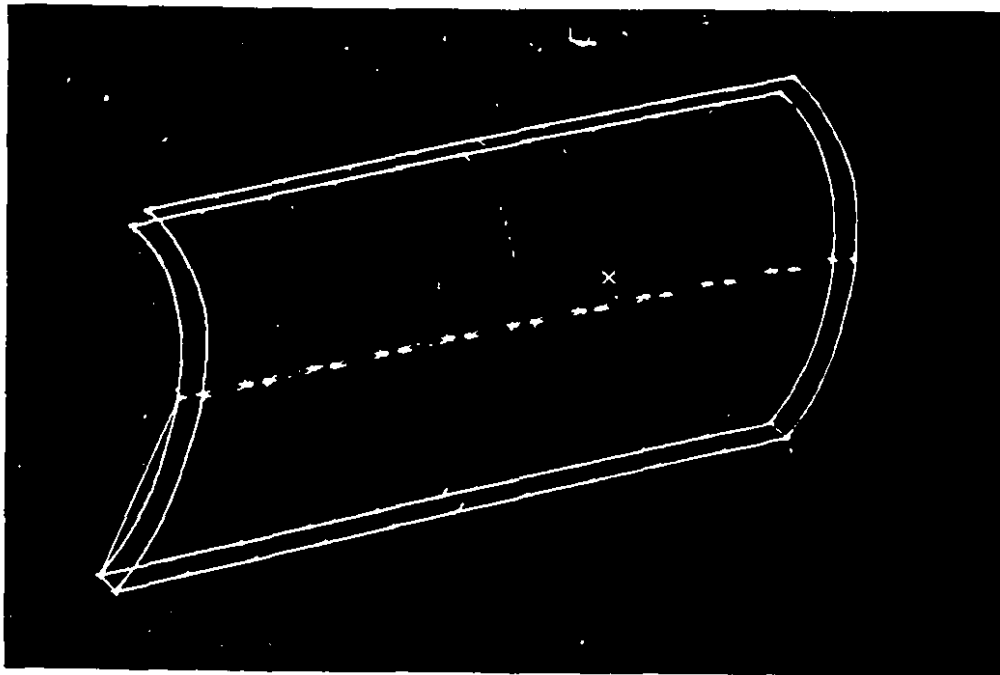


Figure A.2: Geometric model and finite-element mesh used for analysing the two-layered pulp fibre model.

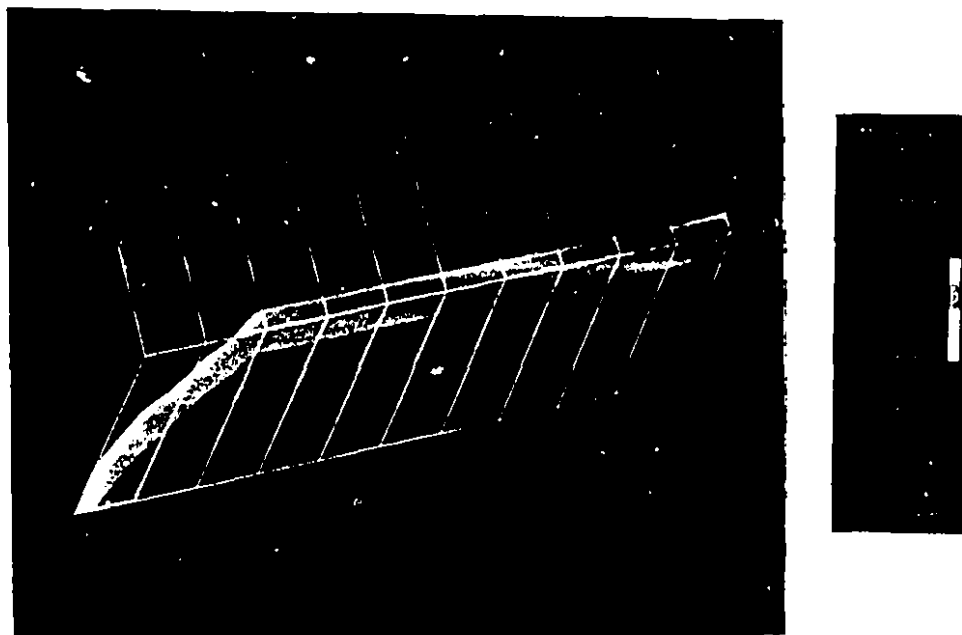


Figure A.3: Strain distribution for a pulp fibre with 30° fibril angle.

Appendix B

Calibrations

B.1 Photonic Sensor Calibration

Definition A photonic sensor¹ consists of a light source, mounted together with a photocell, a light probe and an amplifier — as diagrammatically indicated in Figure B.1. The light probe consists of a number of fibre bundles in a random arrangement. The inner bundle (see also magnification in Figure B.1(b)) transmits the light rays from the light source to the object surface. However, the outer fibre bundle collects the reflected light from the object surface and sends it to the photocell. Hence, the difference between the transmitted and reflected light intensities can be obtained from the photocell and amplified for accurate measurements. The difference of these intensities is a function of the gap size of the light probe tip and the test surface, which may be characterised by the output characteristic curve of the device, shown in Figure B.2: In actuality, the gap size is chosen so that only the linear range on the output curve is used — the region bounded by points A and B in Figure B.2.

Calibration This is necessitated by the need to use the photonic probe and sensor to calibrate the single-fibre tensiometer and stepping motor, as well as performing alignment adjustments of the loading jaws: since, in this manner, a highly precise set of measurements may be obtained.

The methodology and set-up used for calibrating the photonic probe are as follows:

¹The usual commercial name is *photonic* sensor.

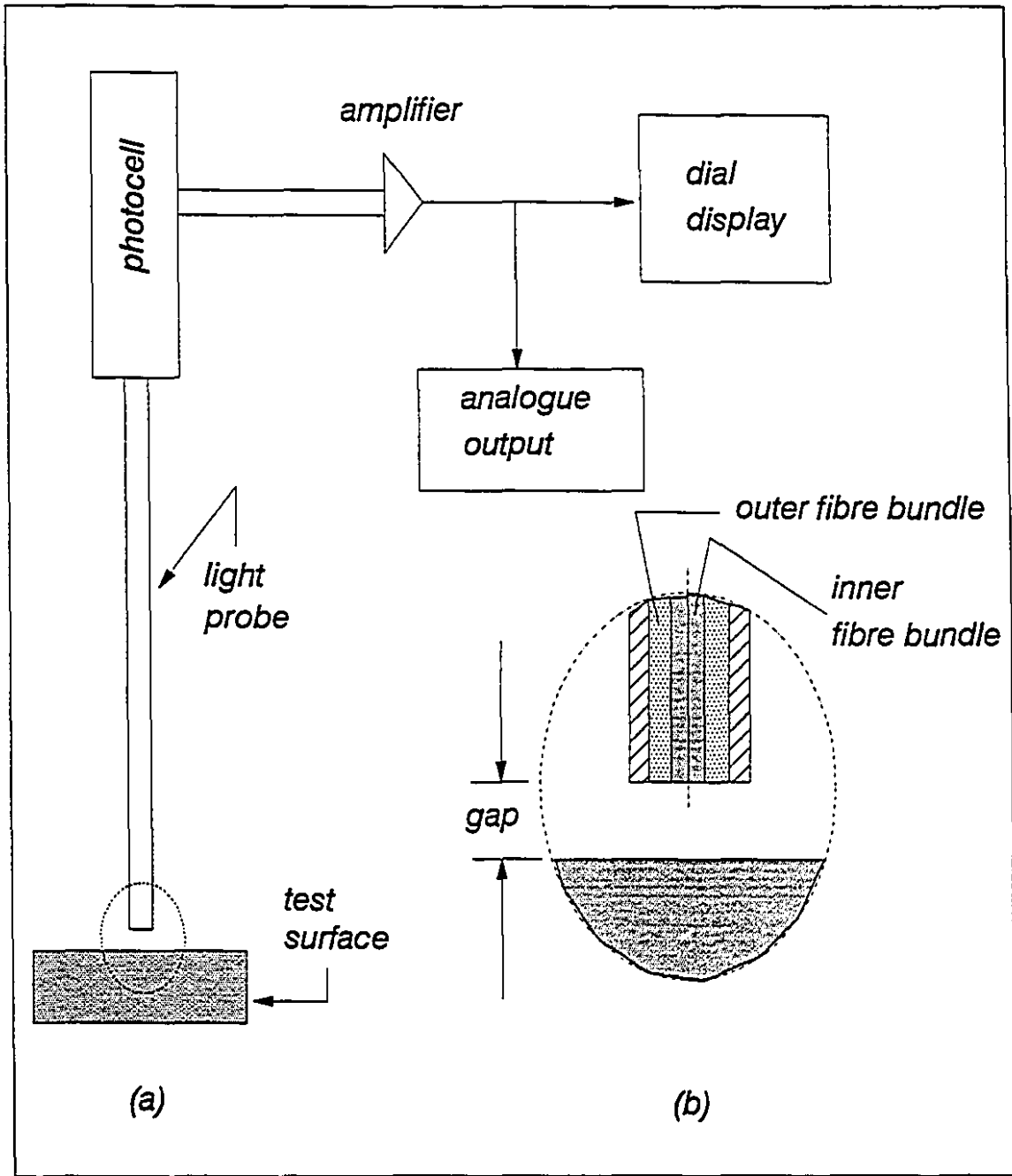


Figure B.1: Schematic of a photonic sensor.

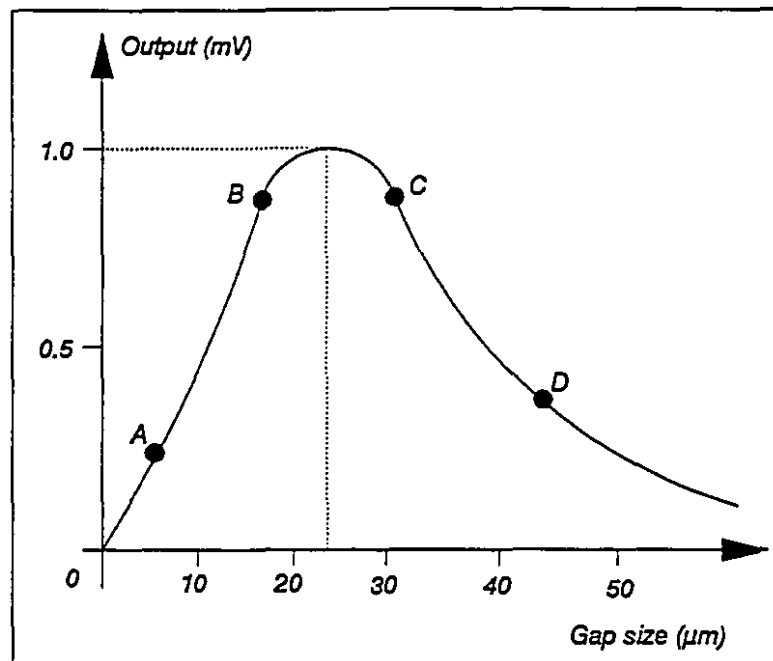


Figure B.2: Output characteristics of the photonic sensor.

• Equipment:

1. Milli-voltmeter.
2. Photonic probe and sensor.
3. A holding fixture for mounting the photonic probe so that the axis of the probe is perpendicular to the observed surface. This surface must be similar to the one observed when calibrating the tensiometer—a silver ribbon was used.
4. All components are to be placed on an optical bench to ensure that any vibrations are completely dampened.

• Procedure:

1. Turn on the sensor box and let it warm up for 15 minutes to ensure a good response.
2. Move the probe into contact with the surface to be observed, maintaining the probe perpendicular to the surface. Adjust the zero control to obtain

zero on the panel meter.

3. Carefully move the probe away from the surface until a maximum reading is obtained on the panel meter. Adjust the intensity control until full scale is obtained at this gap setting.
4. Repeat the latter two steps until proper zero and full scale values are obtained.
5. Having ensured a proper zero, apply known displacements (using a micrometer screw head) and monitor the voltage output. Record both sets of values. The way in which very small displacements are applied with accuracy is described in Figure B.3 below.

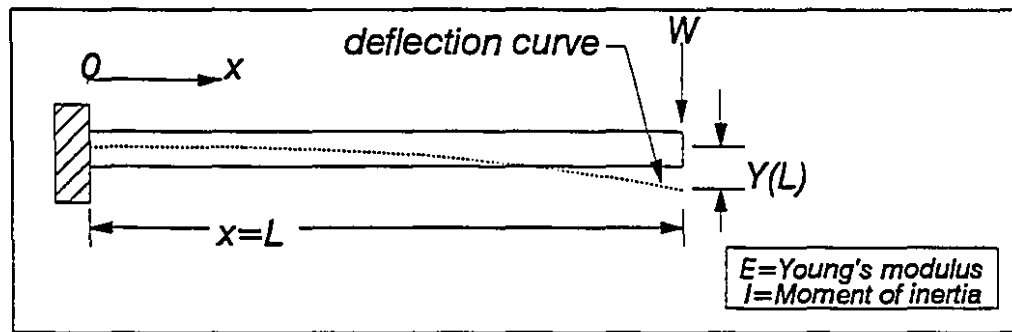


Figure B.3: Deflection of a cantilever beam.

With reference to the Figure B.3, when a displacement is applied at the end $x = L$ of the beam, a displacement is induced at x . The value of the displacement can be calculated from Euler beam theory which, for the present case, states that:

$$Y(x) = \frac{W}{EI} \left(\frac{Lx^2}{2} - \frac{x^3}{6} \right),$$

so that:

$$\frac{Y(x)}{Y(L)} = \left(\frac{Lx^2}{2} - \frac{x^3}{6} \right) \left(\frac{3}{L^3} \right) = \left(\frac{3x^2}{2L^2} - \frac{x^3}{2L^3} \right).$$

Knowing the beam length, the probe location and the end deflection, the displacement induced at position x can be calculated. For our case, the length of the beam

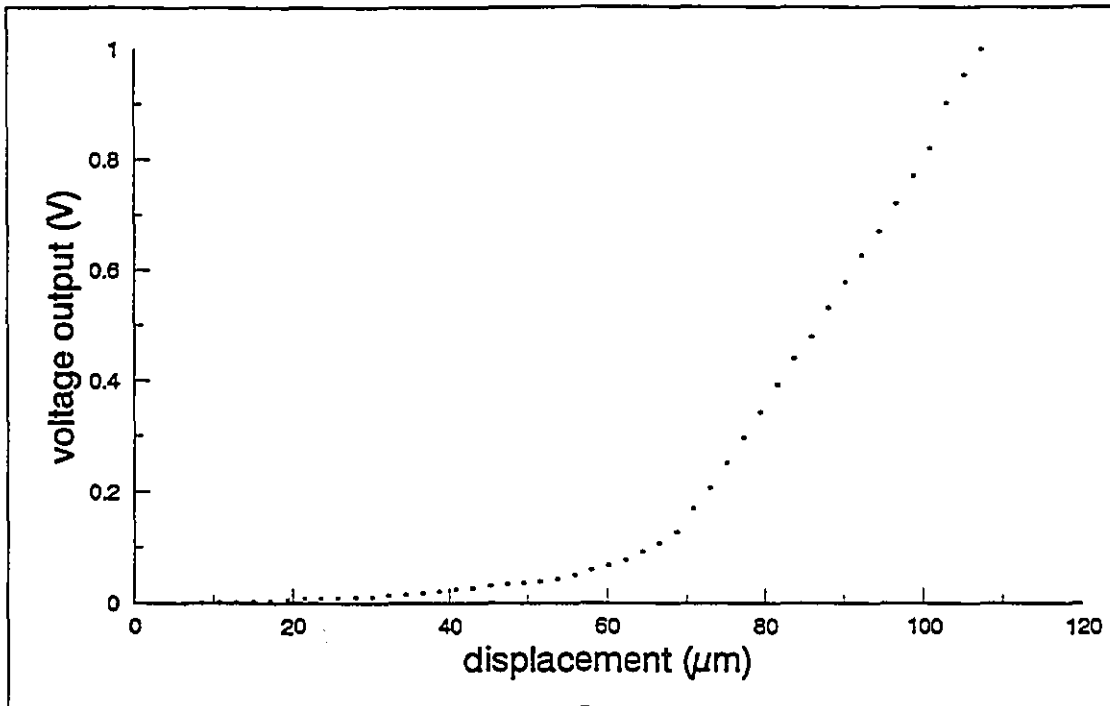


Figure B.4: Photonic sensor calibration curve.

used for calibration was 287 mm while the photonic sensor was positioned at 117 mm. Thus, the relation between $Y(X)$ and $Y(L)$ becomes:

$$Y(X) = 0.215Y(L).$$

Moreover, the end deflection was applied using a micrometer with a precision of $\pm 0.01\text{ mm}$. The resulting data are shown below in Table B.1 along with the calibration curve, Figure B.4. In the linear portion of this curve, the sensitivity² is found to be $54.6\ \mu\text{m}/\text{V}$.

²N.B. The manufacturer's calibration yielded a sensitivity of $2.07\ \mu\text{in}/\text{mV}$ ($52.578\ \mu\text{m}/\text{V}$).

Table B.1: Calibration data of photonic sensor.

$\Delta Y(L)$ (mm)	$\Delta Y(x)$ (μm)	Voltage Output (V)	$\Delta Y(L)$ (mm)	$\Delta Y(x)$ (μm)	Voltage Output (V)
0	0	-.001	.29	62.35	.078
.01	2.15	-.002	.3	64.50	.092
.02	4.3	-.002	.31	66.65	.107
.03	6.45	0	.32	68.80	.128
.04	8.6	.001	.33	70.95	.170
.05	10.75	.001	.34	73.10	.207
.06	12.9	.002	.35	75.25	.251
.07	15.05	.003	.36	77.40	.296
.08	17.2	.004	.37	79.55	.342
.09	19.35	.006	.38	81.70	.392
.1	21.5	.007	.39	83.85	.439
.11	23.65	.008	.4	86.00	.478
.12	25.8	.009	.41	88.15	.531
.13	27.95	.010	.42	90.30	.577
.14	30.1	.011	.43	92.45	.626
.15	32.25	.013	.44	94.60	.668
.16	34.40	.015	.45	96.75	.72
.17	36.55	.018	.46	98.90	.77
.18	38.70	.021	.47	101.05	.820
.19	40.85	.025	.48	103.20	.902
.2	43.0	.027	.49	105.35	.953
.21	45.15	.031	.5	107.50	.998
.22	47.30	.035	.51	109.65	1.055
.23	49.45	.036	.52	111.80	1.108
.24	51.60	.039	.53	113.95	1.145
.25	53.75	.043	.54	116.10	1.190
.26	55.90	.050	.55	118.25	1.231
.27	58.05	.059	.56	120.40	1.278
.28	60.20	.068	.57	122.55	1.307

B.2 Single-Fibre Tensiometer and Stepping Motor Calibration

Having performed the photonic sensor calibration, a precise calibration of the tensiometer and the stepping motor may now be carried out. Two modes of cycling were calibrated; viz., the *automatic* and the *step-by-step* cycling modes. For both calibrations, the set-up was identical and included the following:

- the fixed jaw was replaced by the photonic probe which is in turn connected to the photonic sensor,
- the moving jaw was cylindrical whose surface was the same as that used in the photonic sensor and probe calibration, namely, silver; and
- all components were carefully placed on an optical bench.

It is worth mentioning that meticulous care need be exercised at every stage of the calibration, particularly when adjusting the zero on the photonic sensor. Below is a detailed discussion of the results thus obtained.

B.2.1 Automatic-Cycling Mode

The automatic cycling mode was performed by instructing the $\mu\text{mac-5000}$ to activate the oscillator of the motor's driver for a specified time interval. A program in $\mu\text{mac-BASIC}$ was written for this purpose—refer to Figure B.5. Upon repeating this procedure for a suitable time range and simultaneously monitoring the voltage output on a chart recorder, the desired results may be obtained.

The automatic mode calibration was performed for step rates = 3–9. For step rates lower or higher than the aforementioned, obvious stalling of the stepping motor was detected. The complete results thus obtained are shown in Tables B.2 and B.3. Furthermore, the calibration was sporadically repeated for some time intervals and the results agreed well with the previous ones (% error = 2–5%). The highest sensitivity obtained was $13.1 \mu\text{m/s}$ for step rate = 3—refer to Figure B.6. As the step rate increased the sensitivity decreased; the lowest being $4.54 \mu\text{m/s}$ for step rate = 9.

```
1 REM This is a simple routine to calibrate the motor and
2 REM tensiometer in the AUTOMATIC mode.
3 REM ***** 8 June, 1992.
4 REM N.B.: Place the motor driver in automatic, tension
5 REM and cyclic. *****
10 REAL TIME
12 LET DOT(1,0,0)=1
16 INPUT "input wait time in seconds: " TIME
17 LET DOT(1,0,0)=0
30 LET DOT(1,1,1)=1
40 WAIT(TIME)
50 LET DOT(1,1,1)=0
55 WAIT(TIME)
80 LET DOT(1,0,0)=1
85 PRINT "finished! "
90 STOP
```

Figure B.5: Automatic-mode calibration program.

Table B.2: Stepping motor calibration — automatic mode.

	step rate=2		step rate=3	
Wait Time (sec)	Voltage Output (V)	Displacement (μm)	Voltage Output (V)	Displacement (μm)
1.0	0.252	13.759	0.130	7.098
1.2	0.291	15.889	0.160	8.7336
1.4	0.341	18.619	0.200	10.920
1.6	0.366	19.984	0.240	13.104
1.8	0.409	22.331	0.290	15.334
2.0	0.477	26.044	0.333	18.182
2.2	0.533	29.102	0.435	23.751
2.4	0.598	32.651	0.467	25.498
2.6	0.607	33.142	0.510	27.846
2.8	0.668	36.473	0.551	30.085
3.0	0.643	35.108	0.600	32.760
3.5	0.724	39.530	0.717	39.148
4.0	0.812	44.362	0.800	43.680
	step rate=4		step rate=5	
Wait Time (sec)	Voltage Output (V)	Displacement (μm)	Voltage Output (V)	Displacement (μm)
1.0	0.132	7.207	0.120	6.552
1.2	0.166	9.064	0.155	8.463
1.4	0.198	10.811	0.177	9.664
1.6	0.252	13.759	0.203	11.084
1.8	0.282	15.397	0.230	12.558
2.0	0.310	16.926	0.255	13.923
2.2	0.350	19.110	0.282	15.397
2.4	0.383	20.912	0.308	16.817
2.6	0.413	22.550	0.341	18.619
2.8	0.453	24.734	0.359	19.601
3.0	0.497	27.136	0.392	21.403
3.5	0.570	31.122	0.462	25.225
4.0	0.642	35.053	0.551	30.085

Table B.3: Stepping motor calibration — automatic mode (Cont'd.).

Wait Time (sec)	step rate=6		step rate=7	
	Voltage Output (V)	Displacement (μm)	Voltage Output (V)	Displacement (μm)
1.0	0.080	4.368	0.070	3.822
1.2	0.105	5.733	0.096	5.242
1.4	0.131	7.153	0.118	6.443
1.6	0.152	8.299	0.137	7.480
1.8	0.184	10.046	0.165	9.009
2.0	0.203	11.084	0.180	9.828
2.2	0.228	12.449	0.206	11.248
2.4	0.251	13.705	0.237	12.940
2.6	0.280	15.288	0.250	13.650
2.8	0.298	16.271	0.275	15.015
3.0	0.319	17.417	0.292	15.943
3.5	0.380	20.748	0.342	18.673
4.0	0.438	23.915	0.382	20.857
Wait Time (sec)	step rate=8		step rate=9	
	Voltage Output (V)	Displacement (μm)	Voltage Output (V)	Displacement (μm)
1.0	0.062	3.385	0.041	2.239
1.2	0.083	4.532	0.056	3.058
1.4	0.102	5.569	0.070	3.822
1.6	0.120	6.552	0.090	4.914
1.8	0.140	7.644	0.106	5.788
2.0	0.160	8.736	0.132	7.207
2.2	0.186	10.156	0.144	7.862
2.4	0.197	10.756	0.162	8.845
2.6	0.222	12.121	0.173	9.446
2.8	0.245	13.377	0.188	10.265
3.0	0.261	14.251	0.203	11.084
3.5	0.305	16.653	0.245	13.377
4.0	0.343	18.728	0.299	16.325

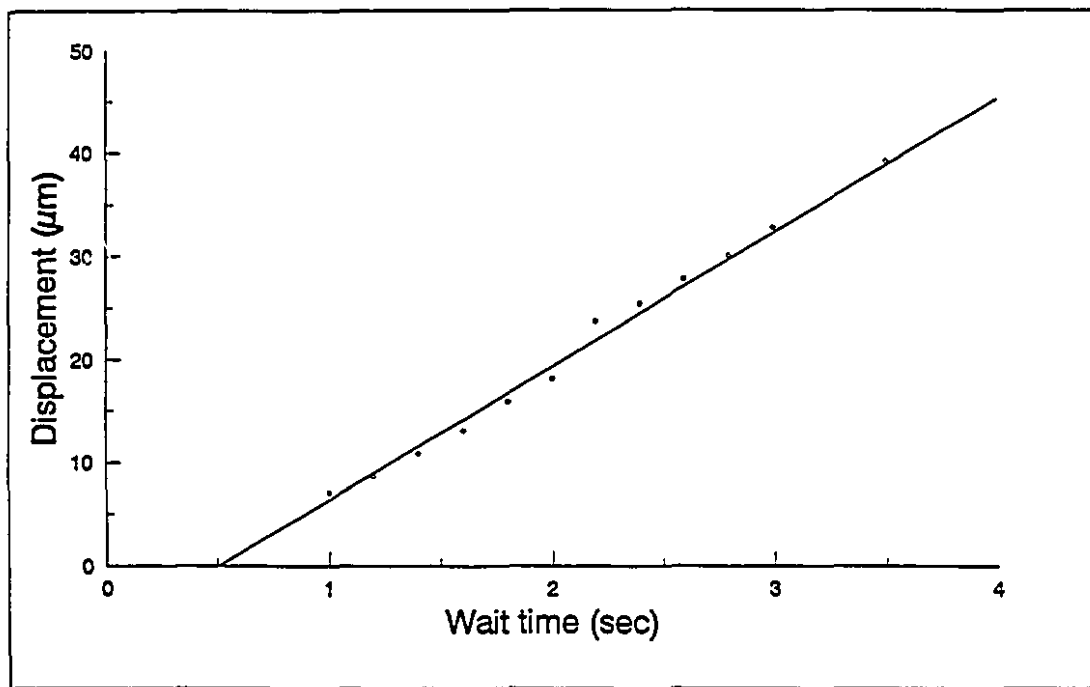


Figure B.6: Displacement versus wait-time plot for step rate=3 (automatic mode).

B.2.2 Step-by-step Cycling Mode

Under this category of the stepping motor calibration procedure a different program (see Figure B.7) was written in which the oscillator of the motor's driver is bypassed, however the latter was instructed to move 50 steps at a time. As before, the photonic sensor's outputs were monitored on a chart recorder and the comprehensive data thus obtained were recorded and duly analysed.

Here, the calibration was performed for step rate = 3 on two separate occasions and the sensitivity of the motor was found to be 3.85 and 4.2 μm per 100 steps respectively; thus giving an average of 4 μm per 100 steps. The entire results for both runs are depicted in Tables B.4 and B.5 accompanied with the respective displacement versus number of steps plots—refer to Figure B.8. Moreover, the calibration for the step-by-step mode was carried out at different step rates (5 & 7) to ensure compatible results and, indeed, they compared well.

```
1 REM This is a simple routine to calibrate the motor and
2 REM tensiometer in the STEP-BY-STEP mode. *****
3 REM ***** 8 June, 1992.
4 REM N.B.: Place motor driver in manual, tension and
5 REM unidirectional. *****
7 INTEGER N,I
9 LET DOT(1,0,0)=1
10 INPUT " input the number of steps " N
20 LET DOT(1,0,0)=1
30 LET DOT(1,1,1)=1
40 FOR I=1 TO N
50 LET DOT(1,3,3)=1
55 WAIT(3)
60 LET DOT(1,3,3)=0
65 WAIT(3)
70 NEXT
80 REM LET DOT(1,1,1)=0
90 REM FOR L=1 TO N
95 REM LET DOT(1,3,3)=1
97 REM LET DOT(1,3,3)=0
100 REM NEXT
105 PRINT "finished! "
110 STOP
```

Figure B.7: Step-by-step mode calibration program.

Table B.4: Stepping Motor Calibration — step-by-step mode (step rate=3) [1st run].

No. of Steps	Voltage Output (V)	ΔV (V)(10 ⁻²)	Δx (μm)	x (μm)
0	0	0	0	0
50	0.032	3.2	1.7472	1.7472
100	0.071	3.9	2.1294	3.8766
150	0.100	2.9	1.5834	5.4600
200	0.121	2.1	1.1466	6.6066
250	0.151	3.0	1.6380	8.2446
300	0.172	2.1	1.1466	9.3912
350	0.189	1.7	0.9282	10.3194
400	0.208	1.9	1.0374	11.3568
450	0.239	3.1	1.6926	13.0494
500	0.253	1.4	0.7644	13.8138
550	0.278	2.5	1.3650	15.1788
600	0.365	8.7	4.7502	19.929
650	0.388	2.3	1.2558	21.1848
700	0.418	3.0	1.6380	22.8228
750	0.438	2.0	1.0920	23.9144
800	0.5075	6.95	3.7947	27.7095
850	0.570	6.25	3.4125	31.1220
900	0.5725	0.25	0.1365	31.2585
950	0.601	2.85	1.5561	32.8164
1000	0.643	4.2	2.2932	35.1078
1050	0.645	0.2	0.1092	35.2170
1100	0.669	2.4	1.3104	36.5274
1150	0.703	3.4	1.8564	38.3828
1200	0.746	4.3	2.3478	40.7316
1250	0.925	17.9	9.7734	50.5050
1300	0.9375	1.25	0.6825	51.1875
1350	0.990	5.25	2.8665	54.0540
1400	1.011	2.1	1.1466	55.2006
1450	1.0775	6.65	3.6309	58.8315
1500	1.120	4.25	2.3205	61.1520

Table B.5: Stepping Motor Calibration — step-by-step mode (step rate=3) [2nd run].

No. of Steps	Voltage Output (V)	ΔV (V)(10 ⁻²)	Δx (μm)	x (μm)
0	0	0	0	0
50	0.043	4.3	2.3478	2.3478
100	0.077	3.4	1.8564	4.2042
150	0.101	2.4	1.3104	5.5146
200	0.124	2.3	1.2558	6.7704
250	0.134	1.0	0.546	7.3164
300	0.153	1.9	1.0374	8.3538
350	0.198	4.5	2.4570	10.8108
400	0.249	5.1	2.7846	13.5954
450	0.268	1.9	1.0374	14.6328
500	0.354	8.6	4.6956	19.3284
550	0.367	1.3	0.7398	20.0382
600	0.460	9.3	5.0778	25.1160
650	0.500	4.0	2.1840	27.3000
700	0.530	3.0	1.6380	28.9380
750	0.546	1.6	0.8736	29.8116
800	0.561	1.5	0.8190	30.6306
850	0.589	2.8	1.5288	32.1594
900	0.606	1.7	0.9282	33.0876
950	0.652	4.6	2.5116	35.5992
1000	0.832	18.0	9.8280	45.4272
1050	0.842	1.0	0.546	45.9732
1100	0.880	3.8	2.0748	48.0480
1150	0.910	3.0	1.6380	49.6860
1200	0.913	0.3	0.1638	49.8498
1250	0.947	3.4	1.8564	51.7062
1300	0.980	3.3	1.8018	53.5080
1350	1.007	2.7	1.4742	54.9822
1400	1.025	1.8	0.9828	55.9650
1450	1.042	1.7	0.9282	56.8932
1500	1.078	3.6	1.9656	58.8588

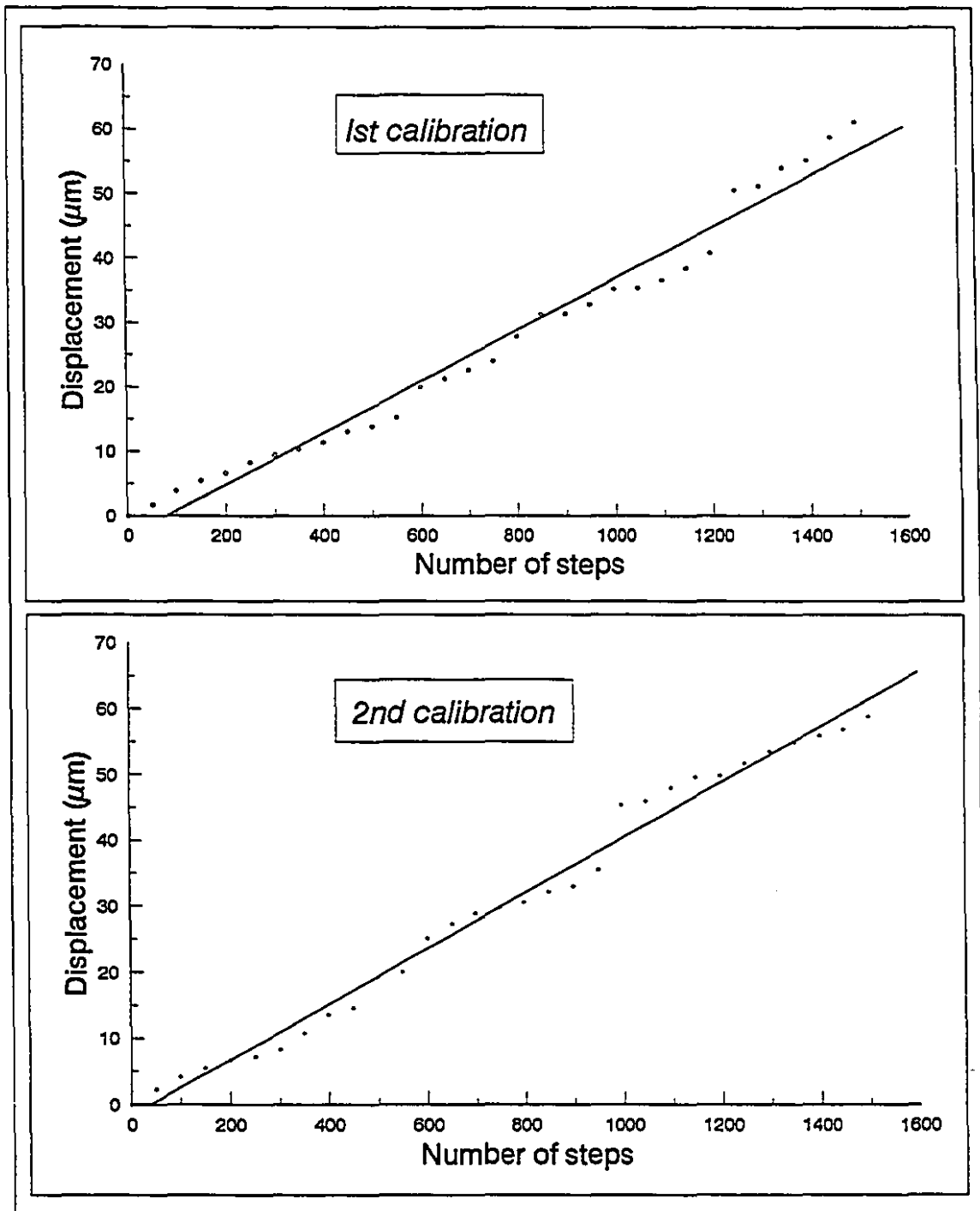


Figure B.8: Displacement versus number of steps plots, step rate=3 (step-by-step mode).

B.3 Load-Cell Calibration

The calibration of the load cell was carried out by comparing the electrical output of the transducer to a known static weight. The data obtained is found in Table B.6, while the resulting graph is shown in Figure B.9.

The calibration of the load cell is obtained from the slope of the linear curve of Figure B.9. The sensitivity of the load cell is found to be 7.52 mV/lb when the signal is fed into a 100x amplifier located in the load cell power supply.

Table B.6: Calibration of the ± 1 -lb load cell.

Weight (g)	100x amplifier Output (V)	Weight (g)	100x amplifier Output (V)
0	-0.524	92.7	-2.09
22.7	-0.906	102.7	-2.26
27.7	-0.994	112.7	-2.42
32.7	-1.080	122.7	-2.54
37.7	-1.169	172.7	-3.40
42.7	-1.255	222.7	-4.21
47.7	-1.344	272.7	-5.02
52.7	-1.430	322.7	-5.84
62.7	-1.600	372.7	-6.64
72.7	-1.768	422.7	-7.45
82.7	-1.930	452.7	-7.94

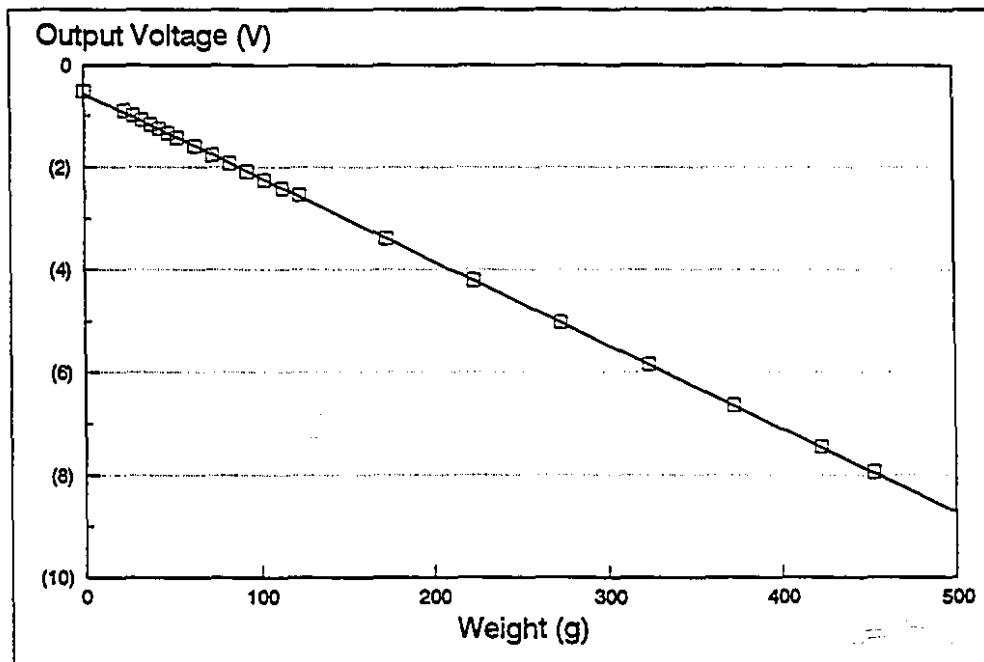


Figure B.9: Load cell calibration under static load.

B.4 Vertical displacement Calibration of the Tensiometer and Support/Stage Set-up

As enunciated in Chapter 7, when performing *in situ* confocal scanning of the fatigued fibres, the stepping stage of the CLSM is not utilised owing to the particular characteristics of the set-up; however, the support/stage mechanism is used to perform the function of a stepping stage and as such the vertical movement of the tensiometer with respect to the former need be precisely known.

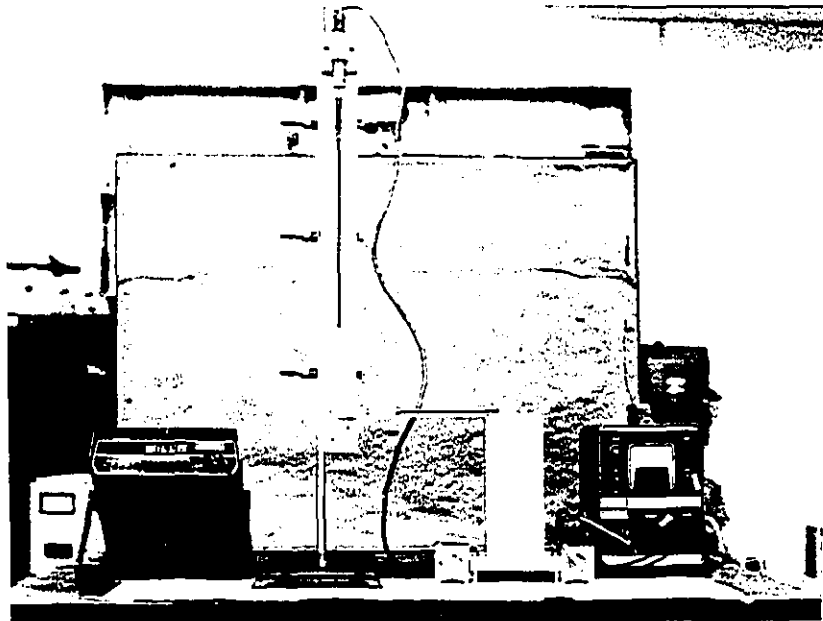


Figure B.10: Pictorial representation of the vertical displacement calibration of the tensiometer-support set-up.

The set-up, pictorially depicted in Figure B.10, principally comprises a photonic probe and a sensor box that are used in a manner similar to what has been canvassed hereinbefore. The calibration is performed for the locality where the loading jaws are situated and the surfaces are prepared exactly as detailed at the beginning of this appendix. The calibration was performed on two separate occasions, with the data presented in Table B.7, and the engendered actual versus applied displacement curves in Figure B.11: the slopes of the latter curves produce a sense of the actual displacement to every applied displacement. The two plots yield sensitivities of 0.836

μm and $0.933 \mu\text{m}$ for each applied μm , giving an average of $0.8845 \mu\text{m}$.

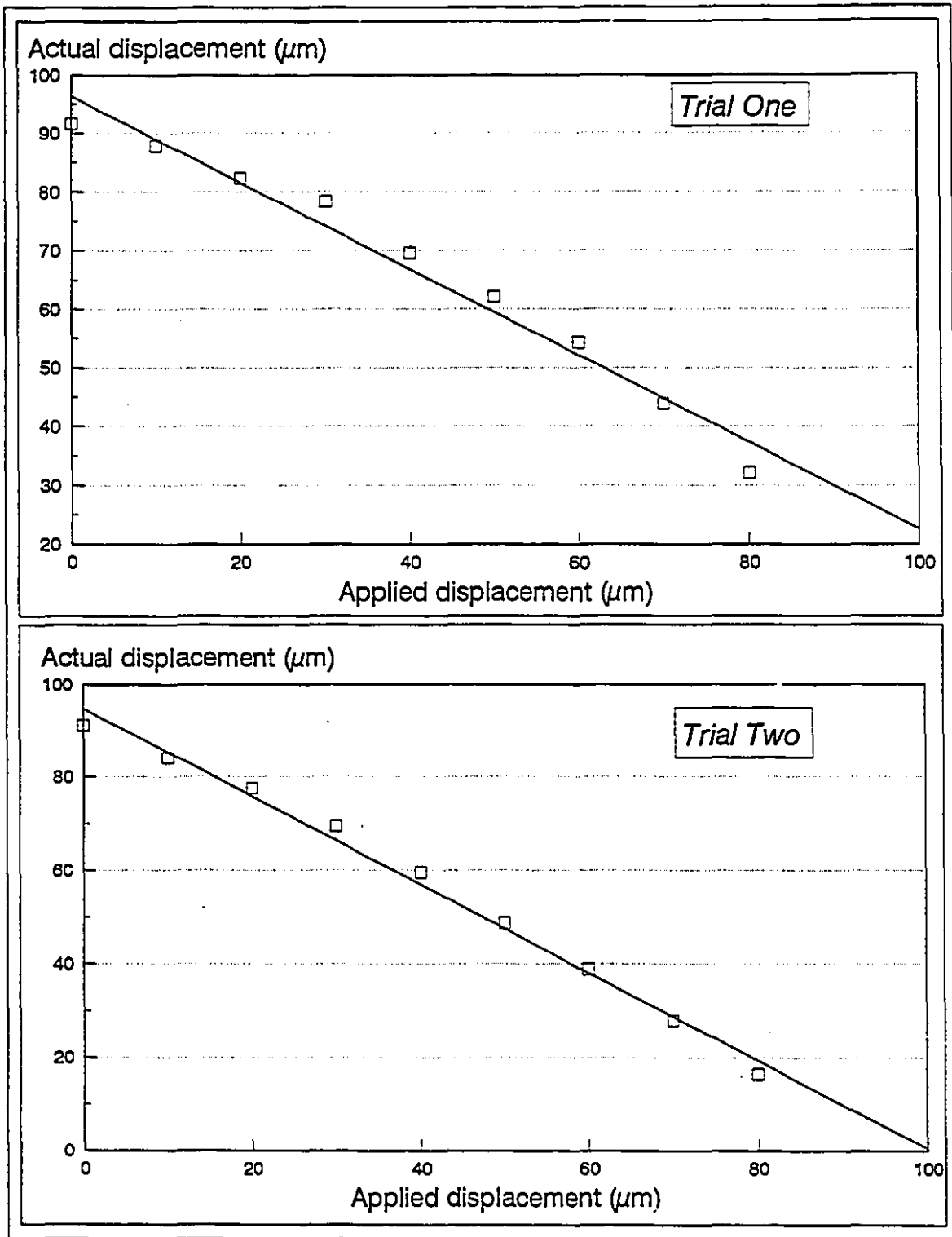


Figure B.11: Plots of vertical displacement calibration of the tensiometer-support set-up.

Table B.7: Data for the vertical displacement of the tensiometer-support set-up.

Applied Displ. (μm)	Trial One		Trial Two	
	Voltage Output (V)	Actual Displ.† (μm)	Voltage Output (V)	Actual Displ.† (μm)
0	1.687	91.6188	1.667	91.0182
10	1.609	87.8514	1.540	84.0840
20	1.507	82.2822	1.420	77.5320
30	1.434	78.2964	1.270	69.3420
40	1.275	69.6150	1.090	59.5140
50	1.137	62.0802	0.893	48.7578
60	0.995	54.3270	0.712	38.8752
70	0.803	43.8438	0.510	27.8460
80	0.587	32.0502	0.300	16.3800

† Actual displacement = applied displacement \times 54.6 $\mu\text{m}/\text{V}$.

Appendix C

Illustrations and Schemas

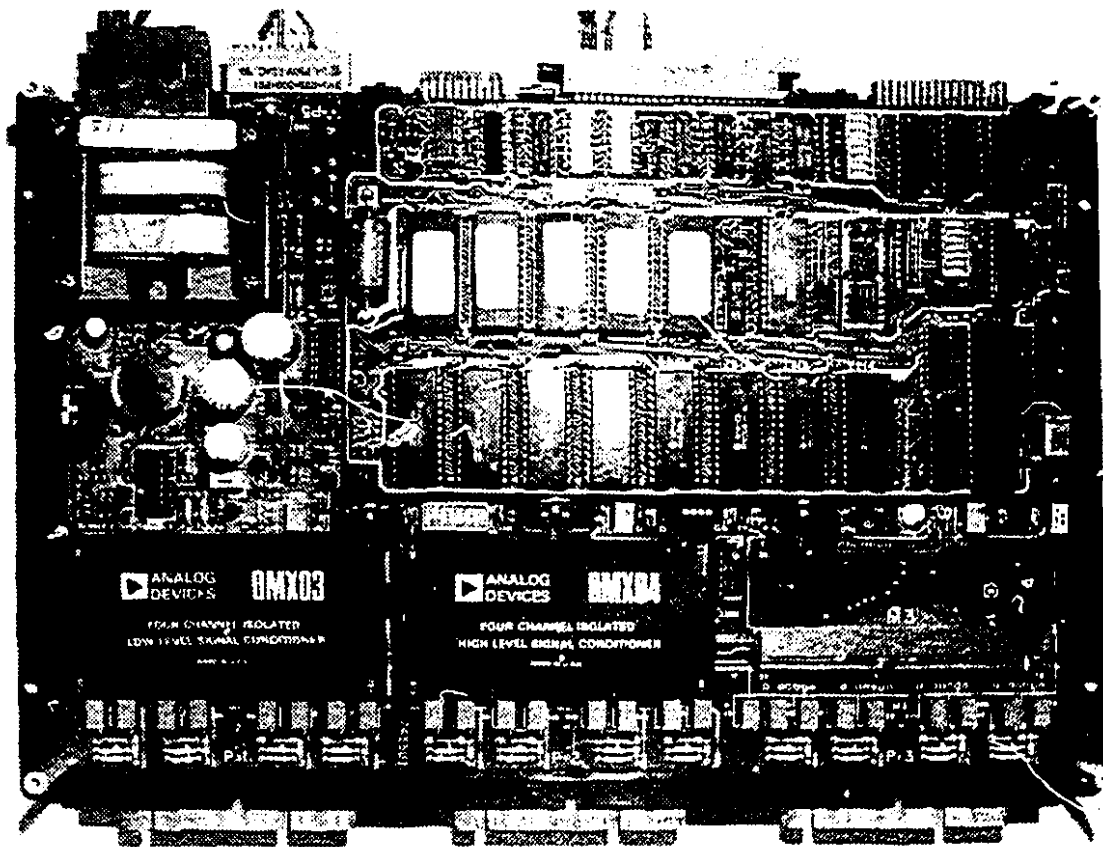


Figure C.1: Photographic depiction of the interior of the μ mac-5000 microcomputer.

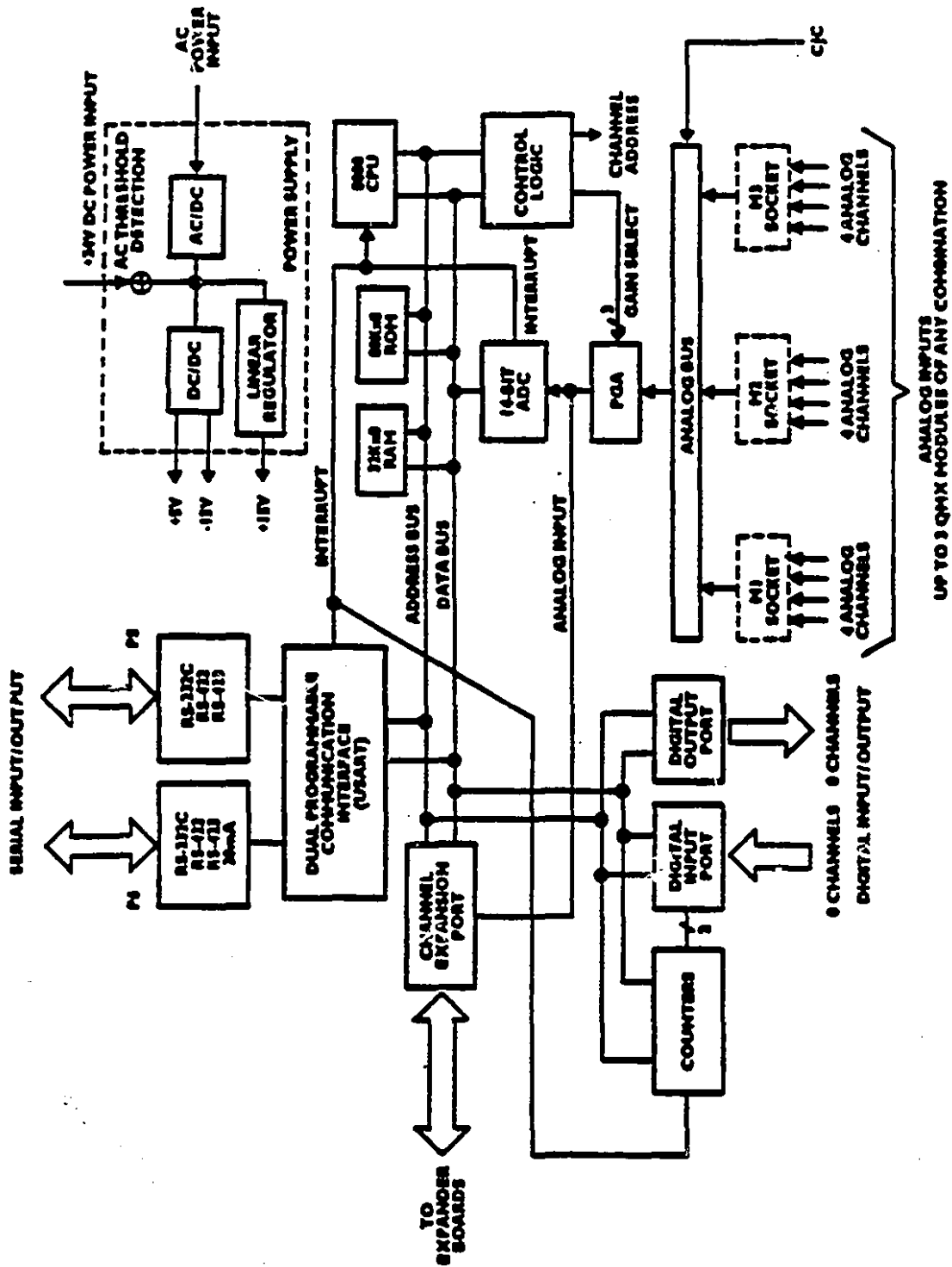


Figure C.2: Block diagram of the μ mac-5000 microcomputer.

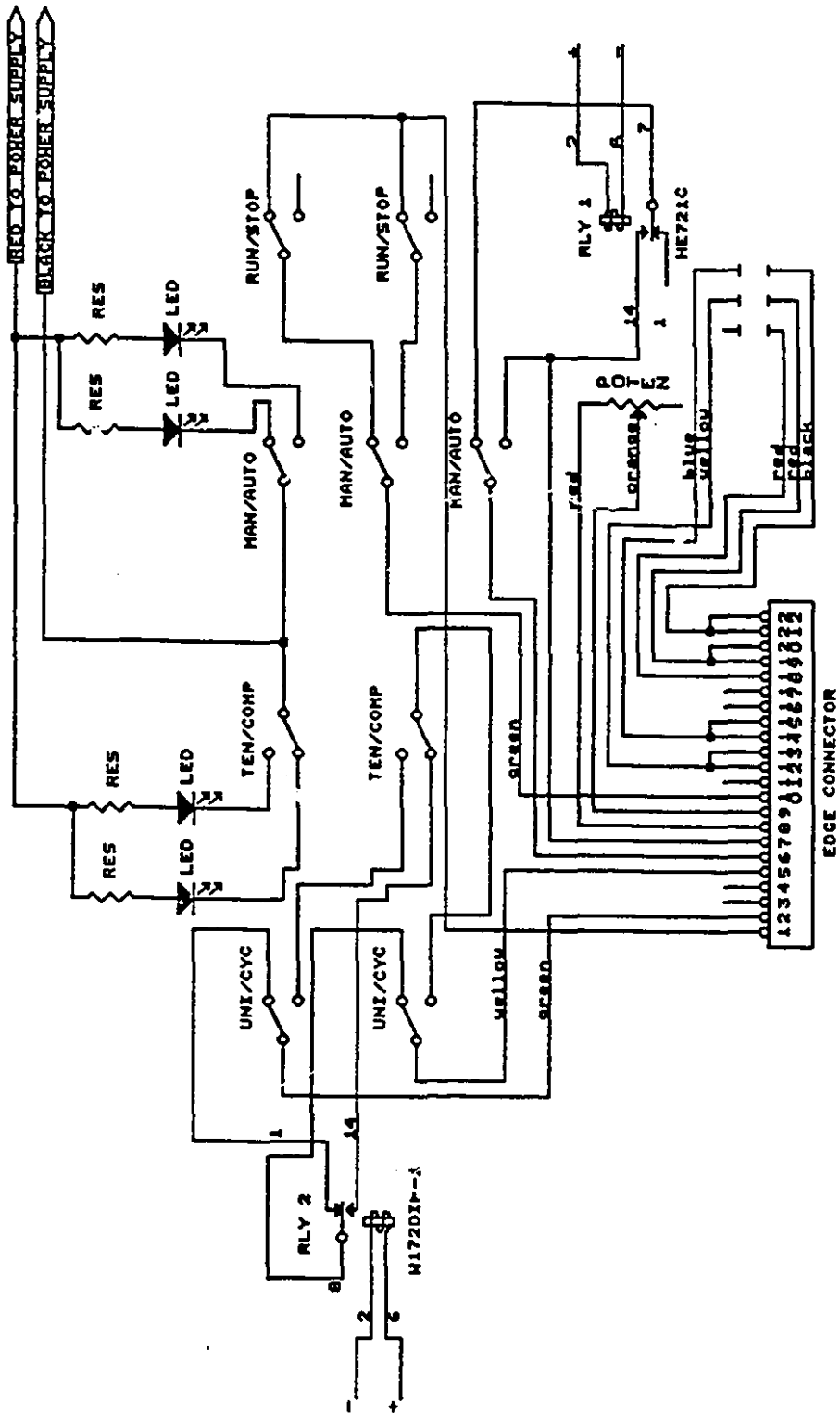


Figure C.3: Schematic representation of the motor driver.

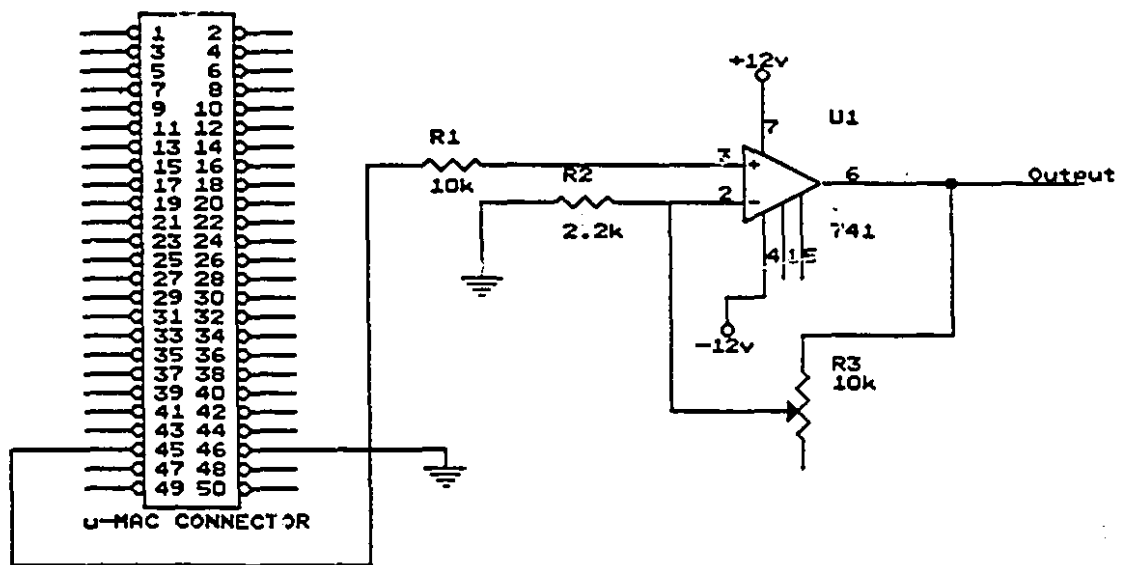


Figure C.4: A schema of the 2x amplifier.

Appendix D

Fatigue-Testing Algorithm

The computer algorithm below used to operate and control the entire running of the fatigue-testing procedure is written in μ mac-BASIC, a real time language¹. Main routines in the structure of the algorithm are explained via comment statements; throughout the whole body of the program, the steps are rather easy to follow if one is made cognisant of preceding, relevant discussions in Chapters 7 and 8.

D.1 Program

```
6000 REM *****
6001 REM *****
6002 REM ** **
6003 REM ** FATIGUE-TESTING ALGORITHM **
6004 REM ** (Constant-amplitude, displacement-controlled) **
6005 REM ** **
6006 REM ** updated 14th, August, 1992. **
6007 REM ** **
6008 REM *****
6009 REM *****
6010 REM
```

¹Refer to details discussed in Sections 7.5 and 8.1 of Chapters 7 and 8, respectively.

```
6011 REM
6012 REM ***** Variable Dictionary *****
6013 REM RESUME, SURE, MODE = strings in INTERRUPT procedure
6014 REM CHOICE, FULL, RESPONSE, SAY, ANSWER, MORE -cont'd.-
6015 REM OPTION = strings in MAIN program
6016 REM X, Z, L, I, P, A, INDEX, INDICE = variables
6017 REM CYCLE = number of cycles performed
6018 REM W = limit cycle in automatic mode
6019 REM M = W/50 = loop limit (automatic mode)
6020 REM O = integer remainder of W/50
6021 REM MICRON = peak-to-peak displ. of applicator (aut. mode)
6022 REM TICAL = calibration variable = 0.076336 (aut. mode)
6023 REM TEMPS = waiting time = MICRON x TICAL
6024 REM LIM = cycle limit (ste-by-step mode)
6025 REM CALIB = 100 steps per 1 um = 25 (stepping motor calib.
6026 REM in step-by-step mode)
6027 REM GAP = gap input for positioning the applicator at start
6028 REM STEP = GAP x CALIB (positioning of applicator)
6029 REM REALGAP = STEP / CALIB
6030 REM PEAK = peak-to-peak displ. of applicator in microns
6031 REM (step-by-step mode)
6032 REM AUTOSTEP = PEAK x CALIB
6033 REM REALPEAK = AUTOSTEP / CALIB
6034 REM TEMPO = initialiser (used in step-by-step cycling)
6035 REM *****
6036 REM
6037 REM The routine below permits interruption at any moment.
6038 REM
7000 interrupt procedure handler
7002 string resume, sure, mode
7003 REM Turn oscillator off
```

```
7005 let dot(1,0,0)=1
7009 REM
7010 REM *****
7020 REM ** WAITING PROCEDURE **
7030 REM *****
7033 REM
7037 REM This procedure enables the program to be stopped at any
7039 REM time during execution, without losing any information.
7042 REM To activate the procedure, one needs to press the
7044 REM percentage sign.
7046 REM
7048 REM
7050 on intr goto 7060, 7060, 7060, 7060, 7060, 7065, 7060
7060 exit
7065 let dot(1,0,0)=1
7070 Print " In which mode were you cycling : "
7080 Print " a) automatic "
7090 Print " b) step by step "
7100 Print " c) slower rate "
7110 Print " "
7120 Input " The cycling mode is : " mode
7125 Print " "
7130 If Follow = "a" then 7140 else 7160
7140 Print " The cycling mode is automatic "
7150 Goto 7220
7160 If Follow = "b" then 7170 else 7190
7170 Print " The cycling mode is step by step "
7180 Goto 7220
7190 If Follow = "c" then 7200 else 7070
7200 Print " The cycling mode is a slower rate "
7210 Print " "
```

```
7220 Input " Are you sure ? " sure
7230 If Zut = "y" then 7250 else 7240
7240 If Zut = "n" then 7070 else 7125
7250 Input " Waiting, to resume test press c : " resume
7260 If Suite = "c" then 7270 else 7250
7270 If Follow = "a" then 7280 else 7300
7279 REM Turn oscillator on
7280 Let Dot(1,0,0)=0
7290 Exit
7300 If Follow = "b" then 7320 else 7310
7310 If Follow = "c" then 7320
7311 REM Oscillator off
7320 Let Dot(1,0,0)=1
7330 Exit
main
5 REM ***** MAIN PROGRAM *****
6 REM
10 INTEGER CYCLE, STEP, X, W, Z, L, M, O, P, A, AUTOSTEP, LIM
20 INTEGER INDEX, INDICE
30 REAL MICRON, TEMPS, TICAL, GAP, CALIB, REALGAP, PEAK
40 REAL REALPEAK, TEMPO
50 STRING CHOICE, FULL, RESPONSE, SAY, ANSWER
60 STRING MORE, OPTION
61 REM
70 REM This dot command is to make sure that the driver is
80 REM off at the beginning of the testing and is turned on
90 REM only by the program.
91 REM
99 REM Oscillator off
100 LET DOT(1,0,0) = 1
110 REM *****
```

```
120 REM ** CYCLIC-DISPLACEMENT, FATIGUE-TESTING PROGRAM **
130 REM *****
131 REM
136 REM
138 REM These statements enable the interrupt procedure.
139 REM
140 SETINT(7,37)
150 ON INTERRUPT HANDLER
151 REM
160 PRINT CHR$(24)
170 PRINT "CYCLIC DISPLACEMENT FATIGUE TESTING EXPERIMENT"
180 PRINT "_____ "
190 PRINT
200 PRINT " Menu : 1) constant displacement cycling "
210 PRINT " 2) positioning "
230 PRINT " 4) exit "
240 PRINT
260 PRINT
270 INPUT "type 1/2/4 " CHOICE
271 REM
272 REM ** These statements branch the program to the right ***
273 REM ** routine depending on the programmer's choice. *****
274 REM
280 IF ASC(CHOICE) < 49 OR ASC(CHOICE) > 52 THEN GOTO 160
290 ON VAL(CHOICE) GOSUB 390,1680
340 IF CHOICE <> "4" THEN GOTO 160
341 REM
350 LET DOT(1,0,0)=1
360 STOP
370 REM
380 REM
```

```
390 REM *****
400 REM ** CONSTANT-DISPLACEMENT ROUTINE **
410 REM *****
420 REM
422 REM This routine permits the specimen to be cycled at a
423 REM given peak-to-peak displacement, in one of 3 different
424 REM modes. Most of the parameters are chosen by the user.
425 REM
426 REM Cycling starts at the closest position, i.e., it starts in
427 REM tension. The cycling also ends at the closest position.
428 REM
430 REM Initialisation of the calibration variable (automatic mode):
440 REM Sensitivity = 13.1 micron/sec, or 0.076336 sec/micron.
450 REM
460 LET TICAL = 0.076336
470 REM
480 PRINT CHR$(24)
490 PRINT " CONSTANT DISPLACEMENT CYCLING TEST "
500 PRINT " _____ "
510 PRINT
520 PRINT " Menu : 1) automatic cycling "
530 PRINT " 2) step-by-step cycling "
540 PRINT " 3) slower rate cycling"
550 PRINT " "
560 INPUT "Choose the option : " OPTION
561 REM
562 REM These statements branch the program to the right
563 REM subroutine depending on the cycling mode chosen.
564 REM
570 IF ASC(OPTION) < 49 OR ASC(OPTION) > 51 THEN GOTO 510
580 ON VAL(OPTION) GOSUB 590, 1180, 1230
```

```
581 REM
582 REM Automatic cycling routine
583 REM _____
584 REM
585 REM This routine makes the motor step at its fastest
586 REM possible speed without stalling.
587 REM The internal oscillator of the driver is used.
588 REM
590 PRINT " Automatic Cycling "
600 PRINT " "
610 PRINT " Position the driver in Auto, Tension &: Cyclic "
620 PRINT
630 PRINT
640 INPUT "Enter the peak-to-peak displacement in microns : " MICRON
650 TEMPS = MICRON * TICAL
660 PRINT " "
670 PRINT "waiting time = ", TEMPS
680 PRINT " "
690 CYCLE = 0
700 INPUT "what is the cycle limit (in 50's) ? " W
710 PRINT " "
720 PRINT "the cycle limit is ", W
730 PRINT " "
740 INPUT "do you want to change the cycle limit ? " SAY
750 PRINT " "
760 IF PARLER = "y" GOTO 700 ELSE GOTO 770
770 IF PARLER = "n" GOTO 780 ELSE GOTO 720
771 REM
780 IF W < 50 GOTO 790 ELSE GOTO 810
781 REM
790 LET O = W
```

```
800 GOTO 1005
810 LET M = W / 50
820 LET O = W MOD 50
829 REM Oscillator on
830 LET DOT(1,0,0)=0
831 REM
832 REM
840 FOR X = 1 TO M
850 FOR Z = 1 TO 50
859 REM In tension
860 LET DOT(1,1,1)=1
870 WAIT(TEMPS)
879 REM In compression
880 LET DOT(1,1,1)=0
890 WAIT(TEMPS)
900 CYCLE = CYCLE + 1
910 PRINT "cycle = ", CYCLE
920 NEXT
921 REM
922 REM This next loop repositions the loading jaws to the
923 REM right opening. It is executed after each 50 cycles.
924 REM
925 REM N.B. Adjustments are calibrated every 50 cycles
926 REM Put in tension; oscillator off
930 LET DOT(1,1,1)=1
940 LET DOT(1,0,0)=1
950 FOR L = 1 TO 280
960 LET DOT(1,3,3)=1
970 LET DOT(1,3,3)=0
980 NEXT
981 REM
```

```
990 LET DOT(1,0,0)=0
1000 NEXT
1001 REM
1003 IF O=0 THEN GOTO 1090 ELSE 1005
1004 REM
1005 LET DOT(1,0,0)=0
1010 FOR P = 1 TO O
1020 LET DOT(1,1,1)=1
1030 WAIT(TEMPS)
1040 LET DOT(1,1,1)=0
1050 WAIT(TEMPS)
1060 CYCLE = CYCLE + 1
1070 PRINT "cycle = ", CYCLE
1080 NEXT
1081 REM
1082 REM
1083 REM
1090 LET DOT(1,0,0)=1
1100 PRINT " "
1110 PRINT " "
1120 PRINT "Note that ", O , "cycles were not calibrated"
1130 PRINT " "
1140 PRINT " "
1150 INPUT "do you want to cycle more ? " RESPONSE
1160 IF RESPONSE = "y" GOTO 720 ELSE GOTO 1170
1170 IF RESPONSE = "n" GOTO 160 ELSE GOTO 1150
1171 REM
1172 REM Step by step cycling
1173 REM _____
1174 REM
1175 REM This routine makes the motor step at a slower rate than
```

```
1176 REM the automatic mode. The internal oscillator is bypassed
1177 REM and the motor is triggered by the digital output of the
1178 REM umac-5000.
1179 REM
1180 PRINT " "
1190 PRINT " Step by step cycling "
1200 PRINT " "
1210 LET TEMPO = 0.0
1220 GOTO 1270
1230 PRINT " "
1240 PRINT " Slower rate cycling "
1245 PRINT " "
1250 INPUT " Enter the waiting time : " TEMPO
1260 PRINT " "
1270 PRINT " Position the driver in Auto, Tension & Cyclic "
1280 PRINT " "
1290 LET CALIB = 25.0
1300 INPUT " Enter the p to p displacement in microns : " PEAK
1310 LET AUTOSTEP = PEAK * CALIB
1320 LET REALPEAK = AUTOSTEP / CALIB
1330 PRINT " "
1340 PRINT " The real displacement is ", REALPEAK
1350 PRINT " The number of steps is ", AUTOSTEP
1355 PRINT " The waiting time is ", TEMPO
1360 PRINT " "
1370 CYCLE = 0
1380 INPUT " What is the cycle limit ? " LIM
1390 PRINT " "
1400 PRINT " The cycle limit is : ", LIM
1410 PRINT " "
1420 INPUT " Do you want to change the cycle limit ? " ANSWER
```

```
1430 PRINT " "
1440 IF ANSWER = "y" GOTO 1380 ELSE GOTO 1450
1450 IF ANSWER = "n" GOTO 1460 ELSE GOTO 1400
1460 LET DOT(1,0,0)=1
1470 FOR A = 1 TO LIM
1480 LET DOT(1,1,1)=1
1485 REM Passing the signal through the 2x amplifier (0 and 10 V)
1490 FOR INDEX = 1 TO AUTOSTEP
1500 LET DOT(1,3,3)=1
1510 LET DOT(1,3,3)=0
1520 NEXT
1522 IF OPTION = "2" THEN GOTO 1530 ELSE 1525
1525 WAIT(TEMPO)
1530 LET DOT(1,1,1)=0
1540 FOR INDICE = 1 TO AUTOSTEP
1550 LET DOT(1,3,3)=1
1560 LET DOT(1,3,3)=0
1570 NEXT
1572 IF OPTION = "2" THEN GOTO 1580 ELSE 1575
1575 WAIT(TEMPO)
1580 CYCLE = CYCLE + 1
1590 PRINT "cycle = ", CYCLE
1600 NEXT
1610 PRINT " "
1620 INPUT "do you want to cycle more ? " MORE
1630 IF MORE = "y" GOTO 1400 ELSE GOTO 1640
1640 IF MORE = "n" GOTO 160 ELSE GOTO 1620
1641 REM
1642 REM
1650 REM *****
1660 REM ** POSITIONING ROUTINE **
```

```
1670 REM *****
1680 REM
1681 REM This routine does NOT cycle the specimen. It only moves
1682 REM the applicator in one direction (chosen by the user)
1683 REM for a given distance. This movement is done by bypassing
1684 REM the oscillator.
1685 REM
1686 REM
1690 REM Initialisation of the calibration variable (step-by-step mode):
1700 REM Sensitivity = 0.04 micron/step, or 25 steps/micron.
1710 REM
1720 LET CALIB = 25.0
1730 REM
1740 PRINT CHR$(24)
1750 PRINT " INITIAL GAP POSITIONING ROUTINE "
1760 PRINT " _____ "
1770 PRINT
1780 PRINT
1790 PRINT " Position the driver in Auto, Run and Uni-directional "
1800 PRINT " Make sure the driver is set in the right direction:"
1810 PRINT " -Ten or Com "
1820 PRINT " "
1830 INPUT " Enter the displacement in microns : " GAP
1840 STEP = GAP * CALIB
1850 REALGAP = STEP / CALIB
1860 PRINT "real gap is : ", REALGAP
1870 PRINT "# of steps is : ", STEP
1880 LET DOT(1,0,0)=1
1890 FOR I= 1 TO STEP
1900 LET DOT(1,3,3)=1
1910 LET DOT(1,3,3)=0
```

1920 NEXT

1930 LET DOT(1,0,0)=1

1940 REM

1950 RETURN

Appendix E

Supplementary Results

In addition to the plethora of results presented in Chapter 8, a few more have been selected to further confirm the analysis of the fatigue cumulative damage properties, both material degradation and structural breakdown; and to corroborate the theory proposed for explicating fatigue-failure in wood pulp fibres.

Figure E.1: The underlying themes typifying fatigue cumulative damage are chemical degradation and structural breakdown of the cell wall material. The latter are evinced by particular phenomena, e.g., the propagation of cracks, inter-laminar separation, and partial peeling-off, of the cell wall material — travelling successively inwards. (a) Shows a pulp fibre sample: Jack pine RMP, refined at 4.4 GJ/t whose extractives are removed, subjected to 350 cycles in shear at 0.0262 Hz. (b) Similar to (a) except that the extractives are *not* removed, and the fibre is cycled 1200 times.

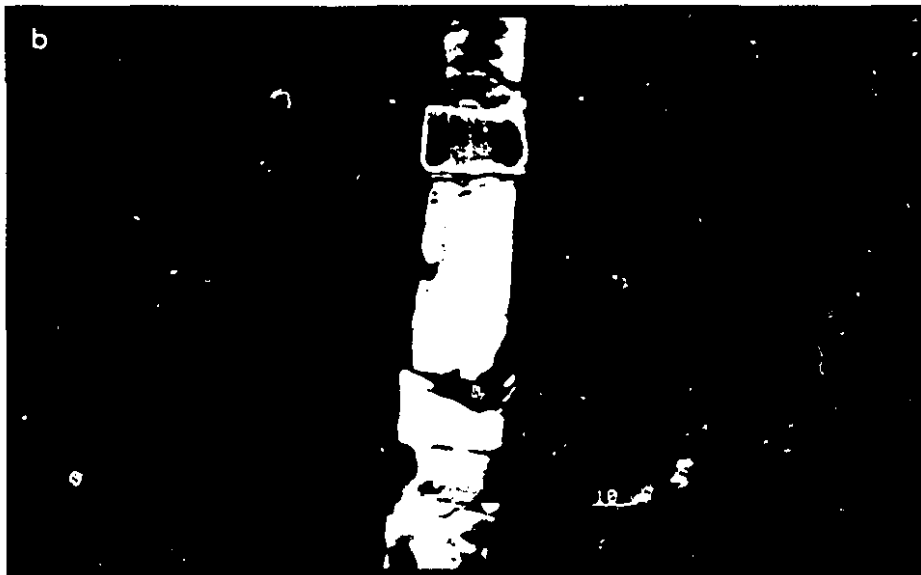


Figure E.2: The above micrographs depict the typical material property degradation phenomena characterising damage accumulation due to cyclic-shear loading: A myriad of microcracks combine to form a dominant macrocrack spanning the length of the fibre. Regions of high stress concentration, such as bordered pits, force the cracks to re-orient themselves around these regions of natural bias. Moreover, intensive material degradation cumulates with cycling causing the eventual peeling-off of parts of the external cell wall layers (a). Concomitantly, the cell wall also undergoes extensive external fibrillation (b), as well as internal fibrillation; the latter being evinced by the apparent volumetric expansion of the cell wall layers (c). It should be noted that the transverse cracks are responsible for one mode of failure, as explained *in extenso* in Chapter 8. (Tested sample is: Jack pine RMP, refined at 6.5 GJ/t, subjected to 1050 cycles in shear at 0.0262 Hz.)

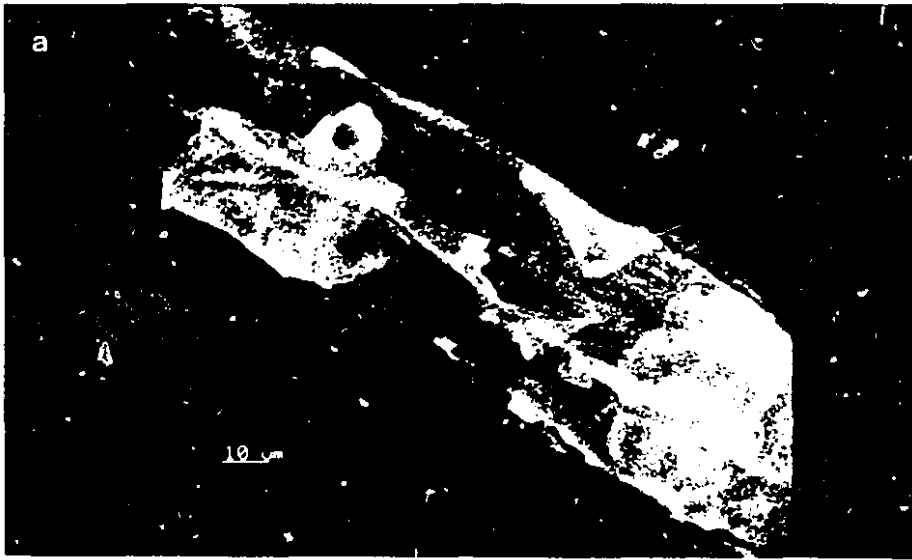
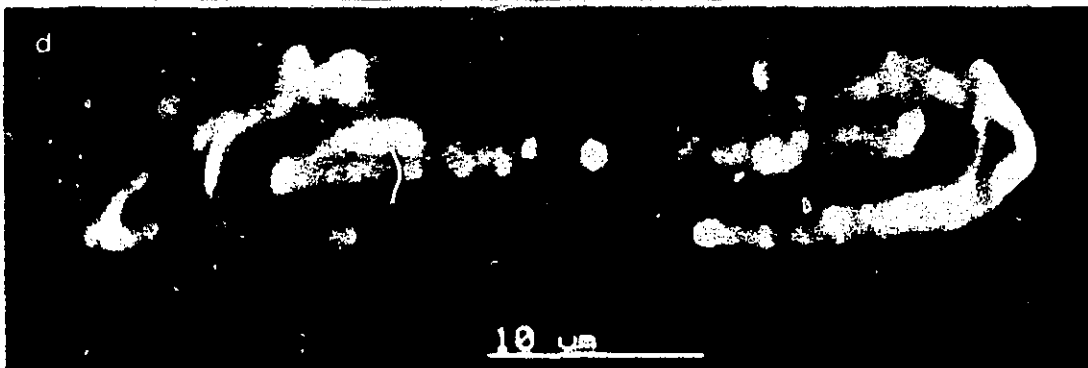
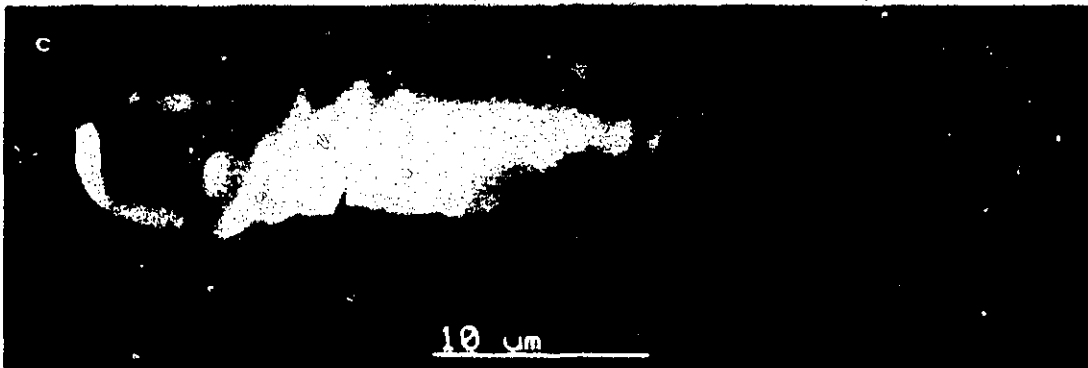
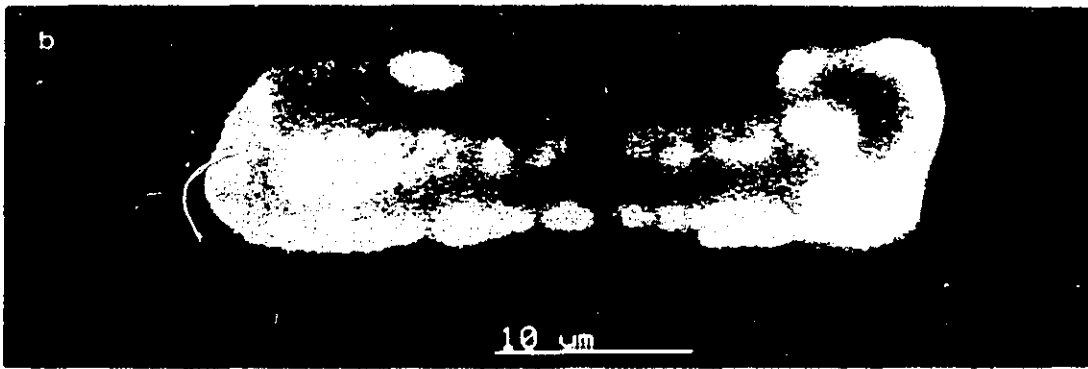


Figure E.3: Owing to the continued chemical degradation and structural breakdown—which traverses across the fibre width, the structural integrity of the laminated composite fibre is successively compromised as evinced by the clear cell wall collapse, and inter-laminar delamination as well. Cross-sectional micrographs (a)–(d), which are 30 μm apart, are of black spruce RMP, refined at 8.5 GJ/t, and subjected to 1200 cycles in shear at 0.0262 Hz. Whilst these shown in (e)–(g) are of jack pine RMP, refined at 6.5 GJ/t, and cycled 1750 times in shear.



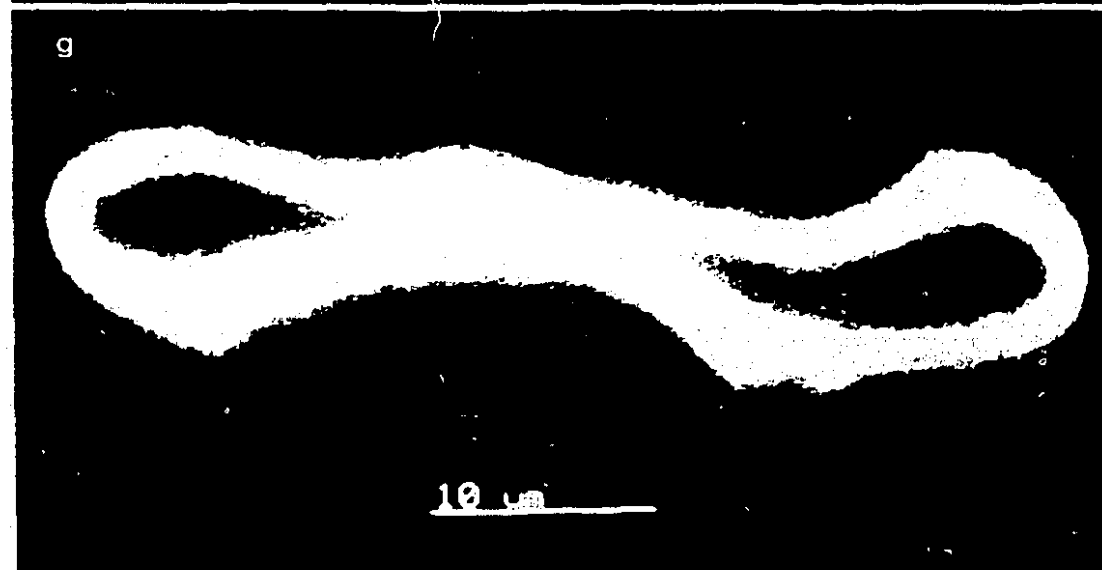
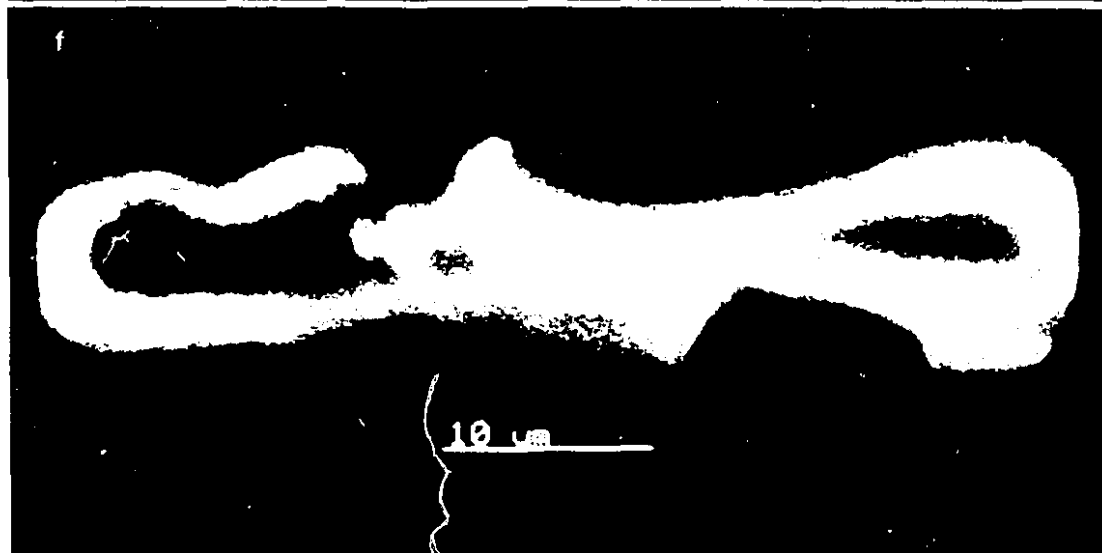
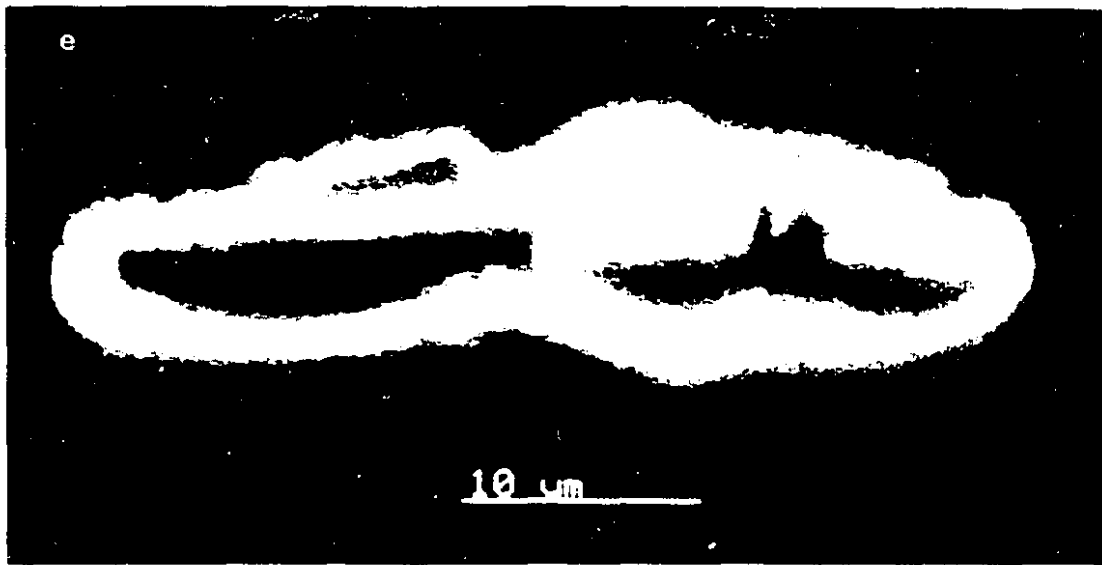


Figure E.4: The propagation of developed cracks in the manner illustrated in the above micrograph, provides further support to theory proposed for the micro-mechanisms of fibre fatigue-failure (see section 8.4, Chapter 8): Essentially, the crack initiates at the surface and propagates longitudinally until deflected by the presence of natural bias. The shown photomicrograph is of jack pine RMP, refined at 6.5 GJ/t, subjected to 1050 cycles in shear.



Figure E.5: Although, under radial compression testing, a much larger number of cycles is required to effectively cause the material degradation and structural breakdown, in the fibre cell wall material, the overall mechanisms of failure and material property degradation phenomena are principally the same as for shear-testing. Shown above are such characteristics of: (a) jack pine RMP, refined at 6.5 GJ/t, subjected to 3400 cycles at 0.187 Hz; (b) black spruce RMP, refined at 8.5 GJ/t, subjected to 5400 cycles.

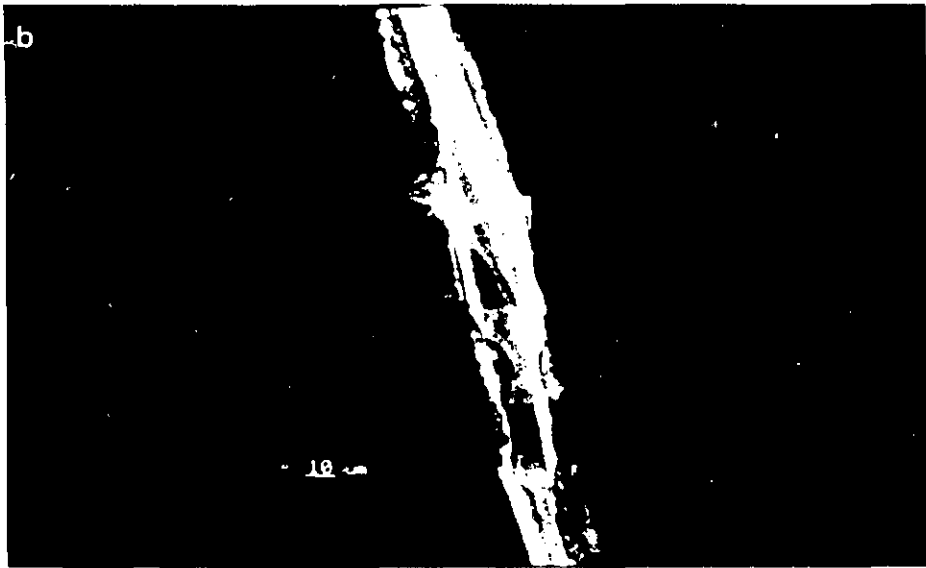
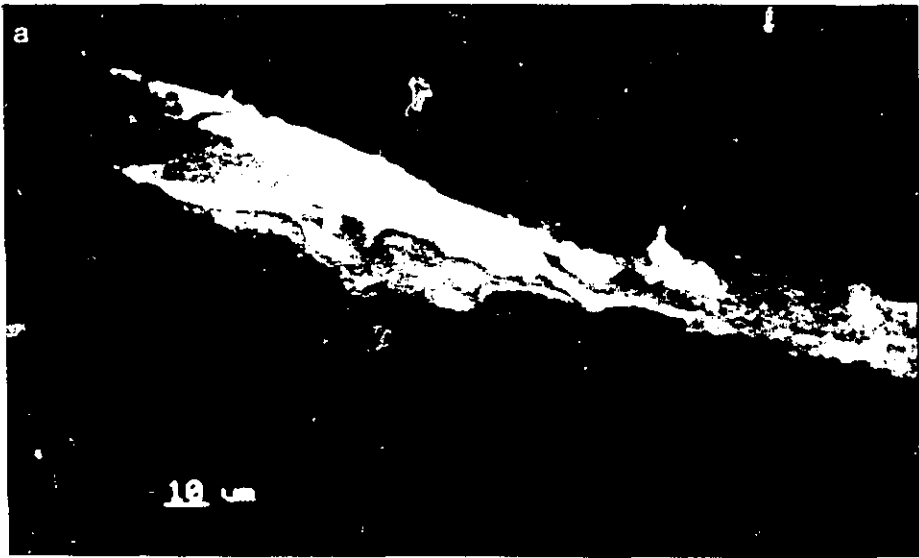


Figure E.6: The cell wall collapse, due to radial compression testing, is by far less than that due to shear-testing since the extent of damage accumulation is less pronounced here. Cross-sectional images (a)-(b), 30 μm apart, are of jack pine RMP, refined at 6.5 GJ/t, and subjected to 3400 cycles at 0.187 Hz.

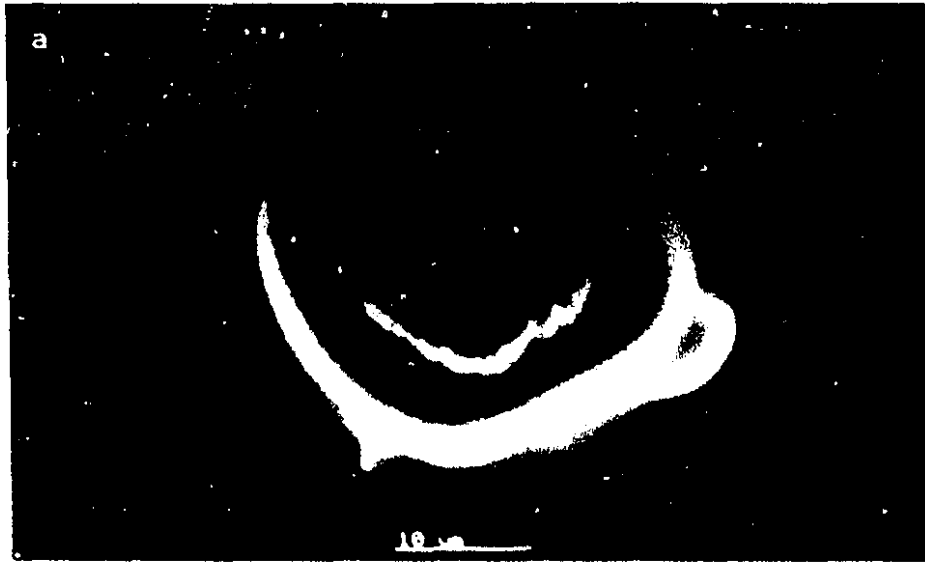
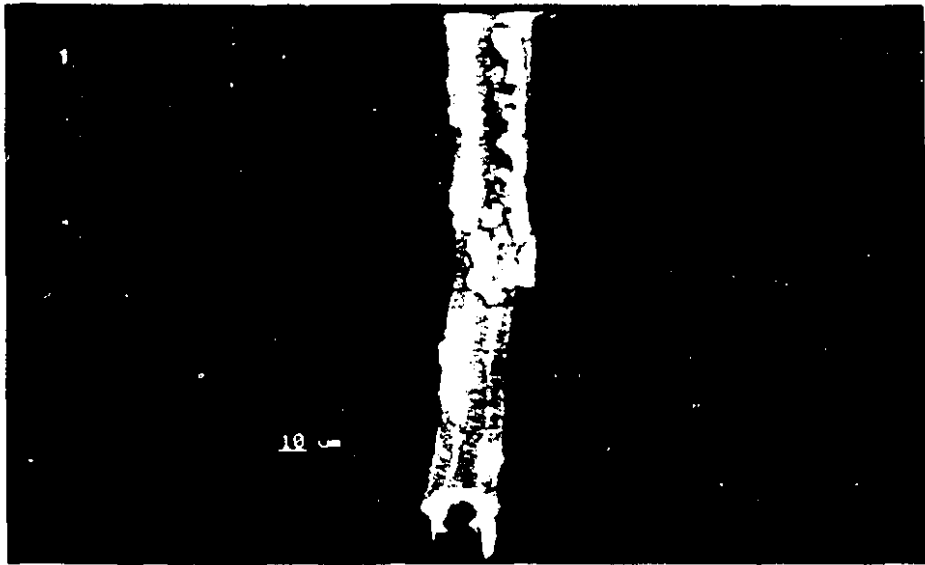


Figure E.7: In the micrograph shown here, a pulp fibre was forced to rupture by driving the steel-alloy wire, housed in the applicator, through it. As clearly evidenced, the rupture is oriented along the dominant cracks which indicates the pre-eminence of the latter. This particular fibre is jack pine RMP, refined at 6.5 GJ/t, and radially compressed 2700 times at a frequency of 0.187 Hz.



18

Figure E.8: Cyclic tension stroke is the least effective mode at which material degradation could occur, even as the number of cycles exceeds 6000—i.e. three-fold the maximum experienced under shear testing. Hence, very insignificant degradation phenomena and structural collapse would be expected: Micrograph (a) shows external fibrillation in the external layer of the fibre cell wall; whilst (b)–(c) depict two cross-sectional micrographs, 30 μm apart, of the above region. The tested fibre is: jack pine RMP, refined at 8.5 GJ/t, cycled 6100 times at 0.187 Hz.

